TECHNICAL PROGRESS REPORT

CONTRACT EY-76-C-02-0535.A002

November 1, 1978

COO/535-766

NOTICE

This report was prepared as an account of work sponsored by the United States Government. Neither the United States nor the United States Department of Energy, nor any of their employees, makes any warranty, express or implied, or assumes any legal liability or responsibility for the accuracy, completeness, or usefulness of any information, apparatus, product or process disclosed, or represents that its use would not infringe privately owned rights.

DISCLAIMER

TABLE OF CONTENTS

I. INTRODUCTION

This report summarizes the work carried out at the Nuclear Physics Laboratory of the University of Colorado during the period November 1, 1977 to November 1, 1978, under contract EY-76-C-02-0535.A002 between the University of Colorado and the United States Department of Energy.

The research activities of the laboratory have spanned a broad range of interests over the past year. Numerous topics in charged-particle spectroscopy and reaction studies, neutron time-of-flight measurements and gamma-ray investigations performed at the cyclotron laboratory are covered in this report. In addition, several items in intermediate energy nuclear physics as studied at Los Alamos and Indiana by members of the laboratory are reported. The efforts in nuclear theory include studies in nuclear reaction mechanisms and pion scattering as related to the experimental program.

In terms of journal publications and conference presentations the laboratory productivity was at an all-time high this year.

II. EXPERIMENTAL PROGRAM

A. Nuclear Physics

1. Nuclear Reaction Studies

a. Single-Nucleon Transfer Reactions

i. The ^{198}Pt(d,p)^{199}Pt Reaction - R. J. Peterson, N. J. DiGiacomo and G. R. Smith

Angular distributions for several levels of ^{199}Pt were obtained at a deuteron energy of 17.3 MeV in an attempt to follow the shifting single neutron states for the heavier Pt isotopes.[1] This beam energy is too low, and even ℓ=1 cross sections were small. The largest cross sections seen were only 500 μb/sr. Data for the first four levels are compared to DWBA predictions in Fig. A1-a1. Few firm spin assignments are available for ^{199}Pt from the literature.[2]

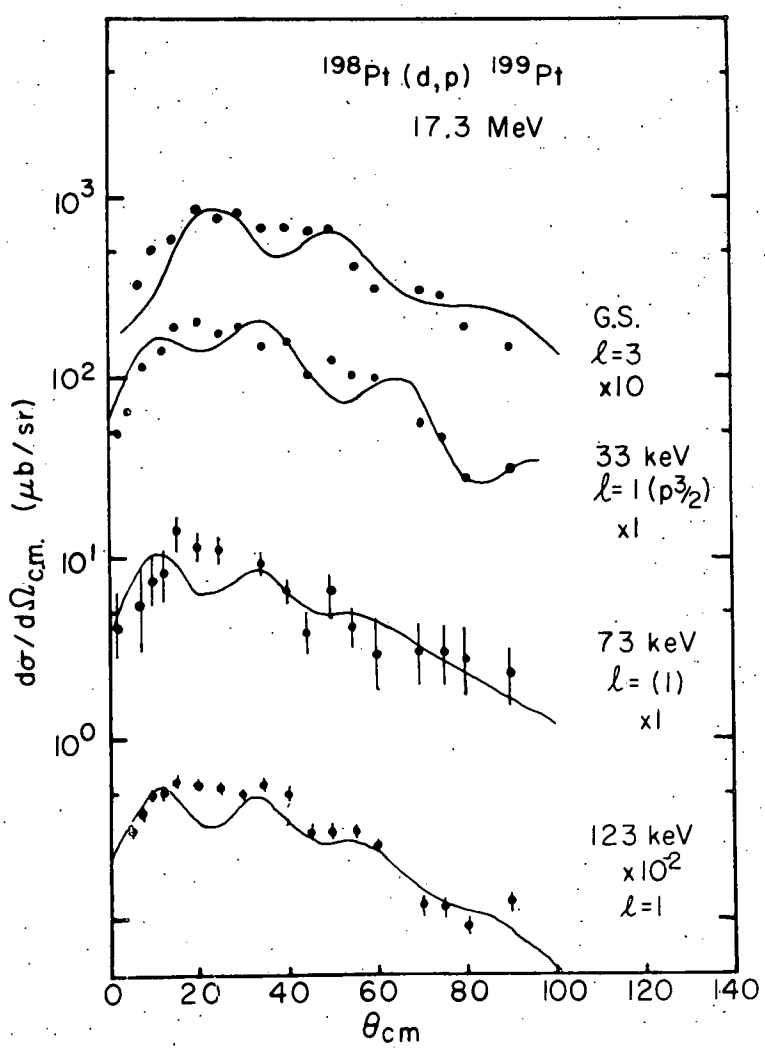

Fig. A1-a1. Angular distributions for several low-lying states of ^{199}Pt are compared to DWBA calculations. The ℓ=1 curves are for $p_{3/2}$ transfer, which fit better than those for $p_{1/2}$ transfer.

The ℓ=3 fit for the ground state is in agreement with the compiled result, but the first excited state could be a doublet of ℓ=1 and ℓ=3 transitions. The lack of distinction between ℓ=1 and ℓ=3 predictions precludes a detailed assignment. States at 32 keV $(7/2^-)$ and 0.05 MeV $(1/2,3/2)^-$ are known.[2] The 73 keV state is only weakly excited, and even the strong 123 keV state is not fit well by the ℓ=1 prediction. Spectroscopic factors for the low-lying states of ^{199}Pt are listed in Table A1-aI.

The poor ℓ=1 fits, the lack of clear distinction between ℓ=1 and ℓ=3 shapes and the total lack of strength to the known high spin states are all due to the low beam energy. No further work on this experiment is planned, since the present deuteron beam energy is not sufficient to answer the relevant questions.

Table A1-AI
Spectroscopic factors from the ^{198}Pt(d,p)^{199}Pt reaction at 17.3 MeV.

Excitation (keV)	ℓ	J^π (assumed)	C^2S
0	3	$5/2^-$	0.10
33	1	$3/2^-$	0.08
73	(1)	$1/2^-$	0.010
		$3/2^-$	0.005
123	1	$1/2^-$	0.055
		$3/2^-$	0.028
193	n.s.	--	--
331	(1)	$1/2^-$	0.025
		$3/2^-$	0.013

ii. Proton Stripping and Pickup on ^{14}C - R. R. Sercely, R. J. Peterson and E. R. Flynn (LASL)

The ^{14}C(^{3}He,d)^{15}N reaction at 25.4 MeV has been studied. Very good fits to DWBA predictions are found for a number of known states of ^{15}N. Samples are shown as Fig. A1-a2. Proton pickup by the ^{14}C(t,α) reaction at 23 MeV was also studied with the LASL 3-stage accelerator. Only the ground state of ^{13}B was strongly populated; the data and DWBA fit are shown as Fig. A1-a3.

The main purpose of this study was to determine the admixture of $p_{1/2}$ protons into the $p_{3/2}$ shell expected to dominate for ^{14}C, since the neutron shell closure is expected to decrease the strong deformation found for ^{12}C. For the proton stripping, the $p_{3/2}$ spectroscopic factor is 0.036 times that for $p_{1/2}$ transfer. No $1/2^-$ states are known in ^{13}B, but neither of the two candidates has a pickup spectroscopic factor larger than one percent of the $p_{3/2}$ pickup strength.

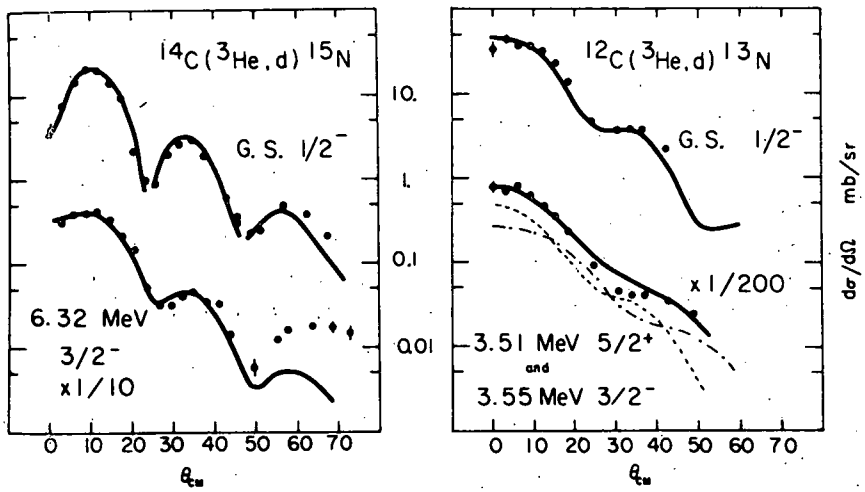

Fig. A1-a2. Angular distributions to known $1/2^-$ and $3/2^-$ states in ^{15}N and ^{13}N are compared to DWBA predictions. The $3/2^-$ state of ^{13}N is not resolved from the broad $5/2^+$ level.

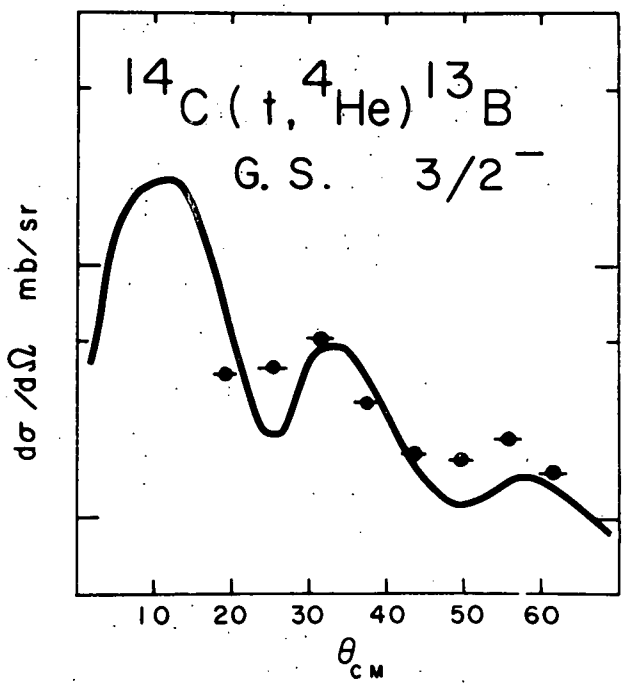

Fig. A1-a3. Data for the proton pickup from ^{14}C at 23 MeV to the $3/2^-$ ground state of ^{13}B are compared to a DWBA prediction. No other levels of ^{13}B below 4 MeV were populated with strength sufficient for a detailed analysis.

[1] W. P. Alford and K. H. Purser, Nucl. Phys. A132 (1969) 86.
[2] F. E. Cecil et al. 1975 Progress Report, Univ. of Colorado, p. 73.

iii. Proton Spectroscopy of ^{96}Tc from the (^{3}He,d) Reaction - R. A. Emigh, J. J. Kraushaar, and S. Shastry (SUNY, Plattsburgh, NY)

The level structure of the odd-odd nucleus ^{96}Tc is of interest primarily to investigate the residual nucleon-nucleon interaction in a region removed from doubly magic nuclei. Although relatively thorough studies have been made of ^{98}Tc (Ref. 1) and ^{94}Tc (Ref. 2-5), only γ-ray related reaction studies have been made on ^{96}Tc. The low-lying positive parity multiplet of ^{94}Tc appears to have a relatively pure $\pi 1g_{9/2}^{3} \otimes \nu 2d_{5/2}$ configuration while the positive parity multiplet of ^{98}Tc has principally a $\pi 1g_{9/2}^{3} \otimes \nu 2d_{5/2}^{-1}$ configuration. Only the low-lying positive parity multiplet of ^{96}Tc remains to be identified for the even mass Tc isotopes between the semi-shell closures at N=50 and N=56, where the $2d_{5/2}$ orbital is expected to be the most active.

The ^{94,98}Tc nuclei are of interest because most of the single particle strength lies in the multiplet constructed from the $\pi 1g_{9/2}$ and $\nu 2d_{5/2}$ orbitals. Although there is extensive configuration mixing in the level structure of ^{94,98}Tc, so little single particle strength resides in levels other than the low-lying $g_{9/2}$-$d_{5/2}$ multiplet that mixing should not significantly shift the relative location of the members of this multiplet. Consequently, relatively simple shell model calculations should reproduce the locations of the members of the $g_{9/2}$-$d_{5/2}$ multiplet. This in fact appears to be the case for ^{94,98}Tc. If the addition of two neutrons (neutron holes) to ^{94}Tc (^{98}Tc) does not significantly alter the nuclear structure, then one would expect similar structural characteristics in ^{96}Tc as in ^{94,98}Tc.

The reaction was studied using the University of Colorado spectrometer at a $^{3}He^{++}$ energy of 33.6 MeV. The target consists of approximately 100 μgm/cm^2 of 94% ^{95}Mo sputtered onto a 50 μgm/cm^2 ^{12}C backing. The energy resolution is about 28 keV (FWHM). Sample deuteron spectra are shown in Fig. A1-a4.

The relative normalization between data taken at various scattering angles was obtained by the use of a Faraday cup and a solid state detector monitor placed at an angle fixed with respect to the incoming beam. Absolute normalization was obtained by comparing the experimental elastic cross sections to those predicted from ^{3}He optical model parameters.

The energies of the various peaks in ^{96}Tc are based on the calibration data taken from the ^{106}Pd(^{3}He,d)^{107}Ag reaction.[6,7] The uncertainties in the calculated energies range from less than 5 keV for the lower-lying peaks to 15 keV for some of the higher-lying peaks.

The experimental angular distributions were compared to DWBA curves generated by the computer code DWUCK4[8] in order to obtain ℓ-transfers and spectroscopic factors. Proton optical model parameters were taken from the work of Becchetti et al.[9] and the deuteron parameters from Childs and Daehnick.[10] Energies and spectroscopic

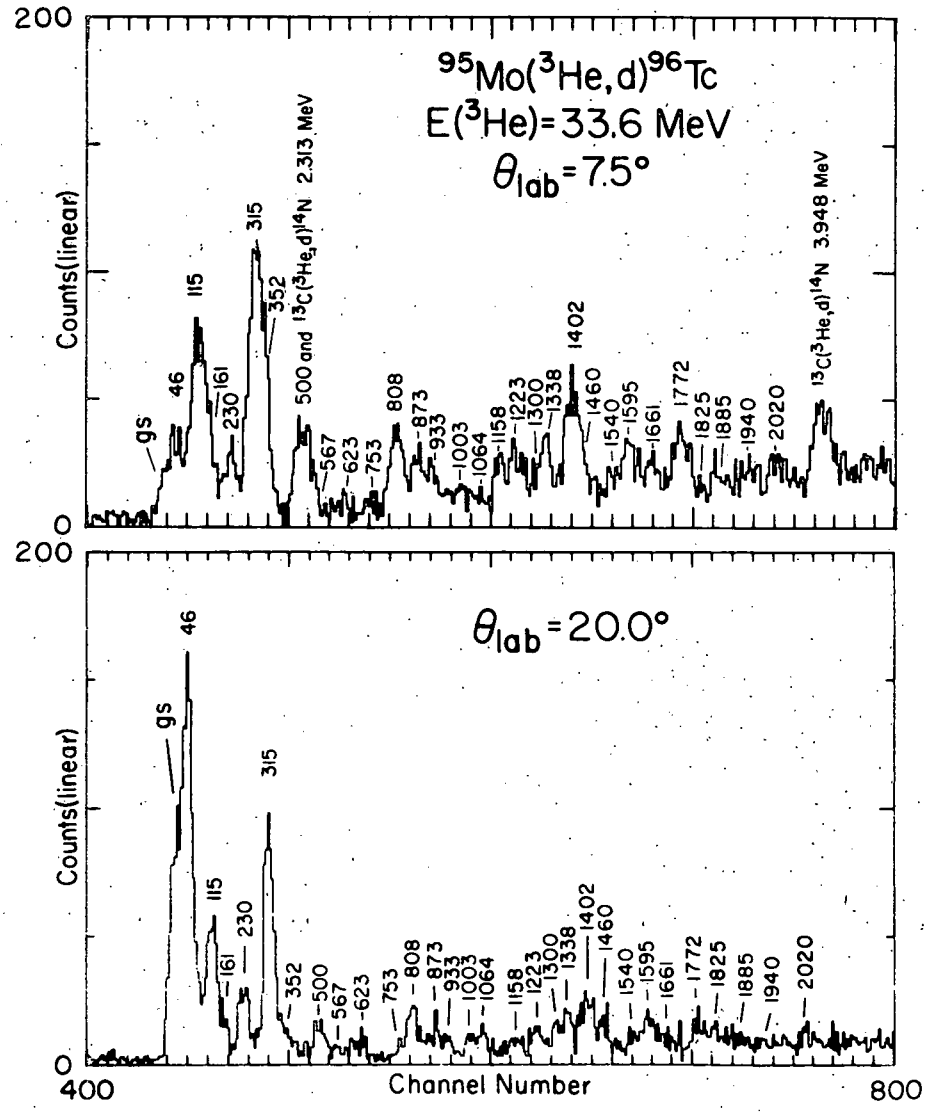

Fig. A1-a4. Sample spectra of the $^{95}Mo(^{3}He,d)^{96}Tc$ reaction at $\theta_{lab}=7.5^{o}$ and 20.0^{o}. Level energies are given in keV.

strengths are listed in Table A1-AII. Angular distributions and DWUCK4 fits are shown in Figs. A1-a5 through A1-a11.

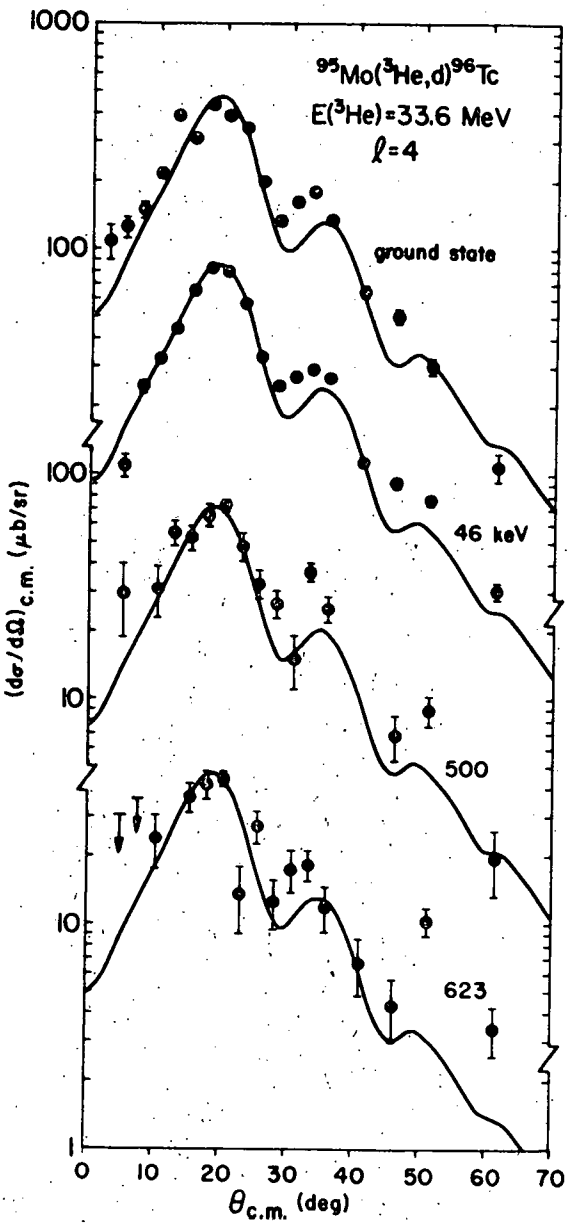

Fig. A1-a5. Angular distributions which have ℓ=4 transfer in the ^{95}Mo(^{3}He,d)^{96}Tc reaction.

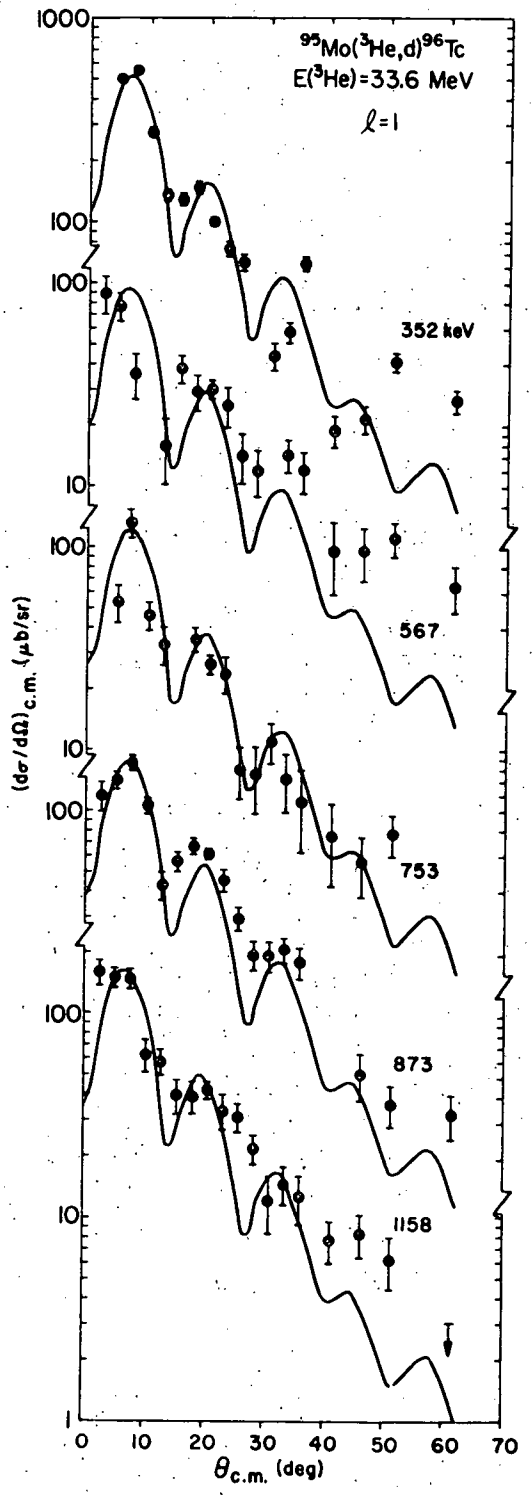

Fig. A1-a6. Angular distributions which have ℓ=1 transfer in the ^{95}Mo(^{3}He,d)^{96}Tc reaction.

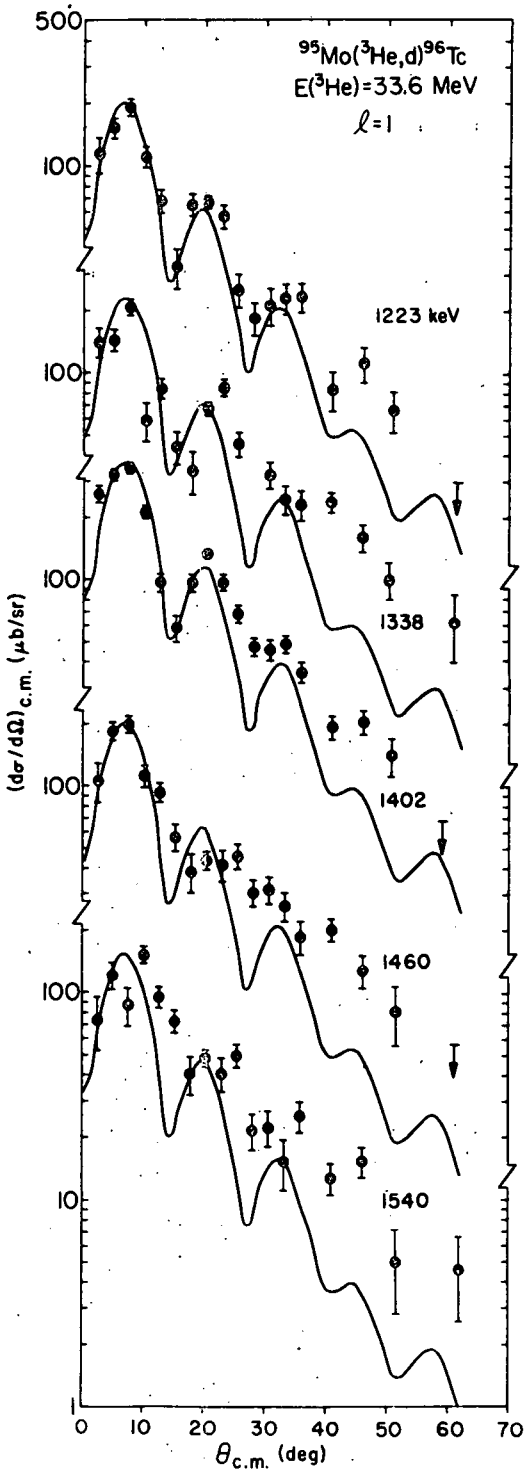

Fig. A1-a7. Angular distributions which have ℓ=1 transfer in the ^{95}Mo(^{3}He,d)^{96}Tc reaction.

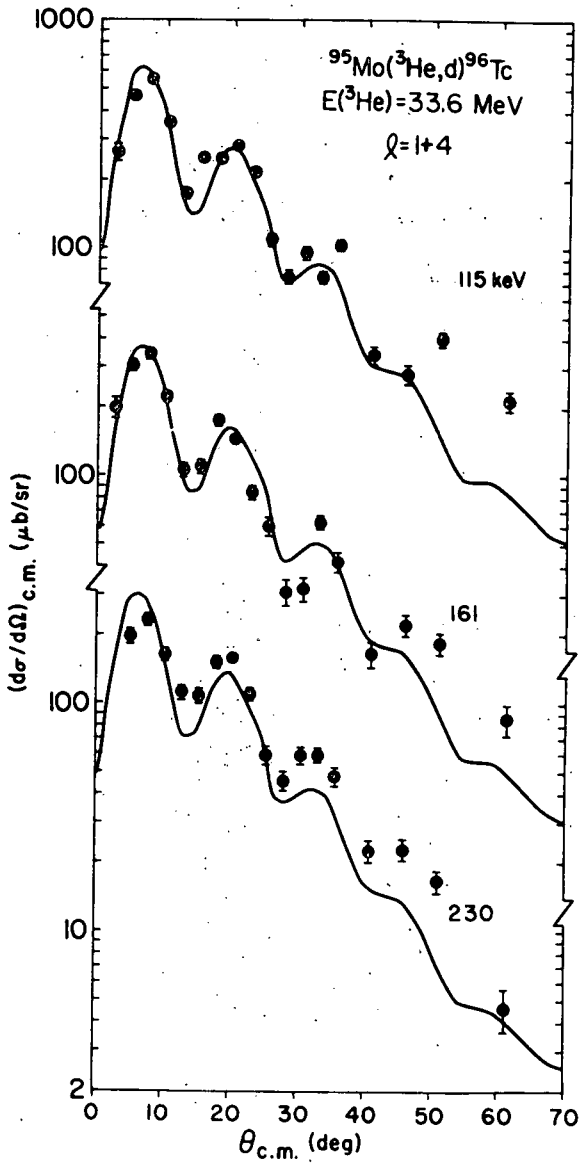

Fig. A1-a8. Angular distributions which have ℓ=1+4 transfer in the ^{95}Mo(^{3}He,d)^{96}Tc reaction.

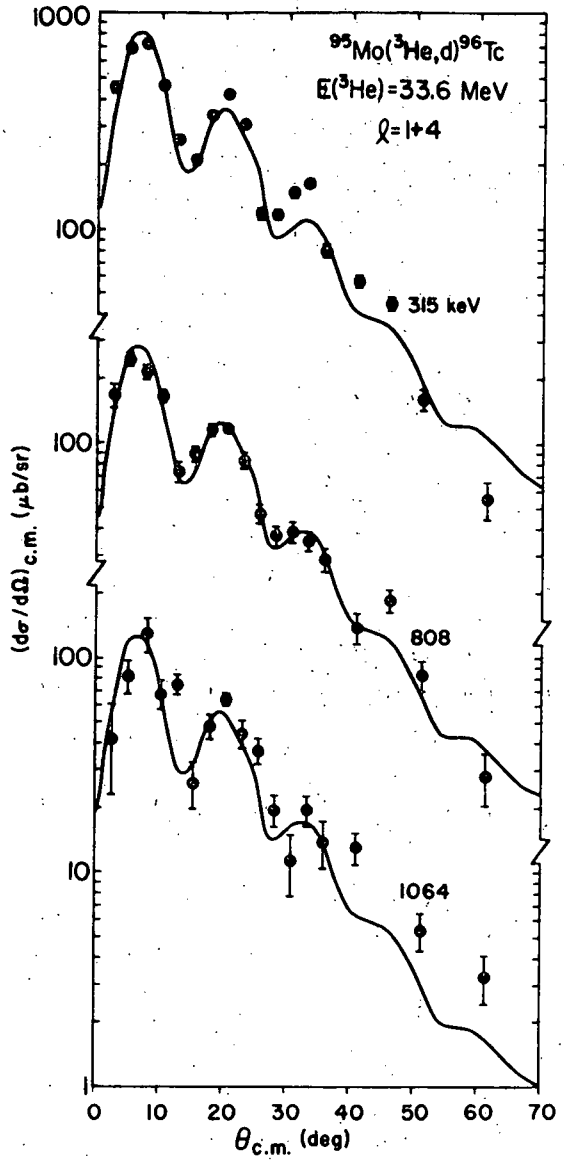

Fig. A1-a9. Angular distributions which have ℓ=1+4 transfer in the ^{95}Mo(^{3}He,d)^{96}Tc reaction.

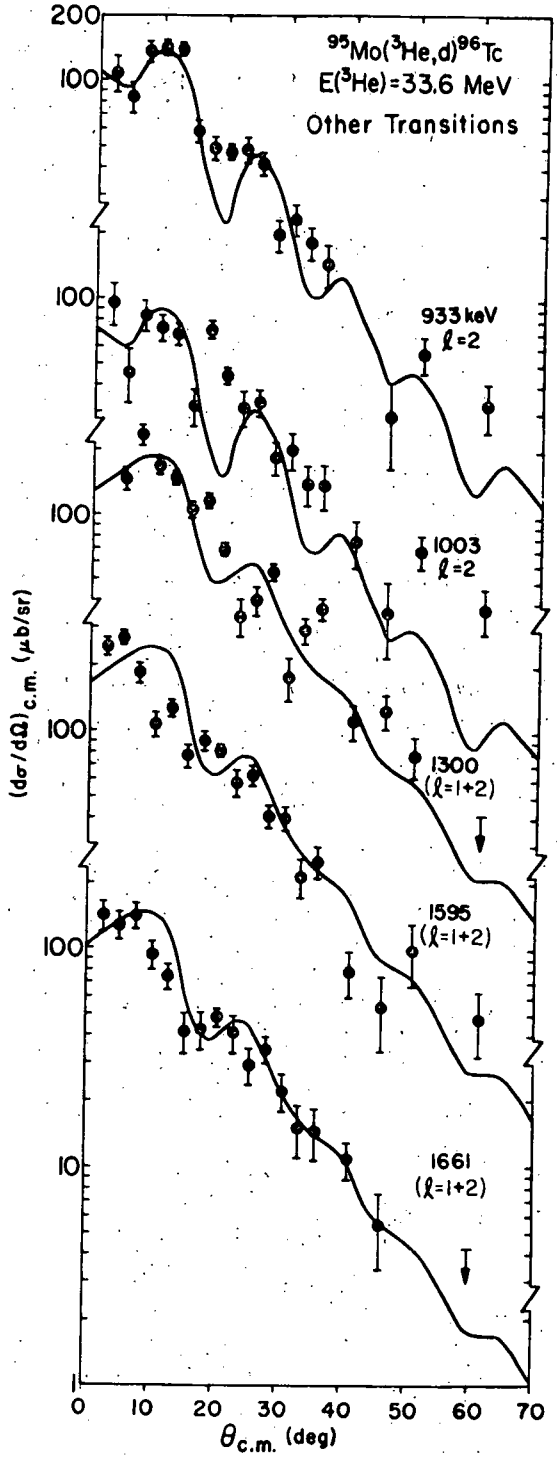

Fig. A1-a10. Angular distributions which have ℓ=2 or ℓ=1+2 transfer in the ^{95}Mo(^{3}He,d)^{96}Tc reaction.

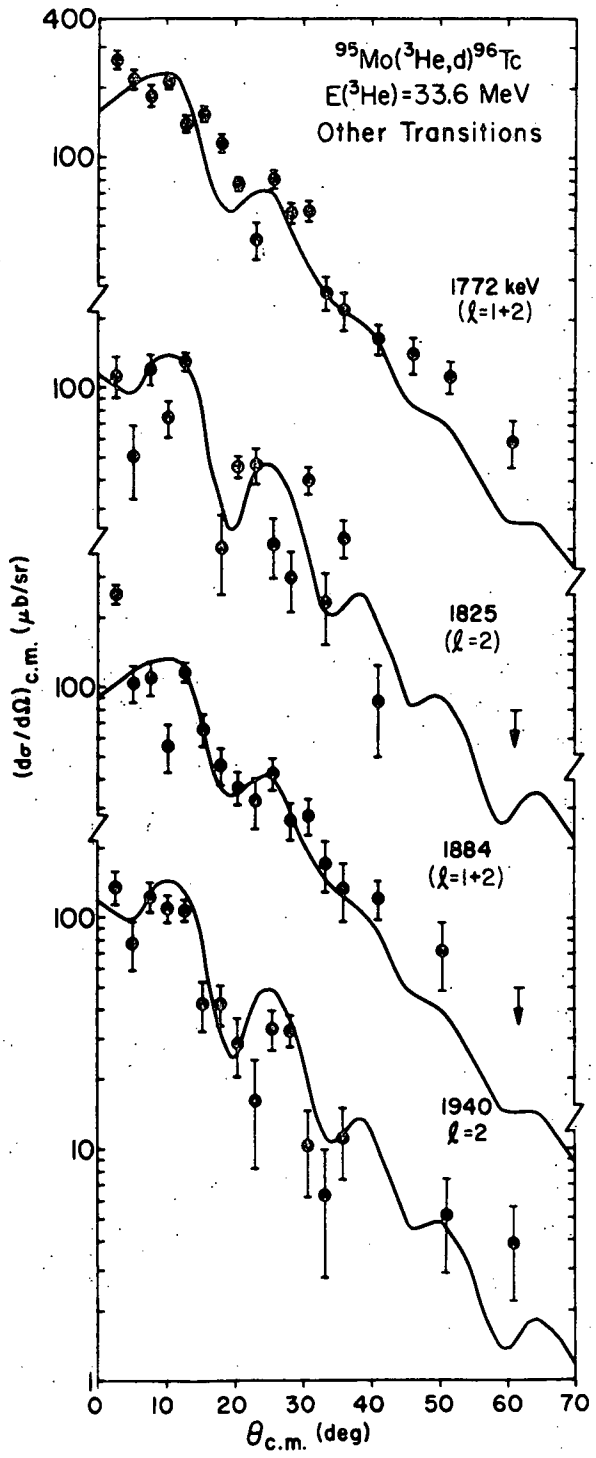

Fig. A1-a11. Angular distributions which have ℓ=2 or ℓ=1+2 transfer in the ^{95}Mo(^{3}He,d)^{96}Tc reaction.

Table A1-AII

Summary of the $^{95}Mo(^{3}He,d)^{96}Tc$ reaction measurements.

Present work ($^{3}He,d$)				
Energy (keV)	Uncertainty (keV) [a]	ℓ-transfer	J^{π} [b]	$(2J+1)C^{2}S$ [c,d]
0	4	4	7^{+}	2.42
46	2	4	$3^{+},4^{+},(6)^{+}$	4.24
115	3	1+4	$1\text{-}4^{-}$	0.22
			$2\text{-}7^{+}$	0.94
161	3	1+4	$2\text{-}7^{+}$	0.64
			$1\text{-}4^{-}$	0.14
230	3	1+4	$1\text{-}4^{-}$	0.10
			$2\text{-}7^{+}$	0.50
315	4	1+4	$1\text{-}4^{-}$	0.29
			$2\text{-}7^{+}$	1.29
352	2	1	$1\text{-}4^{-}$	0.21
500	3	4	$2\text{-}7^{+}$	0.35
567	4	1	$1\text{-}4^{-}$	0.04
623	2	4	$2\text{-}7^{+}$	0.22
753	7	1	$1\text{-}4^{-}$	0.05
808	5	1+4	$1\text{-}4^{-},2\text{-}7^{+}$	0.09,0.36
873	3	1	$1\text{-}4^{-}$	0.07
933	5	2	$0\text{-}5^{+}$	0.08

Table A1-AII (continued)

1003	5	2	$0\text{-}5^+$	0.05
1064	9	1+4	$1\text{-}4^-, 2\text{-}7^+$	0.04,0.16
1158	4	1	$1\text{-}4^-$	0.05
1223	4	1	$1\text{-}4^-$	0.07
1300	10	1+2	$1\text{-}4^-, 0\text{-}5^+$	0.03,0.08
1338	8	1	$1\text{-}4^-$	0.08
1402	6	1	$1\text{-}4^-$	0.13
1460	10	1	$1\text{-}4^-$	0.06
1540	15	1	$1\text{-}4^-$	0.05
1595	10	1+2	$1\text{-}4^-, 0\text{-}5^+$	0.03,0.02
1661	8	1+2	$1\text{-}4^-, 0\text{-}5^+$	0.02,0.06
1772	9	1+2	$1\text{-}4^-, 0\text{-}5^+$	0.03,0.07
1825	8	2	$0\text{-}5^+$	0.06
1885	15	2	$0\text{-}5^+$	0.06
1940	15	2	$0\text{-}5^+$	0.07
2020	15	--	--	--

a) These uncertainties are the standard deviations of the energies calculated from the calibration target at three angles.

b) Only the least restrictive spin-parity assignments are given here.

c) Orbits are assumed to be $2p_{1/2}$, $2d_{5/2}$ and $1g_{9/2}$ for ℓ=1, ℓ=2 and ℓ=4, respectively. For $2p_{3/2}$ multiply by 0.95, for $2d_{3/2}$ multiply by 1.24 and for $1g_{7/2}$ multiply by 1.52.

d) States with double ℓ-value assignments have relative sensitivities of the order of 10% for ℓ=1+4 transfers and 40% for ℓ=1+2 transfers.

The low-lying positive parity multiplet of ^{96}Tc should be primarily the $[(\pi 1g_{9/2})^3_{9/2} \otimes (\nu 2d_{5/2})^3_{5/2}]_{J=2^+-7^+}$ configuration. The (^{3}He,d) reaction populates the levels by ℓ=4 transfer, the bulk of which lies below 500 keV excitation. The ground state, which has been previously assigned a spin-parity of 7^+ (Ref. 11), is seen with a spectroscopic strength of 2.42. In the absence of seniority and configuration mixing, the predicted $(2J+1)C^2S$ should be less than 2.0. Due to the steep functional dependence of the calculated spectroscopic factors upon the bound state parameters, this difference is not important. This level should have a relatively pure configuration as few other simple configuration multiplets have a $J^\pi=7^+$ member. Consequently, all other ℓ=4 transfer strength in this report will be compared to this one.

The group at 46 keV excitation populated by an ℓ=4 transition has a spectroscopic strength of almost twice that of the ground state, indicating the presence of more than one state at this location. There are known states at 34.2 kev ($J^\pi=4^+$) and at 35.0 keV ($J^\pi=(3^+)$)(Ref. 5,12-15). Also, a level at 49.1 keV with a spin and parity of 6^+ has been proposed.[4,13] Three levels with spin-parities 3^+, 4^+ and 6^+ are consistent with spectroscopic factors from our data.

The lowest lying $J^\pi=2^+$ level tentatively identified in other studies is located at 240 keV. This level corresponds to the positive parity member of the unresolved doublet seen in this work at 230 keV excitation. The $J^\pi=2^+$ level in ^{98}Tc is located at 345 keV and the addition of two $d_{5/2}$ neutron holes to ^{98}Tc should make the $\pi 1g_{9/2}$-$\nu 2d_{5/2}^{-1}$ two-body matrix elements less repulsive, thus lowering the $J^\pi=2^+$ level in energy. This level has an experimental C^2S of 0.50 as compared to a predicted strength of 0.81, indicating that some fragmentation to higher excitations is likely.

The remaining member ($J^\pi=5^+$) of the low-lying multiplet is not so easily identified. A known $J^\pi=5^+$ level must be fragmented over more than one level. This is not surprising due to the large number of levels in ^{96}Tc, although no significant mixing was noted in any member of the $(\pi 1g_{9/2})^3 \otimes (\nu 2d_{5/2})^{-1}$ multiplet in ^{98}Tc. If the bulk of the remaining strength resides in the positive parity level at 115 keV excitation, then the $J^\pi=5^+$ centroid is located at 134 keV with slightly less than the predicted C^2S.

If the positive parity levels are truly as pure in configuration as postulated, then a simple shell model calculation should describe the observed levels well. Using standard shell model techniques, the $[(\pi 1g_{9/2})^3 \otimes (\nu 2d_{5/2})^{-3}]_{2^+-7^+}$ spectrum was calculated from the residual two-body matrix elements obtained from the experimental spectrum of ^{98}Tc (Ref. 1). The calculated spectrum is compared to the experimental spectrum in Fig. A1-a12. The comparison is relatively good when one considers that any mixing in the $J^\pi=4^+,6^+$ levels will drive them lower in excitation. Only the $J^\pi=5^+$ level is not well described by this calculation, implying that the structure of this level is sufficiently complex and that the basis chosen for our calculation is too small to approximate the actual structure.

At least twenty levels in ^{96}Tc are populated by ℓ=1 transfers. In the absence of any configuration mixing one would expect only six levels from the $2p_{1/2}$ and $2p_{3/2}$ orbitals. If the negative parity levels are thoroughly mixed with the nearby neutron orbitals, one would expect to populate twenty-two levels. The negative parity levels, therefore, are severely mixed. Nonetheless, it is expected from shell model considerations that the $J^\pi=2^-,3^-$ levels should have the largest ℓ=1 cross sections. The negative parity levels at 115 keV (C^2S=0.22) and 315 keV (C^2S=0.29) would have spin parities of 2^- and 3^- respectively. The separation between the $[(\pi 1g_{9/2})^3 \otimes \nu 2d_{5/2}^{-1}]_{2^+-7^+}$

and the $[(\pi 1g_{9/2})^2 2p_{1/2} \otimes \nu 2d_{5/2}^{-1}]_{2^-\ 3^-}$ centroids in ^{98}Tc is 174 keV. Using the tentative results given here, the difference between the positive and negative parity multiplets in ^{96}Tc is 167 keV. Such good agreement strongly implies that the 120 keV level has $J^\pi=2^-$ and the 315 keV level has $J^\pi=3^-$.

These results have been submitted for publication.

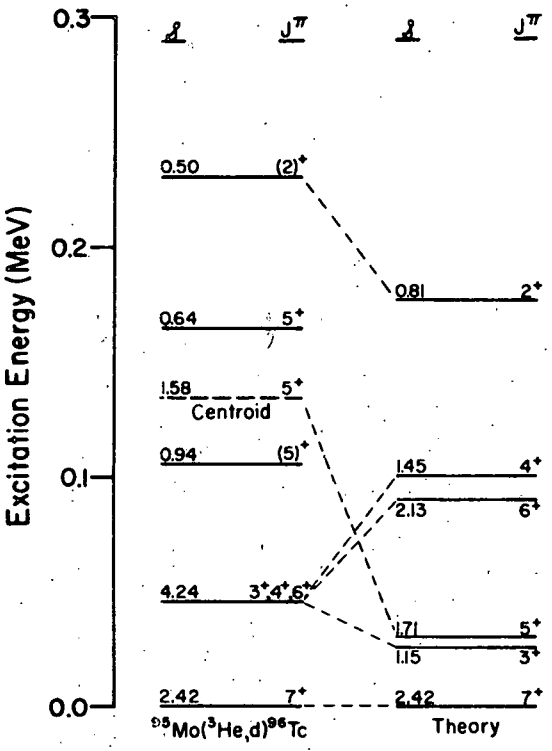

Fig. A1-a12. Comparison of positive parity low-lying levels of ^{96}Tc obtained from this study with a simple shell model calculation. The theoretical spectroscopic factors are normalized to 2.42 for the $J^\pi=7^+$ ground state.

1 See R. A. Emigh and R. E. Anderson, Nucl. Phys. A293 (1977) 379 for a complete list of references.
2 S. I. Hayakawa et al., Nucl. Phys. A277 (1977) 337.
3 M. R. McPherson and F. Gabbard, Phys. Rev. C 7 (1973) 2097.
4 M. S. Zisman and B. G. Harvey, Phys. Rev. C 5 (1972) 1031.
5 D. E. Miracle, Ph.D. thesis, Univ. of KY, (1977); private communication.
6 F. E. Bertrand and D. J. Horen, Nucl. Data Sheets B7 (1972) 1.
7 R. E. Anderson et al., Nucl. Phys. A242 (1975) 75.
8 P. D. Kunz, the program DWUCK4, private communication.
9 F. D. Becchetti et al., Nucl. Phys. A190 (1972) 437.
10 J. Childs and W. W. Daehnick, Bull. Am. Phys. Soc. 20 (1975) 626.
11 R. Ceasareo et al., Z. Physik 205 (1967) 174.
12 G. Doukellis et al., Nucl. Phys. A229 (1974) 47.
13 B. D. Kern et al., to be published.
14 G. Ch. Madueme and K. Arita, Nucl. Phys. A297 (1978) 347.
15 M. Bini et al., Nuovo Cim. 35A (1976) 69.

iv. The $^{91}Zr(^{3}He,d)^{92}Nb$ Reaction - R. E. Anderson, R. A. Emigh, L. E. Samuelson, S. Shastry (State Univ. of New York, Plattsburgh), and P. A. Smith

The nucleus ^{92}Nb has been extensively studied[1] since it has one proton and one neutron outside of the approximate closed core at ^{90}Zr. Effective interaction matrix elements have been obtained from ^{92}Nb for the $(\pi 1g_{9/2} \otimes \nu 2d_{5/2})_{2^+-7^+}$ and $(\pi 2p_{1/2} \otimes \nu 2d_{5/2})_{2^-,3^-}$ multiplets. In spite of the considerable information available on ^{92}Nb, the previous $^{91}Zr(^{3}He,d)^{92}Nb$ reaction results[2] are concerned primarily with levels below 500 keV excitation. Only peaks with $\ell=1$ strength are identified above 500 keV although our work indicates that some of these levels are due to the ^{90}Zr and ^{92}Zr contaminants in the target. Nonetheless, it is hoped that a thorough study of the $(^{3}He,d)$ reaction in conjunction with other available data will help with the interpretation of the $^{90}Zr(\alpha,d)^{92}Nb$ reaction data presently being analyzed at this laboratory.[3]

The $^{91}Zr(^{3}He,d)^{92}Nb$ reaction was studied using a 33.6 MeV $^{3}He^{++}$ beam extracted from the University of Colorado cyclotron. Due to the 5.0% ^{90}Zr and 3.3% ^{92}Zr contamination of the 90.9% ^{91}Zr target, the $^{90}Zr(^{3}He,d)^{91}Nb$ and $^{92}Zr(^{3}He,d)^{93}Nb$ reactions were also observed. The outgoing deuterons were momentum analyzed and detected using the energy-loss spectrometer system. Self-supporting rolled targets were used.

Deuteron spectra were obtained at angles from 2.5° to 35.0° in 2.5° steps and for 35.0° to 60° in 5.0° steps with a typical energy resolution of 35 keV (FWHM). Energy calibration of the levels of ^{92}Nb was obtained using the ^{91}Nb and ^{93}Nb contaminants and the known levels of ^{92}Nb. A typical deuteron spectrum of ^{92}Nb is shown in Fig. A1-a13 with some of the contaminants identified. A complete analysis of this experiment is in progress and the final results will be submitted for publication.

---

[1] A. C. Kocher and D. J. Horen, Nucl. Data Sheets B 7 (1972) 299.
[2] M. R. Cates et al., Phys. Rev. 187 (1969) 1682.
[3] Presented elsewhere in this Technical Progress Report.

v. Single Proton Stripping to ^{100}Ru - R. A. Emigh, R. J. Peterson and R. E. Anderson

The $^{99}Tc(^{3}He,d)^{100}Ru$ reaction has been studied at 33.4 MeV to examine the single particle aspects of the vibrational levels of ^{100}Ru. These results are correlated with the neutron pickup results presented next in this report. A typical spectrum is shown in Fig. A1-a14.

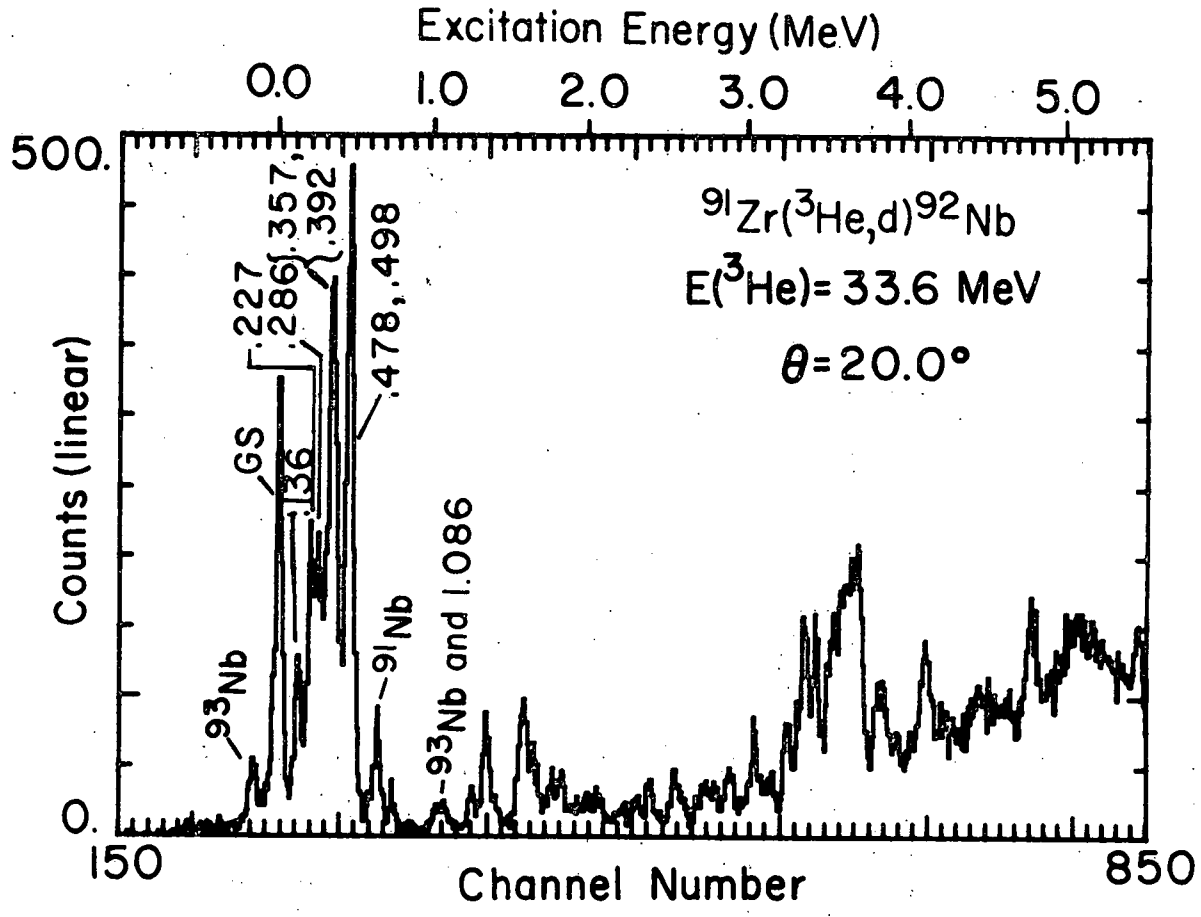

Fig. A1-a13. A deuteron spectrum obtained at 20° from 33.6 MeV ^{3}He on a ^{91}Zr target.

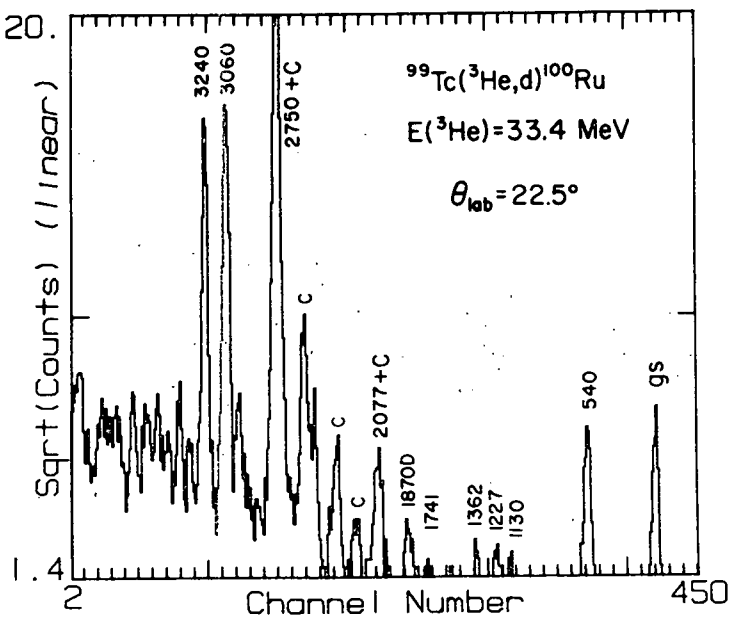

Fig. A1-a14. Sample spectrum of the ^{99}Tc(^{3}He,d)^{100}Ru reaction. Peaks from contaminants are labelled C.

Angular distributions for the first five levels are shown in Fig. A1-a15. The 0^+ states (ground state and 1130 keV) must have ℓ=4 stripping patterns as observed. Mixtures of ℓ transfers to the 2^+ and 4^+ levels are allowed, but not necessary for the fits. This is also found for the (p,d) results.

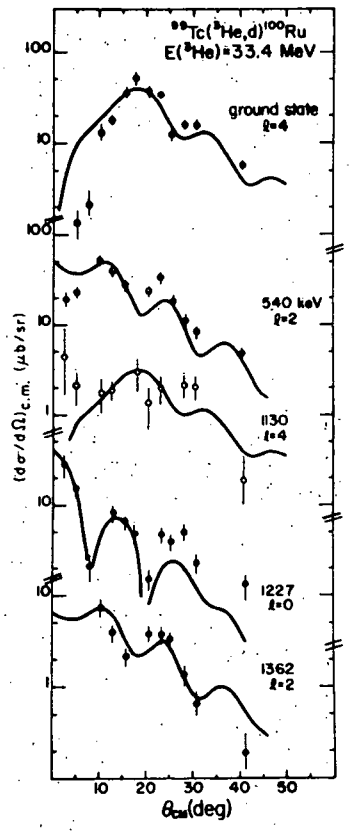

Fig. A1-a15. DWBA calculations for single values of the orbital angular momentum transfer are compared to (^{3}He,d) stripping data to the ground state, one phonon state, and two phonon triplet of ^{100}Ru. Values of ℓ=0, 2 and 4 are allowed for the 1227 keV 4^+ state, but only ℓ=0 is called for by the data.

The shell model with good seniority predicts the cross sections to the $(g_{9/2})^4$ states of seniority zero and two. These are compared to the results of the present work in Table A1-aIII. Very poor agreement is found, and several strong ℓ=4 transitions are found to states other than the known 6^+ and 8^+ levels. The lowest 2^+ and 4^+ states are not even populated by ℓ=4 stripping patterns. A very large discrepancy is found from the simple shell model so successful for ^{99}Tc.[1]

[1] R. J. Peterson, R. A. Emigh and R. E. Anderson, Nucl. Phys. A290 (1977) 155.

Table Al-aIII

Spectroscopic factors predicted by the shell model with good seniority are compared to those observed in the $^{99}Tc(^{3}He,d)^{100}Ru$ reaction.

	Excitation Energy keV	$(2J_f+1)\ C^2S$ Calculated	$(2J_f+1)\ C^2S$ Observed
$J^\pi = 0^+$	0	0.37	0.20
2^+	0.540	0.70	--
4^+	1.227	1.25	--
6^+	2.078	1.81	0.12
8^+	3.062	2.37	1.40

vi. Single Neutron Pickup to ^{100}Ru - R. J. Peterson, R. A. Emigh and R. E. Anderson

The $^{101}Ru(p,d)^{100}Ru$ reaction at 22.9 MeV was studied to examine the single-hole facets of a collective doubly even nucleus. A spectrum showing low-lying levels is given in Fig. Al-al6. These results will be combined with the $^{99}Tc(^{3}He,d)^{100}Ru$ results reported in the previous section of this report.

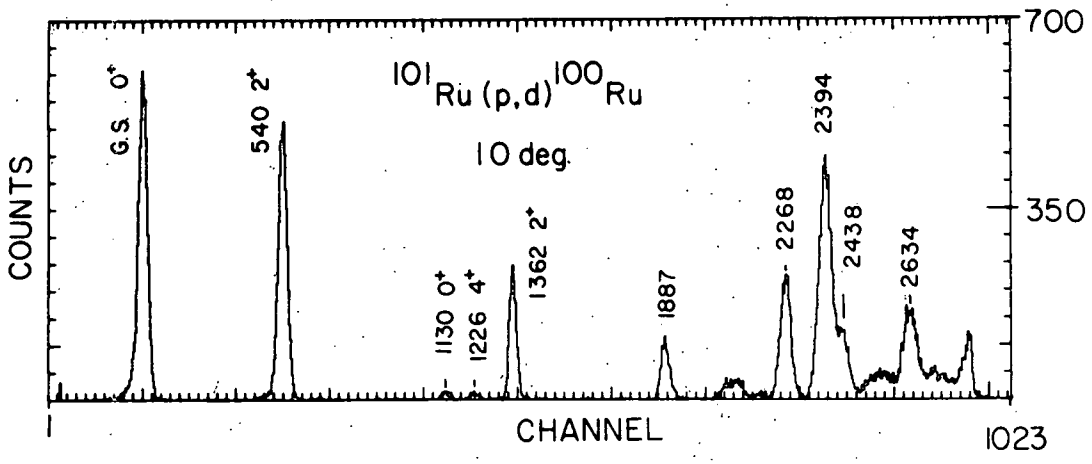

Fig. Al-al6. Sample spectrum of the $^{101}Ru(p,d)^{100}Ru$ reaction at 22.9 MeV.

Angular distributions to the ground state, single phonon state and two phonon triplet are shown in Fig. Al-al7. Although mixtures of ℓ transfers to the 2^+ and 4^+ states are allowed, these are not needed. The ground state and single phonon state are equally strong,

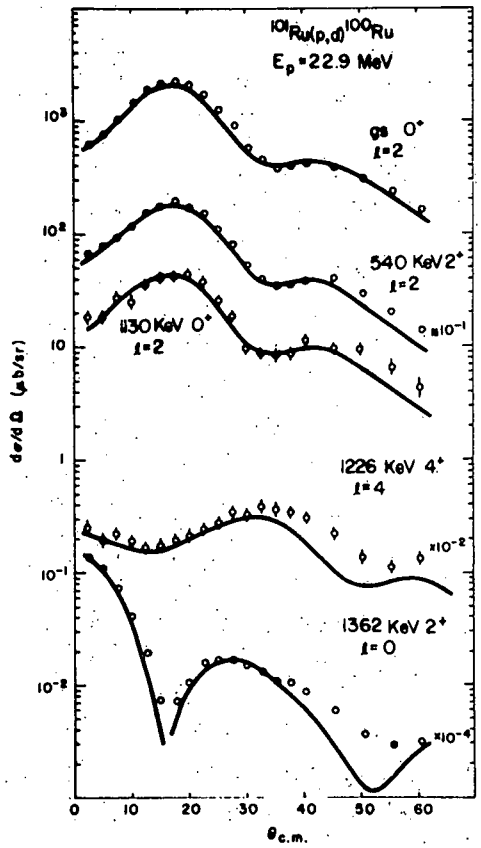

Fig. A1-a17. Angular distributions for the first five levels of ^{100}Ru as seen in the (p,d) reaction at 22.9 MeV are compared to DWBA predictions. Note the strong difference in shape for the two 2^+ states.

while the two phonon states are weaker. The excellent ℓ=4 fit to the 4^+ state and the fine ℓ=0 fit to the 2^+ two phonon state are striking, but not presently understood. States which by their energies and spins might be ascribed to a three phonon structure are more weakly excited. Angular distributions to many states as high as 3.8 MeV are also completly analyzed, but the summed spectroscopic factors for ℓ=0, 2 and 4 are far below the allowed sum rule strength. Only a weak, non-stripping pattern is noted for the collective octupole state at 2.194 MeV.

A microscopic collective model calculation correctly predicts the spectroscopic factor to the first 2^+ state. The 2.394 MeV 0^+ state is very strongly excited, but the (p,t) and (t,p) experiments to this level have not been performed and we are not able to compare our results to the pairing vibration picture.

vii. Neutron Hole States in ^{204}Tl - P. A. Smith, R. A. Emigh, R. J. Peterson and R. E. Anderson

Neutron hole states of ^{204}Tl have been populated by the (p,d) reaction at 26.1 MeV on the $1/2^+$ ground state of ^{205}Tl. The energy resolution was as good as 7 keV (FWHM) at the center of the focal plane. The sample spectrum shown as Fig. A1-a18 indicates the complexity of the results, a result which is not observed for the (p,d) reaction on ^{206}Pb.[1] Given the $1/2^+$ target spin, the ^{205}Tl spectrum would be only doubled if a weak-coupling picture were valid.

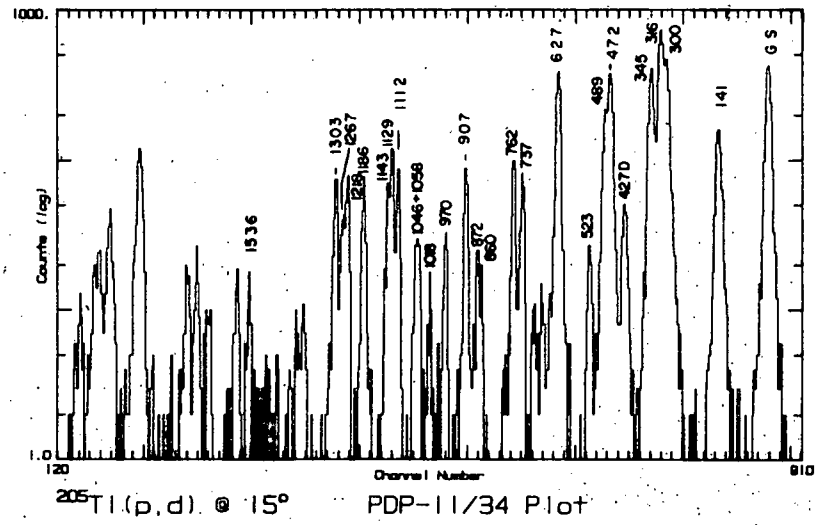

Fig. A1-a18. A spectrum from the ^{205}Tl(p,d)^{204}Tl reaction at 26.1 MeV. Excitation energies are labelled in keV. Most of the strength noted at low excitations is due to ℓ=1 pickup.

In fact, nearly the maximum number of ℓ=1 and ℓ=3 final states allowed for nucleon orbitals above N=82 are found. Very little information on the levels of ^{204}Tl is known,[2] but tight limits on the final spins are established by the present work.

The ℓ=6 neutron pickup proceeds mainly to two final states. The spectroscopic factor to the known 7^+ isomer at 1118 keV is 5.7, while a state at 1303 keV has a spectroscopic factor of 4.9. This is almost certainly the 6^+ state completing the $(\pi s_{1/2}^{-1} \otimes \nu i_{13/2}^{-3})$ doublet. The angular distributions are shown as Fig. A1-a19. The observed splitting of these two states and the purity of the configuration shown by the large spectroscopic factor allow the matrix element for the $(\pi s_{1/2}^{-1} \otimes \nu i_{13/2}^{-1})$ residual interaction to be determined. This will not be possible for the heavily mixed ℓ=1 and ℓ=3 states.

Data for states up to 3 MeV in excitation have been analyzed, and this work is being prepared for publication.

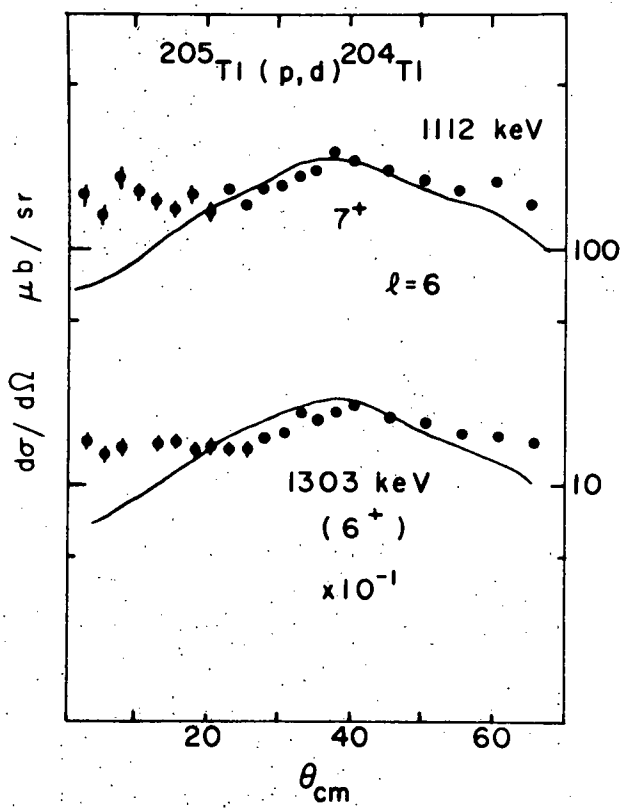

Fig. A1-a19. Angular distributions for two prominent $\ell=6$ ($i_{13/2}$) pick-ups are compared to DWBA calculations. The 1112 keV state corresponds to the known 7^+ isomer, and the other state is the 6^+ member of the $s_{1/2}^{-1}\, i_{13/2}^{-1}$ configuration, based on ^{206}Pb.

[1] W. A. Lanford, Phys. Rev. C 11 (1975) 815.
[2] M. J. Martin, Nucl. Data Sheets B5 (1971) 601.

viii. A Study of the ^{115}In(p,d)^{114}In Reaction - R. A. Emigh, R. E. Anderson and L. E. Samuelson

An investigation of the odd-odd nucleus ^{114}In has been undertaken to study the residual nucleon-nucleon interaction. The proton structure of the ground state of the odd mass indium isotopes is predominantly $\pi 1g_{9/2}^{-1}$. Since the five active neutron orbitals ($3s_{1/2}$, $2d_{3/2}$, $2d_{5/2}$, $1g_{7/2}$, $1h_{11/2}$) in this region are superconducting, one would expect that the main single particle strength would reside in five multiplets. The members of the $(\pi 1g_{9/2}^{-1} \otimes \nu 1h_{11/2})$ multiplet should be relatively pure since it should be the only low-lying negative parity configuration. The positive parity configurations can mix although it is hoped that such mixing is small, allowing for the identification of the members of the various multiplets.

A 27.3 MeV proton beam was used to bombard a 75 μgm/cm^2 thick target of natural ^{115}In evaporated onto a 20 μgm/cm^2 carbon foil. The Colorado energy-loss spectrometer system and helical cathode chamber were used to detect the deuterons. Data were obtained at

twenty-three angles between 2.5° and 60.0° with beam currents of about 1.2 μA. A typical spectrum with 15 keV resolution (FWHM) is shown in Fig. A1-a20. The energy calibration of the ^{114}In spectrum was obtained from the calibration reactions ^{64}Ni(p,d)^{63}Ni and ^{93}Nb(p,d)^{92}Nb at a number of different scattering angles.

Preliminary analysis of the data indicates that almost all of the ℓ=0 strength is located in the levels at 190 keV and 220 keV. Consequently, the $(\pi 1g_{9/2}^{-1} \otimes \nu 3s_{1/2})$ configuration appears to be quite pure. The $J^\pi=1^+$ ground state is populated by a pure ℓ=4 shape as expected. The level at 288 keV excitation, which has $J^\pi=(2,3)^+$, appears to be populated primarily by an ℓ=4 transfer although ℓ=2 transfer is allowed. Consequently, initial indications are that the ^{115}In nucleus may not have as much configuration mixing as other odd-odd nuclei studied in this region. A complete analysis of these data should be finished soon.

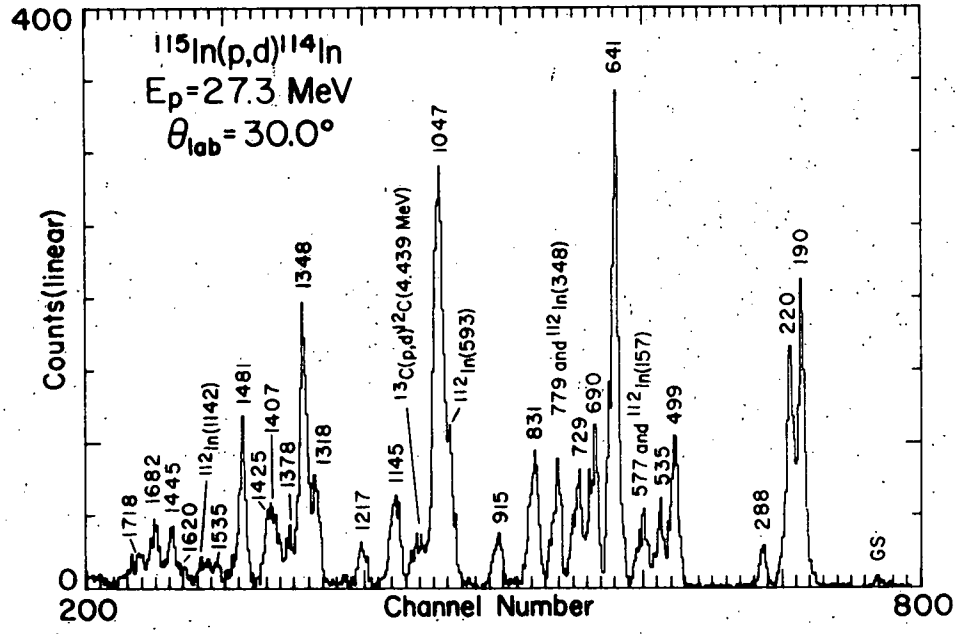

Fig. A1-a20. A spectrum taken at 30.0° for the ^{115}In(p,d)^{114}In spectrum. Peaks from the ^{113}In target contamination are identified. Energies are given in keV.

ix. The (^{3}He,α) Reaction on ^{7}Li, ^{13}C and ^{28}Si - G. R. Smith, N. J. DiGiacomo, J. R. Shepard and R. J. Peterson

In an effort to study neutron pickup at high momentum transfers, the (^{3}He,α) reaction has been performed on targets of ^{7}Li, ^{13}C and ^{28}Si. The bombarding energy was 43 MeV. Since solid state detectors were employed, a broad region of excitation was

covered, from 35 MeV at small angles (10^{o}) to about 10 MeV at the largest angles (140^{o}). The resolution was typically 150 to 250 keV, determined primarily by kinematic broadening. Through the use of an Ortec particle identifier, data were taken simultaneously on the reactions (^{3}He,α), (^{3}He,^{3}He), (^{3}He,t) and (^{3}He,d).

The purpose of taking the (^{3}He,α) data was to compare it to 800 MeV (p,d) data recently taken at HRS at LAMPF. It is part of a comprehensive study of neutron pickup at large momentum transfers being undertaken by this laboratory. The third member of this comparison is the (π^{+},p) reaction which is to be carried out soon at EPICS at LAMPF.

Typical spectra are shown in Figs. A1-a21, A1-a22 and A1-a23 for the three targets. The main difference between ^{7}Li(p,d) and ^{7}Li(^{3}He,α) is the relative strength of the first three states. In 800 MeV (p,d) the 3.56 MeV 0^{+} state is not seen, and the 2.18 MeV 2^{+} state has about 10 times the cross section of the ground state. For (^{3}He,α) the two states are populated with nearly equal strength. For the ^{13}C target, one sees about the same relative intensities for the two reactions until 16.1 MeV of excitation, beyond which the 800 MeV (p,d) reaction strongly populates high-lying levels which are not seen in (^{3}He,α). The ^{28}Si spectrum shows an absence of strongly populated clusters

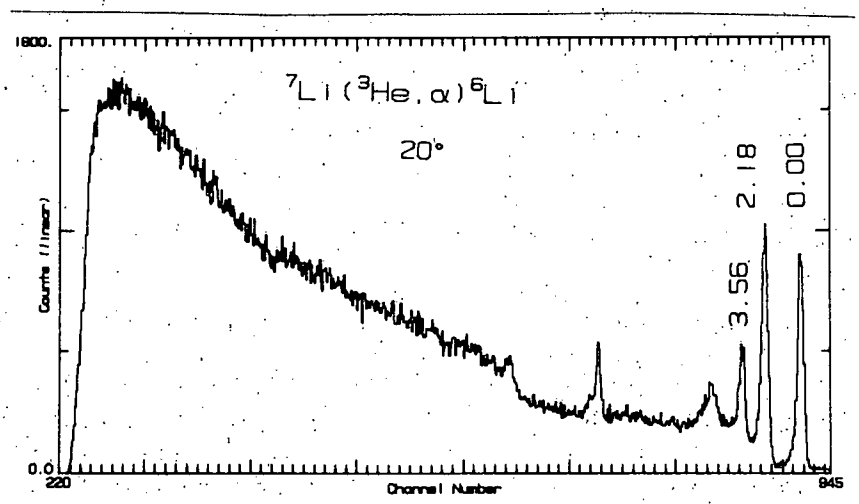

Fig. A1-21. A typical spectrum of the ^{7}Li(^{3}He,α)^{6}Li reaction.

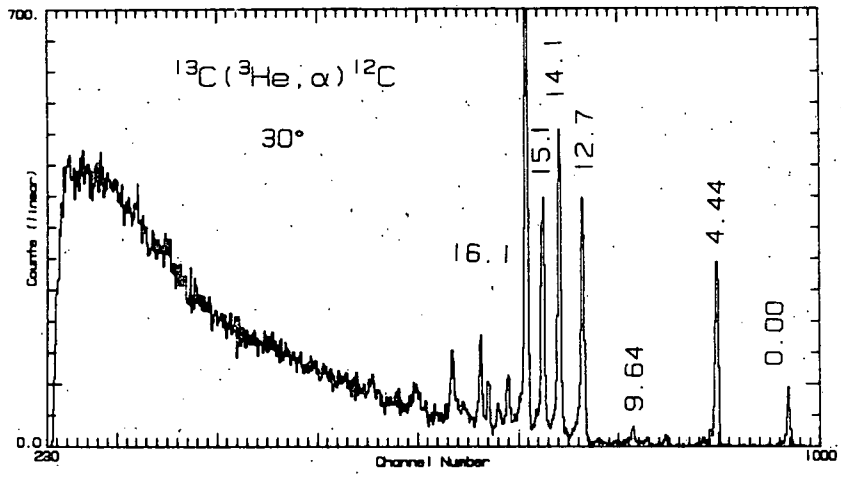

Fig. A1-a22. A typical spectrum for the $^{13}C(^{3}He,\alpha)^{12}C$ reaction.

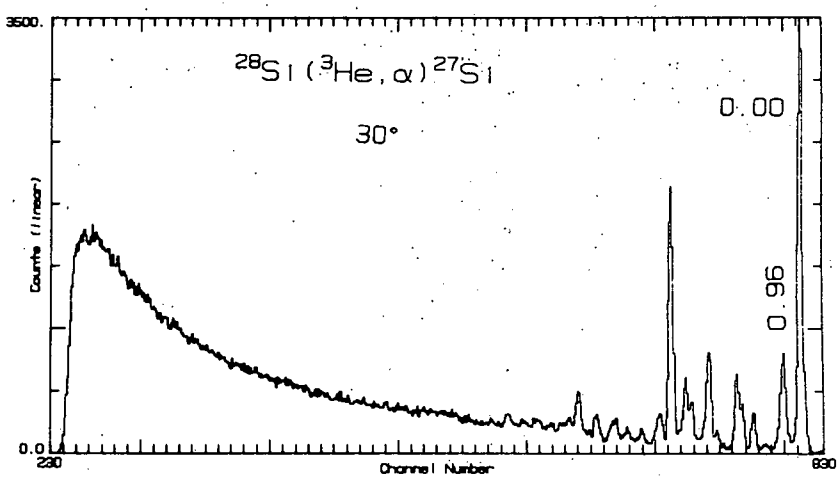

Fig. A1-a23. A typical spectrum for the $^{28}Si(^{3}He,\alpha)^{27}Si$ reaction.

of states seen at high excitation in all the even A targets used in (p,d). We also looked at $^{12}C(^{3}He,\alpha)$ and saw no such structure, although in 800 MeV (p,d) they are very prominent at ∿13.5 MeV excitation. Reference may also be made to the figures in sect. II-B-16 of this report.

Angular distributions are currently being generated for all three targets, and DWBA and CCBA calculations will be performed.

b. Two Nucleon Transfer Reactions

i. The $^{110}Cd(\alpha,d)^{112}In$ Reaction - L. E. Samuelson, R. E. Anderson, R. A. Emigh and P. A. Smith

The members of the $\pi 1g_{9/2} \otimes \nu 1h_{11/2}$ multiplet are quite elusive experimentally for a number of reasons. The $\pi 1g_{9/2}$ orbital is effectively closed at Z=50, restricting few nucleon transfer studies to elements with $40 \lesssim Z \lesssim 50$. Multiplet members are located high in excitation in elements with proton number at the low end of this range. Consequently, multiplet members cannot be securely identified due to little single-particle strength in them and a high level density. With increasing Z, the pairing force manifests itself by the lack of $J^\pi = 9/2^+$ ground states in most stable odd mass-odd proton nuclei. Also, no $J^\pi = 1/2^-$ odd mass-odd neutron nuclei exist in this region. Single-particle transfer cannot, therefore, populate members of the $\pi 1g_{9/2} \otimes \nu 1h_{11/2}$ except through configuration mixing, a highly unsatisfactory method. Two important exceptions are the ground states of ^{113}In and ^{115}In, which have a predominantly $\pi 1g_{9/2}^{-1}$ proton configuration. The level structure of $^{112,114,116}In$ can therefore be investigated via neutron pickup and for stripping reactions. The $^{113,115}In(p,d)^{112,114}In$ reactions are discussed elsewhere in this report. Unfortunately, single-particle reactions have no J-dependence, only a 2J+1 intensity rule which can be negated by seniority and configuration mixing. It should be noted that the γ-ray studies of odd-odd nuclei in this region are beset with problems, due primarily to the many low-lying high spin isomeric states. For example, the presently available spin assignments from γ-ray studies of ^{112}In are dubious at best due to the presence of two closely separated levels, one of which is isomeric (see the discussion of the level structured ^{112}In elsewhere in this report).

The present study of ^{112}In via the (α,d) reaction was done in hopes of identifying members of the $(\pi 1g_{9/2}^{-1} \otimes \nu 1h_{11/2}^{-1})$ and $(\pi 1g_{9/2}^{-1} \otimes \nu 2d_{5/2}^{-1})$ multiplets and the spin-parities of the isomeric states. A beam of 35.6 MeV $^4He^{++}$ particles was used to bombard a 200 $\mu gm/cm^2$ isotopically enriched ^{110}Cd target. The deuterons were analyzed by the Colorado energy-loss spectrometer. A sample spectrum is shown in Fig. A1-b1. The energies of the levels were obtained from the calibration reaction $^{90}Zr(\alpha,d)^{92}Nb$ and identified light contaminants in the ^{110}Cd target. Angular distributions were taken in 5.0^o steps from 5.0^o to 60.0^o. The relative normalization of the data was accomplished by use of a Faraday cup and solid state monitor counter.

Further analysis of this data is in progress, including cluster DWBA calculations. We are planning to study other In isotopes with the (α,d) reaction in the near future.

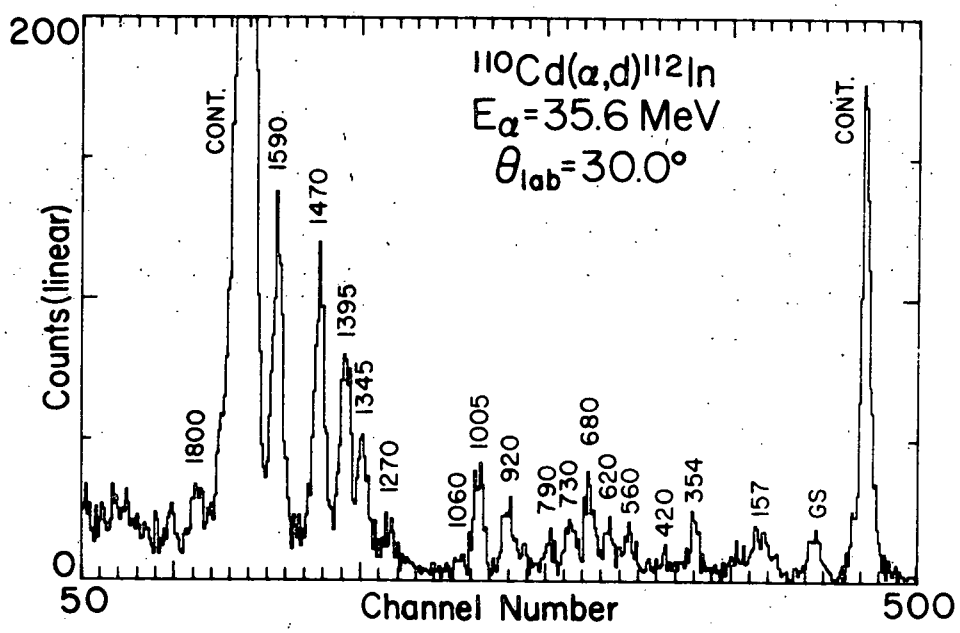

Fig. A1-b1. A typical spectrum of the $^{110}Cd(\alpha,d)^{112}In$ reaction at 30°. Two light mass contaminants are marked.

ii. A Study of Levels in ^{92}Nb Populated via the Direct (α,d) Reaction - R. E. Anderson, R. A. Emigh, L. E. Samuelson and P. A. Smith

The $^{90}Zr(\alpha,d)^{92}Nb$ reaction has been investigated with a view towards studying high spin states in nuclei in the $90 \leq A \leq 120$ mass region. We use the known selectivity of the (α,d) reaction to populate states with $j_n+j_p=L+1$. A study of ^{92}Nb was performed because the members of the $\pi 1g_{9/2} \otimes \nu 2d_{5/2}$ and $\pi 1p_{1/2} \otimes \nu 2d_{5/2}$ multiplets are well known.[1] We have tried to fit the data for the known transitions using a cluster DWBA calculation incorporating well-matched optical model potentials. If the known transitions are fit well, then it is hoped that levels with unknown parentage can be investigated with this reaction in conjunction with DWBA calculations. Furthermore, we hope to be able to extend the knowledge gained from the $^{90}Zr(\alpha,d)^{92}Nb$ reaction studies to other nuclei in this mass region. A previous $^{90}Zr(\alpha,d)^{92}Nb$ reaction[2] study suffers from worse resolution and no attempts were made to fit the data with DWBA calculations.

A beam of 35.6 MeV $^4He^{++}$ particles produced by the University of Colorado AVF cyclotron was used to bombard a self-supporting 330 μgm/cm^2 target of ^{90}Zr. The deuterons were analyzed by the Colorado energy-loss spectrometer system. A helical cathode proportional counter was used to detect the deuterons. A sample spectrum is shown in Fig. A1-b2. Angular distributions were taken in 5.0° steps from 5.0° to 60.0°. The data were normalized to the charge collected in the Faraday cup except for the 5.0° point which

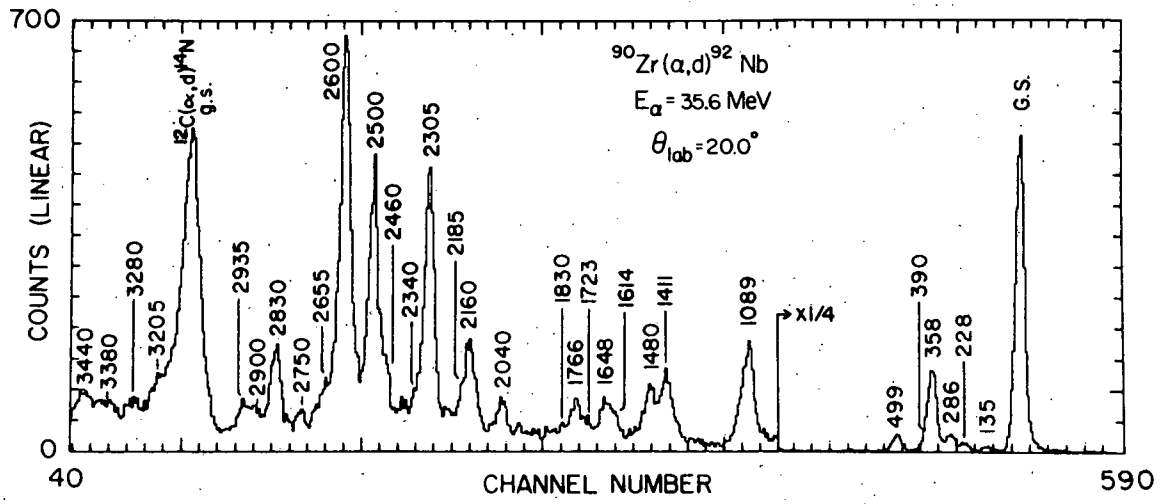

Fig. A1-b2. A sample spectrum of the $^{90}Zr(\alpha,d)^{92}Nb$ reaction at E_α =35.6 MeV.

was normalized by a comparison of elastic scattering and elastic cross sections derived from optical model parameters. This method is believed to be accurate to better than 25%.

The levels of ^{92}Nb were energy calibrated from known level energies and light contaminants in the target. The energies, which are given in Fig. A1-b2, are accurate to 15 keV or less.

We have performed DWBA calculations for the $^{90}Zr(\alpha,d)^{92}Nb$ reaction data discussed above. Since the semi-classical angular matching value for this reaction is about $6\hbar$, we expect that angular momentum transfers of $5\hbar$, $6\hbar$ and $7\hbar$ will be favored by the reaction kinematics. The calculations were performed using a dinucleon cluster form factor, taken to be the wave function of a mass-two particle bound in a Woods-Saxon well. The depth of this well was adjusted to give the proper deuteron binding energy while the number of nodes was determined by analogy to the harmonic oscillator approach. The single particle quantum numbers used in the calculation are determined by assuming that the low-lying positive states belong to the $\pi 1g_{9/2} \otimes \nu 2d_{5/2}$ multiplet and the low-lying negative parity states belong to the $\pi 2p_{1/2} \otimes \nu 2d_{5/2}$ multiplet. The $\nu 1h_{11/2}$, $\nu 1g_{9/2}$ and $\nu 3s_{1/2}$ orbitals were also used for levels above 1 MeV excitation.

Fig. A1-b3 shows the angular distributions for the low-lying levels of ^{92}Nb. In addition, the levels at 1.089 MeV and 2.600 MeV are shown. The curves are the results of the DWBA calculations using the code DWUCK4. In general, the data are very well fit by the curves. An exception is the unresolved $J^\pi=5^+,3^-$ peak. The energy calibration indicates that this is primarily the $J^\pi=5^+$ level although the DWBA calculation indicates that this should be the 3^- level. We have not yet resolved this discrepancy.

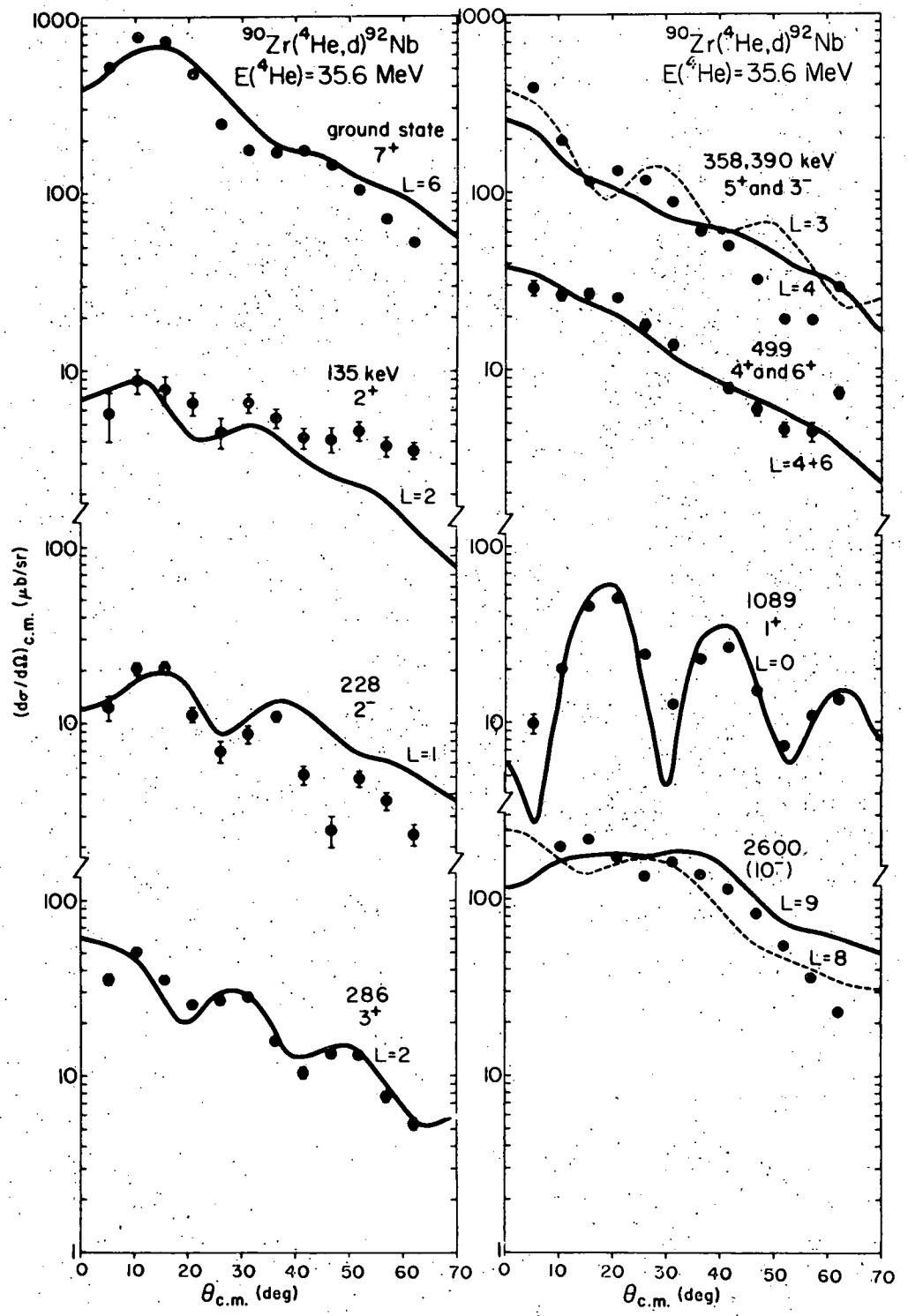

Fig. A1-b3. Angular distributions for selected levels populated by the $^{90}Zr(\alpha,d)^{92}Nb$ reaction. The curves are the results of DWBA calculations discussed in the text. Only the dominant L-transfers are shown. For example, the $J^\pi=7^+$ level can be populated by both L=6 and L=8 transitions. Since the reaction mechanism is dominant for J=L+1, only the L=6 shape is shown for this level.

The DWBA calculations imply that the 1.089 MeV level has $J^{\pi}=1^{+}$, in conflict with the results of the previous $^{91}Zr(^{3}He,d)$ reaction study,[3] which assigns negative parity to this level. We have undertaken a study of the $^{91}Zr(^{3}He,d)^{92}Nb$ reaction (see elsewhere in this report) to determine the spin-parity of this level. Unfortunately, this level is contaminated by an $\ell=1$ transition in the $^{92}Zr(^{3}He,d)^{93}Nb$ reaction so no firm assignment can be made for this level from this reaction. We were, however, able to study this level via the $^{93}Nb(p,d)^{92}Nb$ reaction at 23 MeV. The available (d,t) data make no assignments for this level.[4] In the (p,d) study the level is populated by an $\ell=4$ as shown in Fig. A1-b4. If it were of negative parity, it would most likely be populated by an $\ell=5$ transition.

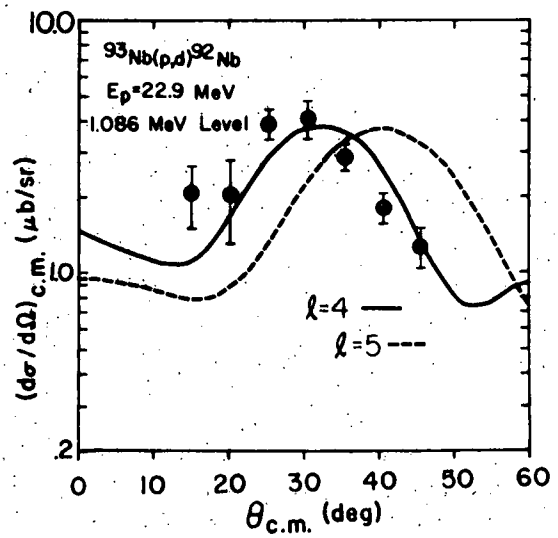

Fig. A1-b4. Angular distribution for the $^{93}Nb(p,d)^{92}Nb$ (1.086 MeV) reaction. The least restrictive spin parity for this level is 0^{+}-8^{+}.

The 2.600 MeV level is best fit by an L=9 curve although it is possible that it may also be fit by an L=8 shape. Nuclear structure factors indicate that if it is an L=8 transition to a $J^{\pi}=8^{+}$ level, then there must be another level with a larger cross section populated by an L=9 transition. As no such states are observed, we tentatively identify this level as the $J^{\pi}=10^{-}$ number of the $\pi 1g_{9/2} \otimes \nu 2d_{5/2}$ multiplet.

Further level identification and DWBA calculations are in progress.

1
2 D. C. Kocher and D. J. Horen, Nucl. Data Sheets B7 (1972) 299.
3 M. S. Zisman and B. G. Harvey, Phys. Rev. C 5 (1972) 1031.
4 M. R. Cates et al., Phys. Rev. 187 (1969) 1682.
T. S. Bhatia et al., Phys. Rev. C 3 (1971) 1361.

iii. Preliminary Investigation of the (α,d) Reaction on $^{104,106,108,110}Pd$ - R. E. Anderson, R. A. Emigh, L. E. Samuelson, P. A. Smith and D. Lingle

The investigation of some of the odd-odd silver isotopes via the (α,d) reaction is being undertaken in an attempt to locate high spin states belonging to the $\pi 1g_{9/2} \otimes \nu 1h_{11/2}$ and $\pi 1g_{9/2} \otimes \nu 2d_{5/2}$ multiplets. The (α,d) reaction, which preferentially excites levels having J=L+1, populates levels with high spins due to the large momentum mismatch. Consequently, one would hope to be able to identify the $(\pi 1g_{9/2} \otimes \nu 1h_{11/2})_{10^-,8^-,6^-}$ and the $(\pi 1g_{9/2} \otimes \nu 2d_{5/2})_{7^+,5^+}$ states. Preliminary results from the $^{90}Zr(\alpha,d)^{92}Nb$ reaction analysis indicate that we can reasonably expect to use cluster DWBA calculations as a tool for level identification along with empirical shapes.

A beam of 35.6 MeV $^4He^{++}$ particles was used. Beam currents on target varied between 4 μa and 8 μa. Target thicknesses were of the order of 200 $\mu gm/cm^2$ evaporated onto 25 $\mu gm/cm^2$ carbon. The ejectiles were momentum analyzed by the University of Colorado energy-loss spectrometer. Analysis of our data is now in progress.

iv. The $(^3He,n)$ Reaction on Tellurium Isotopes - W. P. Alford, R. E. Anderson, P. A. Batay-Csorba, R. A. Emigh, D. A. Lind, P. A. Smith and C. D. Zafiratos

One of the useful features of two-nucleon transfer is the reaction's selectivity in populating nuclear states with strong pairing correlations. This is reflected in strong L=0 transitions leading to the ground state of doubly even nuclei. Similarly, intense L=0 transitions leading to excited states serve to identify those levels with strong pairing correlations in their wave functions.

The present $Te(^3He,n)Xe$ reaction studies are an extension of previously reported measurements of the $(^3He,n)$ reaction on isotopes of Cd and Sn. The $Cd(^3He,n)$ reactions showed a strong L=0 transition to the ground state of the residual Sn nucleus and also to the expected pairing vibrational states at the closed proton shell Z=50. The $Sn(^3He,n)$ reactions might be expected to excite only the ground state L=0 transition with appreciable strength, but fairly strong transitions were observed in states near 2 MeV excitation for the heavier tin targets. This result was explained by the crossing of the $d_{5/2}$ and $g_{7/2}$ proton orbitals in this mass region.

Measurements were made using the 25.4 MeV ^3He beam from the CU cyclotron. The cyclotron was tuned for single-turn extraction, giving a time resolution of 1 nsec or less for beam currents of about 750 na. The targets, about 1 mgm/cm^2 in thickness, were prepared by evaporation of isotopically enriched tellurium onto gold backings. Angular distributions of neutrons were measured between 0^o and 22^o using the neutron time-of-flight facility.

A sample time-of-flight spectrum for each target at 0^{o} is shown in Fig. A1-b5. Excitation energies were calculated using the measured time dispersion and the location of the ground state. The measured angular distributions of the observed states are shown in Figs. A1-b6 through A1-b11. Absolute cross sections are believed to be accurate to better than 20%. The maximum cross sections in levels populated by L=0 transitions in this work are presented in Table A1-bI.

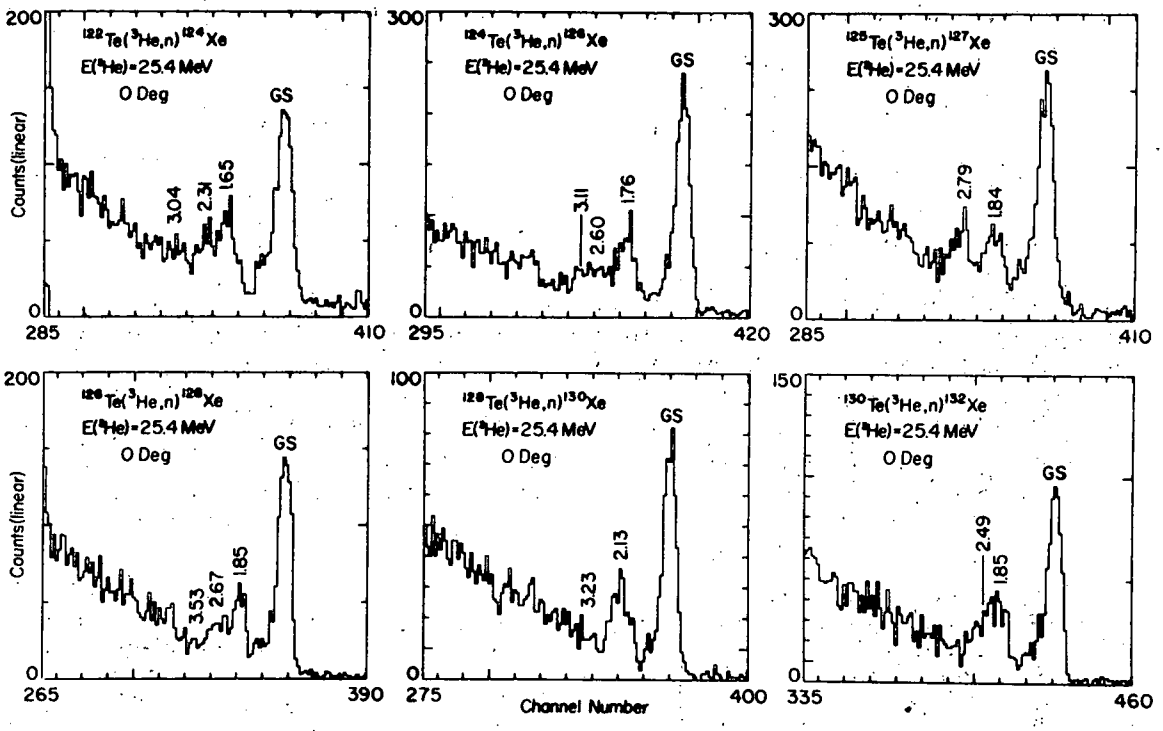

Fig. A1-b5. Neutron time-of-flight spectra for each target at 0 degrees.

For each target studied a strong L=0 transition was observed leading to a state near 2 MeV excitation in the residual nucleus. This is similar to the results found for the heavier Sn targets, but in the present measurements, the ratio of excited state to ground state strength is almost independent of the neutron number of the target.

Calculations are in progress to determine whether these results can be understood in terms of the known properties of the proton single-particle states in this region.

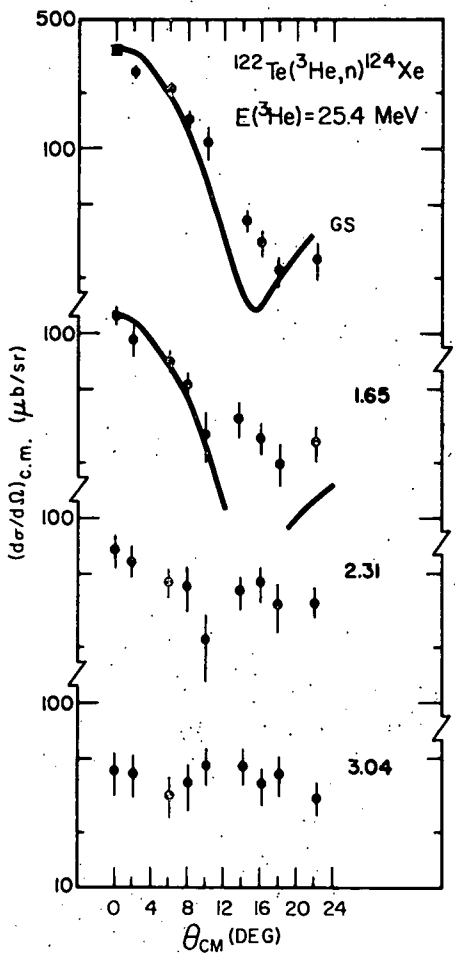

Fig. A1-b6. Angular distributions for the ^{122}Te(^{3}He,n)^{124}Xe reaction. The solid lines are DWBA predictions for L=0 transitions.

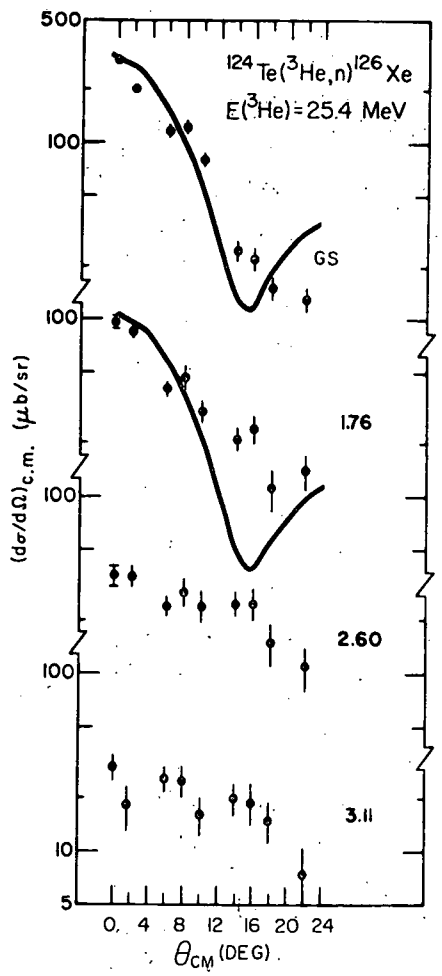

Fig. A1-b7. Angular distributions for the ^{124}Te(^{3}He,n)^{126}Xe reaction The solid lines are DWBA predictions for L=0 transitions.

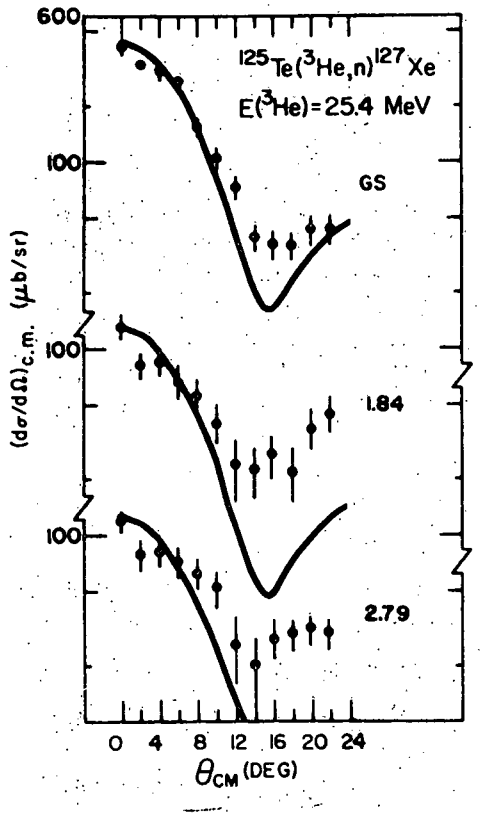

Fig. A1-b8. Angular distributions for the ^{125}Te(^{3}He,n)^{127}Xe reaction. The solid lines are DWBA predictions for L=0 transitions.

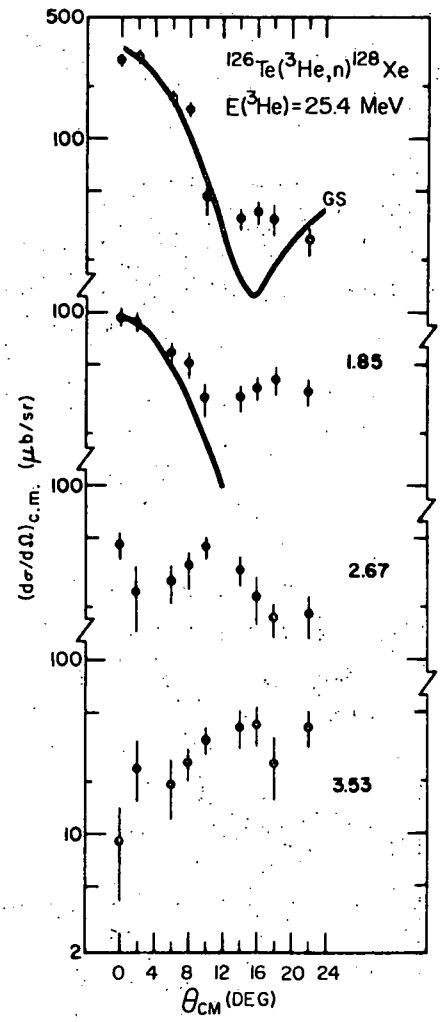

Fig. A1-b9. Angular distributions for the ^{126}Te(^{3}He,n)^{128}Xe reaction. The solid lines are DWBA predictions for L=0 transitions.

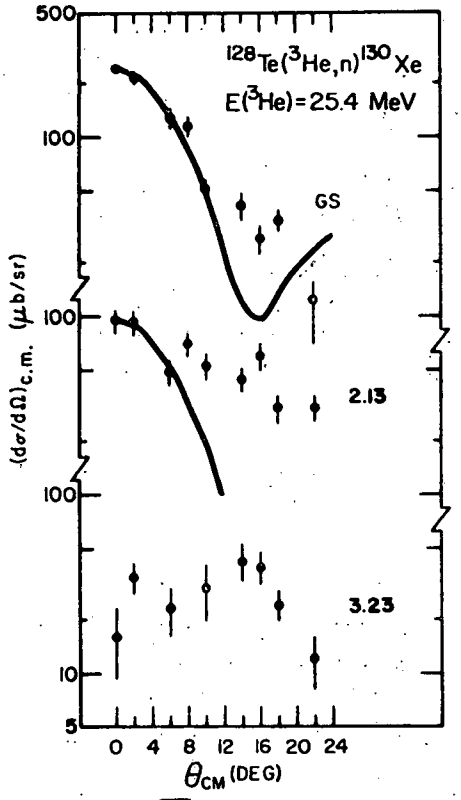

Fig. Al-b10. Angular distributions for the $^{128}Te(^{3}He,n)^{130}Xe$ reaction. The solid lines are DWBA predictions for L=0 transitions.

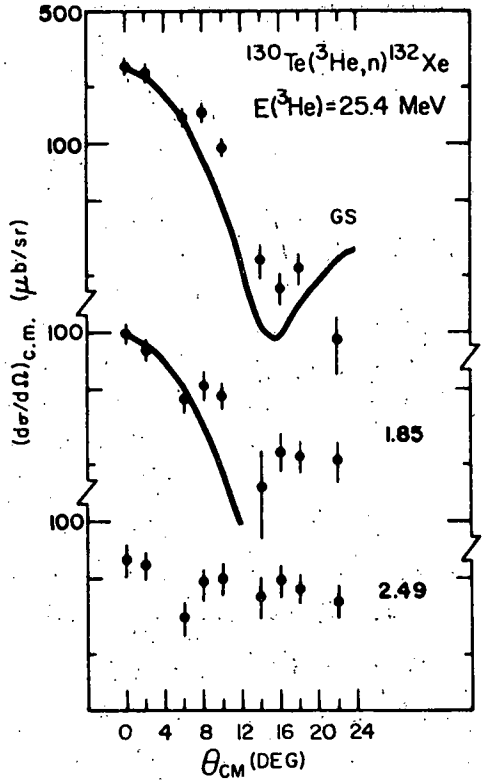

Fig. Al-b11. Angular distributions for the $^{130}Te(^{3}He,n)^{132}Xe$ reaction. The solid lines are DWBA predictions for L=0 transitions.

Table Al-bI

Comparison of experimental data on ground state and excited 0^+ state strengths

Final Nucleus	$\sigma_{g.s.}(0^o)$ (mb/sr)	$\sigma_{ex}(0^o)$ (mb/sr)	$\frac{\sigma_{ex}}{\sigma_{g.s.}}$
^{124}Xe	0.34	0.12	0.35
^{126}Xe	0.30	0.10	0.33
^{127}Xe	0.41	0.13	0.32
^{128}Xe	0.28	0.09	0.32
^{130}Xe	0.24	0.09	0.38
^{132}Xe	0.25	0.10	0.40

v. (^{3}He,n) Reaction Studies near N=82 - R. E. Anderson, P. A. Batay-Csorba, R. A. Emigh, D. A. Lind, P. A. Smith, C. D. Zafiratos, and W. P. Alford (Univ. of Western Ontario)

In addition to results presented in last year's report, measurements have been carried out for targets of ^{139}La and ^{144}Sm. For ^{139}La, a strong L=0 transition proceeds to the 0.15 MeV level in ^{141}Pr. Transitions with $L \geq 2$ are also observed to levels at 1.49, 2.28 and 3.20 MeV, but no L=0 excited state transitions are seen. For ^{144}Sm, excited state transitions are observed to levels in ^{146}Gd at 1.58 MeV (L=3), 2.09 MeV (L=0+2), 2.80 MeV (L=0(+2?) and 3.50 MeV (L=0).

DWBA calculations have been carried out with a simple $(d_{5/2})^2$ form factor ($d_{5/2}$, $h_{11/2}$ for L=3) to obtain relative strengths of all observed transitions. The ground state strengths show a smooth dependence on proton number as shown in Fig. A1-b12. Enhancement factors for all observed transitions are summarized in Table A1-bII. Model calculations are now in progress to obtain more realistic wave functions for the analysis of these results.

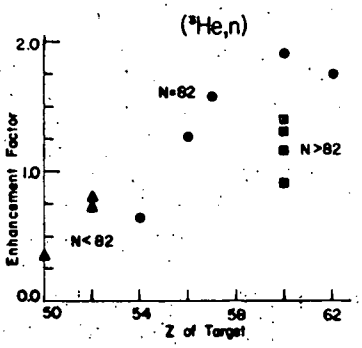

Fig. A1-b12. Enhancement factors for ground state transitions in the (^{3}He,n) reaction on targets near N=82.

These results provide the first direct measurement of the mass of the nuclide ^{146}Gd. The energy of neutrons from the ^{144}Sm(^{3}He,n)^{146}Gd (g.s.) transition was measured relative to that of the ground state transition for ^{58}Ni(^{3}He,n), yielding a value Q_o=977±30 keV. This corresponds to a ground state mass of 145.918324±.000032 amu for ^{146}Gd or a mass defect of 76.081±.030 MeV.

Table A1-bII

Summary of results for (^{3}He,n) reaction studies in the region of N=82.

Target	Final State E_x - MeV	Transfer L	Enhancement Factor
^{136}Xe	0.0	0	0.65
	1.44	2	0.24
	2.34	0+2	0.12,0.33
	2.85	2	0.37
	4.13	2	0.23
	4.86	0+2	0.06,0.22
	5.74	0	0.10
	6.28	0+ ?	0.10
	6.83	0	0.10
^{138}Ba	0.0	0	1.27
	1.91	0+2	0.15,0.41
	2.54	2	0.41
	4.15	2	0.61
	7.37	0	0.23
^{139}La	0.15	0	1.62
	1.49	2	2.0
	2.28	≥2	≥1.7 *
	3.20	≥2	≥1.8 *
^{142}Nd	0	0	1.91
	1.68	2	1.08
	2.69	2	0.76
	3.18	3	0.72
	3.91	3(?)	0.59
	4.48	0	0.34
	4.93	0	0.34
^{144}Sm	0	0	1.62
	1.58	3	0.42
	2.09	0+2	0.44,0.53
	2.80	0(+2?)	0.19
	3.50	0(+?)	0.35
^{144}Nd	0	0	1.16
	2.47	2	0.33
	3.86	0	0.12
^{146}Nd	0	0	1.42
^{148}Nd	0	0	1.31
^{150}Nd	0	0	0.84

* Spin of final state unknown.

vi. Measurement of the $(\vec{t},p)$ Reaction on ^{126}Te and ^{106}Pd - W. P. Alford and E. Sugarbaker (U. of Colorado); E. R. Flynn, D. Hanson and J. A. Cizewski (LASL)

A recent study[1] of the $(\vec{p},t)$ reaction on Te and Pd isotopes showed that the analyzing powers for the first excited 2^+ states can reflect significant sensitivity to the interference between direct and inelastic multistep processes. An investigation of the $^{126}Te(\vec{t},p)$ and $^{106}Pd(\vec{t},p)$ reactions has been initiated to search for similar effects in the $(\vec{t},p)$ reaction. The LASL polarized triton source and Van de Graaff accelerator were used to produce a 17 MeV triton beam having a polarization of typically 0.80. The reaction protons were analyzed with the LASL QDDD spectrometer and detected with a helical wire focal plane detector. Measurements have been made for both spin-up and spin-down beam configurations over an angular range of $\theta_{lab}=15^o$ to 60^o. A preliminary analysis of the 2^+ data indicates only small differences between the differential cross sections and analyzing powers observed for these two nuclei. The data reduction and analysis are currently in progress.

---

[1] K. Yagi, S. Kunori, Y. Aoki, Y. Higashi, J. Sanada and Y. Tagishi, Phys. Rev. Lett. 40 (1978) 161.

vii. Particle-Vibration Multiplets in $^{207,203}Tl$ via the (p,t) and (t,p) Reactions - R. E. Anderson, J. J. Kraushaar, R. A. Ristinen, and R. Weiss (U. of Colo.); E. R. Flynn (LASL); S. Shastry (SUNY, Plattsburgh)

Since the odd mass Tl nuclei lie close to the doubly magic ^{208}Pb nucleus, they represent excellent test cases for the various theoretical models which are available. In particular, the concept of constructing the properties and locations of energy levels of odd-A nuclei from the three elementary modes of nuclear excitation (pairing, single particle and shape excitations) and their interactions is intriguing. Calculations based on such a model have the potential to reproduce a wide variety of data and the Tl nuclei are examples of a fairly wide range of nuclear behavior. In ^{207}Tl the fundamental excitations interact only weakly and thus remain quite pure, while in ^{203}Tl the interactions are much stronger and much fragmentation results. We intend to study the (t,p) and (p,t) reactions on ^{203}Tl and ^{205}Tl, thus collecting data on the residual nuclei $^{201,203,205,207}Tl$. Data on the $^{205}Tl(t,p)^{207}Tl$ and $^{205}Tl(p,t)^{203}Tl$ reactions have been obtained thus far.

Data for the (t,p) (LASL) and (p,t) (Colorado) reactions were obtained at bombarding energies of 17.0 and 26.2 MeV, respectively, with resolutions of about 20 keV in both cases. In order to study

the core transition strengths, (t,p) data on ^{204,206}Pb were collected, as were (p,t) data on ^{208,206}Pb. The Pb data has been analyzed (only previously known levels were observed) and DWBA calculations are in progress. Enhancement factors will be obtained for these levels and for those in ^{203}Tl and ^{207}Tl.

Some preliminary calculations based on the method of Bohr and Mottelson[1] have been performed for $1/2^+$ and $3/2^+$ states in ^{203}Tl. There is a general resemblance between the data (including (t,α) spectroscopic factors and other data from the literature[2] and the calculations. This is encouraging given the complexity of this nucleus, but there still remain some discrepancies to be resolved. In particular, there appear to be more levels found experimentally than are predicted, a situation which we expect will be accentuated when calculations for the $5/2^+$ states are run.

---

[1] Bohr and Mottelson, Nuclear Structure, Vol. II, W. A. Benjamin, 1975.

[2] Nuclear Data Sheets 24 (1978) 117.

c. Three Nucleon Transfer Reactions

The three nucleon transfer reactions (α,p), (p,α) and (α,n) are effective tools for investigating many aspects of nuclear structure. Even though quantitative analysis of the reaction mechanism is quite difficult, the features of these reactions are well understood on a microscopic basis.

The following features are especially attractive:

1) The ability to measure masses and spectra of previously unknown nuclei. The (α,n) reaction, which has not been extensively reported in the literature, leads to many nuclei to the left of the stability line.

2) In many instances three nucleon transfer reactions are the only means to locate single hole or single particle states. One such case, which is currently being studied, is ^{201}Tl via the ^{204}Pb(p,α)^{201}Tl reaction. This study may extend our knowledge of the proton hole energies in the Z=82 closure.

3) Even when a nucleus has been extensively studied, the three nucleon transfer reactions can be used to locate states that are not accessible via simple reactions. The analogs of neutron hole states can be reached by the (p,α) reaction, whereas they cannot be made with the corresponding (d,^{3}He) reaction. For example, the T=5/2 proton hole states that cannot be made with the ^{42}Ca(d,^{3}He)^{41}K reaction are strongly populated by the ^{44}Ca(p,α)^{41}K reaction.

Another class of states unique to the three nucleon transfer reactions consist of those states made up of the target state plus three nucleons. The 3p-1h states of ^{42}Ca, which are discussed below, can be populated by the ^{39}K(α,p)^{42}Ca reaction. The high spin couplings of these three particle configurations are of special interest because they represent unmixed shell model wave functions.

4) The large angular momentum mismatch leads to two interesting phenomena. The first is the population of high spin states. A number of studies using this feature are discussed below where ℓ=9, 10 and 12 transitions have been observed. Secondly, because the angular momentum matching value for the (p,α) reaction decreases as the Q-value becomes more negative, deep proton hole states are kinematically favored. This is quite unlike the (d,^{3}He) reaction.

5) The angular distributions display noticeable j-dependence for ℓ=1, 2, 3 transfers. This is a dramatic effect for ℓ=1 transfers and a measurable effect for ℓ=2 and 3 transfers if the angles between 0° and 20° are studied carefully.

6) Cluster model DWBA calculations, using properly matched optical potentials, reproduce the experimental angular distribution shapes quite well.

During the last two years we have concentrated on the study of high spin states populated with the (α,p) and (p,α) reactions. Targets were chosen because of interesting nuclear structure questions that are discussed below. In order to understand the data, we have developed a systematic approach to cluster model DWBA calculations.

Quite recently we have also developed the capability of studying the (α,n) reaction.

1. The $^{40}Ca(\alpha,p)^{43}Sc$ Reaction - P. A. Smith and R. J. Peterson

The $^{40}Ca(\alpha,p)^{43}Sc$ reaction is the basis of our study of high spin states because the $15/2^-$ and $19/2^-$ states of ^{43}Sc are known states. Sample spectra showing these states are given in Fig. A1-c1.

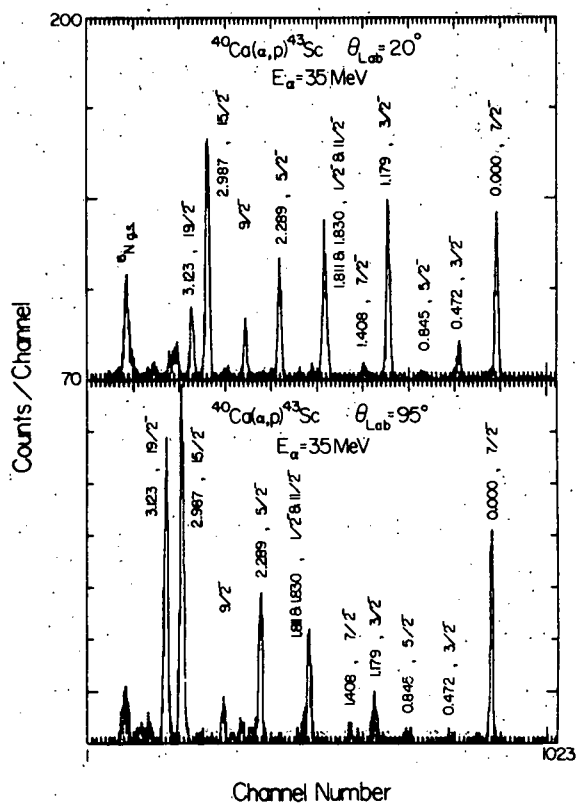

Fig. A1-c1. Spectra for the $^{40}Ca(\alpha,p)^{43}Sc$ reaction.

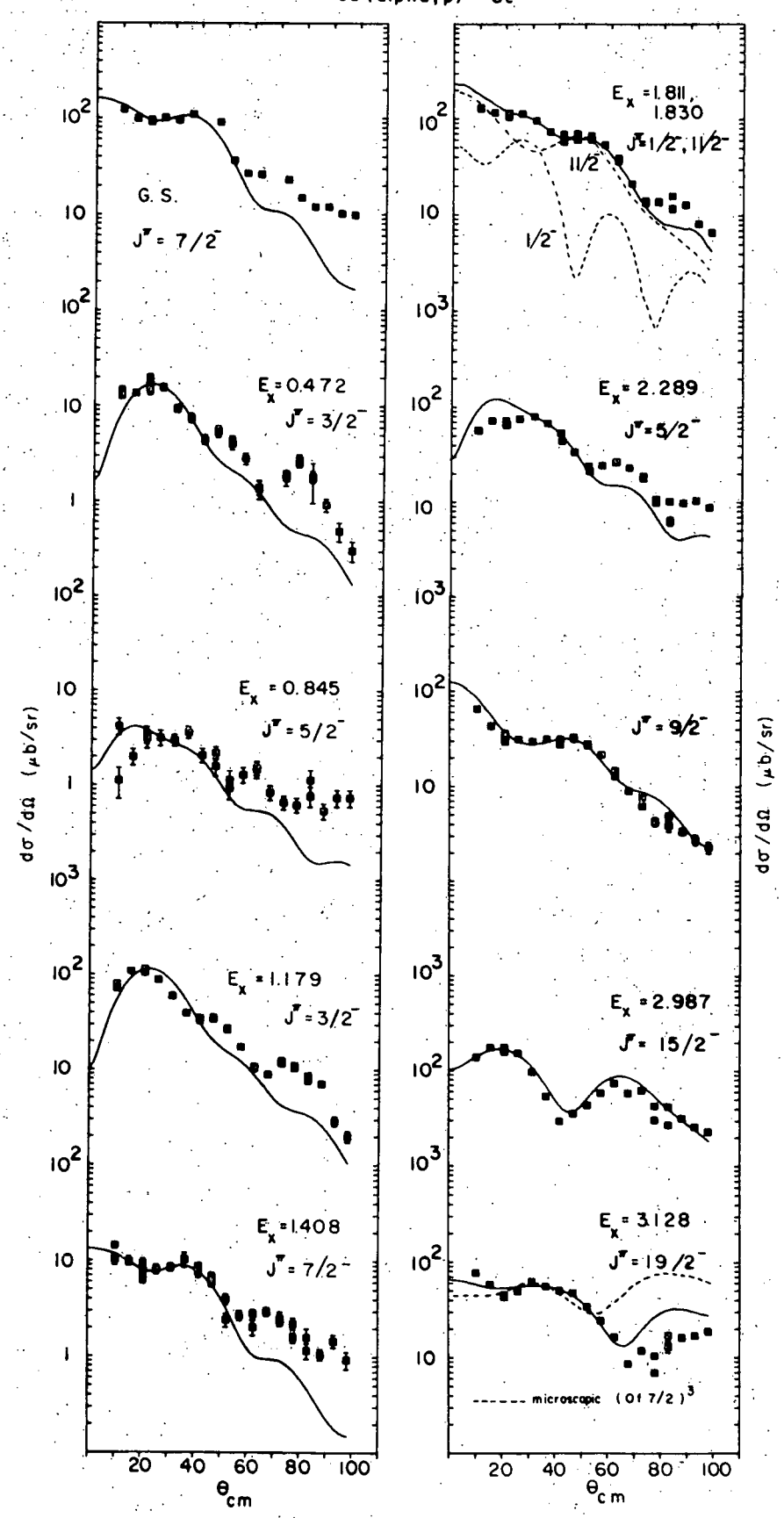

Fig. A1-c2. Angular distributions for the $(f,p)^3$ states of ^{43}Sc.

The angular distributions are given in Fig. A1-c2. Because the $15/2^-$ and $19/2^-$ assignments are unambiguous, these data provide empirical angular distributions to be used for similar assignments in neighboring nuclei. Furthermore, these data test our ability to predict large angular momentum transfers with DWBA calculations. The results of such calculations are shown as solid curves in Fig. A1-c2.

Our failure to observe either $13/2^-$ or $17/2^-$ states is in good agreement with microscopic considerations presented in a later section of this report. Semi-microscopic calculations using $(f_{7/2})^3$ wave functions for ^{43}Sc are currently in progress.

ii. The $^{39}K(\alpha,p)^{42}Ca$ Reaction - P. A. Smith, R. J. Peterson, N. J. DiGiacomo and G. R. Smith

The high spin spectrum of ^{42}Ca has been extensively studied with heavy-ion fusion-evaporation reactions. At least six γ-decay experiments have attempted to unravel this level scheme. The resulting level schemes fall into two categories that are summarized in Fig. A1-c3.

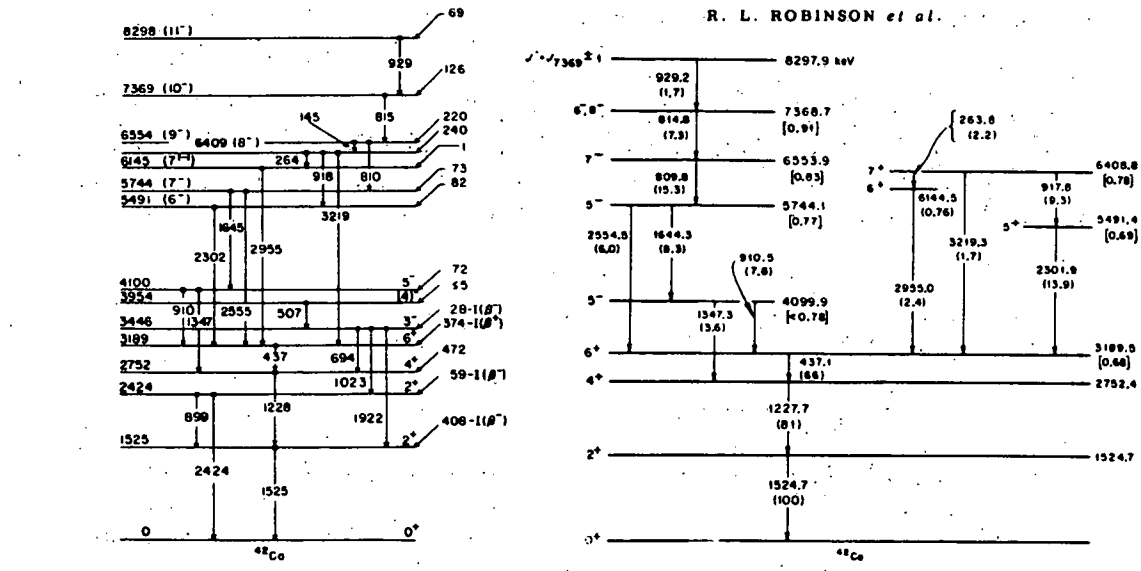

Fig. A1-c3. Proposed level schemes for the high spin states of ^{42}Ca, as taken from Refs. 1 and 2.

We have performed the $^{39}K(\alpha,p)^{42}Ca$ reaction in order to locate those states which have large $[\pi d_{3/2}^{-1}(\pi f_{7/2}\nu(f_{7/2})^2)]_{15/2}$ and $[\pi d_{3/2}^{-1}(\pi f_{7/2}\nu(f_{7/2})^2)]_{19/2}$ components. Such states will have

$6^- \leq J \leq 9^-$ and $8^- \leq j \leq 11^-$, respectively. Sample spectra are shown in Fig. A1-c4. The angular distributions for some of the high-lying states are shown in Fig. A1-c5. The solid curves are the empirical shapes obtained from the $^{40}Ca(\alpha,p)^{43}Sc$ data.

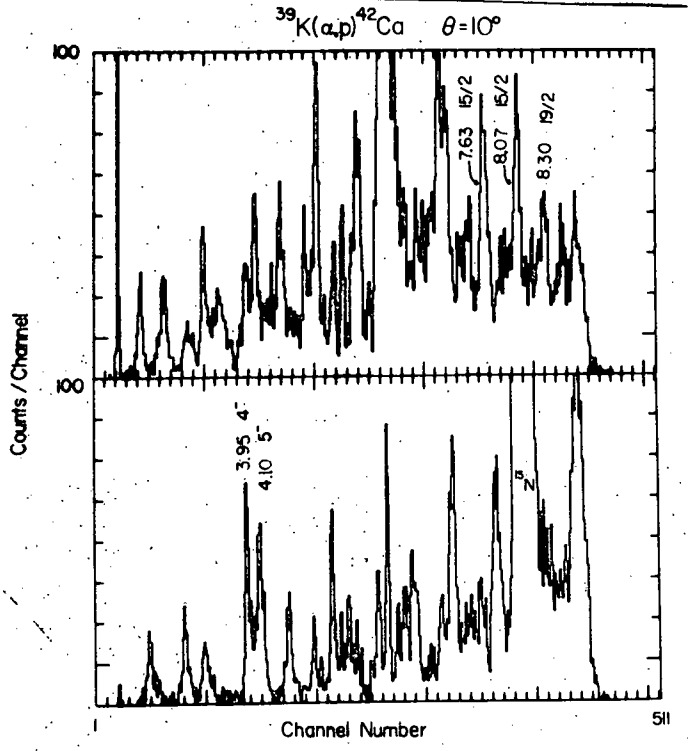

Fig. A1-c4. Spectra for the $^{39}K(\alpha,p)^{42}Ca$ reaction at E_α=35 MeV. Excitation energies are given in MeV. The 15/2 and 19/2 notation is discussed in the text.

Although the analysis of the low-lying states is not quite complete, it is clear that states which have been observed with $15/2^-$ transfers have not previously been reported in either level scheme shown in Fig. A1-c5. The one definite 19/2 transfer is consistent with both level schemes where 9^- and 11^- assignments are suggested.

This work, which has been reported at the Nuclear Physics Division meeting, is nearly completed.

---

1 E. K. Warburton, J. J. Kolata and J. W. Olness, Phys. Rev. C 11 (1975) 700.

2 R. L. Robinson, H. J. Kim, J. B. McGrory, G. J. Smith, W. T. Milner, R. O. Sayer, J. C. Wells, Jr. and J. Lin, Phys. Rev. C 13 (1976) 1922.

iii. The $^{116}Sn(\alpha,p)^{119}Sb$ Reaction - P. A. Smith, N. J. DiGiacomo, R. A. Emigh, R. J. Peterson and G. R. Smith

The high spin states of Sn and Sb nuclei that have previously been located with (^6Li,^3n) experiments are the members of a rotational band built on an excited 0^+ state in the Sn nuclei and a $9/2^+$

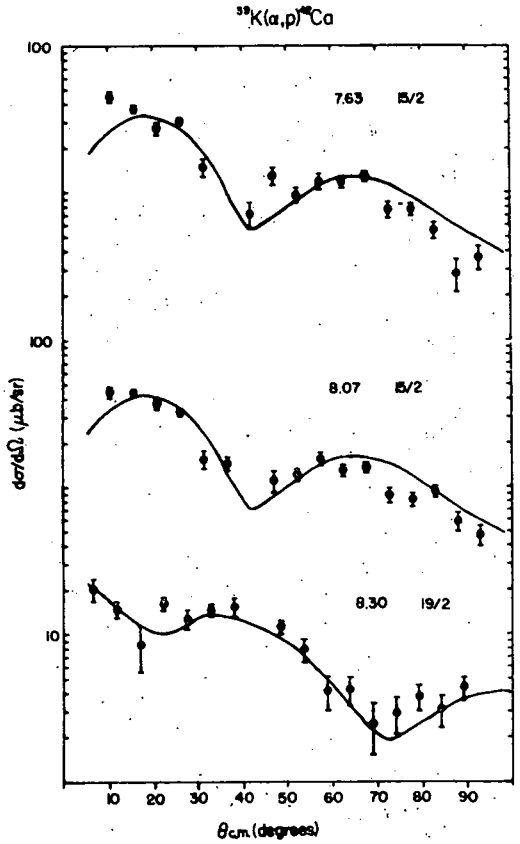

Fig. Al-c5. Angular distributions for the high-lying states of ^{42}Ca. The solid curves are the empirical shapes of the $15/2^-$ and $19/2^-$ angular distributions observed in the $^{40}Ca(\alpha,p)^{43}Sc$ reaction.

state in the Sb isotopes. These excited band heads represent deformed states of nuclei that have spherical ground states. It is likely that these nuclei have spectra that can be separated into spherical and deformed subgroups which are nearly orthogonal.

We have studied the $^{116}Sn(\alpha,p)^{119}Sb$ reaction in order to test this coexistence hypothesis. If the hypothesis is correct, the addition of three nucleons to a spherical ground state will not populate the members of the rotational band. On the other hand, we can expect to see the spherical high spin states whose wave functions are of the form $[\pi s_{1/2}(\nu h_{11/2})^2_{10}]_{19/2^+,21/2^+}$, $[\pi d_{5/2}\nu(h_{11/2})^2_{10}]_{25/2^+}$ and $[\pi g_{7/2}\nu(h_{11/2})^2_{10}]_{27/2^+}$.

The ^{116}Sn target was chosen because it was the lightest tin isotope that could be purchased cheaply with high purity. Most of the γ-ray studies have been on the light Sb isotopes, ^{119}Sb being the heaviest case that has been published.

Sample spectra are shown in Fig. Al-c6. The large states in the low excitation region are the proton particle states seen in the $^{118}Sn(^3He,d)^{119}Sb$ reaction. None of the known members of

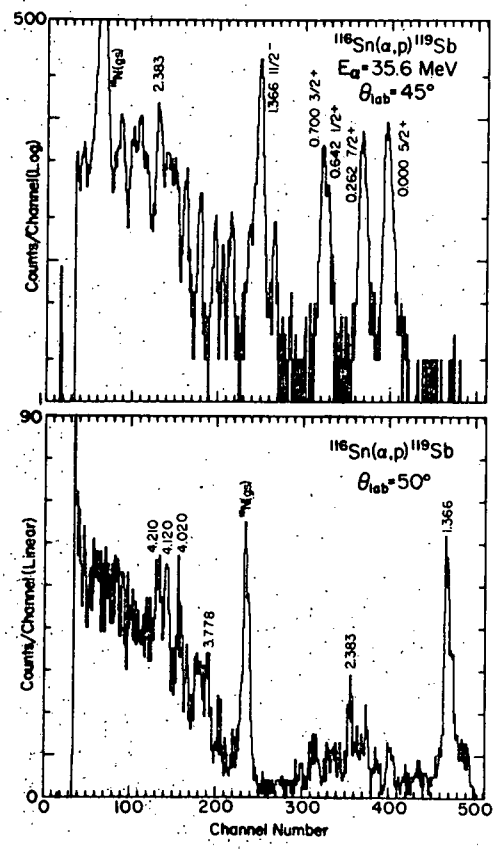

Fig. A1-c6. Spectra for the ^{116}Sn(α,p)^{119}Sb reaction.

the $9/2^+$ rotational band are present in Fig. A1-c6. Furthermore, all the angular distributions that were extracted were fit well by the empirical shapes taken from the known particle states.

Three states slightly above 4 MeV excitation energy appear in the large angle data. The angular distributions of these states are compared with DWBA calculations in Fig. A1-7. Because the background states have forward peaked angular distributions these high spin candidates are obscured at small scattering angles.

The L=9 and 11 assignments would require an $(h_{11/2})^3$ wave function, which seems unlikely, while the L=10 and 12 choices are consistent with the likely wave functions discussed above. This hypothesis is further supported by calculating the $(\pi s_{1/2} \nu h_{11/2})_{5^-,\ 6^-}$ residual interaction matrix elements using our excitation energies and the known $\nu(h_{11/2})^2_{10^+}$ state of ^{118}Sr. The resulting matrix elements are in excellent agreement with matrix element systematics if the assignments 4.120 MeV, $21/2^+$, 4.210 MeV, $19/2^+$, are made.

The energies of the rotational $19/2^+$ and $21/2^+$ states can be determined from the systematics of the lighter Sb isotopes. The expected energies are far enough below the states observed here to

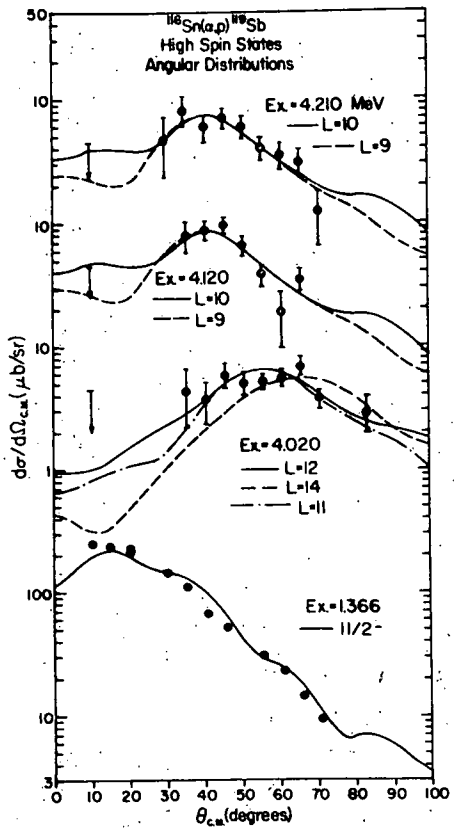

Fig. A1-c7. Angular distributions for the high spin states of ^{119}Sb. The curves are the results of DWBA calculations.

guarantee that they are not the same states.

This work has been submitted to Phys. Rev. C for publication.

iv. The ^{103}Rh(α,p)^{106}Pd Reaction - P. A. Smith, R. A. Emigh, C. R. Emigh (LASL) and L. E. Samuelson

The spectrum of ^{106}Pd displays a well developed ground state rotational band and a number of two quasi-particle states which may form band heads. The ground state rotational band backbends sharply at the 10^+ level. It is likely, however, that the yrast 10^+ is the $\nu(h_{11/2})^2_{10^+}$ quasiparticle state while another 10^+, which was only weakly populated in an earlier heavy-ion experiment used to study the band structure, is the member of the rotational sequence. The sequence is given in Fig. A1-c8.

This hypothesis can be tested with the ^{103}Rh(α,p)^{106}Pd reaction since the intrinsic 10^+ state represents the aligned $[\pi p_{1/2}\nu(h_{11/2})^2_{10}]$ transfer. We have obtained a few spectra. An unresolved set of states is observed at the proper excitation energy. Unfortunately, the 800 μg/cm^2 target limited the resolution to about 100 keV which made identification of the high-lying

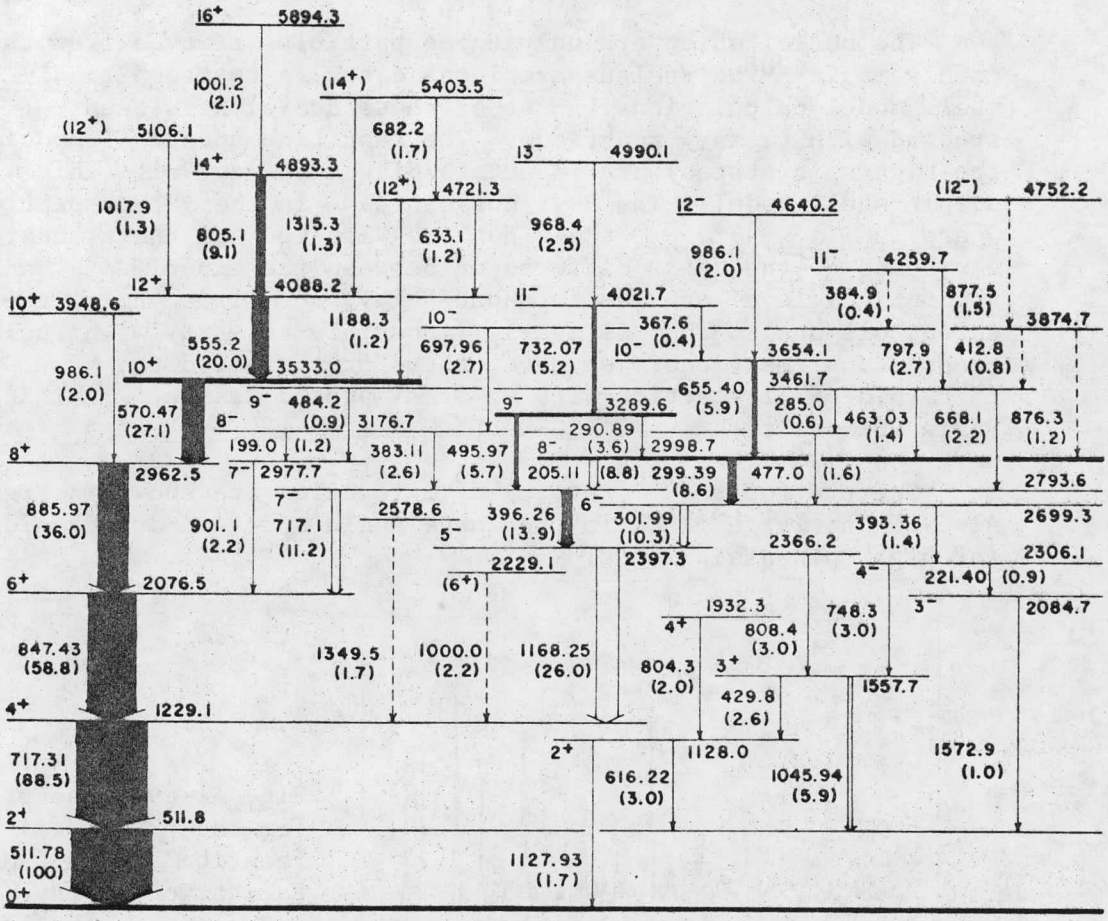

$^{96}Zr(^{13}C,3n)^{106}Pd$

Fig. A1-c8. The level scheme for the high spin states of ^{106}Pd as taken from Ref. 1.

levels impossible. With a thinner target a resolution of 25 keV FWHM should be attainable, although the small count rate may require 100,000 μC runs.

Another attempt at this experiment will be undertaken in the near future after a target of ∿20 μg/cm^2 has been fabricated.

---

[1] J. A. Grau, L. E. Samuelson, F. A. Rickey, P. C. Simms and G. J. Smith, Phys. Rev. C 14 (1976) 2297.

v. The $^{208,206,204}Pb(p,\alpha)^{205,203,201}Tl$ Reactions - P. A. Smith, and G. M. Crawley R. G. Markham and D. A. Weber (Michigan State University)

The nuclei which are only three particles removed from the doubly magic ^{208}Pb nucleus are ideal cases to test empirical shell model calculations. Most of these nuclei have been studied with $(\alpha,xn\gamma)$ reactions. The resulting spectra (especially the high spin states) are in outstanding agreement with this simple shell model. The most notable case is the ^{205}Pb spectrum where the $(i_{13/2})^3_{33/2^+}$ state has been located and the standard deviation of the differences between the experimental and theoretical level schemes is about 6 keV. ^{205}Tl is one of the three hole nuclei that is nearly impossible to study with fusion-evaporation reactions. We have, therefore, studied the $^{208}Pb(p,\alpha)^{205}Tl$ reaction with a 35 MeV proton beam at Michigan State University.

Spectra for the $^{208}Pb(p,\alpha)^{205}Tl$ reaction are shown in Fig. A1-c9. The large peaks in the large angle spectrum are candidates for high spin assignments.

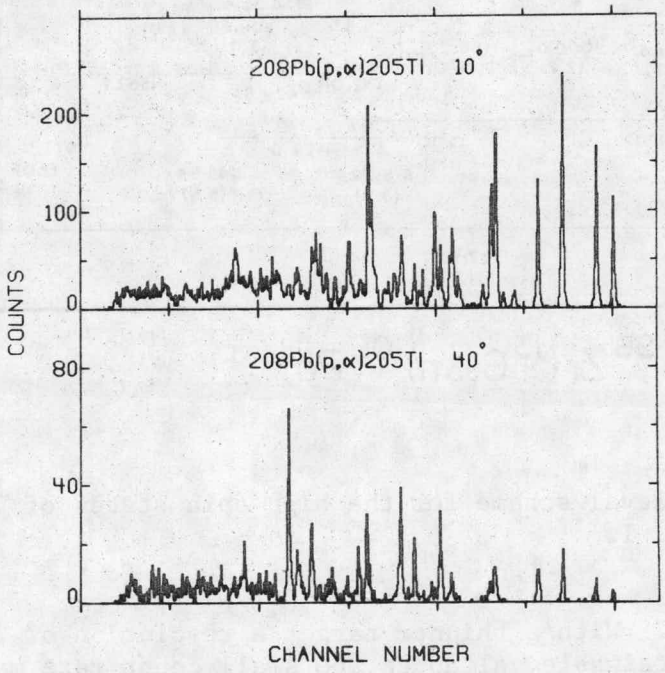

Fig. A1-c9. Spectra for the $^{208}Pb(p,\alpha)^{205}Tl$ reaction at E_p=35 MeV. Excitation energy increases to the left. The six large peaks in the low excitation part of the spectrum are the $1/2^+$, $3/2^+$, $5/2^+$, $7/2^+$, $9/2^+$ and $11/2^-$ states of ^{205}Tl. The large peak in the 40° spectrum is a high spin state.

A few of the angular distributions and cluster model DWBA calculations are shown in Fig. A1-c10. The fits were very good for j-transfers ranging from 1/2 to 21/2.

The work on the ^{208}Pb target has been completed and accepted for publication in Phys. Rev. C.

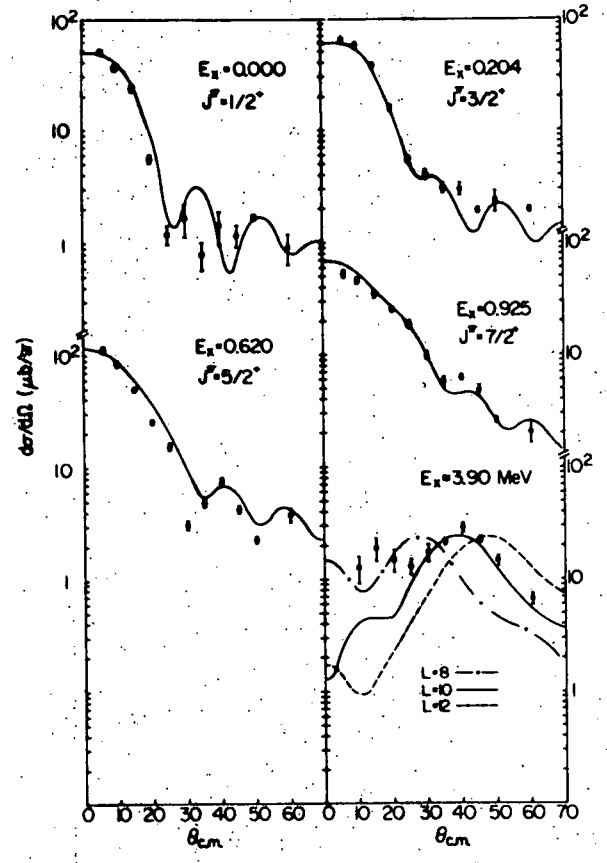

Fig. A1-c10. A few angular distributions for the $^{208}Pb(p,\alpha)^{205}Tl$ reaction.

A sample spectrum from the $^{206}Pb(p,\alpha)^{203}Tl$ reaction is shown in Fig. A1-c11. The correspondence between the strengths and j values of the low-lying states of ^{203}Tl and ^{205}Tl is remarkable.

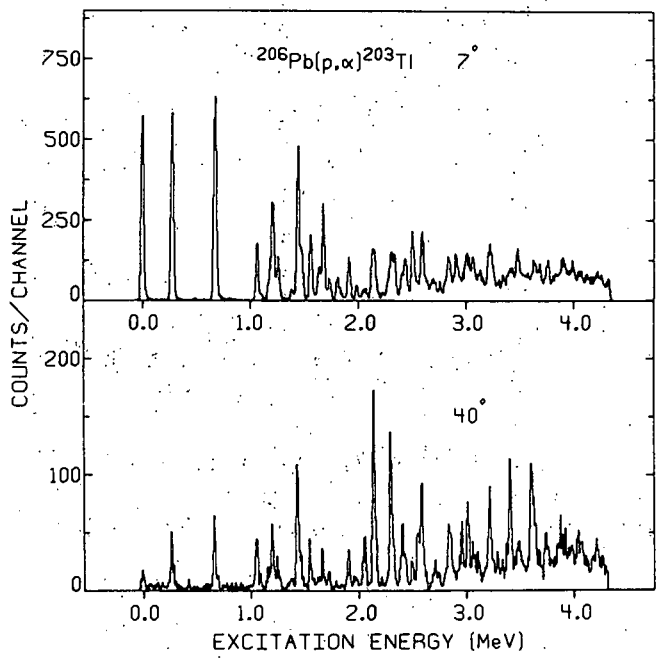

Fig. A1-c11. Spectra for the $^{206}Pb(p,\alpha)^{203}Tl$ reaction.

The analysis of the ^{206}Pb data is complete. In this instance many of the high spin states appear to be unresolved doublets. A first draft of a paper on this reaction is currently under way.

The $^{204}Pb(p,\alpha)^{201}Tl$ reaction is of interest because so little is known about the ^{201}Tl spectrum. The identification of the proton hole states to extend further the systematics for proton-hole energies in the Z=82 shell closure is one point of interest. We have not begun to take data on this target as yet, but the ^{204}Pb target has been transported from Boulder to East Lansing.

vi. The $^{27}Al(\alpha,p)^{30}Si$ Reaction - P. A. Smith, R. E. Anderson and R. A. Emigh

The negative parity states of nuclei in the upper half of the sd-shell have been studied with proton inelastic scattering in the last few years. These states are believed to be the T=1 coupling of $((sd)^{-1}f_{7/2})$ configurations. The concept of an odd sd shell particle coupled to $f_{7/2}$ particles to create particle-hole negative parity states can be extended to include three $f_{7/2}$ particles coupled to an sd-shell particle. In order to look for negative parity states in ^{30}Si, we have studied the $^{27}Al(\alpha,p)^{30}Si$ reaction. It is hoped that the negative parity states can be identified by comparing the angular distributions to those obtained with the $^{40}Ca(\alpha,p)^{43}Sc$ reaction.

The data were obtained while last year's progress report was being written. Spectra and angular distributions of known negative parity states were shown in last year's report. During the past year the data has been analyzed. This analysis, which is currently being examined, should be completed soon.

vii. The $^{13}C(\alpha,p)^{16}N$ Reaction - P. A. Smith, R. R. Sercely and R. J. Peterson

The lowest four states of the A=16, T=1 system have spins $0^-, 1^-, 2^-$ and 3^-, formed largely by a particle-hole promotion from the $p_{1/2}$ shell to the $d_{5/2}$ or $s_{1/2}$ shells. Single nucleon transfer reactions give results in general agreement with this picture, but a more sensitive test may be made using the coherent properties of multinucleon transfer reactions.

The (α,p) reaction on $^{13}C(J^\pi=1/2^-)$ allows convenient access to these states of ^{16}N. The transferred nucleons would be coupled only to $J=1/2^+$ or $J=5/2^+$ if the simple picture were true. The data shown in Fig. A1-c12 show the 2^- and 3^- states to have the same shape, which is in fair agreement with the cluster DWBA prediction for $J=5/2^+$, as shown. Only $J=1/2^+$ is allowed for the 0^- states, but the agreement with the DWBA curve is not good. The data for the 1^- state show a structure different from that for the 0^- state and more like the $1/2^+$ DWBA calculation.

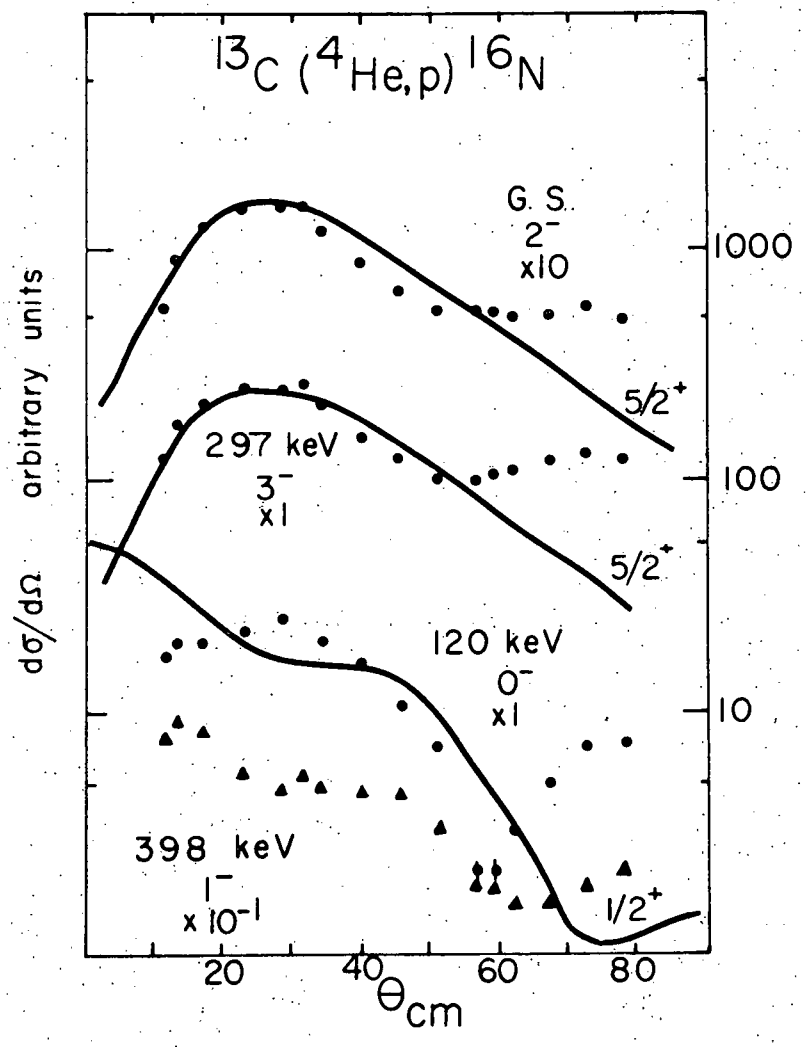

Fig. A1-c12. Angular distributions for the (α,p) transfer reaction on ^{13}C at 35 MeV are compared to cluster DWBA calculations of the indicated angular momentum transfers.

Further DWBA calculations using ^{16}N wave functions based on the known 2p-2h structure[1] of ^{16}O are continuing.

[1] K. S. Rao, Can. Journal of Phys. 53 (1975) 1299.

viii. Microscopic Calculations for Three Nucleon Transfer- P. A. Smith and R. A. Emigh

There have been many microscopic and semi-microscopic calculations for three nucleon transfer reactions published in the last two years. The semi-microscopic approaches have the advantage of using cluster form factors, which are simple to generate and which give good results for angular distribution shapes. Unfortunately, the normalization factors obtained by comparing the cluster DWBA calculations to the data are not easily related to microscopic wave functions.

In order to generate a microscopic three nucleon form factor one must project the center-of-mass motion out of a product of three single nucleon wave functions. If harmonic oscillator single particle wave functions are chosen, this projection results from two successive Moshinsky transformations. The form factor in this formalism also includes an internal overlap integral which is a function of the difference in the nuclear and α-particle size parameters raised to the number of "triton" internal nodes. If the size parameters are set equal, the form factor is zero unless the number of internal nodes is zero. The resulting form factor is a cluster form factor in the oscillator model times numerical coefficients that make up a cluster spectroscopic factor.

A code has been written to calculate these spectroscopic factors for pure configurations. Table CI contains the results for pure $(f_{7/2})^3$ transfers. The spectroscopic factor for $19/2^-$ transfer is 10 times the $17/2^-$ result. Similarly the $15/2^-$ factors are much larger than the $13/2^-$ transfers. This agrees with the $^{40}Ca(\alpha,p)^{43}Sc$ data given earlier. Table CII shows the results for $(\nu h_{11/2})^3_9$ and $[\pi s_{1/2} \nu (h_{11/2})^2_{10}]_{19/2,21/2}$ calculations. It was on the basis of these numbers that the 2-9 assignments for the states observed in the $^{116}Sn(\alpha,p)^{119}Sb$ data were eliminated.

In general, states are linear combinations of the L_n values. A code is currently being written to handle the coherent calculation for all $(f_{7/2})^n$ nuclei.

Table A1-CI

Spectroscopic factors for $(f_{7/2})^3$ transfers.

J = 1/2				
L_n =	0	2	4	6
s^n =	0.0000	0.0000	-.00453	0.0000
J=3/2				
L_n =	0	2	4	6
s^n =	0.0000	-.00518	-.00270	0.000
J=5/2				
L_n =	0	2	4	6
s^n =	0.0000	.00180	.00255	.00355
J=7/2				
L_n =	0	2	4	6
s^n =	.00843	.00449	.00296	.00177
J=9/2				
L_n =	0	2	4	6
s^n =	0.0000	-.00192	-.00259	-.00297
J=11/2				
L_n =	0	2	4	6
s^n =	0.0000	-.00801	-.00467	-.00297
J=13/2				
L_n =	0	2	4	6
s^n =	0.0000	0.0000	.00352	.00412
J=15/2				
L_n =	0	2	4	6
s^n =	0.0000	0.0000	.01231	.00667
J=17/2				
L_n =	0	2	4	6
s^n =	0.0000	0.0000	0.0000	-.00852
J=19/2				
L_n =	0	2	4	6
s^n =	0.0000	0.0000	0.0000	-.02761

Table A1-cII

Cluster spectroscopic factors*

		$(h_{11/2})^3$		
	L=9	J=17/2		
L_n =	4	6	8	10
$\|S\|^2$ =	.015	.025	.031	.032
	L=9	J=19/2		
L_n =	4	6	8	10
$\|S\|^2$ =	.380	.147	.080	.038
		$[\pi s_{1/2} \nu (h_{11/2})^2_{10}]$		
	L=10	J=19/2		
L_n =	10			
$\|S\|^2$ =	1.0			
	L=10	J=21/2		
$\|S\|^2$ =	1.0			

* Normalized so that $|S|^2=1.0$ for $21/2^+$.

d. The (p,n) Quasielastic Reaction on ^{138}Ba, ^{142}Nd and ^{144}Sm at 26.0 MeV - S. D. Schery, D. A. Lind, C. D. Zafiratos, R. E. Anderson, P. A. Smith and R. A. Emigh

The (p,n) quasielastic reaction can be analyzed in terms of a model that employs nuclear matter distributions of the target nucleus. With such a model it is possible to extract information concerning the neutron matter distribution of a nuclide under the assumption that other parts of the model, such as the nucleon-nucleon interaction and proton distribution, are well determined. The sensitivity of the analysis to these other factors can be reduced if comparisons with neighboring nuclides are made rather than single absolute calculations. Previously at this laboratory (p,n) quasielastic data have been taken on the isotopic sequence. The present experiment is designed to obtain data on the N=82 isotonic sequence for analysis in terms of a matter distribution model.

Good precision is needed to resolve differences in angular distributions along our isotonic sequence. Three detectors of two-inch by eight-inch diameter were employed on the 9-meter flight path. An effort was made to obtain 3% or better counting statistics. For a given angle, targets were measured in sequence to minimize relative error. A proton monitor detector was placed at 50° in the scattering chamber and a gate set on the elastic peak for each target. The ratio of neutron counts in the analog peak to the monitor counts provided the angular distributions. The monitor counts also provided the primary relative normalization of the angular distributions using optical potentials to predict the elastic scattering cross sections. This normalization was cross checked with measurements based on absolute target thickness.

Fig. A1-d1 shows a time-of-flight spectrum for ^{144}Sm at 38 degrees and Fig. A1-d2 shows a spectrum for ^{138}Ba at 27 degrees.

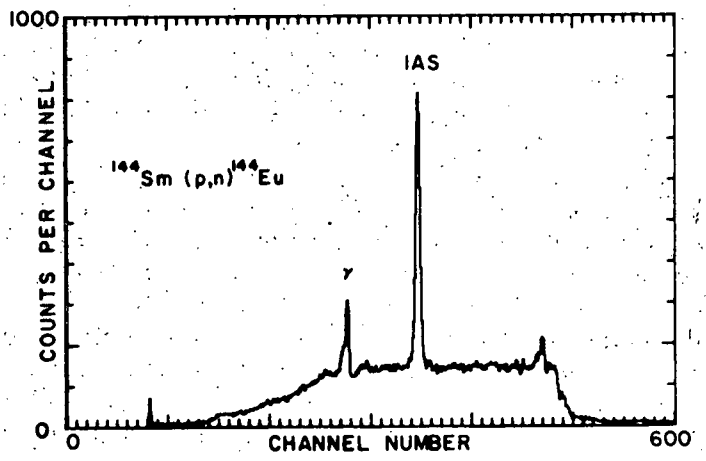

Fig. A1-d1. A time-of-flight spectrum for the $^{144}Sm(p,n)^{144}Eu$ reaction. Decreasing flight time, and hence increasing energy, is toward the right. Time per channel was 0.39 ns and the flight path was 9 meters.

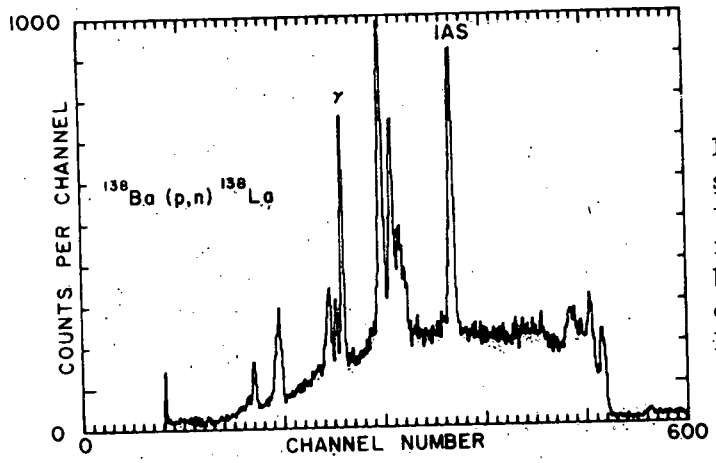

Fig. A1-d2. A time-of-flight spectrum for the $^{138}Ba(p,n)^{138}La$ reaction (as in Fig. A1-d1). The peaks below the IAS are due to oxygen and carbon in the $BaCO_3$ target.

Higher energy neutrons are to the right in each spectrum and the isobaric analog state (IAS) is quite strong. In addition to a peak due to incomplete discrimination against gamma rays in both spectra, there are additional peaks in the Ba spectrum due to C and O in the $BaCO_3$ target.

Fig. A1-d3 shows the angular distributions for the targets ^{138}Ba, ^{142}Nd and ^{144}Sm and Table A1-dI lists the cross sections. The errors listed are random errors based on counting statistics and repeatability of points. The absolute error is ±12% for ^{144}Sm and ±14% for ^{138} and ^{142}Nd based upon uncertainties in detector efficiency, target thickness, neutron attenuation, peak area

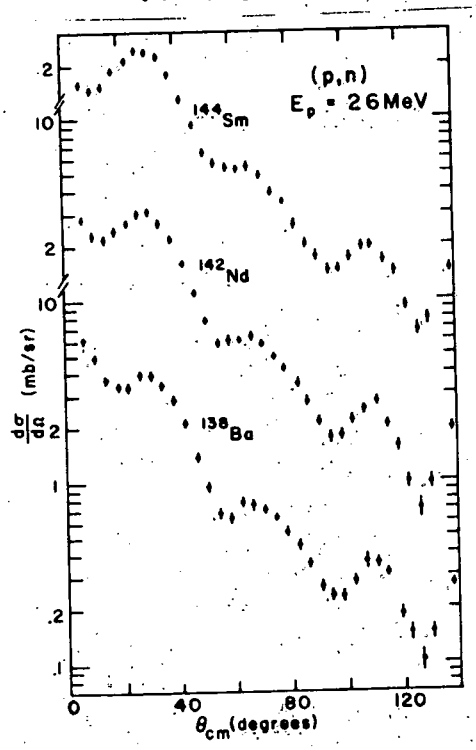

Fig. A1-d3. Angular distributions for the IAS in the (p,n) reaction on the N=82 isotones ^{138}Ba, ^{142}Nd and ^{144}Sm. The trend toward decreasing forward peaking as Z increases is reproduced by preliminary DWBA calculations.

extraction and dead time. However, the error of one angular distribution relative to another is ±6% based on uncertainties in the optical potential cross sections, detector efficiency, and the setting of the elastic monitor gate. Theoretical analysis of these angular distributions is in progress.

Table Al-dI

Cross sections for the isobaric analog of the ground state at a proton energy of 26.0 MeV.

^{138}Ba(p,n)			^{142}Nd(p,n)			^{144}Sm(p,n)		
Angle (c.m.)	$\frac{d\sigma}{d\Omega}(\frac{mb}{sr})$	Error %	Angle (c.m.)	$\frac{d\sigma}{d\Omega}(\frac{mb}{sr})$	Error %	Angle (c.m.)	$\frac{d\sigma}{d\Omega}(\frac{mb}{sr})$	Error %
6.0°	6.11	4	6.1°	2.83	4	6.1°	1.57	4
10.1	4.80	5	10.1	2.32	5	10.1	1.43	3
14.2	3.69	4	14.2	2.19	4	14.2	1.50	3
18.2	3.37	5	18.2	2.46	4	18.2	1.82	3
22.3	3.31	4	22.3	2.69	3	22.3	2.10	3
26.3	3.92	5	26.3	3.01	4	26.3	2.38	2
30.3	3.85	5	30.3	3.10	4	30.3	2.32	4
34.4	3.40	4	34.4	2.65	3	34.4	2.20	3
38.4	2.83	5	38.4	2.16	4	38.4	1.76	4
42.4	2.10	5	42.4	1.60	3	42.4	1.27	5
46.5	1.38	5	46.5	1.10	4	46.5	0.918	4
50.5	0.938	6	50.5	0.770	4	50.5	0.647	4
54.5	0.670	6	54.5	0.574	6	54.5	0.565	5
58.5	0.629	6	58.6	0.605	6	58.6	0.539	5
62.6	0.772	6	62.6	0.601	4	62.6	0.523	3
66.6	0.758	6	66.6	0.629	5	66.6	0.545	5
70.6	0.695	5	70.6	0.571	4	70.6	0.483	3
74.6	0.632	4	74.6	0.481	4	74.6	0.388	5
78.6	0.527	6	78.6	0.424	4	78.6	0.346	3
82.6	0.445	6	82.7	0.349	6	82.7	0.260	6
86.6	0.351	6	86.7	0.277	6	86.7	0.202	6
90.6	0.264	7	90.7	0.212	6	90.7	0.175	6
94.7	0.235	7	94.7	0.175	6	94.7	0.146	6
98.6	0.232	8	98.6	0.179	7	98.6	0.148	6
102.6	0.284	6	102.6	0.221	6	102.6	0.171	6
106.6	0.366	8	106.6	0.248	6	106.6	0.197	6
110.6	0.351	6	110.6	0.277	6	110.6	0.201	6
114.6	0.315	6	114.6	0.205	6	114.6	0.168	6
118.6	0.186	8	118.6	0.156	7	118.6	0.142	6
122.3	0.145	10	122.3	0.0982	10	122.3	0.0924	6
126.5	0.102	14	126.5	0.0715	12	126.5	0.0679	9
130.2	0.147	8	130.3	0.0978	9	130.3	0.0792	8
138.2	0.271	6	138.3	0.194	6	138.3	0.147	6

e. Inelastic Alpha Particle Scattering on ^{89}Y -

J. K. Okamitsu and R. J. Peterson

This inelastic scattering study at 35.6 MeV was performed to provide an up-to-date comparison using a conventional probe to the 800 MeV inelastic proton analysis reported in section IIB9. The energy resolution of 30 keV allowed many of the known states to be analyzed, and βR deformation lengths are extracted from comparisons to DWBA predictions. The optical model parameters were reported in the 1973 Progress Report.

Good fits were found for the DWBA calculation assuming a collective vibrational excitation, even for the 0.91 MeV single-particle $9/2^+$ state. Samples of the data and fits are shown as Fig. Al-el. Tables of the collective strength parameter β are listed in Table Al-eI. No spin factors are included, and β is defined by

$$\beta^2 = \frac{d\sigma}{d\Omega}\ (\text{exp't.}) / \frac{d\sigma}{d\Omega}\ (\text{DWBA})$$

where $\frac{d\sigma}{d\Omega}$(DWBA) is for a spin zero target with β=1.

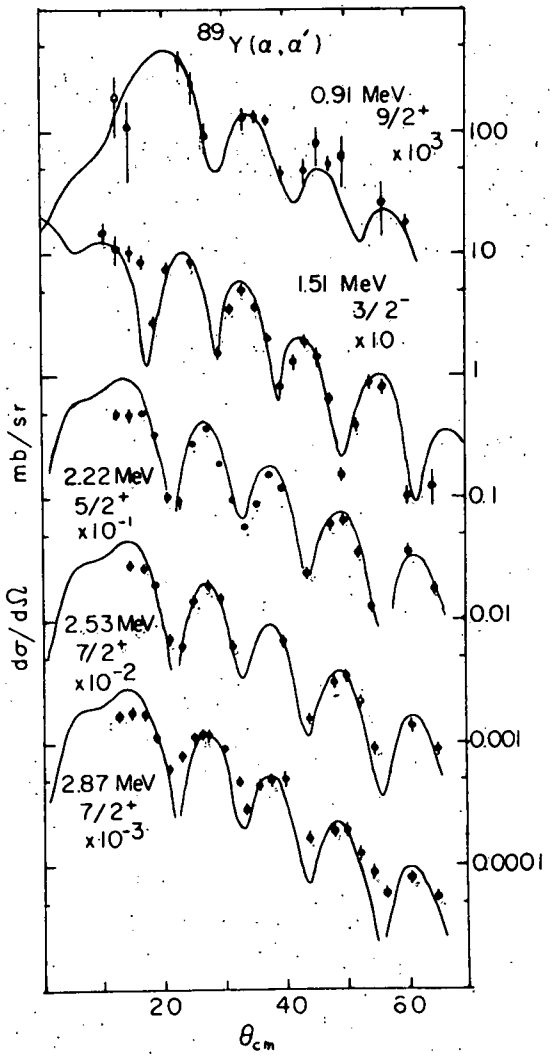

Fig. Al-el. Angular distributions for several states in ^{89}Y populated by the (α,α') reaction. The solid lines represent DWBA fits discussed in the text.

Table A1-eI

Multipolarities and deformation parameters obtained from inelastic scattering of 35.6 MeV alpha particles from ^{89}Y.

Excitation Energy, MeV	J^{π}	L	β
0.91	$9/2^+$	5	0.034
1.51	$3/2^-$	2	0.042
1.75	$5/2^-$	2	0.05
2.22	$5/2^+$	3	0.105
2.53	$7/2^+$	3	0.081
2.62	$9/2^+$	5	0.04
2.87	$7/2^+$	3	0.065

Since no spin transfer is allowed in simple pictures of inelastic alpha particle scattering, these deformation parameters may be compared to those obtained from 800 MeV proton inelastic data to note any strong spin transfer mechanism in the intermediate energy reaction. This alpha particle scattering experiment formed the basis of a senior honors thesis for Jeffrey Okamitsu.

f. Multi-Step Processes in the $^{20}Ne(d,^{6}Li)^{16}O$ (8.88 MeV 2^-) Reaction at E_d=40 MeV - J. R. Shepard and N. S. P. King (LASL)

Measurements of the $^{20}Ne(d,^{6}Li)^{16}O$ reaction done at the University of California, Davis, at a bombarding energy of 40 MeV show that the 8.83 MeV level is appreciably populated; the cross section to this level is roughly one-tenth of that to the ground state.[1] Since the excitation of unnatural parity states via the $(d,^{6}Li)$ reaction on a 0^+ target is forbidden in the simple one-step α-pickup model, other processes must be invoked. Distorted wave Born approximation calculations show that population of the 2^- level via pickup of a non-alpha cluster having spin S=1 is unlikely since the shapes of the calculated angular distributions in no way resemble those observed. Since similar DWBA calculations, assuming alpha pickup, reproduce the shapes of the 0^+ ground state and the 6.13 MeV 3^- angular distributions, it is unlikely that the failure to reproduce the shape of the 2^- angular distribution is due to an improper choice for DWBA input parameters such as optical model potentials.

Compound nuclear processes could in principle be responsible for the excitation of the 2^- level; however, Hauser-Feshbach calculations[2] also give angular distributions whose shapes do not agree with experiment.

A third possibility for excitation of the 2^- level is that the reaction does not take place in a single step. Although it is possible that sequential processes such as successive deuteron pickups may contribute, the present work ignores them and instead focusses on processes involving a single alpha transfer but with inelastic scatterings in the incoming (deuteron) and for outgoing (^{6}Li) channels.

Inelastic scattering on ^{20}Ne predominantly excites the 1.63 MeV 2^+ and 4.25 MeV 4^+ members of the $(\lambda\mu)$ = (80) ground state band. Consequently, in treating inelastic coupling in the d + ^{20}Ne system, including these two levels in addition to the ground state is likely to be sufficient. Such an assumption results in the coupling scheme shown in Fig. A1-f1.

Excitation of the 2^- level can proceed via inelastic excitation of the 1.63 MeV 2^+ (4.25 MeV 4^+) level followed by an alpha pickup involving either an L=3 or an L=1 (5) angular momentum transfer. In order to perform a CCBA calculation of this process, certain quantities reflecting the nuclear structure of the states involved must be determined. These quantities are given in Table A1-fI. The deformation parameters β_2 and β_4 describing the inelastic excitations in ^{20}Ne were determined from comparison with measured inelastic cross sections for the 40 MeV ^{20}Ne (d,d') reaction. The relative spectroscopic amplitudes for the alpha pickups were calculated using a simple SU_3 model of the levels of ^{20}Ne and ^{16}O.[3] As was mentioned above, the levels in ^{20}Ne were assumed to be members of the $(\lambda\mu)$=(80)

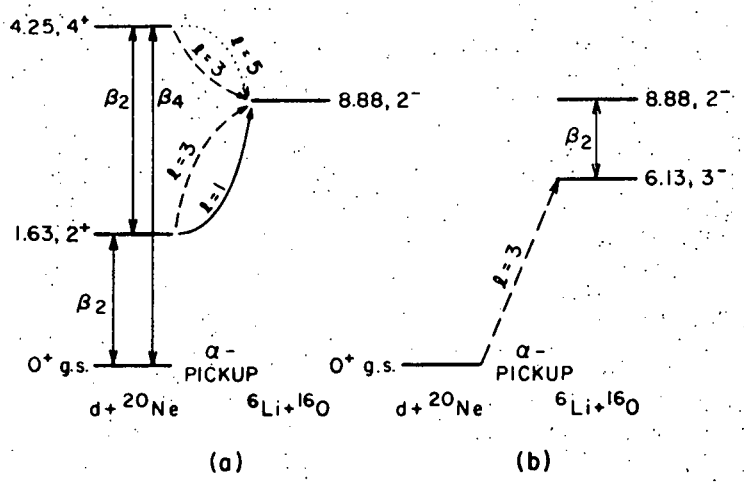

Fig. A1-f1. Coupling scheme used to account for inelastic processes in the d + ^{6}Li channel.

Table A1-fI

Optical model and deformation parameters. Potentials are in MeV, lengths are in fermis.

	V	r	a	W_v	W_s	r'	a'	r_c
d + ^{20}Ne [a]	-70.53	1.25	0.745	-13.0	---	1.25	0.71	1.30
	β_2= +0.33[a], β_4= +0.20[a]							
^{6}Li+^{16}O [b]	-241.0	1.11	0.775	---	-9.51	1.71	0.74	2.50
	$\|\beta_3\|$= 0.260 [c], $\|\beta_2\|$= 0.748[c]							
α + ^{16}O	---[d]	1.45	0.60	---	---	---	---	2.50

a) Ref. 1.

b) Ref. 4.

c) See text.

d) Well depth adjusted to give correct separation energy.

band while the 2^- level in ^{16}O was assumed to be a member of the band with symmetry $(\lambda\mu)=(21)$. Since the magnitudes of the spectroscopic amplitudes are only determined relative to the ground state to ground state amplitude, the overall strength of the CCBA calculations for the 2^- cross section is obtained by normalizing the DWBA prediction for the g.s. to g.s. transition to the experimental results.[4] An extracted spectroscopic factor of S=0.15 is the result of such a process when a zero-range normalization factor of $D_o^2/10^4 = 0.64$ is assumed, and a $^6Li \rightarrow d+\alpha$ spectroscopic factor of 0.75 is used. This value compares favorably with those determined in other studies: Ichimura,[5] S=0.23; Yoshida,[6] S=0.182; G. Audi et al,[7] S≈0.14 (if S=0.5 is assumed for a pickup on ^{12}C to g.s. of ^8Be and the spectroscopic factor is extracted using their most reasonable parameter set, c, of their Table 2).

The CCBA calculations including inelastic coupling in the deuteron channel and normalized as discussed above are compared with the experimental angular distribution for the 8.88 MeV 2^- level in Fig. A1-f1. While the shape of the experimental angular distribution is well described by the CCBA results, the magnitude is under-predicted by about a factor of ten. This suggests that deuteron inelastic scattering followed by alpha pickup is not primarily responsible for the transition to the 2^- level.

An alternative two-step process involves inelastic processes in the $^6Li + ^{16}O$ channel, specifically alpha pickup to the 6.13 MeV 3^- level followed by quadrupole inelastic scattering in the $^6Li + ^{16}O$ channel to the 2^- level. The strength of the transition from the ^{20}Ne ground state to the 6.13 MeV 3^- level is determined by the experimental cross section. Comparison with DWBA predictions yields a spectroscopic factor S=0.31. The strength parameter, $\beta_2 R$, for the inelastic scattering from the 3^- to the 2^- state has been extracted from a CCBA analysis of $^{16}O(\alpha,\alpha')^{16}O$ scattering to the 2^- level which is known to proceed predominantly in two steps through the 3^- level.[8] Using the optical model potentials quoted by Mori[8] and assuming a simple, collective octupole (quadrupole) transition between the 0^+ and 3^- (3^- and 2^-) levels and thereby ignoring exchange effects, CCBA calculations can be compared with the E_α=40.5 MeV measurements of Harvey et al.[9] This results in deformation parameters of β_3=0.260 and β_2=0.748 for a potential radius parameter of $r_o = R/A^{1/3} = 1.77$ fm. Applying these deformation parameters to the $^6Li + ^{16}O$ case is somewhat ambiguous since the real and imaginary radius parameters for the $^6Li + ^{16}O$ optical model potential are both less than 1.77 and are quite different from each other (see Table A1-fI). However, if the product βR is required to be the same in the $\alpha + ^{16}O$ and $^6Li + ^{16}O$ cases, and if r_o=1.40 is chosen for the ^6Li potential radius parameter, the deformation parameters shown in Table A1-fI are obtained.

With these empirically determined strengths, the α pickup spectroscopic factor, and the 3^- to 2^- quadrupole deformation parameter, the CCBA calculation can be absolutely normalized and

the curve appearing in Fig. A1-f2 results. The calculation reproduces the overall magnitude of the cross section quite well while the shape is poorly described beyond $\theta=20^{o}$. Both the theoretical and experimental angular distributions show the forward angle drop-off required by angular momentum considerations for unnatural parity multistep transitions in the absence of strong spin orbit interactions.[10]

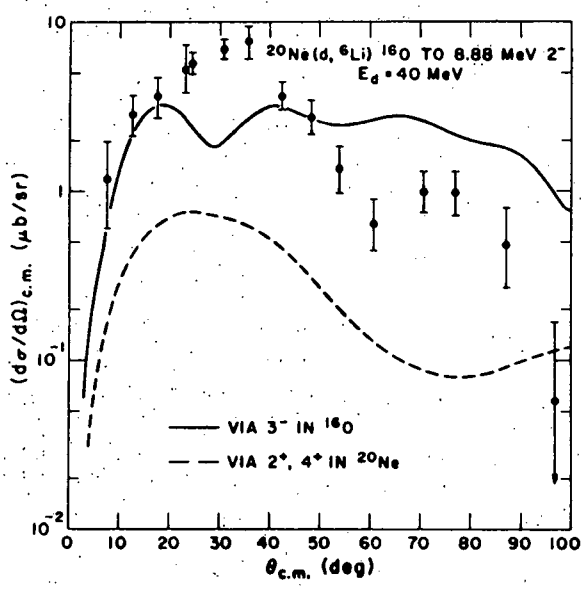

Fig. A1-f2. ^{20}Ne(d, ^{6}Li)^{16}O (8.88 MeV 2$^-$) experimental angular distributions are compared with CCBA calculations. The dashed curve represents inelastic couplings in the d + ^{20}Ne channel. The solid curve represents couplings in the ^{6}Li + ^{16}O channel.

Thus these calculations suggest that the excitation of the 8.88 MeV 2$^-$ level in ^{16}O is primarily due to inelastic excitation from the 6.13 MeV 3$^-$ level with inelastic excitations in the d + ^{20}Ne channel playing a lesser role. The poor quality of the fit to the shape of the experimental angular distribution implies that a more careful treatment of the details of the calculations is required. Refinements to be considered in future calculations include a more precise determination of the shape and magnitude of the 3$^-$ to 2$^-$ form factor and simultaneous treatment of the two (deuteron and ^{6}Li) inelastic channels.

1 M. B. Epstein et al., Bull. Am. Phys. Soc. 19 (1974) 453;
N. S. P. King et al., Bull. Am. Phys. Soc. 18 (1973);
2 G. W. Wolfe, Ph.D. Thesis, Univ. of California, Davis, unpublished.
3 L. Parrish, CUMPND, unpublished.
4 J. Draayer, Louisiana St. Univ., private communication.
5 J. Watson, Nucl. Phys. A198 (1972) 129.
6 M. Ichimura et al., Nucl. Phys. A204 (1973) 225.
7 Quoted in C. Détraz et al., Nucl. Phys. A147 (1970) 488.
8 G. Audi et al., Nucl. Phys. A237 (1975) 300.
9 A. Mori, Phys. Lett. 53B (1974) 234.
10 B. G. Harvey et al., Phys. Rev. 146 (1966) 712.
T. Udagawa and D. K. Olsen, Phys. Lett. 46B (1973) 285.

g. The Level Structure of ^{112}In as Studied by Four Different Reactions - R. A. Emigh, R. E. Anderson and L. E. Samuelson

The residual neutron-proton interaction, which gives rise to the details of the level structure encountered in odd-odd nuclei, is an interesting and appealing subject of study. In the lead region, where the various configuration multiplets remain relatively pure, a great deal has been learned about the dependence of this interaction on such things as the shell model orbitals involved and the spin and isospin of the multiplet members. In other mass regions the members of multiplets are perturbed by configuration mixing, thus precluding easy understanding of experimental results. The nucleus ^{112}In was felt to be a case where the effects of configuration mixing may be minimized since it is one proton removed from the major shell closure at Z=50. Although the neutron shells are superconducting, it is hoped that the neutron configuration purity remains intact. Because of the selectivity encountered in direct reaction studies and because the valence nucleon in the odd mass target is expected to be a spectator in the reaction, any one-particle direct reaction (in the absence of configuration mixing) is expected to reveal only a few of the levels in the residual nucleus. Thus, several reactions were used in this study to reveal the properties of levels in ^{112}In. Specifically, we looked at the ^{113}In(p,d)^{112}In and ^{111}Cd(^{3}He,d)^{112}In charged particle reactions. In addition, we observed the γ-ray emissions of ^{112} levels excited by the ^{109}Ag(α,nγ)^{112}In and ^{112}Cd(p,nγ)^{112}In reactions.

The ^{111}Cd(^{3}He,d)^{112}In reaction was studied at a bombarding energy of 33.6 MeV. Reaction products were momentum analyzed using the Colorado energy-loss spectrometer system. The target consisted of approximately 50 μgm/cm^2 of enriched (96.5%) ^{111}Cd evaporated onto a 40 μgm/cm^2 carbon foil. A typical spectrum is shown in Fig. Al-gl and has a resolution of 18 keV (FWHM). Data were obtained in 2½° steps between laboratory angles of 2.5° and 40.0°. Relative normalization was obtained from a solid state monitor detector mounted in the scattering chamber at a fixed angle with respect to the incoming beam and is believed to be accurate to better than 15%. Absolute normalization of the data was obtained by measuring ^{3}He elastic scattering from the target at a number of angles and comparing these data with the results of DWBA calculations using the parameters given in Table Al-gI. The absolute normalization is felt to be accurate to ±25%. Energy calibration for the ^{112}In spectrum was obtained by observing the ^{62}Ni(^{3}He,d)^{63}Cu reaction at four different angles. The excitation energies of the levels in ^{112}In were generated from a second order polynomial of deuteron momentum versus channel number obtained by fitting the locations of known peaks in the calibration reaction.

The study of the ^{113}In(p,d)^{112}In reaction was accomplished in a manner essentially identical to that just described for the (^{3}He,d) reaction. A proton bombarding energy of 27.3 MeV was used

Table A1-gI

Optical model and DWBA parameters.

Particle	V_r (MeV)	r_r (fm)	a_r (fm)	W (MeV)	$4W_D$ (MeV)	r_i (fm)	a_i (fm)	V_{so} [a] (MeV)	r_{so} (fm)	a_{so} (fm)	r_c (fm)	β [b]
^{3}He	170	1.14	0.723	20	20	1.60	0.81				1.14	0.25
d @ 33 MeV	101	1.15	0.81		66.5	1.34	0.68	6.0	1.15	0.81	1.15	0.54
Proton well	c)	1.25	0.65					25 [d]			1.25	
p	48.67	1.22	0.72	3.20	26.76	1.32	0.60	6.2	1.06	0.68	1.25	0.85
d @ 20 MeV	94.50	1.15	0.79	0.52	55.68	1.33	0.82	13.4	0.98	1.00	1.25	0.54
Neutron well	c)	1.25	0.65					25 [d]			1.25	0.85

The finite range parameter was 0.77 for the (^{3}He,d) reaction and 0.62 for the (p,d) reaction.

a) The spin-orbit potential depths must be multiplied by four for protons and two for deuterons.
b) Non-locality correction.
c) Adjusted to give the correct binding energy.
d) λ=25 using the Thomas spin orbit form.

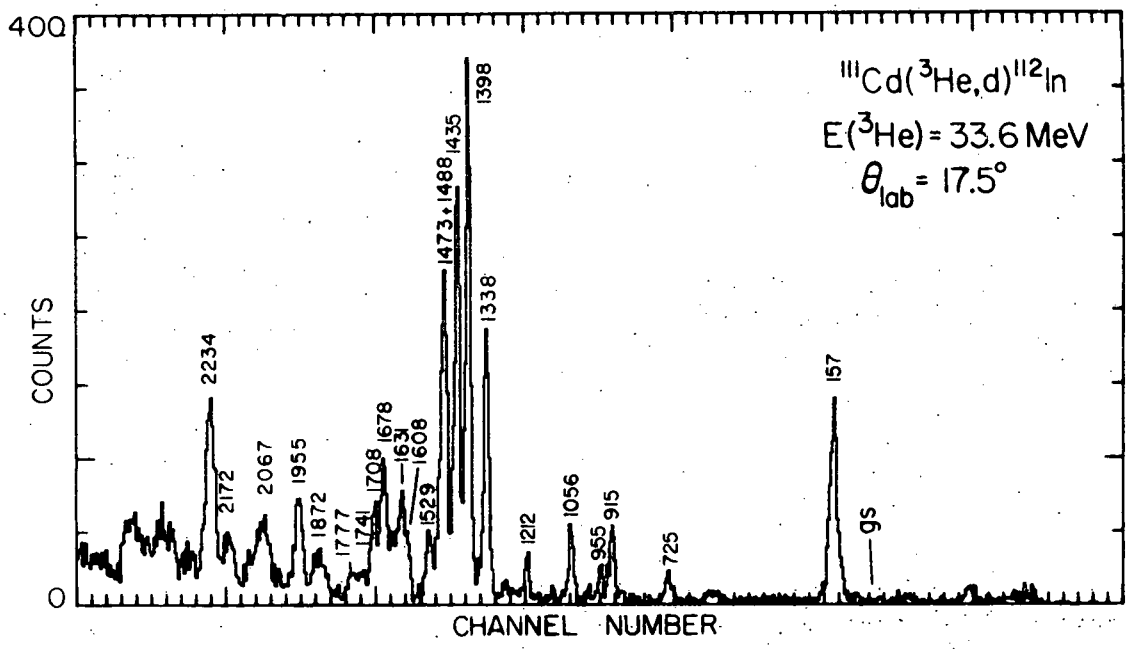

Fig. Al-g1. Deuteron spectrum from the $^{111}Cd(^{3}He,d)^{112}In$ reaction.

and the target consisted of approximately 140 μgm/cm^2 of enriched (96.4%) ^{113}In evaporated onto a 40 μgm/cm^2 carbon foil. A resolution of 12 keV (FWHM) was achieved and a sample spectrum is shown in Fig. Al-g2. Data were collected in 2.5° steps between 2.5°

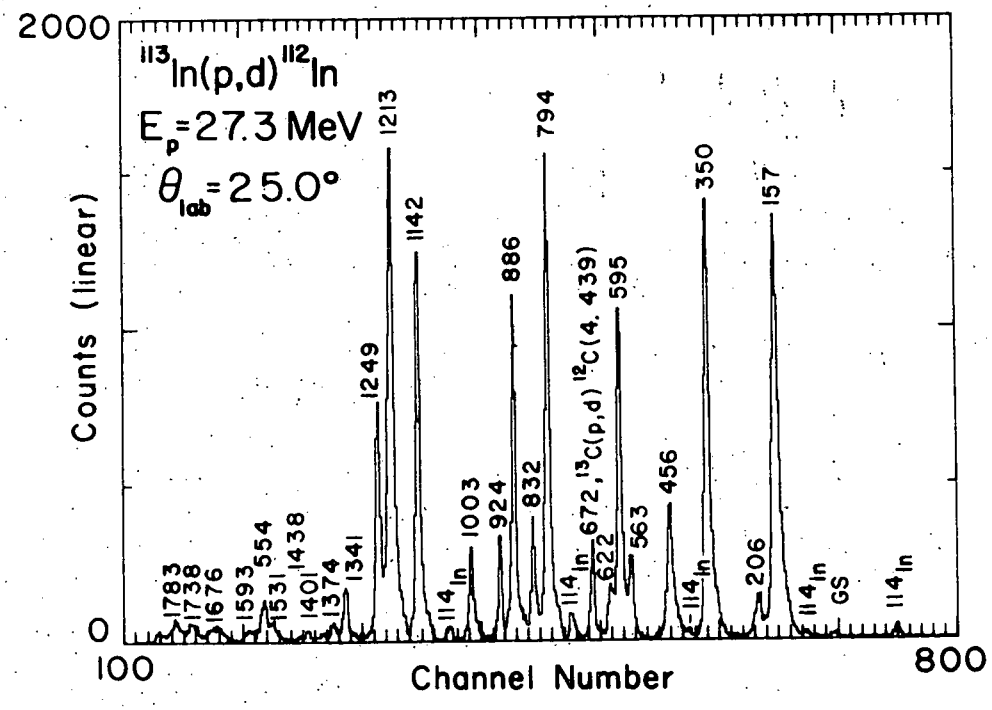

Fig. Al-g2. Deuteron spectrum from the $^{113}In(p,d)^{112}In$ reaction.

and 55.0° with an additional point at 60.0°. Relative and absolute normalizations and the energy calibration using the $^{64}Ni(p,d)^{63}Ni$, $^{93}Nb(p,d)^{92}Nb$ and $^{115}In(p,d)^{114}In$ reactions were obtained in the manner previously described.

Gamma-ray singles, angular distributions and coincidence measurements were taken using the $^{109}Ag(\alpha,n\gamma)^{112}In$ reaction at an alpha bombarding energy of 16.7 MeV. Additional singles measurements were taken at E_α=13.6 MeV, which is below the $(\alpha,2n\gamma)$ threshold, to identify contaminant γ-rays from the $(\alpha,2n\gamma)$ reaction. An enriched (99.3%) self-supporting ^{109}Ag target of 3.3 mgm/cm^2 thickness was used. Two large volume (approximately 50 cm^3) GeLi detectors and two small volume (approximately 1.5 cm^3) HPGe detectors were utilized for both single and coincidence measurements. The former had 2.2 keV resolution (FWHM) at 0.122 MeV. Energy calibrations were made from observations of ^{133}Ba, ^{152}Eu, ^{226}Ra and ^{241}Am sources. Intensity calibrations were obtained using these same sources which were placed inside the aluminum scattering chamber to account for γ-ray attenuation in the chamber walls. A list of γ-ray intensities for the $^{109}Ag(\alpha,n\gamma)^{112}In$ reaction is given in Table Al-gII.

Excitation functions, angular distributions and coincidence data were taken using the $^{112}Cd(p,n\gamma)^{112}In$ reaction. The excitation function was obtained from five incident proton energies between 4.29 and 5.17 MeV. Angular distributions and coincidence data were obtained at E_p=5.17 MeV. The intensities for γ-rays seen from the $^{112}Cd(p,n\gamma)^{112}In$ reaction at 5.17 MeV are given in Table Al-gII.

The experimental angular distributions for the two charged particle reactions were compared to DWBA calculations to determine ℓ-transfers and generate spectroscopic factors. The code DWUCK4 was used in conjunction with the optical model parameters given in Table Al-gI.

Angular momentum transfers of 0, 1, 2 and 4 are seen in the (^{3}He,d) reaction. Figs. Al-g3 through Al-g6 show that the shape for each of these ℓ-transfers is quite nicely reproduced by the DWBA calculations. Spectroscopic factors for the (^{3}He,d) reaction are obtained from the following relationship:

$$\left(\frac{d\sigma}{d\Omega}\right)_{exp} = 4.42 \frac{2J_f+1}{2J_i+1} \left(\frac{d\sigma}{d\Omega}\right)_{DW} \frac{C^2 S_{\ell j}}{2J+1}$$

where $\left(\frac{d\sigma}{d\Omega}\right)$ are the experimental and theoretical cross sections, C^2 is the square of the isotopic coupling coefficient, $S_{\ell j}$ is the spectroscopic factor, and J_f, J_i and J are the total angular momenta of the final state, the initial state and the transferred particle, respectively. The calculated values of $(2J_f+1)\ C^2S_{\ell j}$ are given in Table Al-gIII for the (^{3}He,d) reaction.

Table Al-gII

Results of ^{112}In γ-ray experiments. Only γ rays with energies below 1 MeV are included. The γ-ray angular distributions were least-squares fit to the equation $W(\theta) = A_o [1 + a_2 P_2(\cos\theta) + a_4 P_4(\cos\theta)]$

	^{112}Cd(p,nγ)^{112}In 5.17 MeV			^{109}Ag(αnγ)^{112}In 17.6 MeV		
E_γ [a]	I_γ [b]	a_2	a_4 [c]	I_γ [b]	a_2	a_4 [c]
51.9	[d]			113.6 (33)	-0.084 (14)	-0.008 (18)
99.7				14.3 (8)	-0.15 (8)	
120.0				14.8 (11)		
135.7	46.3 (18)	-0.208 (27)		221 (6)	-0.184 (7)	-0.006 (10)
142.8				7.3 (12)		
146.0	41.0 (16)	-0.145 (19)		276 (7)	-0.104 (8)	0.023 (12)
156.5	[e]			[e]		
185.2	38.0 (16)	-0.125 (19)		152 (5)	-0.126 (14)	0.011 (19)
186.9				225 (6)	-0.105 (14)	0.010 (20)
187.9	44.4 (18)	0.104 (25)		1675 (39)	0.073 (5)	0.001 (7)
189.9	15.7 (10)	0.00 (7)				
195.7	28.1 (13)	0.112 (35)		20.7 (19)		
203.2				98.2 (33)	-0.254 (37)	0.046 (49)
206.7	≡1000	-0.095 (5)	0.001 (6)	≡1000	-0.105 (5)	0.004 (6)
214.2				14.5 (27)		
223.5	17.3 (11)	-0.10 (7)				
249.7 [f]	228 (7)	-0.148 (12)	0.008 (14)	529 (13)	-0.131 (12)	0.016 (16)
255.3	<5.0					
262.9	38.4 (16)	0.037 (28)		1105 (26)	0.046 (6)	0.000 (8)
273.5	12.2 (10)	0.23 (5)		149 (5)	0.176 (35)	-0.019 (48)
277.1	12.9 (11)	0.10 (7)				
279.4	18.0 (11)	-0.07 (7)		42.6 (20)		
281.6	8.0 (10)					
288.8	52.2 (20)	-0.104 (29)		50.0 (23)		
293.4	17.7 (12)	0.01 (7)				
324.0	57.9 (21)	0.001 (24)		32.4 (19)		
326.2	16.2 (12)	-0.06 (8)				
367.3	15.8 (12)	0.05 (6)				

Table A1-gII (continued)

388.2	71.3 (25)	0.092 (22)	-0.014 (24)	52.7 (24)
421.1	9.2 (13)			
428.3	5.9 (12)			
481.7	9.3 (13)			
483.4	6.7 (13)			
522.1 }	33.9 (28)	-0.119(21)		{ 17.8 (18)
523.3 }				{ 73.8 (29)
531.2	7.7 (14)			
573.2	49.1 (22)	-0.200(38)		84.4 (33)
588.3				57.5 (27)
594.8	226 (7)	-0.095(17)	-0.006 (19)	154 (5)
638.0	2.8 (6)			
644.5	14.5 (16)			
666.0	5.0 (12)			
669.0	3.5 (8)			
717.8	54.2 (24)	0.104(39)		47.6 (27)
727.3 }	257 (8)	-0.077(18)	-0.004	{ 43.2 (25)
729.1 }				{ 188 (6)
744.0	2.0 (6)			
761.6	20.4 (19)	-0.08 (8)		
774.5				6.6 (23)
823.8[f]	43.2 (37)			
856.3	32.2 (20)	0.34 (7)		25.6 (26)
918.7	53.1 (23)	-0.023(34)		
928.6	43.4 (21)	-0.038(37)		

a) Errors are ±0.1 keV.
b) If blank, significant intensities were not observed.
c) Where blank, fit with $A_4 \equiv 0.000$.
d) Not measured.
e) Long-lived ^{112}In isomeric decay.
f) Contaminated.

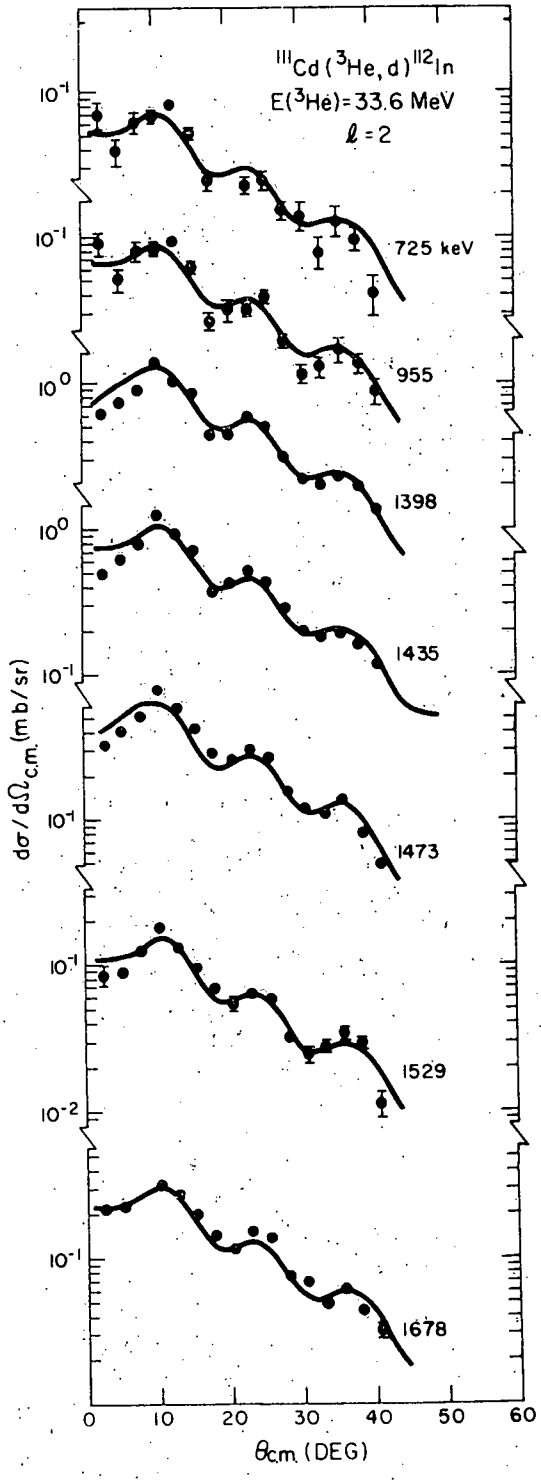

Fig. Al-g4. Angular distributions for ℓ=2 for the $^{111}Cd(^{3}He,d)^{112}In$ reaction.

Fig. Al-g3. Angular distributions for ℓ=2 for the $^{111}Cd(^{3}He,d)^{112}In$ reaction.

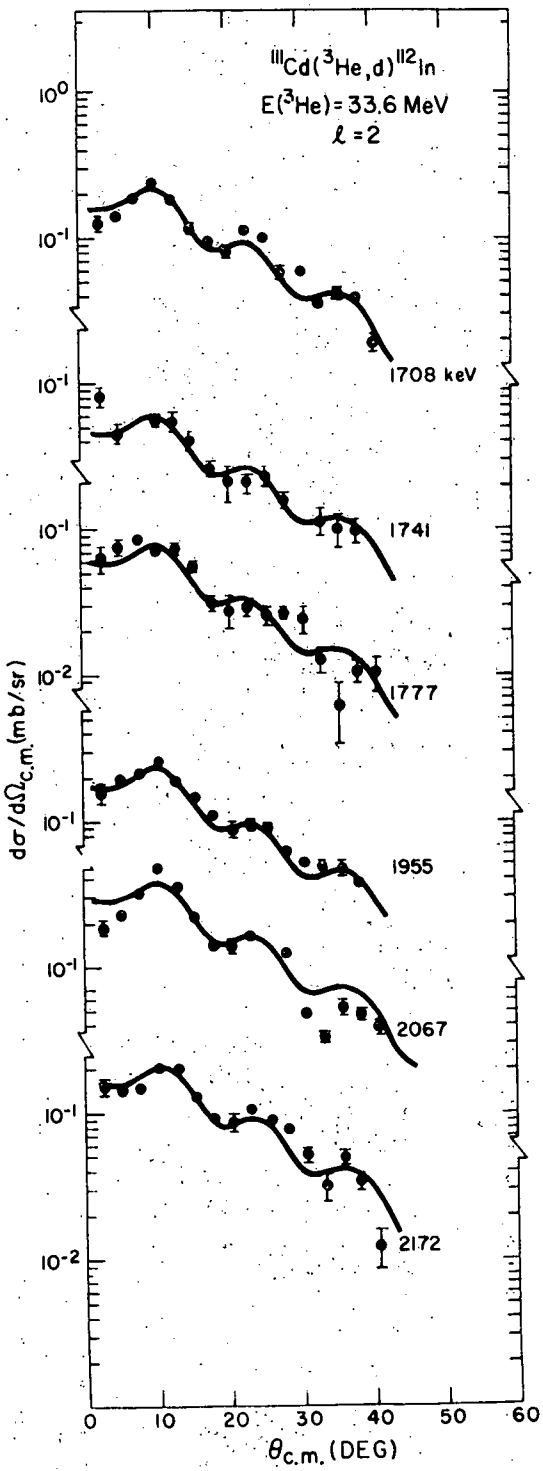

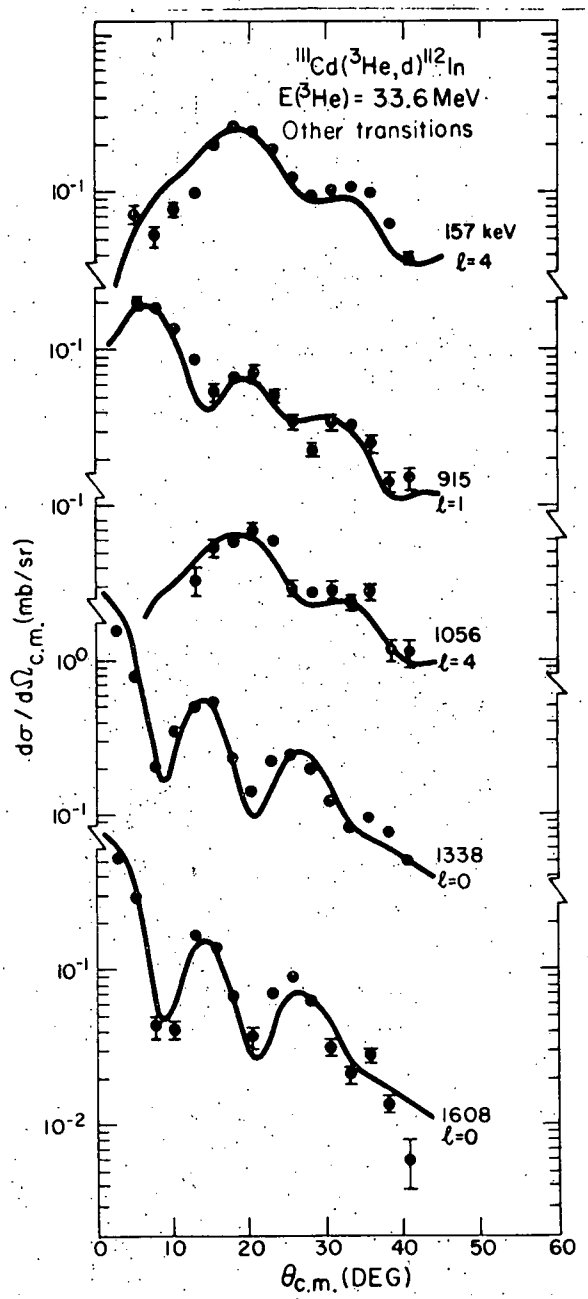

Fig. Al-g6. Angular distributions for various ℓ-transfers for the $^{111}Cd(^{3}He,d)^{112}In$ reaction.

Fig. Al-g5. Angular distributions for ℓ=0, 1 and 4 for the $^{111}Cd(^{3}He,d)^{112}In$ reaction.

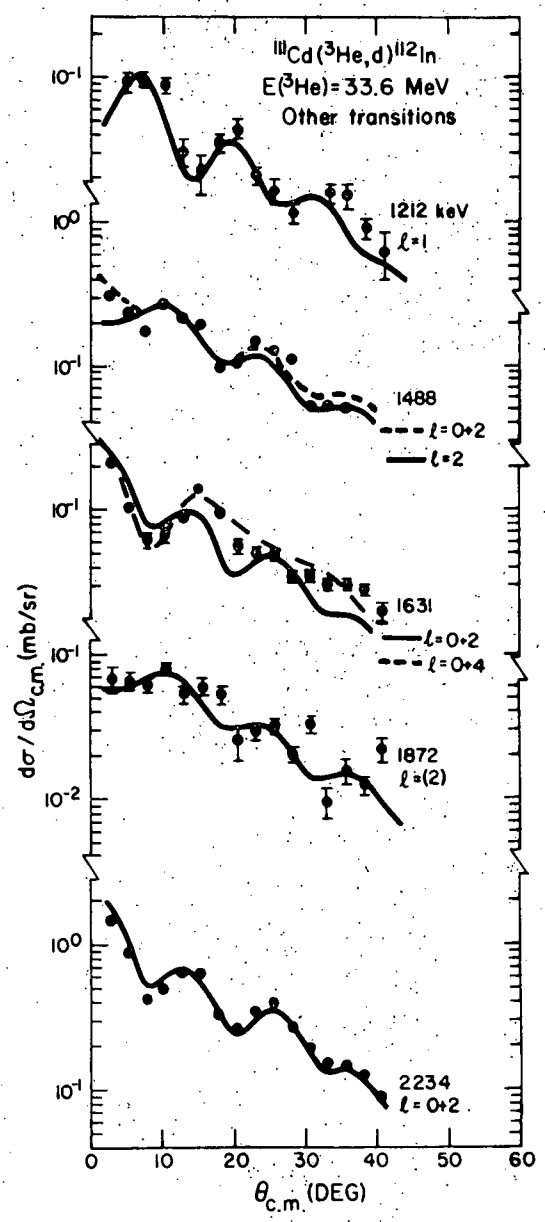

Table A1-gIII

Summary of spectroscopic information obtained from the $^{111}Cd(^{3}He,d)^{112}In$ reaction.

Energy (keV)	ℓ-transfer	(2J+1) C^2S $J_<$	$J_>$
157	4	7.62	3.88
725	2	0.20	0.15
915	1	0.43	0.21
955	2	0.24	0.17
1056	4	1.44	0.74
1212	1	0.21	0.10
1338	0	0.56	0.56
1398	2	0.27	0.20
1435	2	2.43	1.78
1473	2	1.51	1.07
1488	2,0+2	.56, .05+0.45	0.41,0.05+0.33
1529	2	0.33	0.24
1608	0	0.18	0.18
1631	0+2,0+4	0.04+0.11,0.04+1.05	0.04+0.08,0.04+0.62
1678	2	0.67	0.50
1708	2	0.45	0.33
1741	2	0.13	0.10
1777	2	0.18	0.13
1872	2	0.15	0.11
1955	2	0.44	0.33
2067	2	0.81	0.60
2172	2	0.46	0.34
2234	0+2	0.29+1.13	0.29+0.83

Angular distributions for the largest peaks in the $^{113}In(p,d)^{112}In$ reaction are shown in Figs. A1-g7 and A1-g8. Spectroscopic factors are obtained from the following relationship:

$$\left(\frac{d\sigma}{d\Omega}\right)_{exp} = 2.29\left(\frac{d\sigma}{d\Omega}\right)_{DW} \frac{C^2S_{\ell j}}{2J+1}$$

where the various terms are defined above. The values of $C^2_{\ell j}$ are given in Table A1-gIV for the levels which have been analyzed. Complete analysis of the remaining peaks should be completed in the near future.

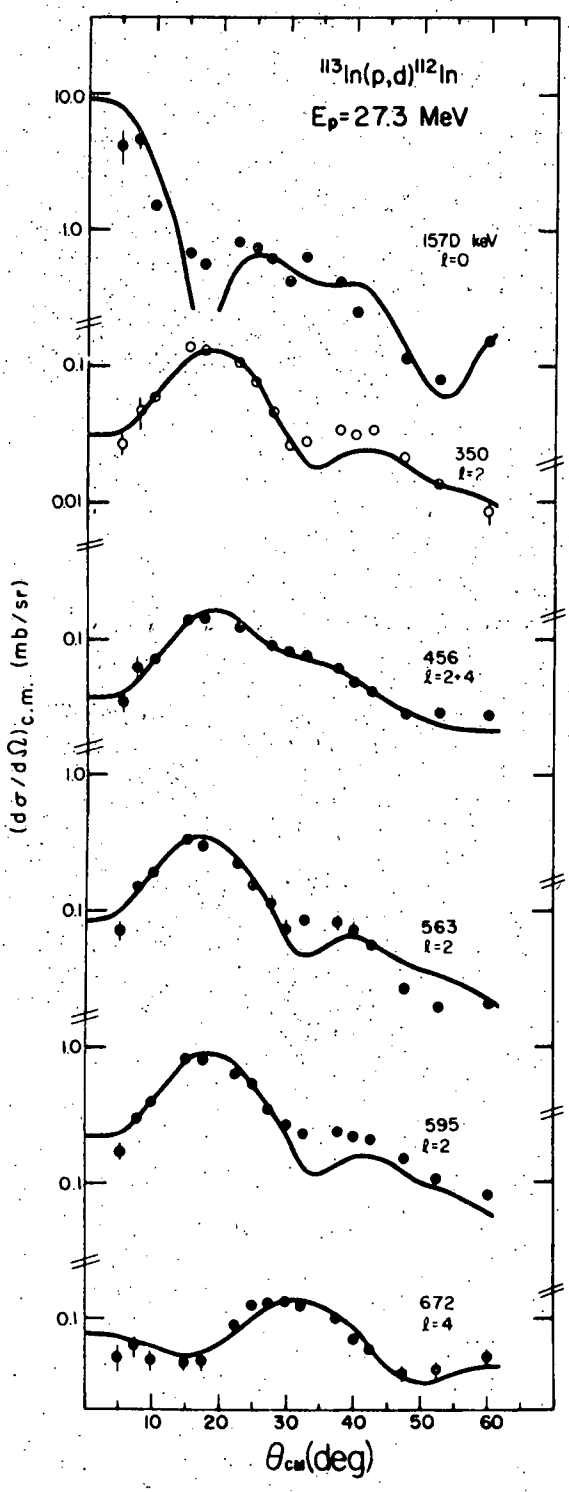

Fig. A1-g8. Angular distributions for various ℓ-transfers for the ^{113}In(p,d)^{112}In reaction.

Fig A1-g7. Angular distributions for various ℓ-tranfers for the ^{113}In(p,d)^{112}In reaction.

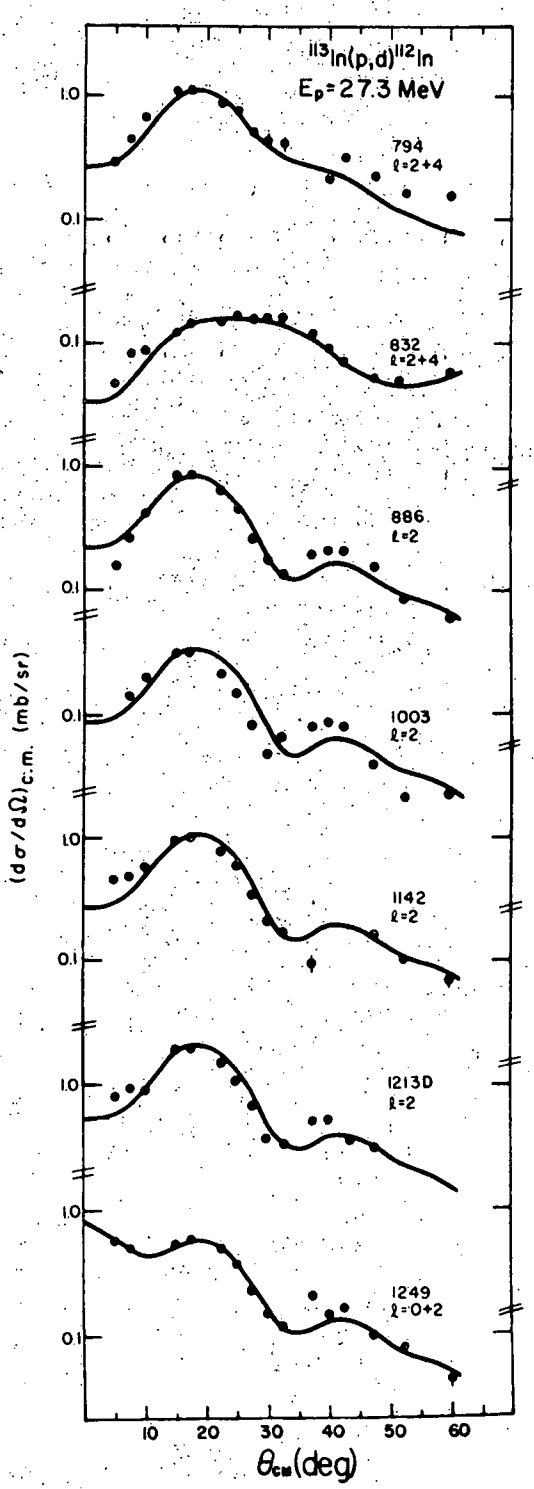

Table Al-gIV

Summary of spectroscopic information obtained from the $^{113}In(p,d)^{112}In$ reaction.

Energy (keV)	ℓ-transfer	C^2S $J_<$	$J_>$
g.s.	4	.05	.03
157	0	.39	--
206	2+4	.03,.15	.03,.10
356	2	.63	.54
456	2+4	.06,.28	.06,.20
563	2	.13	.11
595	2+4	.37,.58	.30,.41
622	4	.39	.27
672	4	.65	.48
794	2	.06	.04
832	2+4	.49,.69	.39,.47
886	2	.40	.31
923	0+2	.02,.09	--,.07
1003	2	.18	.14
1142	0+2	.015,.52	--,.42
1213	0+2	.012,.95	--,.76
1249	0+2	.031,.32	--,.26
1340	Not yet analyzed		
1374	"		
1401	"		
1438	"		
1531	"		
1554	"		
1593	"		
1676	"		
1738	"		
1783	"		

The $^{111}Cd(^3He,d)^{112}In$ Reaction

Since the ground state spin-parity of ^{111}Cd is $1/2^+$, the 1^+ ground state of ^{112}In could be populated in the $(^3He,d)$ reaction by an ℓ=0 or ℓ=2 transition while the known 4^+ isomer at 157 keV could be populated by an ℓ=4 transition. The ground state transition was not seen in spite of the extreme sensitivity of this experiment to ℓ=0 and ℓ=2 transfers. The lowest lying level seen is an ℓ=4 transition taken to be the 157 keV level. Because the

$\pi 1g_{9/2}$ orbital is unfilled, this level is almost certainly populated by $g_{9/2}$ transfer. The large cross section for this level and the lack of another ℓ=4 transfer in this energy region implies that the 157 level is a doublet.

Two ℓ=1 transitions were observed at 915 keV and 1212 keV, whereas four might be expected. From our γ-ray coincidence data, it appears that the 915 keV level is likely both members of the $\pi 2p_{1/2}^{-1} \otimes \nu 3s_{1/2}^{-1}$ doublet. The level at 1212 keV is then either the 1^- or 2^- member of the $\pi 2p_{3/2}^{-1} \otimes \nu 3s_{1/2}^{-1}$ doublet. The other member is not observed.

The paucity of $2p_{1/2}$, $2p_{3/2}$ and $1g_{9/2}$ transitions indicates that the multiplets formed from these proton orbitals and the $3s_{1/2}$ orbital remain quite pure. There are numerous low-lying states of the correct spin and parity but of different configuration which could mix with these states. This is in direct conflict with the results of the $^{105}Pd(^3He,d)^{106}Ag$ reaction, where severe configuration mixing is observed, as observed by the presence of twelve levels populated by ℓ=1 transfer.

The large number of ℓ=2 transitions seen, predominantly above 1300 keV, indicate a different situation for multiplets involving a $2d_{5/2}$ or $2d_{3/2}$ proton. Nominally four ℓ=2 transitions are expected whereas sixteen are definitely seen.

The $^{113}In(p,d)^{112}In$ Reaction

The ^{113}In ground state has a spin-parity of $9/2^+$. The 1^+ ground state can be populated only by an ℓ=4 transfer while the isomeric 4^+ level can be populated by ℓ=0, 2 or 4. The ground state is seen by a pure ℓ=4 shape and the first excited state by an ℓ=0 shape. In conjunction with the (^{3}He,d) reaction data, the ground state must be the 1^+ member of the $\pi 1g_{9/2}^{-1} \otimes \nu 1g_{7/2}^{-1}$ multiplet. The ℓ=0 cross section for the 157 keV peak is approximately twice that of the sum of the 190 keV and 220 keV levels populated by ℓ=0 shapes in the $^{115}In(p,d)^{114}In$ reaction. No other ℓ=0 strength in the $^{113}In(p,d)^{112}In$ reaction is seen below 0.9 MeV excitation. Coupled with the (^{3}He,d) reaction data, the 157 keV peak must be a doublet with the configuration $(\pi 1g_{9/2}^{-1} \otimes \nu 3s_{1/2}^{-1})_{4^+,5^+}$. Analysis of the $^{113}In(p,d)^{112}In$ reaction data is not yet complete although preliminary indications are that configuration mixing is not great.

The $^{112}Cd(p,n)^{112}In$ and $^{109}Ag(\alpha,n\gamma)^{112}In$ Reactions

The decay scheme of ^{112}In for levels below 1.0 MeV of excitation derived from the results of both reactions is shown in Fig. A1-g9. (A multitude of levels are seen between 1.0 and 1.7 MeV excitation. However, only the 1284 keV level has been included for use in this figure for reasons discussed later.) Most of the

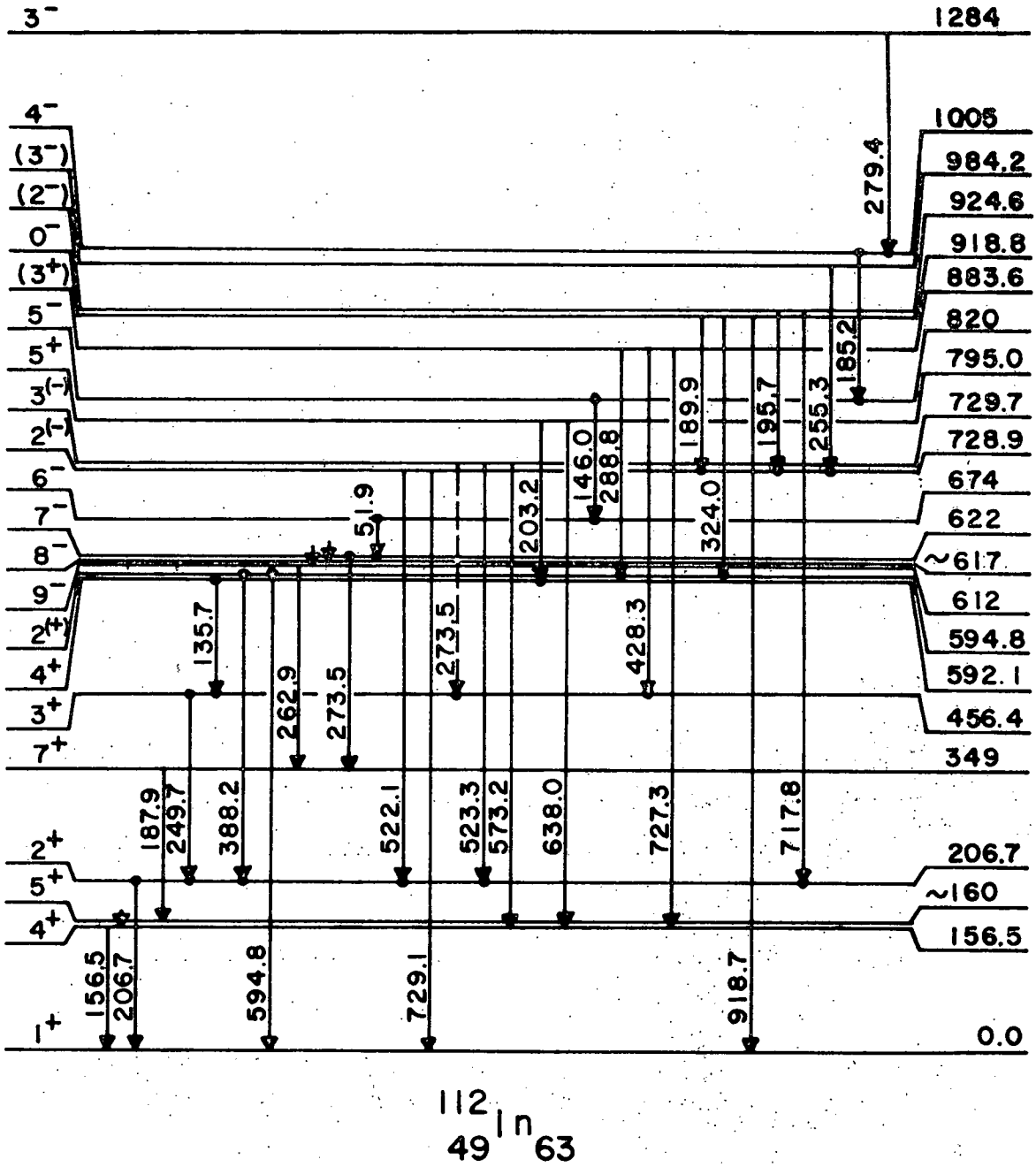

$^{112}_{49}In_{63}$

Fig. A1-g9. Abbreviated decay scheme of ^{112}In. Filled circles indicate observed γ-ray coincidences. Unterminated arrows indicate suspected unobserved (<10 keV) transitions between adjacent levels.

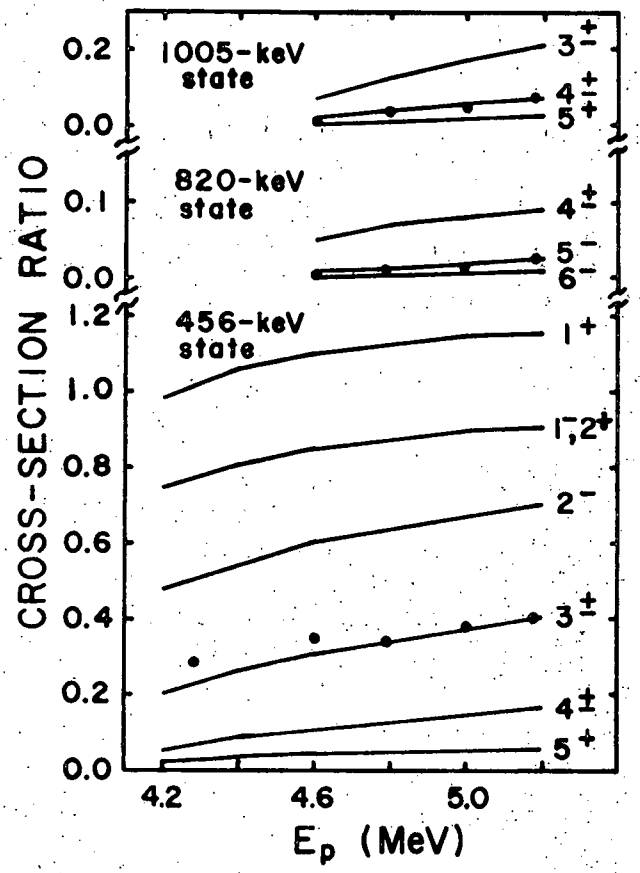

Fig. A1-g10. Examples of cross section ratios determined from the excitation functions measured using the $^{112}Cd(p,n\gamma)^{112}In$ reaction. The ratios are taken with respect to the 2^+ 206.7 keV state. Theoretical statistical compound-nuclear predictions (which depend on the spin and parity of the final state) of these cross section ratios are shown as continuous lines. The errors associated with the data points are on the order of the size of the data.

spin-parity assignments presented in the figure are based upon the comparison of the $^{112}Cd(p,n)^{112}In$ excitation functions with Hauser-Feshbach statistical compound-nuclear calculations in conjunction with the γ-ray angular distribution measurements for both reactions. Three typical examples of these excitation functions are shown in Fig. A1-g10. The 7^+ assignment to the 348 keV state is based upon the E2 nature of the 187.8 keV γ-ray[1] and its surmised feeding to the 5^+ state at approximately 160 keV. The existence of this 5^+ state was previously unknown and it was therefore assumed that the 187.8 keV γ-ray fed the known 4^+ isomer at 156.5 keV. This assumption resulted in a 6^+ assignment to the 348 keV state. Such a 6^+ assignment is now untenable. The energy separation of the 156.5 keV and 160 keV levels cannot be measured accurately and therefore has been estimated to be approximately 3-5 keV from peak shapes observed in the $^{113}In(p,d)^{112}In$ reaction. The 160 keV state is assumed to decay via an unobserved M1 transition to the 156.5 keV isomer.

The 611 keV state, which was previously assigned 8^- because of the M2 262.8 keV γ-ray that feeds the 348 keV state,[1] must now be assigned 9^-. This assignment causes some difficulty because of two reasons. First, the cascade of γ-rays believed to come from negative parity levels which ultimately feed into the 9^- state are observed with the $^{112}Cd(p,n\gamma)$ reaction which, at a proton energy of 5.17 MeV will excite 6^- and higher spin levels with negligible cross section. The cascade must therefore reach to at least 4^- and 3^- states in order to obtain the observed relative cross sections. Secondly, the angular distribution of the 273.5 keV γ-ray believed to feed the 7^+ 348 keV state out of the negative parity cascade, is compatible only with a pure E1 $\Delta I=0$ transition. The 622 keV level must therefore be 7^-. Since much of the cascade intensity bypasses the 273.5 keV transition, and yet finds its way to the 9^- state, unobserved low energy and relatively rapid ($\sim$several nsec) M1 transitions must occur through an intermediate 8^- state. Although this situation is unfortunately not directly provable, it is the only way to explain adequately all the observed data. As a possible answer to this predicament, we have undertaken the study of the $^{110}Cd(\alpha,d)^{112}In$ reaction in the hope that the 10^-, 8^-, 6^- and 4^- states of this cascade, which are favored by the (α,d) reaction, can be identified unambiguously.

Analysis and interpretation of the data are almost complete. When finished, the results of this research will be submitted for publication.

---

[1] M. Ionescu-Bujor, E. A. Ivanov, A. Iordachescu, D. Plostinaru and G. Pascovici, Nucl. Phys. A272 (1976) 1.

2. Gamma Ray Experiments and Beta Decay

a. Decay of ^{198}Au - W. W. Pratt (Pennsylvania State University)

The decay of ^{198}Au, via first forbidden β^- transitions, is known to populate the 0^+ ground state and two 2^+ excited states in ^{198}Hg. The log ft values of the $2^- \rightarrow 2^+$ nonunique transitions are 7.5 and 7.4; that of the $2^- \rightarrow 0^+$ unique transition is 11.2. An alternative mode of decay, which has not to date been observed, can take place by electron capture to the 0^+ ground state of ^{198}Pt. Broyles et al.[1] have searched for this transition by measuring Auger electrons in a magnetic spectrometer. Bashilov,[2] also using a magnetic spectrometer, has measured photoelectrons ejected from a thin radiator foil. Both of these experiments have led to negative results: in the first case, an upper limit of 5×10^{-3} ec/β^- was found, while in the second case an upper limit of 10^{-4} ec/β^- was found. The log ft value corresponding to the latter limit is 7.9.

We have employed a high resolution intrinsic Ge detector to search for the electron capture process through the detection of the Pt K_α x-rays. Sources of 20 μCi of ^{198}Au were prepared by bombarding high purity gold leaf with neutrons in the U.S.G.S. Triga reactor. Very light, thin samples (106 μgm, 135 μgm/cm^2) were used in order to minimize the production of Au x-rays from fluorescence in the source. The source was mounted in a graphite container of sufficient thickness to stop the β rays; the source container was placed at a distance from the detector which was chosen to give a high counting rate without degrading the resolution of the detector. The detector has a resolution of approximately 500 eV at an x-ray energy of 68 keV.

The spectrum in the region of interest is shown in Fig. A2-a1. The large peak at 68.89 keV is the $K_{\alpha 1}$ x-ray of Hg due to internal conversion of the 411 keV γ-ray which follows the β-decay of ^{198}Au. The weak peak at 66.99 keV is the $K_{\alpha 1}$ x-ray of Au due to fluorescence in the source. This region is shown on an expanded scale in the insert in Fig. A2-a1. The region in the spectrum at which the 65.12 keV x-ray of Pt due to electron capture would be expected to appear is indicated by an arrow. The data give no evidence for this x-ray. We estimate that its intensity must be less than 20% of the intensity of the Au fluorescence x-ray and less than 0.066% of the intensity of the Hg $K_{\alpha 1}$ x-ray. When the internal conversion coefficient, α_K=.030, of the 411 keV transition which gives rise to the Hg x-rays is taken into account, our data yield an upper limit of 2×10^{-5} for the e.c./β^- branching ratio in the decay of ^{198}Au. This is lower by a factor of 5 than previously reported limits. The corresponding value for the comparative half life is log ft > 8.6.

The limiting factor in our present failure to detect the electron capture process is the continuous background below the Hg K_α lines. This background is presumably due, for the most part, to the Compton tail of the 411 keV γ-ray which follows the ^{198}Au β-decay. We hope

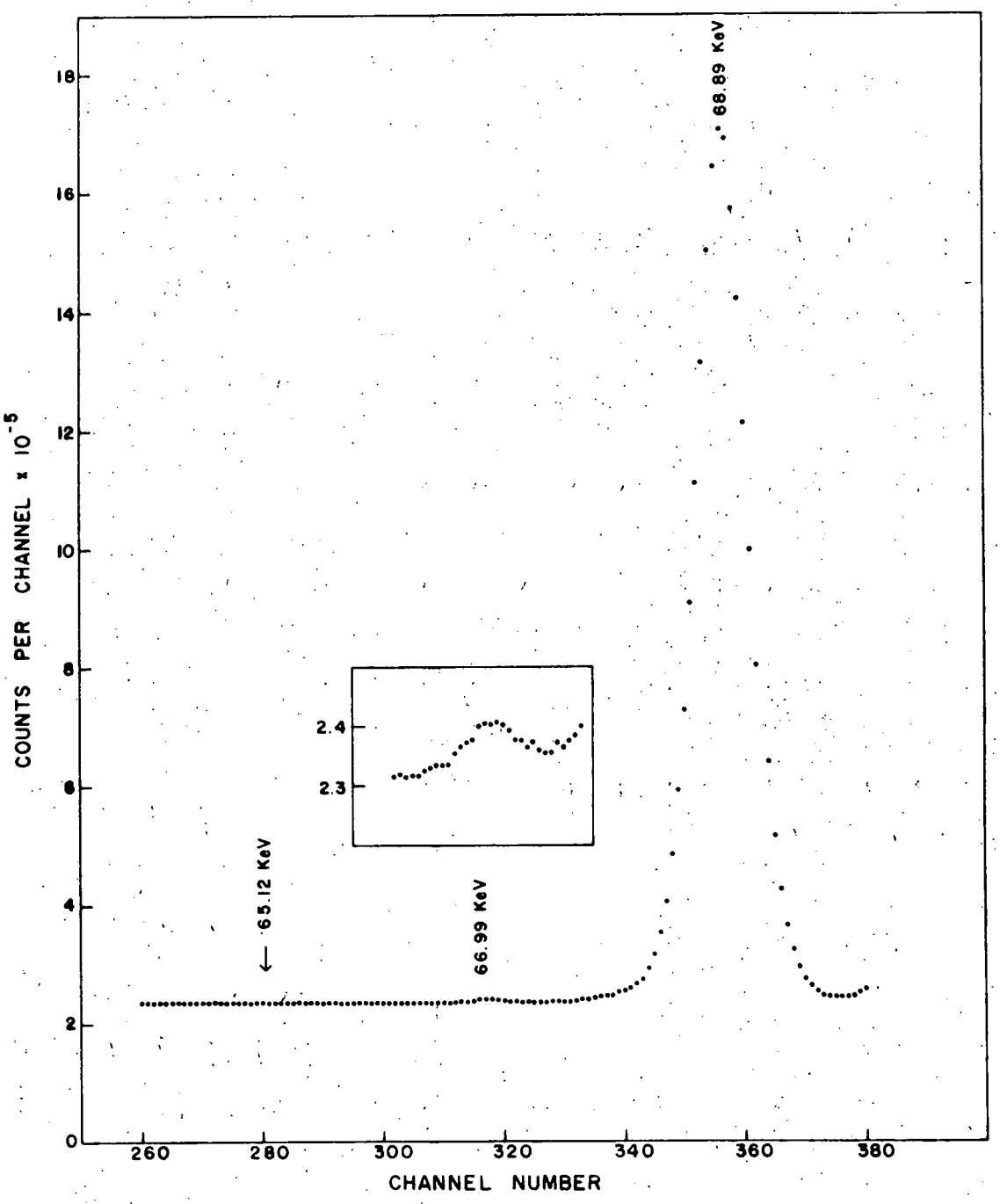

Fig. A2-a1. An x-ray spectrum observed for the decay of ^{198}Au. An upper limit of, 6 x 10^{-2} % was determined for a platinum x-ray at 65.12 keV as compared to the 68.89 keV x-ray of mercury.

at a future date to carry out a similar experiment in which the source is dissolved in a liquid scintillator from which pulses can be derived to feed an anticoincidence gate in the x-ray spectrum analyzer. Since each of the 411 keV γ-rays is accompanied by a β-ray, which would produce a pulse in the liquid scintillator, it should be possible with this arrangement to reduce the background substantially and to carry out a much more sensitive search for the x-rays associated with the electron capture process.

---

[1] C. D. Broyles et al., Phys. Rev. 89 (1953) 715.
[2] A. A. Bashilov, Nucl. Phys. 1 (1956) 629.

b. Levels of ^{106}Ag from the ^{103}Rh(α,nγ)^{106}Ag Reaction - L. E. Samuelson, R. A. Emigh, D. E. Prull, R. E. Anderson, J. J. Kraushaar and R. A. Ristinen

The γ-ray decay scheme of ^{106}Ag from the ^{103}Rh(α,nγ)^{106}Ag reaction at 16.7 MeV has been determined using two sets of γ-γ coincidence data. One set was taken with two small-volume, high-resolution HPGe detectors,[1] while the other set was taken with two large-volume Ge(Li) detectors.[2] In order to obtain accurate energies and relative intensities of the ^{106}Ag γ rays, spectra were measured (both with and without calibration sources) with both an HPGe detector (for low-energy γ rays) and a large volume Ge(Li) detector (for high-energy γ rays) placed at θ=55° with respect to the beam direction. In addition, angular distributions of γ rays having energies of less than 400 keV were taken with an HPGe detector at angles between 15° and 90° in roughly 10° steps. The properly normalized peak areas as a function of detector angle were fit by least squares analysis to the equation

$$W(\theta) = A_o[1 + a_2P_2(\cos\theta) + a_4P_4(\cos\theta)].$$

The A_o coefficient, when corrected for detector efficiency, provided an independent measurement of the relative γ-ray intensities determined above. Finally, since the bombarding α energy of 16.7 MeV is slightly above the (α,2n) threshold, a spectrum was also measured with an HPGe detector at 55° with an α bombarding energy of 13.4 MeV. This measurement ensured correct identification of those ^{106}Ag γ rays which have energies below 400 keV. The results of all of these measurements for γ rays appearing in the decay scheme below 550 keV of excitation are summarized in Table A2-bI.

An abbreviated γ-ray decay scheme of ^{106}Ag to an excitation of 550 keV is presented in Fig. A2-b1. The spin and parity assignments presented are based upon the γ-ray angular distribution results used in conjunction with the results of Anderson et al.,[3] who studied the ^{104}Pd(^{3}He,p)^{106}Ag, ^{105}Pd(^{3}He,d)^{106}Ag and ^{107}Ag(p,d)^{106}Ag reactions. The energy of the 8.4-day 6^+ isomer has been deduced from level energies determined in the ^{105}Pd(^{3}He,d)^{106}Ag reaction and γ-ray decay energies of levels

Table A2-bI

Energies, relative intensities and angular distribution coefficients of some γ rays from the $^{103}Rh(\alpha,n\gamma)^{106}Ag$ reaction. The angular distributions were measured with E_α=16.7 MeV.

E_γ(keV)[a]	I_γ(13.4 MeV)	I_γ(16.7 MeV)	a_2	a_4
87.3	46.8(14)	51.0(14)	-0.189(10)	0.029(14)
95.2	459 (12)	482 (13)	-0.107(6)	0.006(8)
110.6	≡1000	≡1000	-0.098(6)	0.010(9)
113.8[b]	38.8(12)	46.8(14)	-0.159(10)	0.034(14)
139.4	8.1(10)	7.0(5)	0.027(51)	c)
147.9	12.8(10)	11.6(6)	0.145(19)	0.002(27)
153.8	79.6(24)	114.3(31)	-0.359(7)	0.012(10)
154.4[b]	93.3(28)	100.2(28)	-0.108(6)	0.008(8)
158.5	15.2(11)	18.7(8)	0.169(25)	0.030(36)
209.8	7.0(14)	20.4(11)	-0.165(33)	0.06 (5)
213.5[b]	9.2(16)	11.8(10)	0.035(42)	c)
219.1	16.6(16)	13.8(11)	0.06(5)	c)
234.7	61.2(24)	55.8(19)	-0.133(18)	0.016(26)
239.2	198 (6)	268 (7)	-0.103(7)	0.013(11)
243.0[b]	272 (7)	523 (13)	-0.325(5)	0.010(8)
253.8	215 (6)	248 (7)	-0.151(5)	0.005(8)
277.1	403 (11)	356 (9)	-0.092(9)	0.008(12)
278.5	79.8(33)	81.4(28)	-0.080(17)	-0.022(25)
297.0	12.0(22)	34.9(21)	0.002(37)	c)
305.9	27.6(28)	22.9(22)	0.020(61)	c)
312.3	13.2(29)	21.2(20)	-0.10 (6)	c)
314.4	69.8(35)	49.1(24)	0.103(29)	-0.04(4)

a) Errors are ±0.1 keV.

b) Unresolved doublets.

c) Fit with a_4≡0.0.

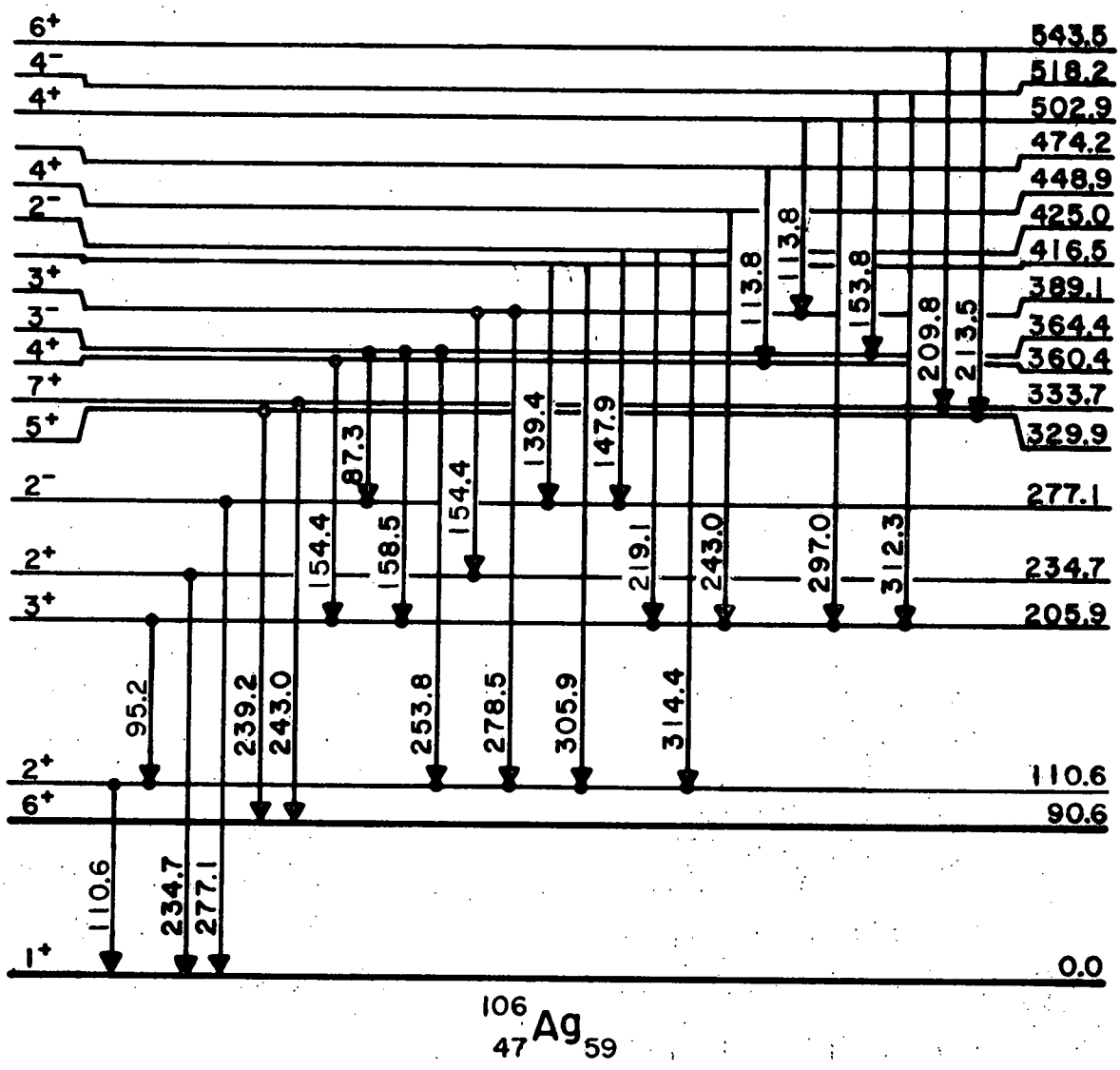

Fig. A2-b1. Abbreviated γ-ray decay scheme of ^{106}Ag from the ^{103}Rh(α,nγ)^{106}Ag reaction at 16.7 MeV. Solid circles indicate observed γ-ray coincidences.

which directly feed the ground state and this isomer. The 275 (1)-keV state seen by Anderson et al.[3] must be the 277.1-keV state (which feeds the ground state) observed here, while the 330 (1) keV state[3] is most certainly a "weighted" average of the 329.9- and 333.7-keV states. Both of these latter states should be excited in the ^{105}Pd(^{3}He,d)^{106}Ag reaction and apparently are, as evidenced by the rather large observed spectroscopic strength.[3] Using 1) the energy difference of 2.1 keV between 275 and 277.1 keV to correct 330 to 332.1 keV, 2) the energy difference of 3.8 keV

between the 239.3 and 243.1 keV γ rays and a 2J+1 weighting of individual centroids to calculate the energies of the individual levels (329.9 and 33.7 keV), and 3) the energies of the decay γ rays, we obtain the value 90.6±1.5 for the isomer energy. This energy is surprisingly close to the value of 85±2 keV deduced by Anderson et al.[3] strictly from charged particle work.

These results are being prepared for publication.

---

[1] University of Colorado Technical Progress Report (1976) p. 84.
[2] University of Colorado Technical Progress Report (1975) p. 70.
[3] R. E. Anderson, R. L. Bunting, J. D. Burch, S. R. Chinn, J. J. Kraushaar, R. J. Peterson, D. E. Prull, B. W. Ridley and R. A. Ristinen, Nucl. Phys. A242 (1975) 93.

c. Multiplet Structure of ^{88,86}Y - W. W. Pratt, C. A. Fields, J. J. Kraushaar, R. A. Ristinen, M. E. Burroughs and L. E. Samuelson

The nucleus ^{88}Y has been studied by both direct reactions and gamma-ray methods. The structure of ^{86}Y is, however, almost completely unknown. A study has been undertaken to clarify the multiplet structure of ^{88}Y, and discover the corresponding structure in ^{86}Y.

To date, the ^{86}Sr(p,nγ-γ)^{86}Y reaction at 14.3 MeV and the ^{85}Rb(α,3nγ-γ)^{86}Y reaction at 35.7 MeV have been studied. Pulsed-beam timing was done in each case, and γ-ray angular distributions were recorded for the ^{85}Rb(α,3nγ) reaction. The data analysis is currently in progress.

The ^{88}Sr(α,d)^{88}Y reaction will be done at 35 MeV to investigate high-spin proton-neutron states. The ^{85}Rb(α,nγ)^{88}Y reaction will be repeated, and the resulting gamma rays observed with a HPGe detector. The main purpose of this experiment will be the determination of the 6^+-7^+ separation.

The ^{86}Y nucleus will also be studied using the ^{86}Sr(^{3}He,t) reaction. Since angular distributions from this reaction often do not conform well to distorted-wave calculations, the angular distributions for known states observed by the ^{88}Sr(^{3}He,t)^{88}Y and ^{90}Zr(^{3}He,t)^{90}Nb reactions will be used to identify ℓ-transfers. An in-beam conversion-electron study of ^{86}Y is also planned. Where possible, the g-factors of long-lived states will be measured by the proton pulsed-beam PAD method.

d. The $[\pi(g_{9/2})\nu(g_{9/2})^{-1}]_{9^+}$ and Higher-Spin States in ^{90}Nb - C. A. Fields, J. J. Kraushaar, R. A. Ristinen and L. E. Samuelson

The $^{89}Y(\alpha,3n\gamma)^{90}Nb$ reaction was studied at 35.7 MeV. The location of the 9^+ member of the $\pi(g_{9/2})\nu(g_{9/2})^{-1}$ multiplet was clarified, and two previously unobserved higher spin states were found.

Gamma-gamma coincidence measurements were made at 20 ns FWHM time resolution using a Ge(Li)-Ge(Li) detector configuration. Angular distribution measurements were made with Ge(Li) and HPGe detectors at 10 angles between 15° and 90° to the incident beam directions. The tentative level scheme and J^π assignments resulting from this study are shown in Fig. A2-d1.

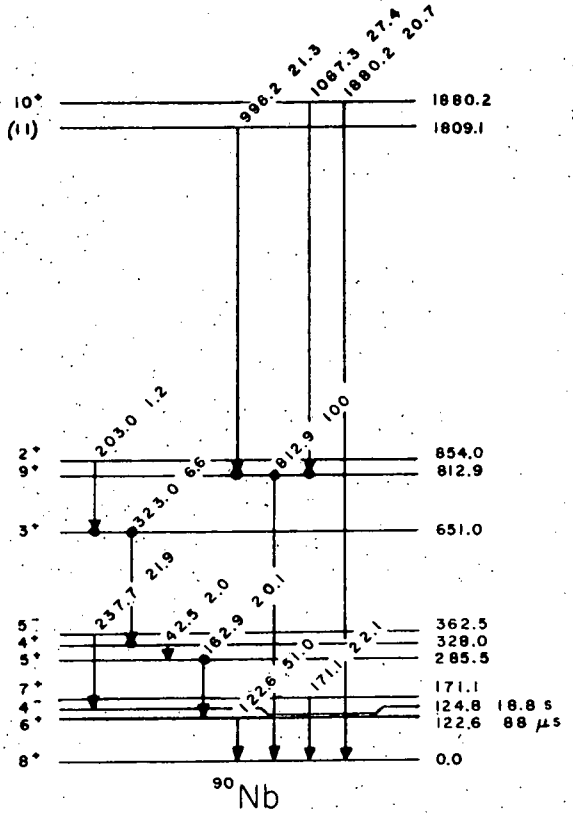

Fig. A2-d1. A partial level scheme for ^{90}Nb deduced from data of this experiment and previous work.

Previously unreported gamma rays of energies 812.9 keV, 996.2 keV, 1067.3 keV and 1880.2 keV were observed. These transitions establish levels at 812.9 keV, 1809.1 keV, and 1880.2 keV. Analysis of the angular distributions and the experimental upper limits which can be placed on branching ratios from these states suggest the assignment of $J^\pi=9^+$ to the 812.9 keV level, 10^+ to the 1880.2 keV level and perhaps J=11 to the 1809.1 keV level.

Several gamma rays reported[1] to be observed in the $^{90}Zr(p,n\gamma)^{90}Nb$ reaction were also observed in this study. The

angular distributions measured in this experiment support the J^{π} assignments made in the earlier work.

With the observation of the 812.9 keV gamma ray from the 812.9 keV 9^+ state, the energies of all of the states thought to comprise the $\pi(g_{9/2})\nu(g_{9/2})^{-1}$ multiplet are known to considerable accuracy. The energy of this 9^+ state is in reasonable agreement with energies previously measured by the $^{90}Zr(^3He,t)^{90}Nb$ [2] and $^{92}Mo(d,\alpha)^{90}Nb$ [3] reactions of states thought to be the 9^+ member of this multiplet.

A recent shell model calculation[4] predicts 10^+ and 11^- states in ^{90}Nb at 2.0 MeV and 1.8 MeV, respectively. These predicted energies are in good agreement with the energies measured in this study for the 10^+ and possible $11^{\pm}$ states. These states may arise from coupling of a $g_{9/2}$ neutron hole to the 2330 keV $\pi(g_{9/2})^3$ $11/2^+$ state and the 2033 keV $\pi(g_{9/2})^2(p_{1/2})$ $13/2^-$ state in ^{91}Nb,[5] respectively.

---

1 Yoshida et al., Nucl. Phys. A187 (1972) 161.
2 Bearse et al., Phys. Rev. Lett. 23 (1969) 864.
3 Comfort et al., Phys. Rev. C 10 (1974) 2399.
4 Serduke et al., Nucl. Phys. A251 (1976) 45.
5 Balanda et al., Acta Phys. Pol. B7 (1976) 355.

e. High-Spin States Above 3.5 MeV in ^{91}Nb - C. A. Fields, J. J. Kraushaar, R. A. Ristinen and L. E. Samuelson

The $^{89}Y(\alpha,2n\gamma)^{91}Nb$ reaction has been studied at 24.0 MeV and 35.7 MeV bombarding energy. Gamma-gamma coincidence data was taken at both beam energies, and γ-ray angular distributions were recorded using the 35.7 MeV beam. A large number of γ rays were observed at 35.7 MeV which were not seen with significant intensity at 24.0 MeV.

The results of our coincidence measurements at 24.0 MeV confirm the known structure of ^{91}Nb below 3.5 MeV excitation.[1] The results of the 35.7 MeV experiment are shown in Fig. A2-e1. The levels at 4097.0 and 4351.3 keV have been previously reported and assigned J^{π} of $19/2^-$ and $21/2^-$ respectively.[1] Our measurements reveal a large (5.9%) quadrupole mixture in the 884.5 keV γ ray, therefore we assign $J^{\pi}=21/2^+$ to the 4351.3 keV state. Our data are consistent with either parity for the 19/2 state at 4097.0 keV. The remaining states above 3.5 MeV have not been previously reported. Spin and parity assignments are tenatively made on the basis of angular distribution measurements.

The high-spin states below 3.5 MeV in ^{91}Nb belong to the

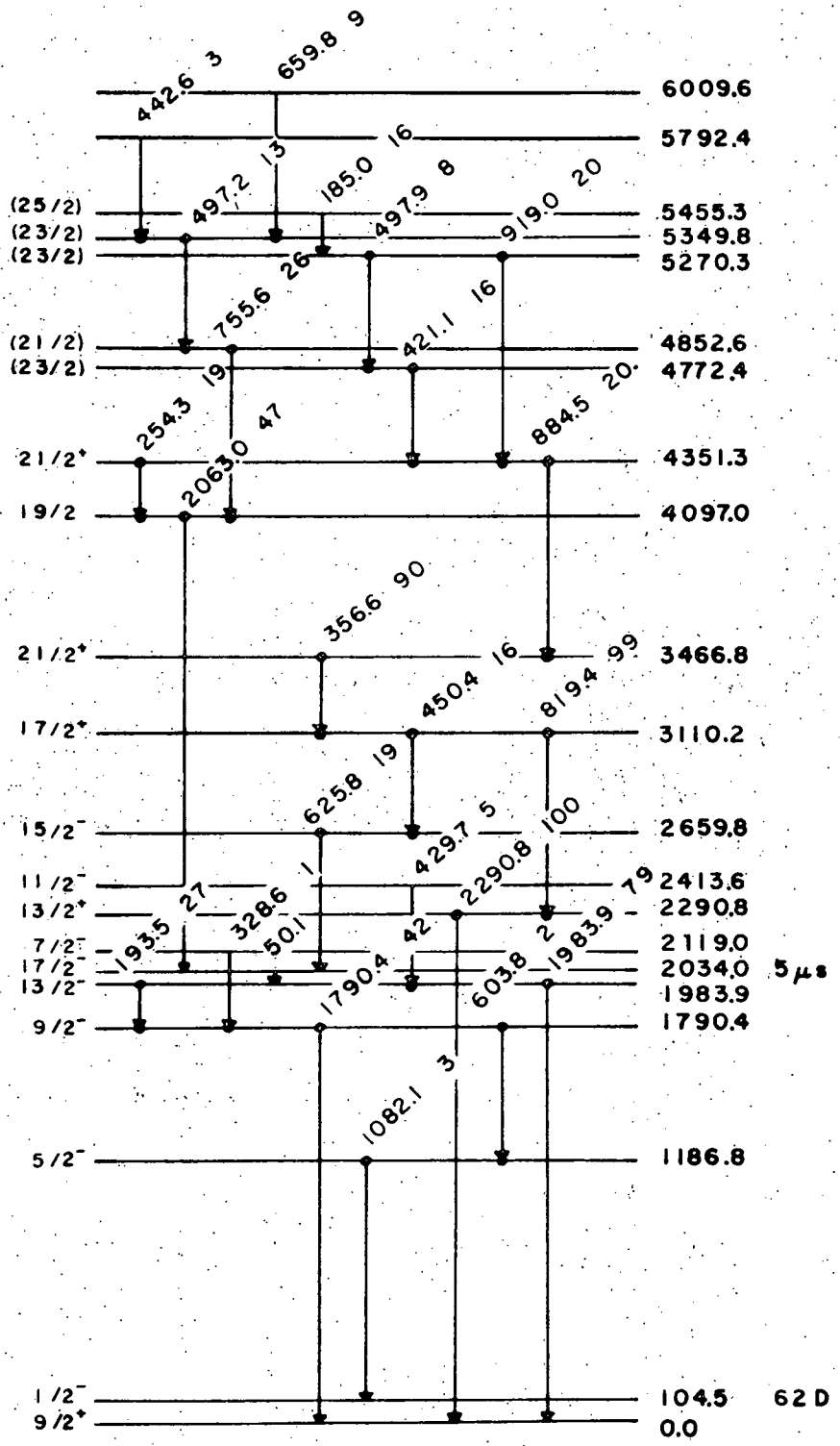

Fig. A2- 1. Gamma rays in ^{91}Nb observed with the ^{89}Y(α,2nγ) reaction at 35.7 MeV. Coincidence relations are shown by dots.

$\pi[p_{1/2}(g_{9/2})^2]$ and $\pi[g_{9/2}]^3$ multiplets. The energies of these states agree well with shell model calculations.[2] The high-spin structure of ^{92}Nb has been successfully described as the coupling of a $2d_{5/2}$ neutron to these two multiplets.[3] It is thus likely that the observed high-spin levels above 3.5 MeV in ^{91}Nb result from the coupling of $\nu[d_{5/2}(g_{9/2})^{-1}]$ to the observed proton structure.

---

1 Balanda et al., Acta Physica Polonica B7 (1976) 355.
2 Gloeckner and Serduke, Nucl. Phys. A220 (1974) 477.
3 D. H. Gloeckner, Nucl. Phys. A253 (1975) 301.

f. The Level Structure of ^{90}Mo, ^{89}Mo and ^{88}Nb -
F. W. N. de Boer, C. A. Fields and L. E. Samuelson

Until now only a few investigations have been performed on the level structure of ^{90}Mo. Besides low spin states observed in the ^{92}Mo(p,t) reaction,[1] the ground state band was observed up to spin 8^+ in the ^{93}Nb(p,nγ) reaction.[2] No levels have previously been reported in ^{89}Mo and ^{88}Nb.

In order to obtain more information about the level structure of these isotopes the present investigation was initiated. Targets of enriched ^{90}Zr and ^{89}Y were bombarded with ^{3}He particles of 33, 38 and 43 MeV. Prompt γ-ray spectra (measured with a 20% Princeton-Gamma Tech Ge(Li) detector, FWHM: 1.8 keV at 1.3 MeV) were analyzed with the peak fitting program SPECFIT[3] using the CDC 6600 computer of NBS. By comparing the measured excitation functions of the γ-rays with calculated cross sections by ALICE[4] it has been possible to assign several γ-rays to either ^{90}Mo, ^{89}Mo or ^{88}Nb. The presence of ^{88}Nb, ^{89}Mo and ^{90}Mo decay lines in the spectra measured immediately after the irradiations supports the fact that levels in these nuclei have been populated. Strong transitions tentatively assigned to ^{88}Mo [5] can now unambiguously be assigned to ^{89}Nb. Gamma-gamma coincidence experiments, angular distribution and conversion electron experiments are underway.

---

1 E. J. Kaptein et al., Nucl. Phys. A260 (1976) 141.
2 M. Ishihara et al., Phys. Lett. 35B (1971) 398.
3 H. P. Blok et al., Nucl. Instr. and Meth. 128 (1975) 545.
4 M. Blann and F. Plasil, USAEC Report C3494-10 (1973).
5 R. Beetz et al., KVI (1976) Annual Report, p. 57.

3. Other Activities

a. Thick Target Measurement of Thermonuclear Reaction Rates - N. A. Roughton (Regis College), C. S. Zaidins, R. J. Peterson, C. J. Hansen (JILA) and M. S. Iverson (Univ. of Northern Colorado)

The measurement of thick target yields and the subsequent use of these experimental results to extract astrophysical thermonuclear reaction rates has continued throughout this year. As discussed in last year's progress report, the analysis of the proton induced reactions is complete and a summary paper and accompanying data were prepared for Atomic Data and Nuclear Data Tables. This work is essentially complete except for minor revisions in the format of the tables. The experimental work and major data analysis effort this past year have been in the area of ^{4}He-induced reactions. The approximately 30 reactions worked on to date are listed in Table II-3aI. The data, where complete, consist of tables of yield Y versus energy, thermonuclear reaction rate $N_A\langle\sigma v\rangle$ versus temperature, and the parameters of a least squares fit to the $N_A\langle\sigma v\rangle$ versus T_9 curves. This fit is of the form suggested by S. E. Woosley and discussed in last year's progress report.

Table II-3aI

^{4}He induced reactions for astrophysical thermonuclear reaction rate determinations from thick target yields

Target Nucleus	Ejectile	Residual Nucleus	Target Nucleus	Ejectile	Residual Nucleus
^{25}Mg	p	^{28}Al	^{58}Ni	p	^{61}Cu
^{26}Mg	p	^{29}Al	^{59}Co	n	^{62}Cu
^{27}Al	n	^{30}P	^{60}Ni	n	^{63}Zn
^{40}Cu	p	^{43}Sc	^{63}Cu	n	^{66}Ga
^{46}Ti	n	^{49}Cr	^{64}Zn	p	^{67}Ga
^{48}Ca	n	^{51}Ti	^{64}Zn	n	^{67}Ge
^{48}Ti	n	^{51}Cr	^{65}Cu	n	^{68}Ga
^{49}Ti	p	^{52}V	^{66}Zn	n	^{69}Ge
^{50}Ti	p	^{53}V	^{70}Zn	n	^{73}Ge
^{50}Cr	n	^{53}Fe	^{70}Zn	p	^{73m}Se
^{51}V	n	^{54}Mn	^{72}Ge	n	^{75}Se
^{53}Cr	p	^{56}Mn	^{74}Ge	n	^{77m}Se
^{54}Fe	p	^{57}Fe	^{76}Ge	n	^{79m}Se
^{54}Fe	n	^{57}Ni	^{92}Mo	n	^{95}Ru
^{55}Mn	n	^{58}Co	^{94}Mo	n	^{97}Ru
^{55}Mn	α,n	^{54}Mn	^{98}Mo	p	^{101}Tc
^{55}Mn	2n	^{57}Co			

In addition to the energy ranges previously studied, the yield measurements have been carried out at both lower and higher energies in order to extend the region of validity for $N_A\langle\sigma v\rangle$. At the lower energies, we are severely limited by low count rate problems and have turned out attention to a better extrapolation of the yields and cross sections to threshold. The higher energy measurements have greatly reduced the error in the high energy extrapolation of $N_A\langle\sigma v\rangle$.

The accurate evaluation of $N_A\langle\sigma v\rangle$ at low temperatures ($T_9 \leq 1$) requires experimental values of the reaction cross sections or yields as a function of energy measured as near to threshold as possible. In the expression

$$N_A\langle\sigma v\rangle \propto \int_{|Q|}^{\infty} \sigma E \exp(-E/KT)dE,$$

we have an integrand which maximizes as a function of E for a fixed value of T_9, and the value of E for which the integral is maximum may be very near the reaction threshold for low T_9. Practical considerations usually prevent good experimental measurements of yields near threshold, especially for (α,p) reactions where the exit channel Coulomb penetrabilities result in very low reaction cross sections. As an example, consider the reaction $^{58}Ni(\alpha,p)^{61}Cu$, $|Q| = 3.108$ MeV. At $T_9=1$, $E_o=4.281$ MeV and an extrapolated prediction of the cross section at this energy is 1.9×10^{-8} barns which, of course, will make measurements by beta-delayed gamma emission very difficult. A practical limit on measurements of (α,p) reactions is about 2 MeV above threshold, but for (α,n) reactions the situation is considerably better, to within a few hundred keV of threshold.

During the past summer, a very careful study of low energy cross section extrapolation forms was made. The forms finally chosen are for (α,p) reactions:

$$\sigma E = S'(0) \exp(-C(E-|Q|)^{n_1} - \alpha(E-|Q|)^{n_2}),$$

and for (α,n) reactions:

$$\sigma E = [E-|Q|]^{\frac{1}{2}} \exp[A + B(E-|Q|)^{n_3} + D(E-|Q|)^{n_4}].$$

In the above equations $S'(0), \alpha, A, B, D$ are obtained by linear least squares techniques with the exponents n_1, n_2, n_3, n_4 as predetermined parameters. The constant C can be calculated from first principles (the Gamow factor), or it can be determined by least squares. For the (α,p) form, n_1 and n_2 are generally taken to be $n_1 = -1/2$, $n_2=1$, after Howard *et al.*[1] In the (α,n) form, preference is given to positive fractional forms and to unity for n_3 and n_4 to prevent possible oscillations in the extrapolation of σE from the lowest measured values to threshold.

The form of σE suggested by Howard *et al.* is

$$\sigma E = A(E-|Q|)^{\frac{1}{2}} [1+B(E-|Q|)^m], \text{ with A, B, and m determined}$$

by least squares. A difficulty we find with this form is that it

requires non-linear least squares techniques. We have found this to be unnecessary by showing that our form for (α,n) can be used to calculate directly Howard's A, B, and m at two points where we have cross section data. This has been done for sample reactions available in Ref. 1.

To check on the accuracy of our extrapolations, we calculate $N_A\langle\sigma v\rangle$ and compare with the values given by Woosley et al.[2] This is a compendium of global calculations of cross sections on the Hauser-Feshbach scheme with rate calculations given primary emphasis. In some cases we find excellent agreement over a wide range of T_9, as shown in Table II-3aII. In other cases the agreement is not as striking and may differ from the work of Ref. 2 by factors of 2 to 5. What is significant here is that the agreement between our data and the calculations of Woosley et al. is as good as it appears to be.

Table II-3aII

Comparison of $N_A\langle\sigma v\rangle$ from this experiment with the predictions of Woosley et al.

	$^{58}Ni(\alpha,p)^{61}Cu$		$^{50}Cr(\alpha,n)^{53}Fe$	
T_9	This Experiment	Ref.2	This Experiment	Ref. 2
1	2.9×10^{-19}	2.23×10^{-19}	1.11×10^{-20}	1.66×10^{-20}
3	1.33×10^{-3}	1.2×10^{-3}	3.15×10^{-3}	2.84×10^{-3}
5	14.8	10.3	26.01	24.5

It must be remembered that calculations of cross sections rely heavily upon experimentally determined level density parameters and assumptions about spin and parity assignments in the level regions where continuum assumptions cannot be made. Our thick target techniques deal with average cross sections and can be expected to give the best possible confirmation of theoretical calculations based on the optical model. Probably the largest source of disagreement between our rates and those of Woosley et al. (aside from the inaccuracies in published branching ratios which trouble the experiment from time to time) lies in the reliance of the calculations of Ref. 2 upon published level densities. We have extended our measurements of thick target yields for (α,x) reactions to the limits of α energies of the cyclotron for the following reasons. Predictions of the rates at high T_9 ($\geq$10) require again knowledge of the cross sections or yields at Gamow peak energies which lie relatively high in energy, and the Gamow peak tends to become very broad with increasing E_o, resulting in an even more important contribution to the reaction yield from α's with high energies in the Boltzmann distribution. To produce an adequate experimental rate at high T_9 therefore requires

study of the reaction at high alpha energies. Other studies of the thick target yields at high energies should also allow us to extract level density parameters for use in Hauser-Feshbach calculations. This topic is currently under study.

In addition to the above work, we have attempted to improve our computer programs in the course of converting them from the old computer system (PDP-9) to the new system (PDP-11).

---

[1] A. J. Howard, H. B. Jensen, M. Rios, W. A. Fowler and B. A. Zimmerman, A.P.J. 188 (1974) 131.

[2] S. E. Woosley, W. A. Fowler, J. A. Holmes and B. A. Zimmerman, Orange Aid Preprint 422, Cal Tech 1975.

b. Fast Neutron Irradiation of Microvasculature - J. R. Fike, E. L. Gillette (Dept. of Radiology and Radiation Biology, Colorado State University), D. E. Prull and J. J. Kraushaar

The use of the laboratory's fast neutron irradiation facility for biological studies continued this past year. The main use was for the endothelial cell response study using single and split dose irradiations of the canine eye. The effects of this and other high linear energy transfer (LET) radiations is of major interest to those using such radiation for cancer therapy.

Surgically induced neovascularization in the avascular cornea was used to quantify the radioresponse of the microvasculature. Capillary endothelial cells have a slow rate of proliferation. The response of a slowly proliferating endothelial cell population was studied by irradiating prior to keratectomy. Once stimulated, the degree of neovascularization was quantified with a morphometric analysis.

A single dose response assay was performed by irradiating 48 hours prior to keratectomy. Forty eyes were randomly distributed into four dose groups receiving 100, 300, 500 and 700 rads of neutrons. There were 28 nonirradiated control eyes.

A split dose response assay was done using two experimental groups. Six eyes were given a single dose of 400 rads 48 hours prior to keratectomy. Eight eyes received two 200-rad doses separated by 24 hours, and keratectomies were done 24 hours after the second dose.

Individual data points from the 300 to 700 rad dose groups were used for a linear regression analysis. A "Do" of 200 rads, which represents the dose required to reduce the percent capillary volume by 63%, was derived from the inverse slope of the regression line. RBE (relative biological effectiveness) values, comparing the neutron single close response with a ^{60}Co gamma ray dose response curve

reported previously,[1,2] were calculated at the 1, 2 and 3% capillary volume levels to be 1.9, 2.1 and 2.3, respectively.

For the split dose study, a mean percent capillary volume was determined for each of the two treatment groups. Dose response curves with slopes equal to that determined in the single dose response assay were drawn through each point. A recovery D_2-D_1 of 130 rads was calculated using the regression parameters and the mean percent capillary volume values. This is a factor of 2 less than that reported for capillary endothelial cells exposed to ^{60}Co gamma rays using the same assay system.[3] The magnitude of recovery is in agreement with that observed in other normal tissues.[4]

The results of these studies indicate that the capillary endothelial cells of the limbal microvasculature are significantly more sensitive to fast neutron irradiation than to ^{60}Co gamma rays. The RBE appears to increase with decreasing dose and some recovery after low doses is observed. The clinical significance of the low dose recovery versus the increasing RBE at lower doses will remain unclear until adequate multifraction studies are completed.

---

1 J. R. Fike, E. L. Gillette, D. E. Prull and J. J. Kraushaar, University of Colorado Technical Progress Report (1977) 99.

2 J. R. Fike and E. L. Gillette, Int. J. Radiat. Onc. Biol. Phys., accepted for publication.

3 J. R. Fike, E. L. Gillette and D. J. Clow, Int. J. Radiat. Onc. Biol. Phys., submitted for publication.

4 S. B. Field and S. Hornsey, Europ. J. Cancer 7 (1971) 161.

c. Proton Spectrum Analysis by Thick Target Radioactivation - T. Intrator, R. J. Peterson, N. A. Roughton and C. S. Zaidins

This idea was first described in the 1977 Progress Report. The (p,n) thick target yields rise steeply above threshold, and for a mixed isotopic target representing a range of thresholds, an examination of the various yields can provide a histogram representation for the incident proton spectrum. This method works well because the steep rise in yield just above threshold sharply delineates energy bins on the histogram. Only very coarse methods of radioactivation analysis are presently being used.

Thick target yields for (p,n) reactions up to 27 MeV proton energy (lab) have been obtained on targets of natural calcium, copper and zinc. These allow histograms to be generated with the lowest boundary near 1 MeV and the highest near 6 MeV. Sample yield curves are shown as Figs. A3-1, A3-2, A3-3 and A3-4.

These thresholds are probably not sufficiently high for the accurate measurement of the highest energy protons from collective acceleration schemes.[1] We have not yet decided on a candidate

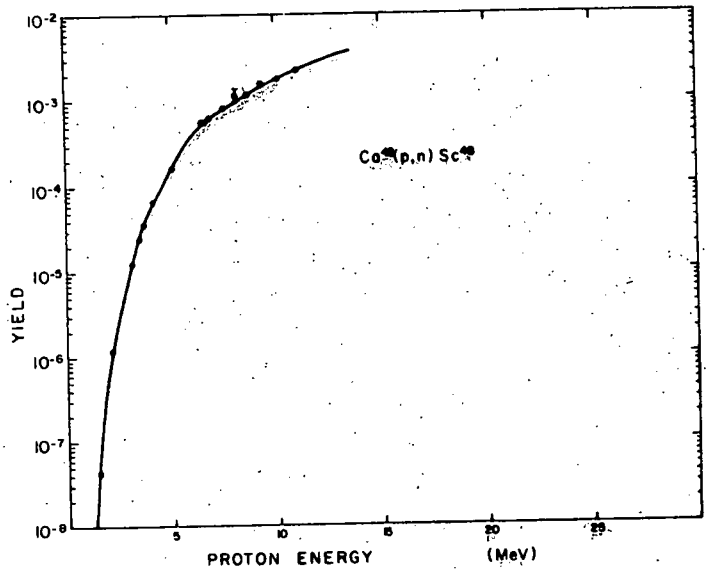

Fig. A3-1. Relative yield curve for the reaction $^{48}Ca(p,n)^{48}Sc$. The threshold proton energy is -0.49 MeV. Error bars are smaller than data points unless shown

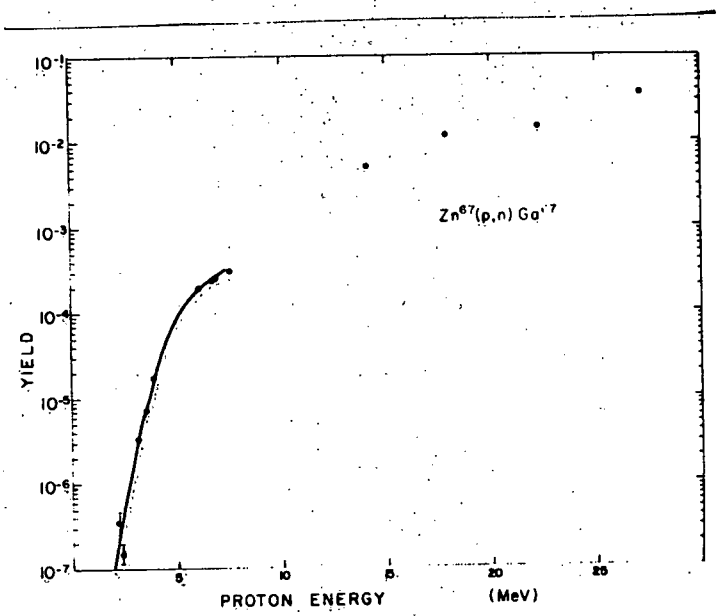

Fig. A3-2. Relative yield curve for the reaction $^{67}Zn(p,n)^{67}Ga$. The threshold proton energy is -1.782 MeV.

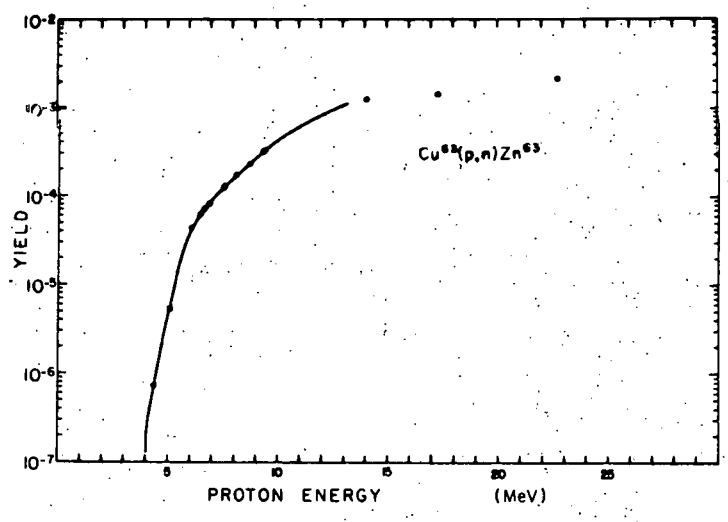

Fig. A3-3. Relative yield curve for the reaction $^{63}Cu(p,n)^{63}Zn$. The threshold proton energy is -4.114 MeV.

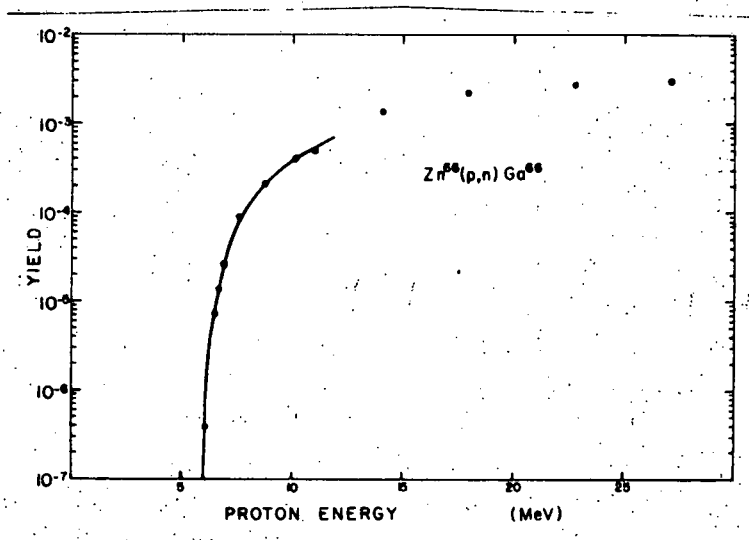

Fig. A3-4. Relative yield curve for the reaction $^{66}Zn(p,n)^{66}Ga$. The threshold proton energy is -5.957 MeV.

reaction for higher energy measurements above 10 MeV, if these prove to be necessary.

A least squares program has been constructed to provide the histograms, but data analysis is not complete.

---

[1] C. W. Robertson et al., Phys. Rev. Lett. 36 (1976) 1457.

d. Production of ^{209}Po via the $^{209}Bi(p,n)$ Reaction - M. L. Gartner, A. B. Phillips, P. A. Smith; E. A. Martell and S. A. Poet (NCAR-Boulder)

Two separate samples of ^{209}Po were produced for the research program of Dr. E. A. Martell of the National Center for Atmospheric Research. They will be used as calibration standards in the study of the mutagenic effects of α radiation.

Thin ^{209}Bi targets on silver backings were used for the production. Each of the targets was approximately 1 cm in diameter and weighed 300 mg. They were mounted in the general purpose target box during the irradiation.

Protons of 9.4 MeV were used for each run; the current measured on the targets was 0.5 μamp. Total irradiation time for each target was 5.25 hours; there was no noticeable damage to the targets caused by the beam. Protons of 9.4 MeV were used to eliminate production of the unwanted ^{208}Po (the threshold for the $^{209}Bi(p,2n)^{208}Po$ reaction is 9.7 MeV) and the thin targets were used to eliminate as much as possible production of ^{210}Po, also an unwanted product, via the $^{209}Bi(p,\gamma)$ reaction.

In each run 2.5 nC of ^{209}Po were produced. No ^{208}Po was produced and virtually no ^{210}Po was produced. The predicted yield of ^{209}Po was approximately 4 nC for each run. This prediction was based on a simple numerical integration using the measured $^{209}Bi(p,n)$ cross section.[1]

---

[1] C. G. Andre et al., Phys. Rev. 101 (1956) 645.

4. X-ray Fluorescence Analysis of Trace Elements - C. A. Crouch, H. Kubo, J. A. Mulvaney, W. R. Smythe and J. W. V. Trish

The major activity in this area has been the NIH sponsored studies of trace element abnormalities in chronic uremia. Autopsy tissue samples have been analyzed from three groups: controls, non-dialyzed uremic patients, and dialyzed uremic patients. The ready availability of the artificial kidney in the United States has made it difficult to obtain an adequate sampling of autopsy tissues from non-dialyzed uremic patients. However, we have been fortunate to have the collaboration of Dr. Peter Craswell of the Royal Brisbane Hospital in Australia, where such tissues are available. Analysis of a large set of Australian tissues from the three groups mentioned is nearing completion. A number of trace element abnormalities which we previously observed in dialyzed uremic patients and presumed to be the result of dialysis, are actually present in non-dialyzed uremic patients. Included in this class are: the general decrease in rubidium and the general increases in tin and strontium. Although there are reasons to believe that the rubidium and strontium abnormalities can be enhanced by use of the artificial kidney, it is now clear that all three of these abnormalities are produced by uremia alone.

The analysis of the Australian samples provided the opportunity to compare control populations between the two continents. The comparison showed that there were some very significant trace element differences between the two populations, the most striking being the elements selenium, bromine and rubidium. Table A4-I lists the average concentration and standard deviation of these three elements in tissues from these two groups. There were typically 16 individuals in the U. S. group and 21 in the Australian group. P is the probability that the difference is not significant, as determined by Student's t-test. On the average, selenium is 28% lower in the Australian tissues while bromine and rubidium are 86% and 96% higher, respectively. The next step is to determine if these trace element differences are caused by environmental factors. Analysis of meat and grain food samples from the two regions is in progress.

In addition to the above work, analytical assistance is being provided to the DOE sponsored study of the trace element problems which might occur with the establishment of an oil shale extraction industry. The primary problems under investigation include identification and study of trace elements which could be released during oil shale retorting operations and the investigation of elements which could be leached from the spent shale dump.

Table A4-I

A comparison of the concentration of selenium, bromine, and rubidium in autopsy tissue samples from Australia and the U.S. Average (±S.D.) concentration figures are given in μg/g on a dry weight basis. P is the probability that the two groups are not significantly different, as determined by application of Student's t-test.

Tissue	Selenium Average Conc. (ppm)			Bromine Average Conc. (ppm)			Rubidium Average Conc. (ppm)		
	U.S.	Aus.	P	U.S.	Aus.	P	U.S.	Aus.	P
Aorta	0.8±0.2	0.7±0.2	n.s.	52±18	76±25	<0.005	8±3	18±4	<0.001
Heart	1.5±0.3	1.1±0.2	<0.001	11±6	21±5	<0.001	16±3	33±7	<0.001
Kidney	4.5±1.4	3.4±0.7	<0.005	27±10	44±13	<0.001	18±8	32±9	<0.001
Liver	2.1±0.5	1.6±0.3	<0.001	9±6	18±5	<0.001	21±7	37±8	<0.001
Lung	1.3±0.3	1.0±0.2	<0.001	25±9	45±11	<0.001	15±5	29±4	<0.001
Muscle	1.4±0.3	0.7±0.2	<0.001	5±4	13±5	<0.001	19±6	37±8	<0.001
Spleen	1.7±0.5	1.1±0.2	<0.001	17±6	28±6	<0.001	20±7	39±8	<0.001

B. Intermediate Energy Physics

1. Observation of Enhanced Excitation of ^{12}C by Inelastic Pion Scattering on the 3-3 Resonance

R. L. Boudrie and R. J. Peterson; C. Fred Moore, W. Cottingame, K. G. Boyer, L. E. Smith, Carol Harvey and W. J. Braithwaite (Univ. of Texas); C. L. Morris, H. A. Thiessen and J. F. Amann (LASL); M. Devereux, G. Blanpied and G. Burleson (New Mexico State University); A. W. Obst, S. Iverson and K. K. Seth (Northwestern University)

Positive pion spectra taken with the EPICS system on ^{12}C show interesting structure at high excitations. Prominent peaks at 19.3, 20.6 and 21.6 MeV (with excitation energies uncertain to ±0.4 MeV) were observed to be larger at energies near 150 MeV than at lower or higher energies. Data were taken at fixed momentum transfer ($q=1.48$ fm^{-1}) at 100, 125, 162, 175, 225 and 291 MeV. At the highest energy, the three peaks were barely seen. An angular distribution at 162 MeV showed a structureless pattern, decreasing less strongly with angle than the cross sections to the 4.4 and 9.6 MeV states. The same peaks are also prominent in preliminary negative pion spectra.

Several states of ^{12}C are known to be in the vicinity of these peaks, and a scheduled run on EPICS in late September will provide better energy resolution to determine the nature of these states. The strongly resonant yield seen is a new effect, presumably related to the pion-nucleon 3-3 resonance in a more direct manner than that observed for the well-known, lower-lying states.

A report of this work has been submitted to Physical Review Letters.

2. New Proposals to LAMPF

R. J. Peterson

A proposal for $\pi^{\pm}$ inelastic scattering on ^{7}Li (#391) was submitted by R. L. Boudrie, J. J. Kraushaar, R. J. Peterson (spokesman) and R. A. Ristinen. The purpose of the experiment is to utilize the large neutron excess in the active p-shell nucleons to examine the role of isovector and isoscalar collective excitations. Very good shell model wave functions are also available for ^{7}Li, and tests of the sensitivity of pion scattering to several variables have been made.[1] This proposal has been granted 300 hours by the LAMPF PAC.

An EPICS proposal to search for giant resonance structure was prompted by the observation of a peak near 63 $A^{-1/3}$ MeV in ^{209}Bi, observed in 180 MeV positive pion scattering. This proposal (#423) was submitted by C. L. Morris and C. Fred Moore (co-spokesmen), H. A. Thiessen, R. L. Boudrie, J. F. Amann, W. J. Braithwaite, G. Burleson, R. J. Peterson, G. W. Hoffman and W. Cottingame, and will be considered at the next LAMPF PAC meeting.

---

[1] D. A. Sparrow, Nucl. Phys. A276 (1977) 365.

3. π^+ and π^- Inelastic Scattering from ^{18}O at 164 MeV and 230 MeV ~~(Exp. 14)~~[2] (Northwestern University; LASL, Univ. of Texas at Austin, Univ. of Colorado, University of Minnesota)

In an earlier version of this experiment[1] we found that the cross section for the excitation of the 1.98 MeV 2_1^+ state in ^{18}O by inelastic scattering of 230 MeV π^- was 1.66±.13 times larger than that for π^+ of the same energy. This was interpreted as indicating that the deformation length for neutrons was greater than that for protons, or $(\beta R)_n \cong 1.3\ (\beta R)_p$. Similar results were found for T_π=164 MeV. At the Zurich conference it was reported that at T_π =163 MeV the experiment has also been done with the SUSI spectrometer at SIN.[2] However, $\sigma(\pi^-)/\sigma(\pi^+)$ was found to be only 1.27±.04, i.e., completely consistent with a ratio of 1.25 expected if $(\beta R)_n=(\beta R)_p$. This disparity between our results and those of SUSI was found to be due to 40% to 50% differences in measured cross sections, both elastic and inelastic. Since the physical result claimed by us is of considerable nuclear structure importance, it was decided to repeat the entire experiment with certain improvements. The small He filled scattering chamber was replaced by a large vacuum scattering chamber. In addition to ionization chambers at 0° to monitor the pion intensity, a three element scintillation counter telescope at ∿30° was used to monitor beam-target interactions. The old ^{18}O (85% enriched) water + gelatine (5%) target was replaced by ^{18}O (94.9% enriched) ice targets of 0.31 and 0.55 gm/cm^2. Data were taken at 2.5° intervals from 17.5° to 80°. An energy resolution (FWHM)=425 keV at T_π=164 MeV and =475 keV at T_π=230 MeV was realized with the 0.31 gm/cm^2 target. Data were analyzed in 2° and 1° bins using the peak fitting program AUTOFIT. The 2_1^+ transition was successfully resolved over the entire angular range. The 3_1^- transition could not be resolved at the most forward angles. A peak was fitted in the 3.70 to 3.95 MeV excitation region in all spectra. At $\theta<40°$ the centroid of this peak was always at ∿3.9 MeV indicating that it is mainly due to the excitation of the level at 3.92 MeV. In the vicinity of 60° the centroid energy was ∿3.7 MeV indicating that near the minimum in the 2_2^+ distribution there is some contribution from the 4_1^+ level at 3.56 MeV.

The results from our new experiment are summarized in Table BI together with our published results[1] at 230 MeV from the first experiment. In summary, they are in excellent agreement with each other but in sharp disagreement with SIN results. We cannot speculate on the possible reasons for the discrepancy in the SIN results. We note that our cross section normalization is based on the well known π^+p cross sections. These were simultaneously measured in our experiment with the hydrogen in the target. We also note that there are obvious problems with the SIN cross sections for the 2_1^+ transition which show a monotonic rise from 30 to 14°, a behavior which is essentially impossible for an L=2 transition.

Since the present experiment fully verifies our published results

at 230 MeV, our conclusions about neutron and proton deformation parameters remain unaltered.

Table BI

Ratios $\sigma(\pi^-)/\sigma(\pi^+)$. Range of integration: Ref. 1, $\theta=30^\circ$ to 90° present, $=17.5^\circ$ to 80°.

T_π	Elastic	2_1^+(1.98 MeV)	2_2^+(4.9 Mev)+(4_1^+)	3_1^-(5.09)MeV
230 MeV (our)[1]	1.05±.05	1.66±.13		0.92±.08
230 MeV(present)	0.98±.04	1.57±.10	1.81±.15	0.96±.04
164 MeV(present)	1.09±.04	1.78±.10	1.71±.20	0.95±.04
164 MeV (SIN)[2]		1.27±.04		0.79±.03

[1] S. Iverson et al., Phys. Rev. Lett. 40 (1978) 17.
[2] E. Boschitz, Proc. 7th International Conference on High Energy Physics and Nuclear Structure, Zurich 1977, p. 133, also J. Jansen et al., SIN preprint, March, 1978.

4. Software Development - R. L. Boudrie, J. F. Amann, C. L. Morris, L. E. Smith, H. A. Thiessen (Los Alamos)

Work has been done to standardize the software for both HRS and EPICS in order to minimize the duplication of effort necessary to keep up two sets of software. This has involved a major internal restructuring of the HRS analyzer in a format closely resembling that of the EPICS analyzer. The chamber software has been modified to accommodate the newly installed drift chambers. The EPICS software for conversion from time differences to position coordinates has been adopted. Together, these have allowed for improved position and angular resolution in all coordinates.

Also included has been a set of EPICS routines which allow the formation of a polynomial in any of the calculated quantities, and the ability to modify both the coefficients and form of the polynomials on-line. This allows one to correct for higher order aberrations in the spectrometer. Central to the utility of this procedure has been the improvement of the program COFEPX (as described in last year's report) to determine automatically a set of coefficients which minimize such calculated quantities as the missing mass or scattering angle.

A large effort was also made to improve and write end-of-run processing programs for both on-line and off-line data reduction.

The amount of data collected at both HRS and EPICS is very large in a short period of time. It is important to have the software calculate "routine" quantities such as live time, chamber efficiencies, and kinematics for each run and then put them in a format that users of these facilities can understand. At the same time it is important to allow the user to do enough work so that he does not "lose touch" with the experiment and thus perpetuate some error throughout his data.

5. Vacuum Phototube Bases - R. L. Boudrie

Work was done in collaboration with the electronics division at LASL to build a photomultiplier base to work reliably in vacuum. The base allows resistor string currents of less than 200 μA for use with 9813B 14-stage EMI phototubes. The resistors are potted in thermally conducting epoxy (H70E) to maximize heat dissipation. For vacuum of less than 10 microns of Hg, there has been no evidence of high voltage breakdown. Some bases in use have survived with no apparent damage or loss in performance when the vacuum box was let up to air with high voltage still applied to the tubes.

These bases are useful at EPICS for veto counters between the dipole magnets. By putting the complete counter in vacuum no special coupling has to be built to allow movement of the counters to intercept more or less of the beam.

This base is also used for a scintillator at the focus of the quadrupoles of EPICS. For experiments where optimum resolution is not required, this scintillator can be moved into the beam and the TOF with the scintillators at the exit of the spectrometer is used to reject electrons. The time resolution of this scintillator system is no worse than that found with conventional phototube bases used in air.

6. Large Angle Proton Elastic Scattering - (Exp. 352/355) - R. L. Boudrie and UCLA, LASL, Univ. Minnesota and Univ. of Texas

Recent work has been done at HRS extending previous data of 800 MeV proton elastic scattering on ^{40}Ca and ^{208}Pb. This present work has extended the ^{40}Ca data to 46° c.m. and 42° c.m. for ^{208}Pb. The cross sections for both of these nuclei fall over 10 orders of magnitude from about 2° c.m. to these largest angles.

7. Elastic Scattering of Pions from ^{12}C - R. L. Boudrie and all EPICS collaborators

A large fraction of the development time at EPICS was spent in a careful study of $\pi^{\pm}$ scattering from ^{12}C at 162 MeV in order to understand normalization problems with EPICS and to compare directly with earlier data taken elsewhere. By using C_9H_{10} targets and

published cross sections for pions on hydrogen at 162 MeV, we compared C to H ratios for these targets for both species of pions. This exercise helped confirm our method of beam monitoring with ion chambers in the scattering chamber and secondary monitors at the pion production target.

With a primary proton beam of reduced intensity, we were able to go forward of 15^{o} lab and normalize to data taken with reduced pion channel acceptance. This kept dead times and efficiencies at manageable levels. Data were taken out to lab angles of 120^{o}.

The elastic scattering data are shown in Figs. B1 and B2 along with data taken at SIN. Rather good agreement has been obtained. The discrepancies are largely in the vicinity of the first minimum where the EPICS data show a slightly deeper minimum and at very large angles where the EPICS data are more nearly identical for π^{+} and π^{-}.

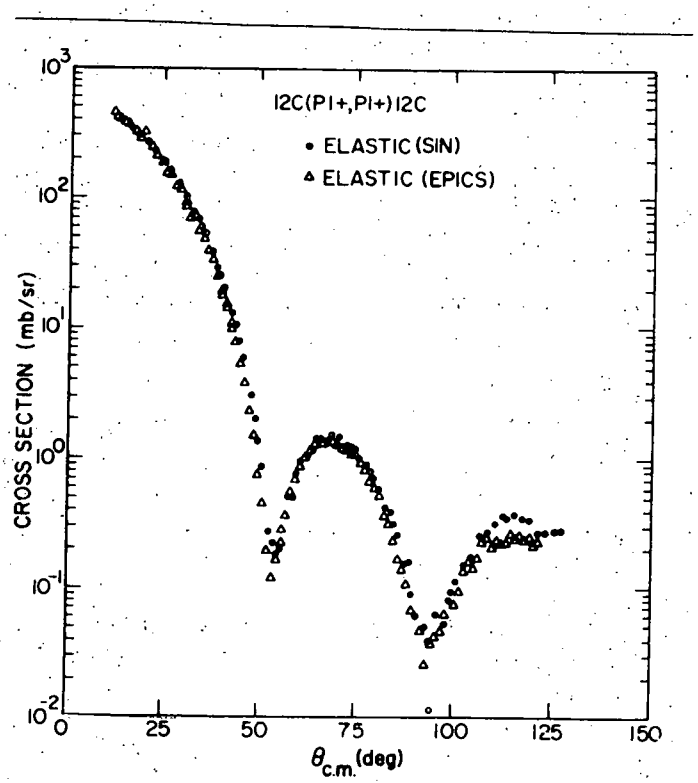

Fig. B1. A comparison of elastic scattering data for π^{+} on ^{12}C.

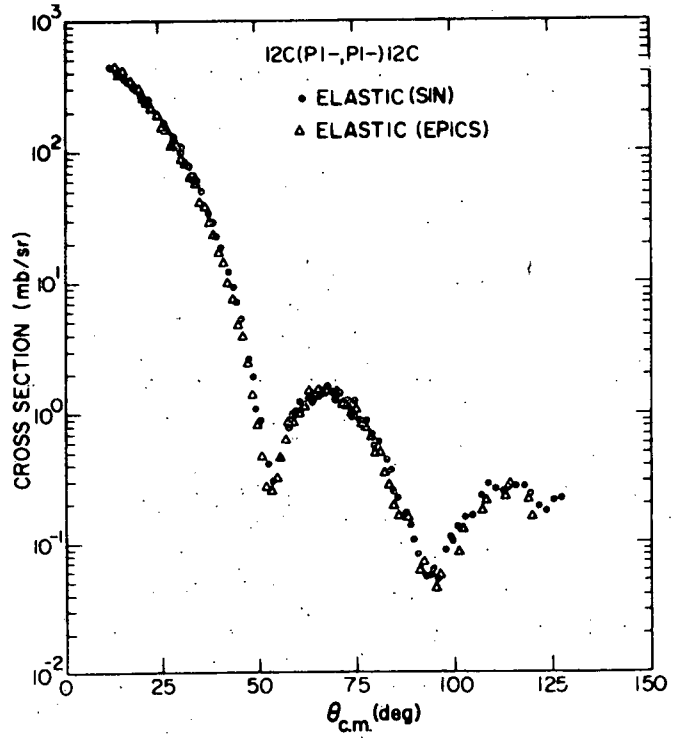

Fig. B2. A comparison of elastic scattering data for π^- on ^{12}C.

8. Pion Elastic Scattering on ^{9}Be, Si, ^{58}Ni and ^{208}Pb - R. L. Boudrie and ANL, LASL, New Mexico State Univ., Northwestern Univ., Oregon State Univ., and Kernfysisch Versneller Institut

The elastic scattering of 162-MeV π^+ and π^- by ^{9}Be, Si, ^{58}Ni and ^{208}Pb has been measured. The measured energy resolution, approximately 350 keV, is limited by target thickness but the energy resolution for all targets is more than adequate for completely resolving the ground-state from excited-state transitions.

The absolute cross sections shown in Fig. B3 are based upon comparison with pion scattering data from carbon given elsewhere in this report. The uncertainty in absolute cross sections is estimated to be less than ±10% and relative cross sections are accurate to better than ±5%, ignoring purely statistical errors. Pronounced oscillations characteristic of strong pion absorption are observed in the angular distributions for Si, ^{58}Ni and ^{208}Pb. The data for ^{9}Be, however, show relatively weak oscillatory structure.

Optical model calculations have been performed using the momentum-space elastic-scattering code PIPIT.[1] In Figs. B3 and B4 the solid lines are the result of calculations with the charge

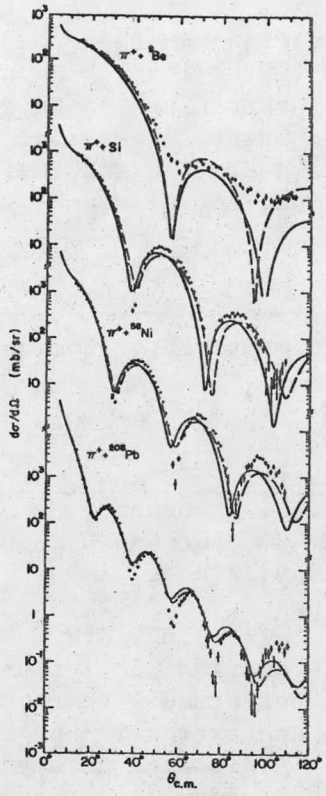

Fig. B3. Elastic scattering data for π^+ on targets of ^{9}Be, Si, ^{58}Ni and ^{208}Pb. The fits are discussed in the text.

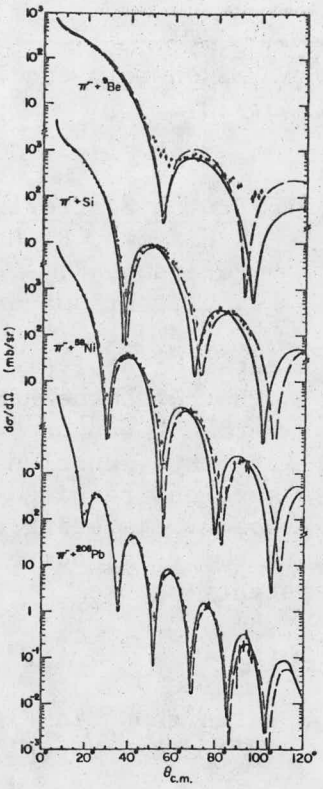

Fig. B4. Elastic scattering data for π^- on targets of ^{9}Be, Si, ^{58}Ni and ^{208}Pb. The fits are discussed in the text.

distributions determined by analyses of electron scattering with a correction for the finite charge radius of the proton. Better agreement with the data is obtained for Si, ^{58}Ni and ^{208}Pb when the rms radii were adjusted such that $\langle r^2 \rangle$ matter = $\langle r^2 \rangle$ charge - $\langle 1.3\ fm \rangle^2$. This is shown in the figures by the dashed lines. Equally satisfactory agreement is achieved, however, if the density distributions retain the values derived from electron scattering, but the calculations are performed for incident pions whose energies range from 5 MeV (Pb) to 12 MeV (Si) lower than in the actual experiment.

The results for ^{9}Be show evidence for quadrupole contributions to the elastic scattering. Inelastic scattering cross sections were obtained for both the $J^\pi = 5/2^-$ (2.43 MeV) and $7/2^-$ (6.76 MeV) members of the ground-state rotational band and showed strengths comparable to that of the elastic scattering. The relative intensities of these elastic states are consistent with assuming only quadrupole scattering. Several potentially important features have been neglected, of which the most obvious are the unusual

structure of ^{9}Be, and the possibilities of spin-flip transitions and coupled-channel effects.

The results of the elastic scattering on these nuclei at 162 MeV have been published (PRL 40 (1978) 1539). A paper showing the evidence for quadrupole scattering in ^{9}Be has been submitted to PRL. In addition, data exist for several inelastic states for these nuclei at 162 MeV and elastic and inelastic data have been obtained at 290 MeV incident pion energy. The results on this work will follow.

---

[1] R. A. Eisenstein and F. Tabakin, Comput. Phys. Commun. 12 (1976) 237.

9. Proton Scattering at 0.8 GeV from ^{89}Y and ^{90}Zr - N. J. DiGiacomo, R. L. Boudrie, J. J. Kraushaar, R. J. Peterson, R. A. Ristinen, E. S. Rost and G. R. Smith, and I. Brissaud (I.P.N., Orsay, France)

A detailed analysis of the ^{89}Y, ^{90}Zr (p,p') 0.8 GeV data taken last August with the HRS at LAMPF is nearing completion. Because the experiment was one of the first performed with the new HRS facility, the reduction of raw data and extraction of reliable cross sections required great care. A detailed documentation of the procedure is being compiled with particular emphasis being paid to empirical corrections, normalization questions, and consistency checks.

The Data

Spectra shown in Figs. B5 and B6 are, respectively, from the ^{90}Zr(p,p') and ^{89}Y(p,p') reactions at 18.5° lab with E_p=0.8 Gev.

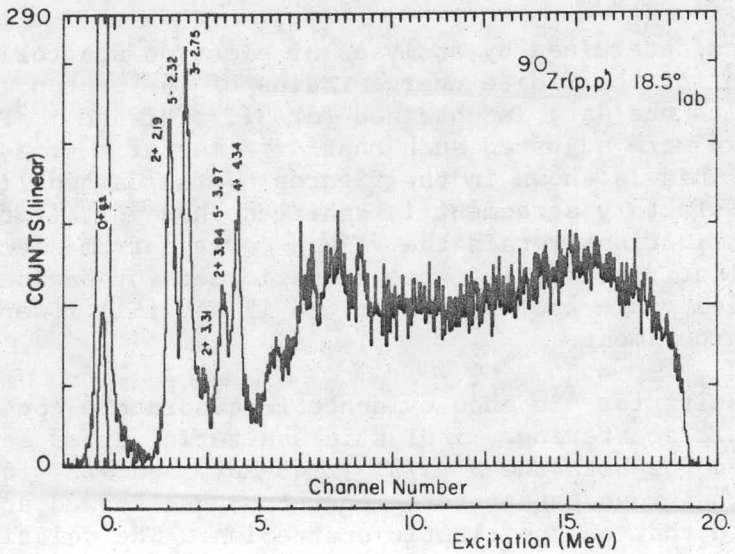

Fig. B5. Spectrum from 0.8 GeV proton scattering by ^{90}Zr at 18.5° (lab).

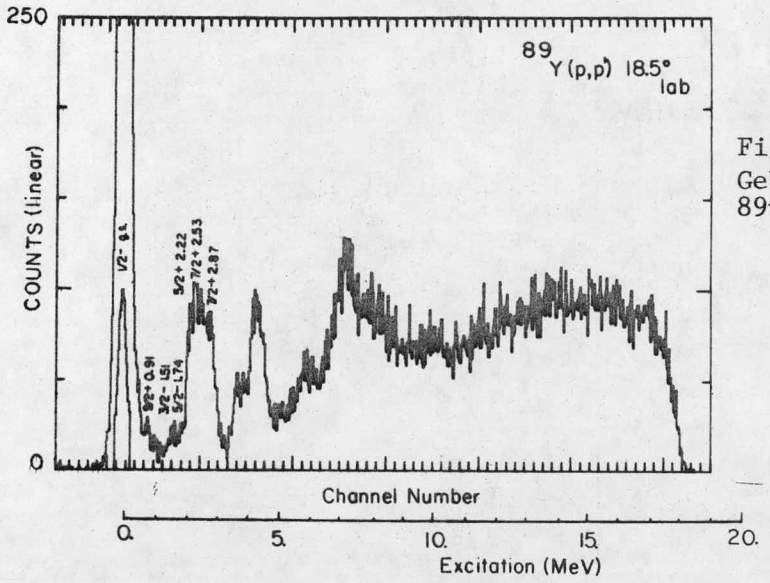

Fig. B6. Spectrum from 0.8 GeV proton scattering by ^{89}Y at 18.5^{o} (lab).

The energy resolution, typically 200 keV (FWHM) allows good resolution of the low-lying nuclear states. Angular distributions out to momentum transfers of 3.8 fm^{-1} for these states are shown in Figs. B7, B8 and B9. Elastic scattering angular distributions to similar momentum transfers are shown in Fig. B10. The elastic scattering polarization data of Fig. B11 for ^{90}Zr are due to Hoffman et al.[1]

Theoretical Analysis: Elastic Scattering

Much of the motivation for the construction of the HRS was based on the anticipation that 0.8 GeV protons would be a good probe of nucleon-nucleon interactions in nuclear matter. It was expected that the 0.8 GeV proton, with a wave length on the order of the internuclear separation (as opposed to, say, a 30 MeV proton with a wave length on the order of the size of the nucleus) would be sensitive to detailed nuclear structure in addition to gross nuclear size and shape. To test this hypothesis, ^{89}Y and ^{90}Zr, both with states known to be well described by simple shell model wave functions, were chosen as targets. In particular, the angular distributions of the $9/2^{+}$ state at 0.91 MeV in ^{89}Y is well described, as a result of reaction studies at lower energies, by a microscopic model where the excitation is due simply to the promotion of a $p_{1/2}$ proton to the $g_{9/2}$ shell. This angular distribution is distinctly different[2] from angular distributions of other states in ^{89}Y with the same (ℓ=5) ℓ transfer. It was hoped that the 0.8 GeV proton would be sensitive to these differences.

The data were analyzed in the Generalized Optical model. The coupling between the elastic and inelastic channels is, however, sufficiently weak that this approach is equivalent to the DWBA.

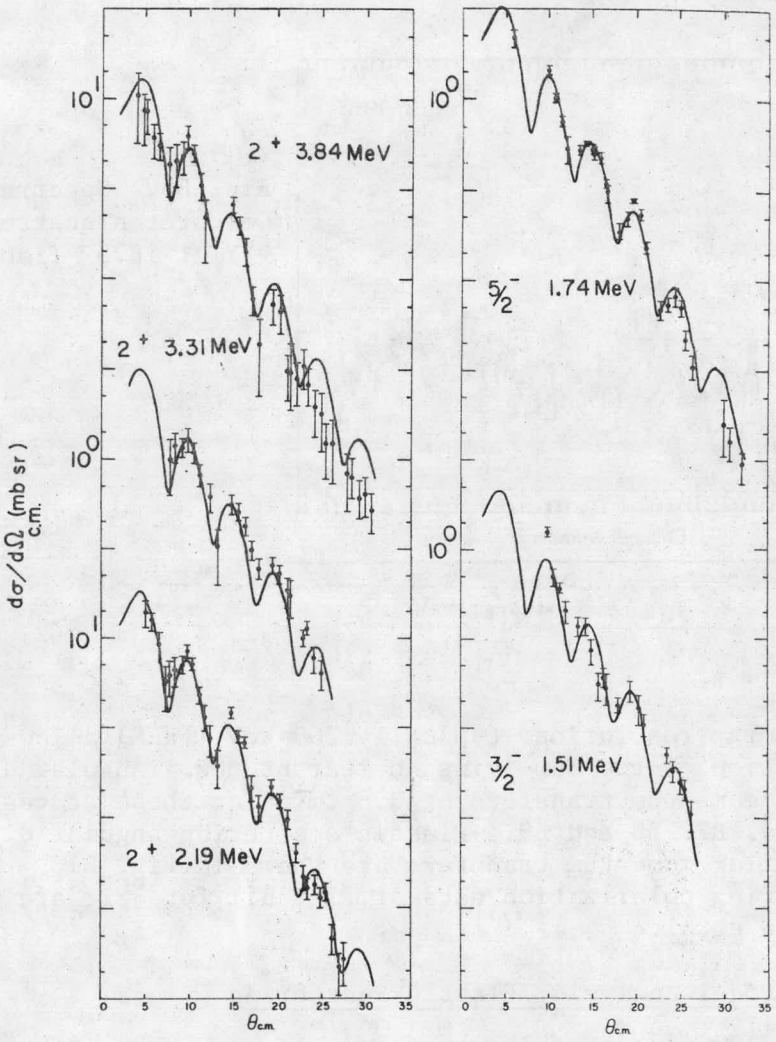

Fig. B7. Angular distributions obtained from inelastic scattering of 0.8 GeV protons by ^{90}Zr (left half of the figure) and ^{89}Y (right half of the figure). The solid curves are ℓ=2 collective DWBA calculations with deformation of only the central part of the best fit ^{90}Zr optical potential of Table BI. The extracted deformation parameters are:

2^+ at 3.84 MeV β_2=0.070,
2^+ at 3.31 MeV β_2=0.053,
2^+ at 2.19 MeV β_2=0.100,
$5/2^-$ at 1.74 MeV β_2=0.058,
$3/2^-$ at 1.51 MeV β_2=0.036.

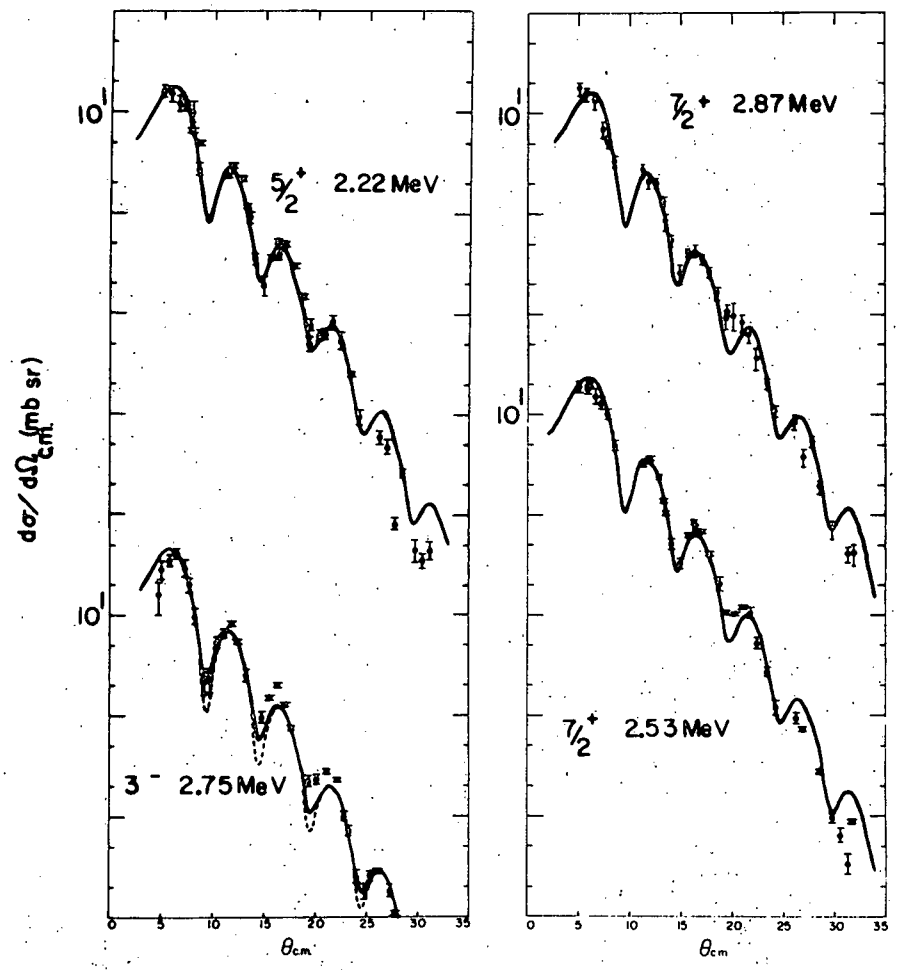

Fig. B8. Angular distributions obtained from inelastic scattering of 0.8 GeV protons by ^{90}Zr (3^-) and ^{89}Y ($5/2^+$, $7/2^+$, $7/2^+$). The solid curves are ℓ=3 collective DWBA calculations with deformation of only the central part of the best fit ^{90}Zr optical potential of Table BI. The extracted deformation parameters are:

$5/2^+$ at 2.22 MeV β_3=0.097,
3^- at 2.75 MeV β_3=0.151,
$7/2^+$ at 2.87 MeV β_3=0.091,
$7/2^+$ at 2.53 MeV β_3=0.106.

The dashed curve through the 3^- data is a ℓ=3 collective DWBA calculation deforming both the central and spin orbit parts of the best fit ^{90}Zr optical potential with $\beta_c = \beta_{so}$. The spin orbit term is deformed using the "Oak Ridge" prescription.

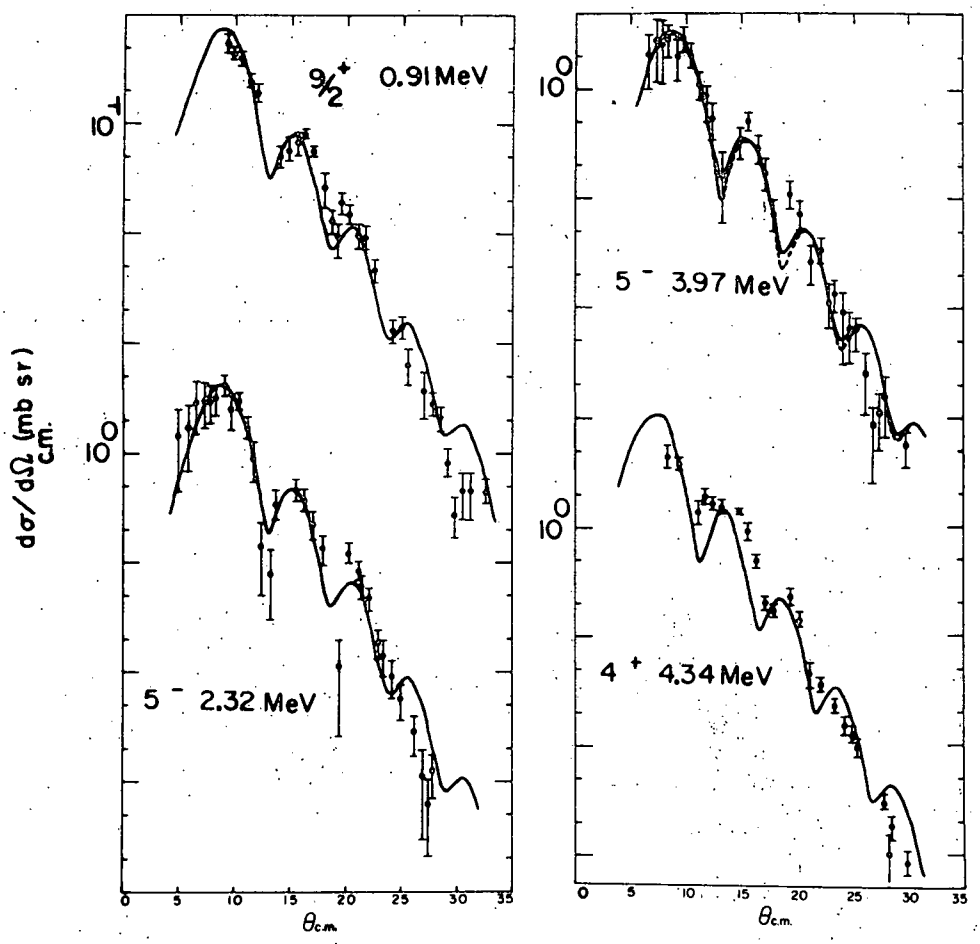

Fig. B9. Angular distributions obtained from inelastic scattering of 0.8 GeV protons by ^{90}Zr (5^-, 5^-, 4^+) and ^{89}Y($9/2^+$). The solid curves are collective DWBA calculations with deformation of only the central part of the best fit ^{90}Zr optical potential of Table BI. The extracted deformation parameters are, for the ℓ=3 transfers:

$9/2^+$ at 0.91 MeV β_5=0.032,
5^- at 2.32 MeV β_5=0.075,
5^- at 3.97 MeV β_5=0.064,

for the ℓ=4 transfer:

4^+ at 4.34 MeV $\beta_4=\beta$= 0.102.

The dashed curve with the 5^- at 3.97 MeV data is a collective DWBA calculation deforming both the central and spin orbit parts of the best fit ^{90}Zr optical potential at Table BI with $\beta_c=\beta_{so}$. The spin orbit potential is deformed according to the "Oak Ridge" prescription.

Table BI*

Optical model parameters used on analysis of 0.8 GeV proton scattering data.

U_c	r_r	a_r	W_c	r_i	a_i	U_{so}	W_{so}	r_{so}	a_{so}	r_c
+28.4 MeV	1.047 fm	0.462 fm	-52.9 MeV	1.115 fm	0.555 fm	-1.34 MeV	0.48 MeV	1.040 fm	0.745 fm	1.113 fm

* A positive potential is repulsive, a negative potential is attractive.

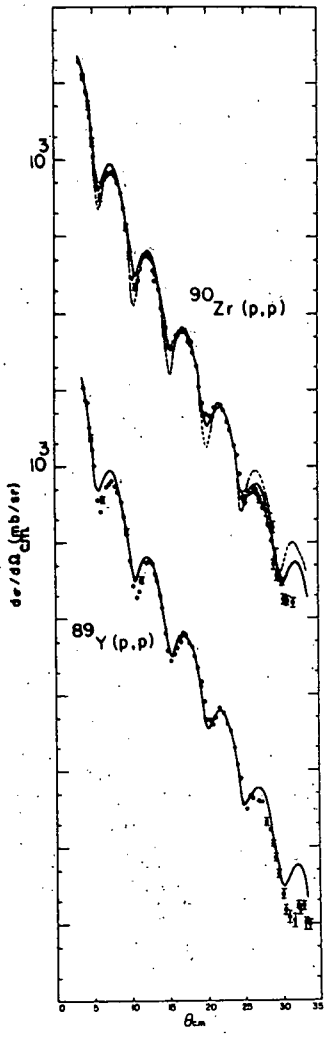

Fig. B10. Angular distributions obtained from elastic scattering of 0.8 GeV protons by ^{90}Zr and ^{89}Y. The solid curves are optical model calculations involving the parameters of Table BI. The dashed curve is an optical model calculation using the parameters of Table BI but with the real volume term set to zero (U_c=0.0 MeV).

The elastic scattering cross sections and polarizations for ^{90}Zr were fit with the following optical potential:

$$U_{opt} = U_{coul}(r,r_c) + U_c f(r,r_r,a_r) + iW_c f(r,r_2,a_2) + \frac{\hbar^2}{m_\pi c}(U_{so} + i W_{so})\, \vec{L}\cdot\vec{S}\, \frac{1}{r}\frac{d}{dr} f(r,r_{so},a_{so})$$

where $f(r,r_o,a_o) = [\exp((r-r_o A^{1/3})/a)+1]^{-1}$

and $U_{coul}(r,r_c)$ is the Coulomb potential of a charged sphere of radius $r_c A^{1/3}$.

The best fit parameters are listed in Table BI. This phenomenological optical model approach, involving parameter searching, is no less fundamental than a KMT calculation using N-N amplitudes and densities from electron scattering, as insufficient knowledge of the 0.8 GeV N-N scattering amplitudes forces one to search for a fit to the data with an essentially equivalent number of parameters.

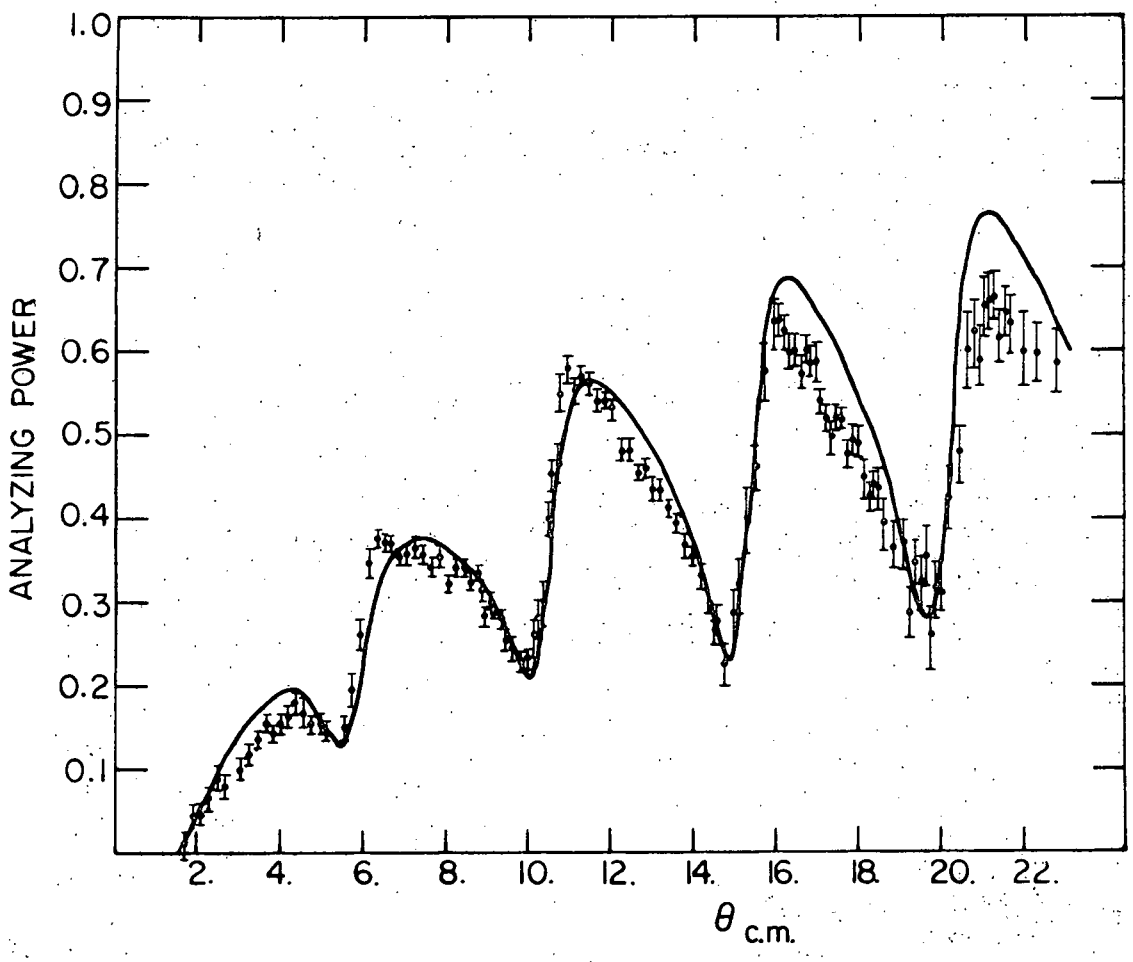

Fig. B11. The analyzing power for 0.8 GeV elastic proton scattering by ^{90}Zr. The data are due to Ref. 2. The solid curve is an optical model calculation using parameters of Table BI.

Care was taken to constrain our search to be consistent with known energy systematics.

The solid curves through the ^{90}Zr and ^{89}Y elastic data in Figs. B10 and B11 are the best fit optical model calculations for ^{90}Zr. The dashed curve in Fig. B10 is the best fit potential with $U_c=0$. It appears, from the similarity of the fits, that the scattering is dominated by the imaginary (absorptive) part of the central potential. Consistent with this observation is the fact that the spacing of the maxima and minima in the angular distributions is very well reproduced by Fraunhofer model calculations. The elastic S matrix elements are also as predicted by this diffractive model.

It is interesting to observe that a potential which better fits the forward angle elastic scattering data at the expense of back angle agreement (obtained by weighing forward angle data more than back angle data in the search procedure) compares quite well with first order KMT calculations. Varma[3] has been able to obtain excellent fits to 0.8 GeV proton elastic scattering data from heavy nuclei with a Glauber calculation plus second order corrections. Our method of analysis does not allow explicit identification of these effects in the elastic scattering. Nonetheless, our observations are not inconsistent with the possibility that the first order potential is inadequate beyond some as yet unestablished momentum transfer.

Collective DWBA Analysis of Inelastic Scattering

Given the apparent diffractive nature of the elastic scattering, it is not surprising that the inelastic scattering would be well described by the collective DWBA. In this model the transition amplitude form factor is surface peaked, being the derivative of the central part of the Woods-Saxon shape optical potential. No information about detailed microscopic nuclear structure is contained in this transition amplitude. The solid curves in Figs. B7, B8 and B9 result from these collective calculations, and are in good agreement with the data.

The deformation parameters, listed in the figure captions, are also in good agreement with those obtained from analyses of reactions at lower energies involving strongly absorbed projectiles, e.g. (α,α') and $(^3He,^3He')$. Also, the angular distributions of the $9/2^+$ state at 0.91 MeV and the 5^- state at 2.32 MeV (see Fig. B9), which are markedly different at lower proton energies, are essentially the same at 0.8 GeV. These results imply that the scattering of 0.8 GeV protons by heavy nuclei is even more strongly surface dominated than at lower proton energies.

Calculations were performed in which the spin orbit part of the optical potential, as well as the central part, is deformed and used in the transition amplitude. The deformation of the spin orbit term is accomplished using the "Oak Ridge" prescription. Predictions using the full Thomas-Fermi form, known to be important at lower proton energies, are not significantly different from the Oak Ridge

form at 0.8 GeV. The dotted curves in Figs. B8 and B9 are collective DWBA calculations involving both deformed central and spin orbit contributions to the transition amplitude. The results indicate that the spin orbit term in the optical potential has a small effect on the predicted scattering and does not improve the fit to the data.

It should be noted that when an optical potential equivalent to the KMT calculations of Ray et al.[4] is used instead of our best fit optical potential, a somewhat larger spin orbit effect in the inelastic scattering is yielded. Their fit to the elastic polarization is, however, significantly different from ours, especially within the first 10^{o}.

Microscopic DWBA Calculations

Preliminary microscopic DWBA calculations involving shell model wave functions and an interaction of the Yukawa form are in poor agreement with the data. More sophisticated calculations using a Gaussian form interaction are being performed.

Giant Resonances

Analysis of the region of excitation greater than ~5 MeV is in progress. The structure around 7 MeV of excitation appears to be the isoscalar giant E3 resonance seen in (e,e'), (α,α') and (^{6}Li,^{6}Li') scattering by ^{90}Zr. This region appears to be interesting enough to warrant high resolution study using the 45 MeV ^{3}He and 35 MeV α beams from the University of Colorado cyclotron. These lower energy data should allow identification of detailed structure, along with isospin and ℓ transfer assignments. Comparison will then be made to the 0.8 GeV results with particular emphasis on differences in excitation strengths.

Elastic Scattering Differences Between ^{89}Y and ^{90}Zr

For purposes of the preceding analysis, ^{89}Y and ^{90}Zr elastic scattering were assumed to be the same. A detailed comparison of the elastic scattering, however, shows systematic variations as a function of angle. The difference is not large enough to affect the DWBA calculations of inelastic scattering. Work is now underway to explain the observed small systematic differences.

---

1 G. W. Hoffman et al., Phys. Rev. Lett. 40 (1978) 1256.
2 M. L. Whitten et al., Nucl. Phys. A181 (1972) 417.
3 G. Varma, Rutgers Univ., SWUM Conference, U. Md., April, 1978.
4 L. Ray, LASL, private communication (1978).

10. Identification of High-lying T=0 Strength in ^{12}C -
J. R. Shepard and N. S. P. King (LASL)

Recent experiments at LAMPF have shown that reactions such as $^{12}C(\pi,\pi')^{12}C^*$ and $^{13}C(p,d)^{12}C$ [1] with E_p=800 MeV strongly excite many levels in ^{12}C with excitation energies above 18 MeV. A large number of levels in this region are known from prior experiments but in most cases the structure and even the excitation energy and spin, parity and isospin quantum numbers are undetermined. As one part of a general program aimed at determining the nuclear structure of high-lying levels in ^{12}C, we have analyzed $^{14}N(p,t)^{12}N$ and $^{14}N(p,^3He)^{12}C$ data for E_p=52 MeV taken at Crocker Laboratory, University of California, Davis. We have extracted relative angular distributions for eight corresponding groups in the residual nuclei up to an excitation energy of about 7.4 MeV in ^{12}N or about 22.5 MeV in ^{12}C. For the 16.1 MeV 2^+ T=1 level, the empirical shapes for t and ^3He agree almost exactly and the ratio of the cross sections is 0.62±0.05. This compares with a value of 0.62±0.06 measured by H. Yokomizo et al.[2], also at a proton energy of 52 MeV.

This empirical (p,t)/(p,^{3}He) cross section ratio for a T=1 final state was used to subtract the ΔT=1 components of the (p,^{3}He) cross section. We defined

$$\left(\frac{d\sigma}{d\Omega}(p,^3He)\right)_{\Delta T=0} = \frac{d\sigma}{d\Omega}(p,^3He)_{Total} - 0.62\,\frac{d\sigma}{d\Omega}(p,t).$$

For all levels in ^{12}C other than the analog of the ∿5.4 MeV state of ^{12}N, the extracted ΔT=0 cross section was consistent with zero at the majority of angles (spectra were measured between 10° and 50° in the lab system). For the analog of the 5.4 MeV state, the ΔT=0 component was determined to account for 50 to 80% of the total strength. Furthermore the shape of the ΔT=0 angular distribution is nearly identical to that for the 0.964 MeV 2^+ level in ^{12}N which is a pure L=2 transition. This suggests that the analog of the 5.4 MeV level having an excitation energy of ∿20.5 MeV in ^{12}C has isospin T=0, and positive parity with $0 \leq J \leq 4$. Since this level is observed in $^{12}C(d,d')$ [3] the T=0 assignment is supported. Since it is not seen in $^{12}C(\alpha,\alpha')$ [4], it is unlikely that the state is a natural parity level. On these bases we can argue that there is a + parity T=0 level in ^{12}C at about 20.5 MeV excitation with a probable angular momentum of 1 or 3. This state is appreciably excited in two nucleon pickup and thus is likely to have a p-shell configuration. The p-shell nuclear structure calculations of Norton and Goldhammer[5] do an excellent job of accounting for the observed + parity levels of ^{12}C up to at least the 18.13 MeV 1^+ T=0 level. These calculations predict no 1^+ T=0 levels between 18.13 and 31.36 MeV. However, 3^+ T=0 levels are predicted at 23.69 and 24.58 MeV. While discrepancies betwen Norton and Goldhammer's predicted excitation energies and experimental values are generally less than 0.5 MeV, it is possible that the observed level at ∿20.5 MeV corresponds to one of 3^+ levels mentioned above. It should be noted that they predict a 3^+ T=1 level at 20.5 MeV and that such a level is shown in the compilaton of Ajzenberg.[6] Since

our assignment of T=0 strength is quite firm, it may be that there are two 3^+ levels degenerate at that excitation, one T=0 and the other T=1.

Future $^{14}N(p,t)$ and $(p,^3He)$ experiments are anticipated so that the above conjectures can be examined more carefully.

---

[1] Elsewhere in this Progress Report.
[2] H. Yokomizo et al., Phys. Lett. 61B (1976) 245.
[3] O. Aspelund et al., Nucl. Phys. A253 (1975) 253.
[4] K. T. Köpfle et al., Phys. Lett. 64B (1976) 263.
[5] J. L. Norton and P. Goldhammer, Nucl. Phys. A165 (1971) 33, and J. L. Norton, Ph.D. Thesis, Univ. of Kansas, unpublished.
[6] F. Ajzenberg-Selove, Nucl. Phys. A248 (1975) 1.

11. Differential Cross Section and Asymmetry Measurements for 800 MeV Proton Scattering from ^{16}O, ^{40}Ca, ^{48}Ca and ^{54}Fe - G. R. Smith -- G. Adams, T. Bauer, C. Whitten, G. Igo, G. Pauletta (UCLA); G. Hoffmann (LAMPF)

Angular distributions for elastic and inelastic scattering on targets of ^{16}O, ^{40}Ca, ^{48}Ca, and ^{54}Fe have been measured at a proton bombarding energy of 800 MeV. In addition, asymmetry measurements were made on the ^{16}O and ^{54}Fe targets by using a polarized beam. The data were taken at the HRS (High Resolution Spectrometer) facility at LAMPF. The angular range (laboratory) of the measurements was from 5° to 30° for ^{16}O, and from 5° to about 23° for the other targets. The energy resolution of the inelastic spectra, which include about 25 MeV of excitation energy, varied from about 100 keV FWHM for the heavier targets to about 190 keV for the large-angle ^{16}O spectra.

Data for exciting the ground state, 6.13 (3^-), 6.92 (2^+), 7.12 (1^-) and 8.87 (2^-) MeV states in ^{16}O have been reduced. The cross section for exciting the 2^-, T=0 state at 8.87 MeV is comparable to that which was measured at 135 MeV.[1] However, the 4^- states populated at 135 MeV are not strongly excited at 800 MeV relative to the neighboring levels.

Fig. B12 shows the angular distribution for the $^{16}O(p,p)^{16}O$ (0.00 MeV) reaction. The data fall 4 orders of magnitude in 20°. The large angle data were taken to provide a constraint for theoretical models which predict different large angle behavior. Fig. B13 shows the asymmetry measurements for the ^{16}O ground state. The asymmetry is quite large and displays considerable structure. Solid curves shown in both figures result from a phenomenological optical model fit. Data from other targets are presently being reduced.

---

[1] B. M. Spicer et al., IUCF Technical and Scientific Report, Feb. 1, 1977 to Jan. 31, 1978, p. 105.

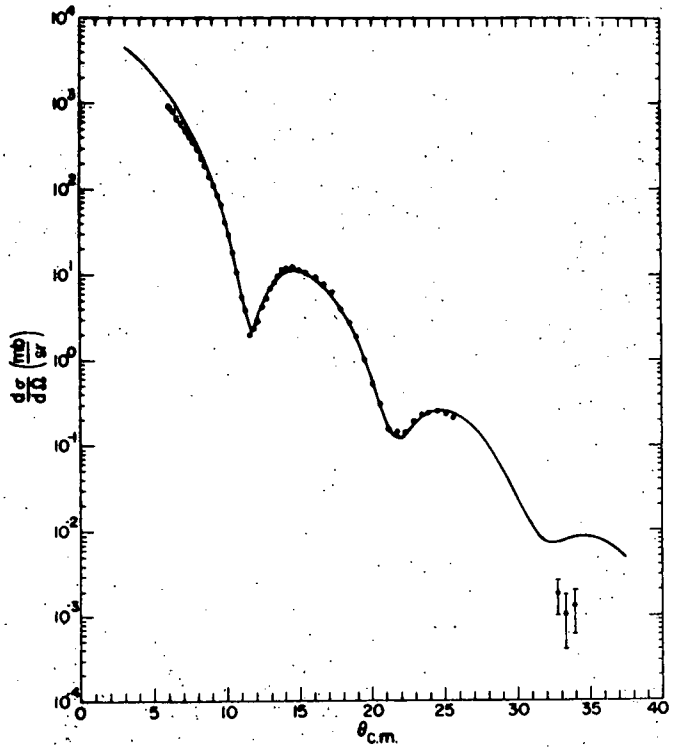

Fig. B12. Angular distribution for the $^{16}O(p,p)^{16}O$ (ground state). The error bars are too small to be seen at all but the largest angles. The solid curve is from a phenomenological optical model fit.

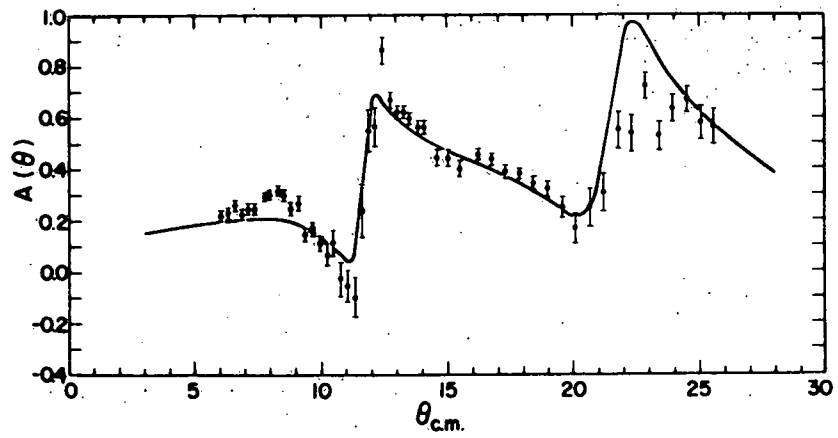

Fig. B13. Asymmetry measurements for the reaction $^{16}O(\vec{p},p)^{16}O$ (ground state). The solid curve is derived from a phenomenological optical model fit.

12. Enhanced Spin-Flip Probability in $^{9}Be(p,n)^{9}B$ at E_p=120 MeV - J. R. Shepard and C. D. Zafiratos (Univ. of Colo.); C. D. Goodman (ORNL); D. E. Bainum and J. Rapaport (Ohio Univ.); C. A. Goulding and M. B. Greenfield (Florida A & M); C. C. Foster (IUCF) and S. D. Schery (Texas A & M)

Neutron spectra from the $^{9}Be(p,n)^{9}B$ reaction with E_p=120 MeV were measured at several angles at IUCF using two large volume (15 cm x 15 cm x 100 cm) plastic scintillation neutron detectors at a 30-meter flight path. Overall time resolution was below 1 ns fwhm. The spectra were dominated by transitions to the ground state and to a state at 2.4 MeV excitation. Comparison of the observed angular distributions to DWBA calculation indicates that both transitions are dominated by ℓ=0.

These results are of interest for two reasons. First, the level at 2.4 MeV is presumably the known $5/2^-$ state but DWBA calculations indicate that the $1/2^-$ state expected from a variety of theoretical models should be quite strong and dominated by an ℓ=0 spin-flip transition from the $3/2^-$ ground state of the target. Thus, the absence of a third strong state in these observations points to near-degeneracy of the expected $1/2^-$ state in ^{9}B with either the ground state or the 2.4 MeV state.

The second point of interest in this study is the dramatic increase in the strength of the 2.4 MeV level as the proton energy is raised from 16 to 120 MeV. Comparison was made to published and unpublished data at 16, 23, 30, 50, 62 and 80 MeV. Since either the $5/2^-$ state or an assumed $1/2^-$ state near 2.4 MeV excitation can be reached by a spin-flip transition from the $3/2^-$ target, this implies that the ratio $V_{\sigma\tau}/V_{\tau}$ grows rapidly with energy. However, if the ground state transition is assumed to be an incoherent sum of Fermi-like and Gamow-Teller-like transitions the observed increase is too great to be consistent with published values of $V_{\sigma\tau}/V_{\tau}$.

13. The ^{12}C, ^{54}Fe and $^{208}Pb(p,t)$ Reactions at E_p=80 MeV - J. R. Shepard, R. E. Anderson, J. J. Kraushaar, and R. A. Ristinen (Univ. of Colo.), in collaboration with J. R. Comfort (Univ. of Pittsburgh), N. S. P. King (LASL) and A. Bacher and W. Jacobs (Univ. of Indiana).

We measured angular distributions for strongly excited levels up to ~4 MeV excitation for the ^{12}C, ^{54}Fe and $^{208}Pb(p,t)$ reactions at a bombarding energy of 80 MeV.

The experiment was carried out at the Indiana University Cyclotron Facility using the QDD spectrograph with a helical cathode position sensing proportional chamber in the focal plane. Tritons were identified by using a pair of plastic scintillators positioned behind the proportional chamber. Energy resolution was roughly 130 keV (fwhm). A natural carbon target and ^{54}Fe and ^{208}Pb

targets enriched to better than 97% isotopic purity were employed.

The $^{12}C(p,t)^{10}C$ Reaction

A spectrum comprised of two momentum bites joined together appears in Fig. B14. Three states of ^{10}C are observed, the 0^+ ground state, the 2^+ level at 3.3 MeV and a level at 5.3 MeV which has a tentative spin-parity assignment of 2^+.[1] Experimental angular distributions for these levels are shown in Fig. B15 along with DWBA results. The parameters used in the calculations appear in Table BI. The geometry of the well used to bind the neutrons in ^{12}C was obtained via a best fit to $e^- + {}^{12}C$ electron scattering data using a technique described elsewhere.[2] The binding energies of the neutrons were chosen to be half of the two neutron separation energy appropriate to the excitation energy of the final state. For these calculations the pickup of two $1p_{3/2}$ neutrons was assumed.

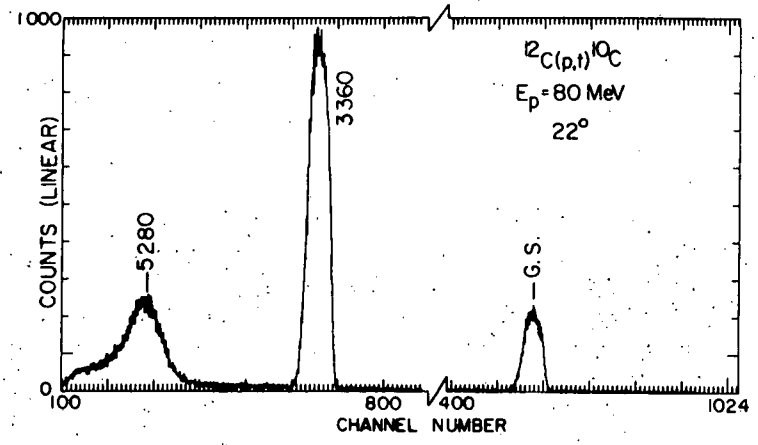

Fig. B14. A $^{12}C(p,t)^{10}C$ triton spectrum at a laboratory angle of 22°. This figure shows two momentum bites of the magnetic spectrometer spliced together. Energies shown are in keV and are taken from Ref. 1.

The angular distributions calculated for the 0^+ transition were extremely sensitive to the optical model parameters used, especially for the triton potential. While no calculation reproduced the data with precision, many choices could obviously be excluded. Furthermore, all triton potentials giving reasonable results were quite similar while variation among and sensitivity to proton parameters appearing in the literature were slight. A set of proton and triton optical model parameters representative of the best agreement with the 0^+ data are shown in Table BI. The DWBA results are in reasonable agreement for the 0^+ g.s. while the 2^+ angular distributions are not too well reproduced. Finite range corrections did not appreciably improve the agreement.

Enhancement factors, ε, are given in Table BII for all three levels of ^{10}C. The quantity ε is essentially the renormalization

Table BI
DWBA input parameters, potentials are in MeV, lengths are in fermis.

	V	r	a	W	W_V	r'	a'	V_{so}	W_{so}	r_{so}	a_{so}	r_c
$^{12}C(p,t)^{10}C$												
p + ^{12}C P1C[a]	-25.44	1.13	0.49	--	-8.51	1.45	0.45	--	--	--	--	1.33
t + ^{10}C T2C[b]	-160.0	1.39	0.542	-12.58	--	1.96	0.571	--	--	--	--	1.30
n + ^{10}C k)	-c)-	1.44	0.38	--	--	--	--	-d)-	--	1.44	0.38	--
$^{54}Fe(p,t)^{52}Fe$												
p + ^{54}Fe P6F[e]	-32.04	1.17	0.75	-14.9	--	1.32	0.536	-6.2	--	-1.01	0.75	1.25
P8F[f]	-30.2	1.228	0.764	- 7.29	--	1.456	0.505	-4.46	-0.40	1.052	0.611	1.25
t + ^{52}Fe T6F[g]	-117.4	1.165	0.802	--	-21.95	1.278	0.755	--	--	--	--	1.30
T7F[h]	-138.4	1.20	0.720	-14.6	--	1.43	0.840	--	--	--	--	1.30
n + ^{52}Fe	-c)-	1.29	0.65	--	--	--	--	-d)-	--	1.29	0.65	--
$^{208}Pb(p,t)^{206}Pb$												
p + ^{208}Pb P5P[i]	-39.5	1.211	0.769	-6.58	--	1.460	0.523	4.61	--	1.083	0.766	1.25
t + ^{206}Pb T2P[j]	-160.2	1.20	0.672	--	-23.39	1.095	0.931	--	--	--	--	1.30
n + ^{206}Pb k)	-c)-	1.27	0.90	--	--	--	--	-d)-	--	1.27	0.90	--

a) Ref. 9.
b) Ref. 10.
c) Well depth adjusted to give correct neutron binding energy.
d) Spin orbit strength tied to central well depth; λ=25.
e) Ref. 11.
f) Ref. 12.
g) Ref. 13.
h) Ref. 11
i) Ref. 12
j) Ref. 8
k) Ref. 14.

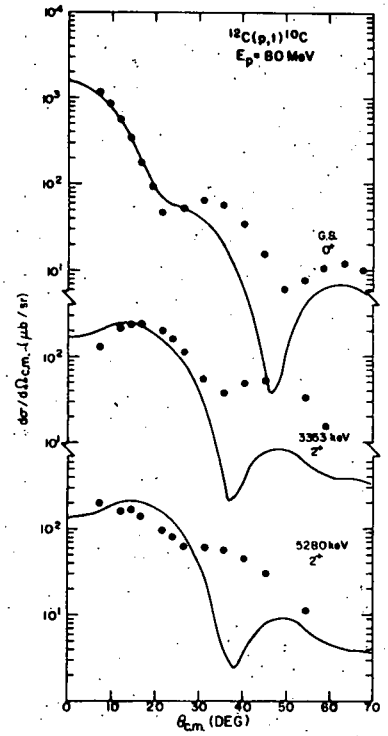

Fig. B15. Experimental angular distributions for $^{12}C(p,t)^{10}C$. The DWBA predictions shown were obtained using the input parameters of Table BI. The normalizations shown resulted in the enhancement factors of Table BII.

Table BII
Enhancement factors for $^{12}C(p,t)^{10}C$.

E_x	J^π	ε [a]
0	0^+	0.863
3353	2^+	0.255
5280	(2^+)	0.255

a) DWBA calculations used parameters of Table BI without either finite-range or non-locality corrections - configurations of picked-up neutrons assumed to be $(1p_{3/2})^2$.

factor required to bring the DWBA calculation into agreement with data. Specifically we have

$$\sigma_{expt.} = \varepsilon(S^{\frac{1}{2}})^2(D_o^2/10^4)\ \frac{\sigma_{DWUCK4}}{2L+1}\ ,$$

where $S^{\frac{1}{2}}$ is the two neutron spectroscopic amplitude, D_o is the zero range normalization factor and L is the angular momentum transfer. All calculations reported in this work use $D_o^2/10^4 = 25$ MeV $fm^{3/2}$. The enhancement factors quoted in Table BII refer to DWBA calculations without finite range (or non-locality) corrections.

The $^{54}Fe(p,t)^{52}Fe$ reaction

Cross sections were extracted for the ground state, 850 keV (2^+), 2385 keV (4^+) and 3583 keV (4^+) states. The spectrum is shown in Fig. B16 and the resulting angular distributions are shown in Fig. B17 along with the DWBA predictions. The DWBA

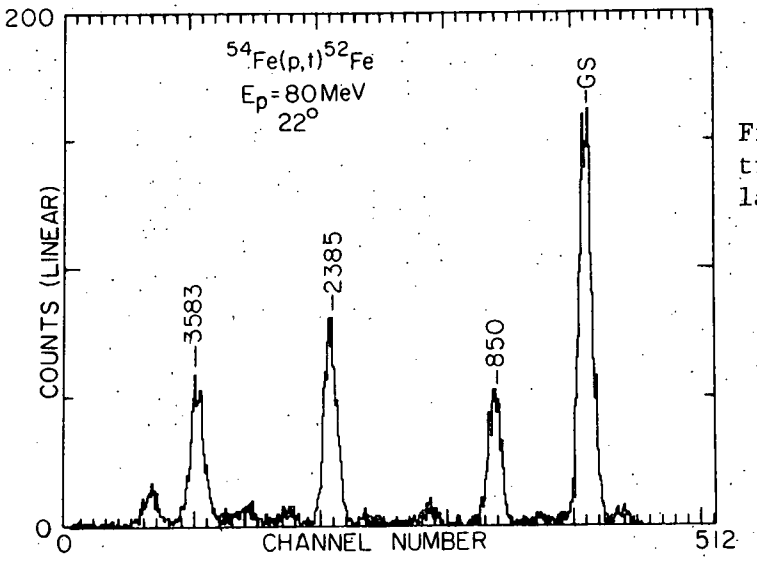

Fig. B16. A $^{54}Fe(p,t)$ triton spectrum at a laboratory angle of 22°.

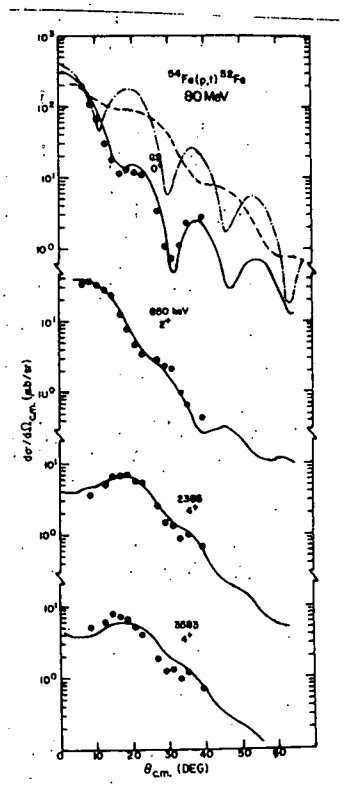

Fig. B17. Experimental angular distributions for $^{54}Fe(p,t)^{52}Fe$. The solid curves are DWBA predictions using optical model parameter sets P8F and T7F and the bound state geometry given in Table BI. The dashed and dashed-dot curves shown for the ground state transition were obtained by substituting optical model parameter sets T6F and P6F, respectively, in the original calculation. The normalizations of the solid curves reflect the enhancement factors quoted in Table BII.

optical model parameters that are appropriate for the projectile and ejectile were not immediately obvious and a number of parameter sets were tried in order to adequately describe the ground state transition. Table BI lists the various optical model parameter sets which were tried as well as the neutron bound state geometry employed. Also, the configuration of the picked-up neutrons was assumed to be $(1f_{7/2})^2$.

Sensitivity to optical model parameters was found to be great as is illustrated in Fig. B17 where calculations using different proton and triton potentials are compared with the ground state angular distribution. A glance at Table BI shows that, numerically, proton potentials P8F and P6F are quite similar, yet the resulting DWBA cross sections are very different. Triton potential T6F has a real volume integral per nucleon pair of -344 MeV fm^3 and, hence, is a "shallow" potential. The corresponding value for T7F is -417 MeV fm^3, classifying it as a "deep" potential. It is obvious from the results shown in Fig. B17 that the deep potential is preferred, in accord with the findings of several previous studies at lower energies.[3]

The DWBA results also proved to be sensitive to the choice of the neutron binding well geometry. Agreement with the shape of the experimental angular distributions was optimized when the well radius parameter was set to r_o=1.29 fm. Using r_o=1.25 fm as in Ref. 4 significantly worsened the shape agreement although the overall magnitude of the calculations was unaltered.

Comparison of calculated and measured cross sections resulted in the enhancement factors quoted in Table BIII where they are compared with those extracted in a similar analysis at E_p=40 MeV.[4] Two

Table BIII

Enhancement factors for ^{54}Fe(p,t)^{52}Fe.

E_x	J^π	[a] ε (80 MeV)	[a] $\varepsilon/\varepsilon_{g.s.}$ (80 MeV)	[b] ε (40 MeV)	[b] $\varepsilon/\varepsilon_{g.s.}$ (40 MeV)
g.s.	0^+	0.966	---	3.72	---
850	2^+	0.173	0.179	0.488	0.131
2385	4^+	0.019	0.020	0.092	0.025
3583	4^+	0.021	0.022	0.087	0.023

a) DWBA calculations used parameters of Table BI without either finite-range or non-locality corrections; optical model parameter sets P8F, T7F were used--configuration of picked-up neutron assumed to be $(1f_{7/2})^2$.
b) Ref. 4.

features are worth noting. The ratios of the enhancement factors for excited states to the enhancement factor for the ground state are in very good agreement for the two energies. However, the 80 MeV enhancement factors are roughly one-fourth as large as those for 40 MeV.

The $^{208}Pb(p,t)^{206}Pb$ Reaction

Triton energy spectra were measured up to ~4.5 MeV of excitation in ^{206}Pb. An example is given in Fig. B18. However, due to limited experimental resolution only eight states up to 3.243 MeV in excitation were analyzed. Angular distributions for these eight levels appear in Figs. B19 along with the DWBA results. As shown in Fig. B20, maximum cross sections are typically one order of magnitude smaller than those observed at 40 MeV,[5] with the exception of the 9^- state which, due to favorable angular momentum matching at 80 MeV, has roughly the same strength at the two energies.

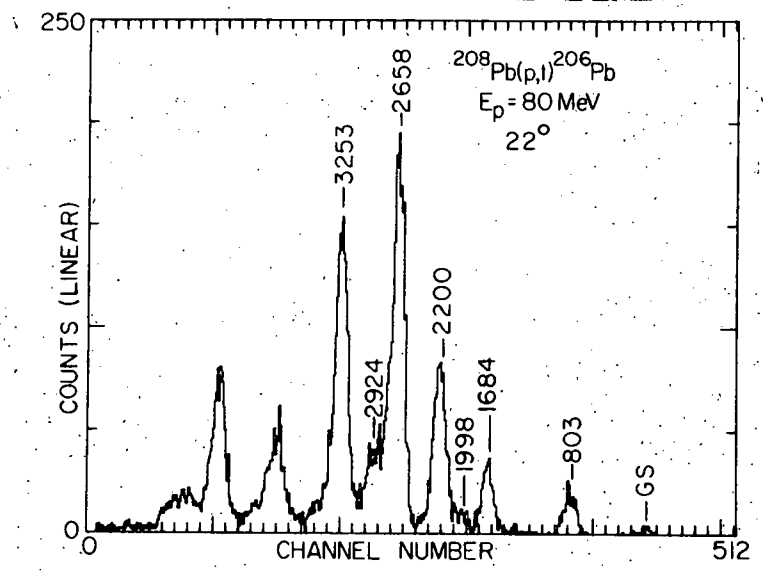

Fig. B18. A $^{208}Pb(p,t)$ triton spectrum at a laboratory angle of 22°.

The configurations of the transferred neutrons assumed in the calculation were determined by the leading components of the ^{206}Pb wave functions of True[6] and are quoted along with the extracted enhancement factors in Table BIV. Agreement with the shapes of the experimental angular distributions is generally excellent.

In Table BIV the extracted enhancement factors for E_p=80 are compared with those obtained from the 40 MeV data of Smith et al.[5] The 40 MeV DWBA calculations employed the optical model parameters used by Smith et al. and the neutron configurations

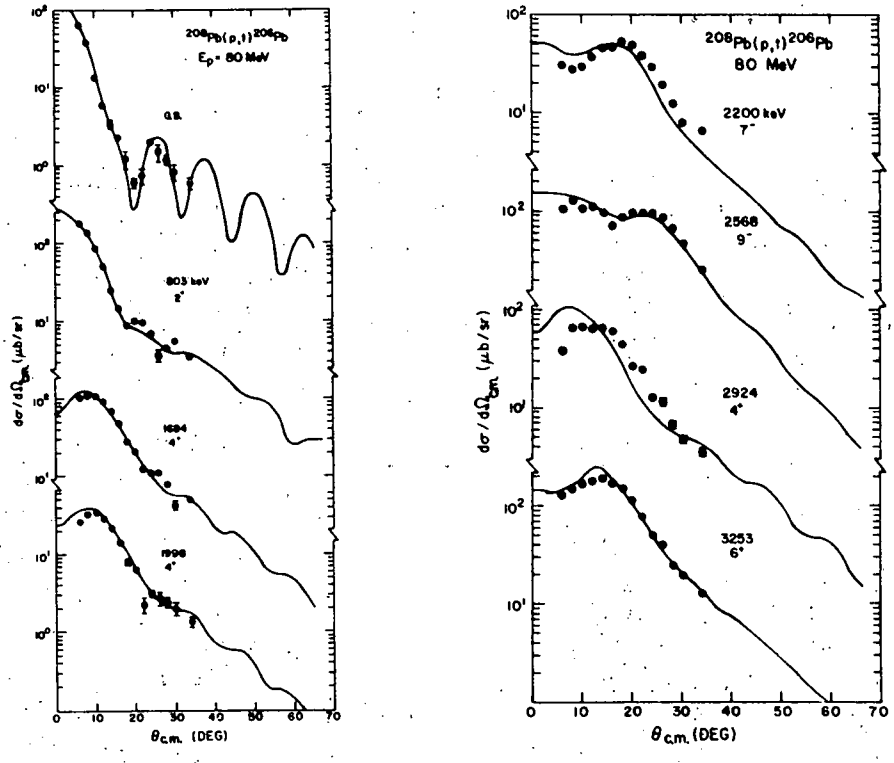

Fig. B19. Experimental angular distributions for $^{208}Pb(p,t)^{206}Pb$. The DWBA predictions shown were obtained using the input parameters of Table BI. The normalizations shown reflect the enhancement factors quoted in Table BIV.

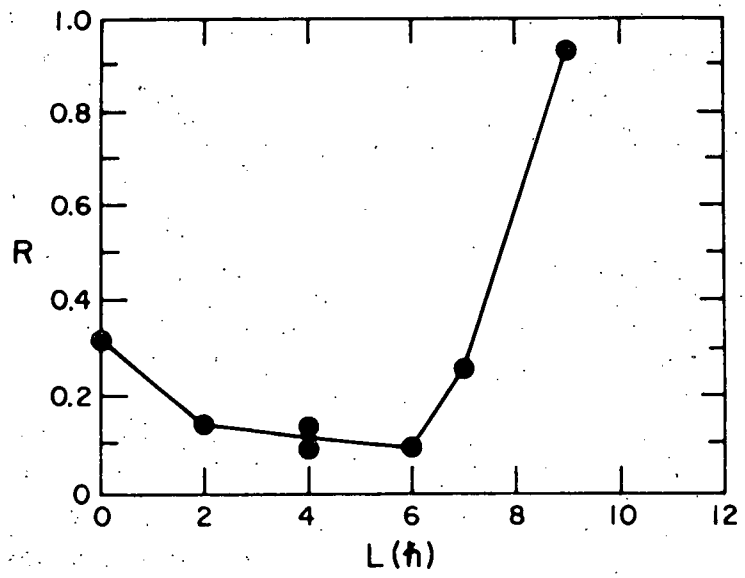

B20. The ratios, R, of maximum experimental differential cross sections at E_p=80 and 40 MeV are shown for $^{208}Pb(p,t)^{206}Pb$ transitions having various L transfers. $R=(d\sigma/d\Omega)_{max}(80\ MeV)/(d\sigma/d\Omega)_{max}(40\ MeV)$. Note that the most favorable angular transfer, classically, is $\Delta KR=(K_p-K_t) \times 1.25 \times 208^{1/3} \sim 9.4$. Hence, as is observed in the data, an L=9 transfer is strongly favored. At E_p=40 MeV, $\Delta KR \sim 6.3$.

Table BIV

Enhancement Factors for $^{208}Pb(p,t)^{206}Pb$

E_x	J^π	Config.	ϵ (80 MeV) [a]	$\epsilon/\epsilon_{g.s.}$ (80 MeV) [a]	ϵ (40 MeV) [b]	$\epsilon/\epsilon_{g.s.}$ (40 MeV) [b]
g.s.	0^+	$(3p_{1/2}^{-2})$	0.279	---	3.36	---
803	2^+	$(3p_{1/2}^{-1}, 2f_{5/2}^{-1})$	0.279	1.00	2.81	0.835
1684	4^+	$(3p_{3/2}^{-1}, 2f_{5/2}^{-1})$	0.099	0.353	1.17	0.348
1998	4^+	$(2f_{5/2}^{-2})$	0.329	1.18	6.56	1.951
2200	7^-	$(3p_{1/2}^{-1}, 1i_{13/2}^{-1})$	0.062	0.221	1.00	0.297
2568	9^-	$(2f_{5/2}^{-1}, 1i_{13/2}^{-1})$	0.064	0.228	0.795	0.236
2924	4^+	$(3p_{1/2}^{-1}, 2f_{7/2}^{-1})$	0.075-0.113	0.270-0.404	0.506	0.150
3253	6^+	$(2f_{5/2}^{-1}, 2f_{7/2}^{-1})$	0.131	0.471	1.37	0.407

a) DWBA calculations used parameters of Table BI without either finite-range or non-locality corrections.

b) Used data of Ref. 5. DWBA calculations used optical model potentials of Ref. 5 and neutron bound state geometry of Table BI. No finite-range or non-locality corrections were used.

and binding well geometry of the present work. As as the case for ^{54}Fe(p,t), the ratios of enhancement factors to the ground state enhancement factor agree well for the two energies (except for the 2.924 MeV 4^+ level). However, the 80 MeV values are smaller than those for 40 MeV, in this case, by a factor of 12.

^{206}Pb At this point the simplicity of the wave functions of the levels can be exploited. According to the calculations of True,[6] the 7^- and 9^- levels are essentially single configuration states, $(3p_{1/2}^{-1}, 1i_{13/2}^{-1})_{7^-}$ and $(2f_{5/2}^{-1}, 1i_{13/2}^{-1})_{9^-}$, respectively. It is then reasonable to assume that if the (p,t) reaction is adequately described by the present DWBA calculations, enhancement factors for these two levels would be nearly unity. At E_p=40 MeV such is the case. At 80 MeV, however, the 7^- and 9^- enhancement factors are both about 0.064 while that for the ground state is 0.279, much less than unity. This result, taken together with the similar findings for ^{54}(p,t), suggests that there is an overall energy dependence of the (p,t) cross section which is not reproduced by the single-step DWBA. Specifically, for ^{208}Pb, the observed (p,t) strength drops twelve times faster between 40 and 80 MeV than is predicted by the simple DWBA. Furthermore, this effect appears not to be a function of L-transfer or nuclear structure, but suggests that there is an energy dependence to the overall (p,t) normalization.

Variation with energy of the normalization of the zero range DWBA has been examined in previous papers for the (p,d)[7] and the (^{3}He,α)[8] reactions and it is not unreasonable to expect a like phenomenon for the (p,t) reaction. Such an energy dependence, when observed, can be traced to the variation of momentum transfer to the ejectile, in this case the triton. Specifically, the Fourier transform of the quantity $V_{p-2n}\phi_{p-2n}$ which "drives" the (p,t) reaction is not a constant as implied by the zero range assumption but is likely to decrease as the momentum transfer $q=|\vec{K}_p - \frac{1}{2}\vec{K}_t|$, increases. (Note that such a finite range effect is far beyond the ability of the simple first order corrections to account for.) Such a speculation can be tested only via careful exact finite range DWBA calculations utilizing a realistic triton wave function. We intend to perform such calculations in the immediate future.

It is possible, too, that the apparent change in overall DWBA normalization is due to complicated phenomena such as interference between multi-step and one-step modes which the DWBA is able to describe phenomenologically. This possibility, too, will be explored in the future as reliable techniques for calculating the two-step contributions are developed.

---

[1] F. Ajzenberg-Selove and T. Lauritsen, Nucl. Phys. A227 (1974) 1.
[2] J. R. Shepard and P. Kaczkowski, Bull. Am. Phys. Soc. 22 (1977) 529.

3 J. R. Shepard and N. S. P. King, to be published, and J. R. Shepard et al., Bull. Am. Phys. Soc. 18 (1973) 604.
4 P. Decowski et al., Nucl. Phys. A302 (1978) 186.
5 S. M. Smith et al., Nucl. Phys. A158 (1970) 479.
6 W. W. True, Phys. Rev. 168 (1968) 1391.
7 S. D. Baker et al., Phys. Lett. 52B (1974) 57, and E. Rost and J. R. Shepard, Phys. Lett. 59B (1975) 413.
8 J. R. Shepard, W. R. Zimmerman and J. J. Kraushaar, Nucl. Phys. A275 (1977) 189.
9 C. Rolland et al., Nucl. Phys. 80 (1966) 625.
10 Gordon C. Ball and Joseph Cerny, Phys. Rev. 177 (1969) 1466.
11 F. D. Becchetti and G. W. Greenlees, Phys. Rev. 182 (1969) 1190.
12 P. Schwandt, Indiana Univ., private communication.
13 H. H. Chang et al., Nucl Phys. A297 (1978) 105.
14 J. R. Shepard and P. Kaczkowski, Bull. Am. Phys. Soc. 22 (1977) 529.

14. Population of 1^+ and 4^+ States in ^{12}C by Inelastic Scattering of 180 MeV π^+ - R. L. Boudrie, N. J. DiGiacomo, J. J. Kraushaar, R. J. Peterson, R. A. Ristinen and G. R. Smith, Univ. of Colorado; K. Boyer, W. Cottinghame and C. F. Moore, Univ. of Texas, Austin; N. S. P. King, C. L. Morris and H. A. Thiessen, LAMPF, LASL.

We have recently examined inelastic scattering of 180 MeV π^+ by ^{12}C to excitations up to 25 MeV with the EPICS facility at LAMPF. Figs. B21 and B22 are representative of the data obtained.

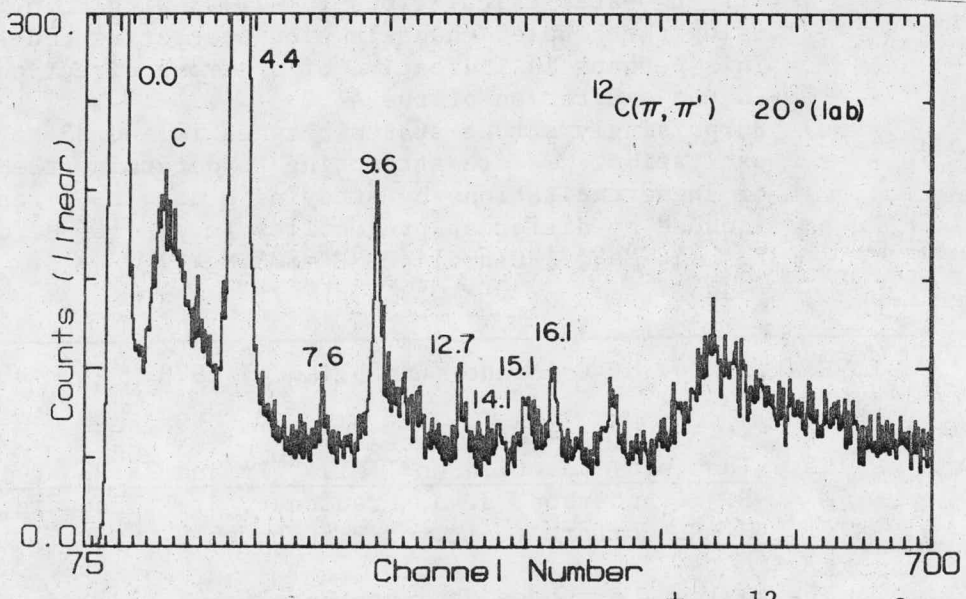

Fig. B21. Inelastic scattering of 180 MeV π^+ by ^{12}C at 20^o (lab). Excitation energies are in MeV.

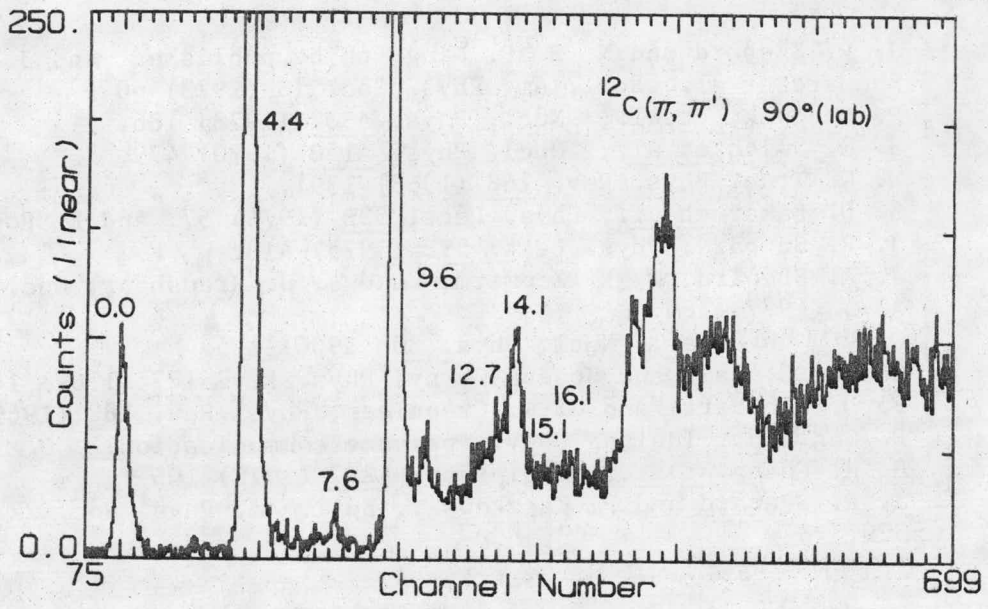

Fig. B22. Inelastic scattering of 180 MeV π^+ by ^{12}C at 90° (lab). Excitation energies are in MeV.

Energy resolution was approximately 250 keV FWHM. Preliminary examination of the spectra reveals, in addition to previously observed low lying states,

a) The T=1 and T=0 1^+ states at 12.7 MeV and 15.1 MeV clearly resolved.

b) The 4^+ state at 14.1 MeV. This state appears to be excited much more strongly than expected on the basis of two-step calculations ($0^+ \rightarrow 2^+ \rightarrow 4^+$ with $\beta_2 = 0.56$) using the coupled channels pion scattering code CHOPIN.[1] This perhaps is indicative of a strong direct component in the excitation of the 4^+.

c) Surprisingly strong states between 19 and 23 MeV in excitation. We are attempting to determine the nature of these excitations by studying a number of reactions induced by different projectiles (e.g. $^{11}B(^3He,d)^{12}C$ $E_{^3He}$ =44 MeV, $^{13}C(p,d)^{12}C$ E_p=800 MeV.)

[1] E. Rost, Univ. of Colorado (unpublished) 1978.

15. The (p,d) Reaction on ^{58}Ni, ^{90}Zr and ^{208}Pb at 121 MeV - R. E. Anderson, J. J. Kraushaar, J. R. Shepard; and J. R. Comfort (Univ. of Pittsburgh)

The analysis of these data has been completed and a paper accepted for publication.

The express purpose of the study was to test the usual distorted wave procedures at a bombarding energy that is significantly greater than that normally used. Emphasis was placed on the excitation and study of the strong single-hole states. Values of the zero range normalization factor, D_o^2, were obtained by comparison of exact finite range calculations with zero range calculations and a value of 1.23×10^4 MeV^2fm^3 was extracted. As expected this is reduced from the value in the range of 1.5 to 1.6×10^4 used at lower energies. Deuteron D-state contributions become significant only at scattering angles greater than 30^o or 40^o.

Appropriate optical model parameters at these higher energies are less available and presently offer limitations to the accuracy of the distorted wave calculations that are carried out. Adiabatic-deuteron potentials when used in a DWBA calculation appeared to describe the data better than those derived directly from deuteron elastic scattering.

Important deficiencies have been noted in the ability of the single step calculations to describe adequately the shapes and magnitudes of the angular distributions. While the calculated angular distributions have the correct general shape, many of the details of the experimental angular distributions are not reproduced. The general quality of the fits is considerably poorer than is usually the case at lower energies. There also appears to be an overall normalization problem for ^{58}Ni as well as an ℓ-dependent problem as evidenced in ^{208}Pb. In particular, the high ℓ-transitions appear to be underpredicted both in ^{90}Zr and ^{208}Pb. An example of this is indicated in Table BV where the spectroscopic factors from various neutron pickup reactions on ^{208}Pb are summarized including the present data at 121 MeV. While the agreement with the sum rule and other data is tolerable for the lower spin states, the values of $C^2S_{\ell_j}$ for the $13/2^+$ and $9/2^-$ states are only about one-half the expected value. It is interesting to note, however, that for the $13/2^+$ state several other studies have obtained low values for the spectroscopic factor. It would be interesting to analyze all of the existing data for the neutron pickup reactions to this state in a consistent fashion as a test of the distorted wave method.

In the case of ^{58}Ni and ^{208}Pb, variations were made in the bound state calculations as well as other parameters in the calculations. Although many effects were noted no particular prescription for the bound state calculations resolved all of the problems encountered.

In the case of ^{208}Pb, two-step calculations were carried out with the general conclusion that such contributions are negligible for the strong single particle states. As with lower bombarding energies, however, such two-step contributions can play an important role if the single step process is very weak. There appears no obvious enhancement of two-step contributions at a bombarding energy of 121 MeV.

Table BV

Spectroscopic factors for neutron pickup reactions on ^{208}Pb

		$C^2S_{\ell j}$							
		(p,d)						(d,t)	(^{3}He,α)
E(keV) [a]	j^π	22 MeV [b]	22 MeV [c]	35 MeV [d]	40 MeV [e]	55 MeV [f]	121 MeV [g]	17 MeV [h]	28 MeV [i]
G.S.	$1/2^-$	2.2	2.0	1.8	2.15	1.68	2.5		3.2
570	$5/2^-$	4.0	6.0	5.2	6.3	6.0	5.3	6.8	6.0
898	$3/2^-$	4.0	3.7	3.2	3.8	3.33	4.8	4.0	6.5
1633	$13/2^+$	6.5	13.0	9.4	8.5	14.0	6.7	14.5	14.0
2340	$7/2^-$	3.4	6.0	4.4	5.1	6.55	6.4	7.1	9.7
2726	$(9/2)^+$				0.05		0.03	0.091	
3409	$9/2^-$	2.2	7.0	4.9	6.8	8.5	4.0	9.8	6.0

a)
b) Ref. 1.
Ref. 2. Various calculations were completed by these authors; the spectroscopic factors shown were obtained with no radial cutoffs in the DWBA calculations.
c)
Ref. 3. Reanalysis of the data of Ref. 2 with adiabatic deuteron potentials.
d)
e) Ref. 4.
f) Ref. 5.
g) Ref. 6.
h) Present study.
i) Ref. 7.
Ref. 8.

An example of the two-step calculations is shown in Fig. B23.

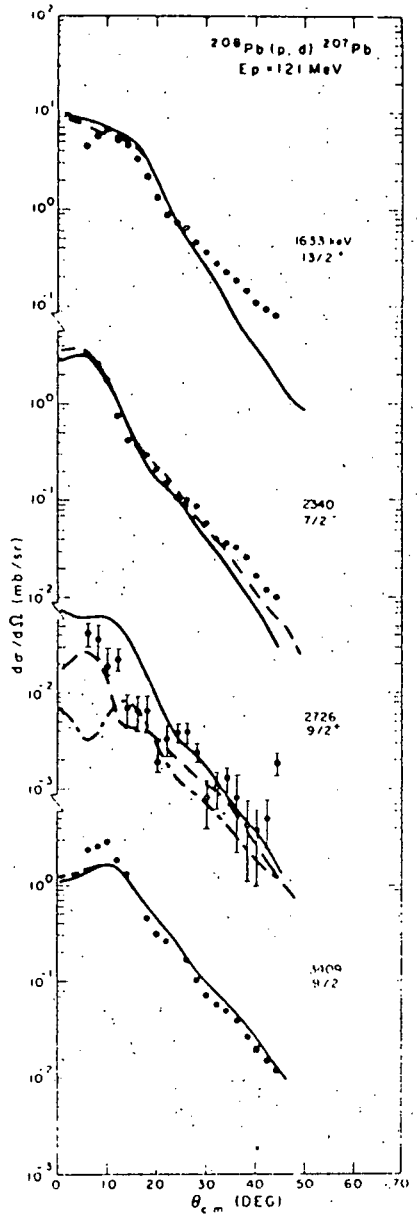

Fig. B23. The effects of two-step processes on the calculated angular distribution for several states in ^{207}Pb. For the states at 1633, 2340 and 3409 keV, the spectroscopic factors listed in Table BV were assumed and the calculations that included the two-step processes are shown for the two choices of relative phase. For the state at 2726 keV a spectroscopic factor of 0.03 was assumed. For all four states the dashed curve was for constructive interference and the solid curve for destructive interference. The dash-dot curve for the 2726 keV state was for two-step processes alone.

Calculations were performed based on the inelastic excitation of the 3^- state at 26.4 keV in ^{208}Pb followed by a $f_{7/2}$ neutron pickup from that state to the $13/2^+$ level in ^{208}Pb. A value of β_3=0.11 was taken for the inelastic excitation and a spectroscopic factor of 2.2 was assumed for the $f_{7/2}$ transition. The value of 2.2 was obtained by dividing the full spectroscopic strength of 8 among the seven levels of the $[3^- \otimes f_{7/2}]_{j^\pi}$ multiplet according to a 2j+1 weighting factor. This gives a much larger two-step component than most structure calculations suggest. Hence our two-step

calculations may be viewed on that basis as an upper limit for such effects. The spectroscopic strength for the direct neutron pickup and the phase of the direct leg relative to the two-step leg were varied to obtain the best fit. The results are shown in Fig. B23 with $C^2S_{\ell j}=9$ for the direct component for both constructive and destructive interference between the two paths. As can be seen, inclusion of the two-step process in the excitation of the $13/2^+$ level results in only very minor changes in shape or magnitude compared to the one-step calculation discussed earlier.

The calculations including two-step processes do tend to be somewhat less diffractive in shape than the one-step process alone, although the differences are insignificant in terms of the data. Clearly the two-step process based on the $[3^- \otimes f_{7/2}]$ configuration alone cannot account for the reduced spectroscopic factor for the 1633 keV level observed within the present study at 121 MeV.

Similar results were obtained for the $7/2^-$ and $9/2^-$ states at 2340 and 3409 keV and these results are also displayed in Fig. B23. The $7/2^-$ level is somewhat more strongly affected by the choice of the relative phase. In cases where the spectroscopic factor for the direct transition is a reasonably large fraction of the sum rule limit, inclusion of the two-step processes makes little difference in the shape and magnitude of extracted spectroscopic factors.

The $9/2^+$ state at 2726 keV can be excited either by a two-step process or directly due to particle-hole admixtures in the ^{208}Pb core. In Fig. B23 a pure two-step calculation is shown and it falls somewhat below the data, while inclusion of a small $2g_{9/2}$ admixture permits the calculation to approximately reproduce the data. Calculations are shown in Fig. B23 for both destructive and constructive interference with a spectroscopic factor of 0.03 for the direct transition. Either relative phase describes the data equally well.

In summary it appears that the (p,d) reaction at 121 MeV falls into the category of low energy reactions in that no new phenomena appear in the analysis of the strong single particle transitions. There are, however, discrepancies encountered that offer a challenge to the full understanding of the reaction at this energy.

---

1 M. R. Schmorak and R. L. Auble, Nuclear Data Sheets 5 (1971) 207.
2 C. A. Whitten, Jr., N. Stein, G. E. Holland and D. A. Bromley, Phys. Rev. 188 (1969) 1941.
3 G. R. Satchler, Phys. Rev. C 4 (1971) 1485.
4 W. A. Lanford and G. M. Crawley, Phys. Rev. C 9 (1974) 646.
5 S. M. Smith, P. G. Roos, C. Moazed and A. M. Bernstein, Nucl. Phys. A173 (1971) 32.
6 K. Yagi, T. Ishimatsu, Y. Ishizaki and Y. Saji, Nucl. Phys. A121 (1968) 161.
7 R. A. Moyer, B. L. Cohen and R. C. Diehl, Phys. Rev. C 2 (1970) 1898.
8 W. P. Alford and D. G. Burke, Phys. Rev. 185 (1969) 1560.

16. The (p,d) Reaction at 800 MeV - G. R. Smith, J. R. Shepard, R. L. Boudrie, R. J. Peterson, N. J. DiGiacomo, and J. J. Kraushaar (Univ. of Colo.); G. Igo, C. A. Whitten, T. S. Bauer, G. Adams and G. Pauletta (Univ. of California, Los Angeles)

We have measured cross sections for the ^{7}Li, ^{12}C, ^{13}C, ^{16}O, ^{25}Mg, ^{28}Si and ^{40}Ca(p,d) reactions at E_p=800 MeV using the High Resolution Spectrometer (HRS) facility at LAMPF. Sample spectra are displayed in Figs. B24 through B30. In addition to the normal strong single-particle levels anticipated on the basis of low-energy single neutron pickup data, we observe new strongly excited levels at high excitation energies. For example, in Fig. B25 a strong group is observed at about 13.5 MeV excitation in ^{11}C; no evidence of such a level is seen in other (p,d) studies at 135[1] and 185 MeV[2] bombarding energies. The strongly excited levels above 19 MeV excitation in ^{12}C and shown in Fig. B26 are barely visible in similar spectra at E_p=185 MeV[2] and 62 MeV.[3] The nature of these states and the reasons for their strong excitation are not well understood at present.

Excitation of the low-lying, strong, single-particle states seems well understood in the case of ^{13}C(p,d)^{12}C, at least insofar as exact finite-range DWBA calculations seem generally able to reproduce the observed cross sections. Calculations[4] done using the parameters of Table BVI are compared with experimental angular distributions in Fig. B31. The calculations are absolutely normalized and employ spectroscopic factors computed from the wave functions of Norton and Goldhammer.[5] Sensitivity to the details of the input parameters is demonstrated by the two curves compared with the ground state angular distribution. The curve which reproduces the forward angle cross sections uses the bound state geometry of Shepard and Kaczkowski obtained by comparison with electron scattering data.[6] The other curve used the Elton and Swift geometry.[7] For the 12.7, 15.1 and 16.1 MeV angular distributions the separation energy method of computing the nuclear bound state wave function (solid line) is seen to be superior to the separation-energy independent method (dashed line). Preliminary CCBA calculations suggest that the disagreement between the calculations and experiment for the 4.44 MeV 2^+ level can be explained on the basis of strong two-step couplings which have been neglected in the DWBA approach.

Agreement between DWBA calculations and measured cross sections for targets other than ^{13}C and ^{12}C is not so good. For instance, the 2.2 MeV 3^+ level excited in ^{7}Li(p,d)^{6}Li is nearly an order of magnitude more strongly excited than the 1^+ g.s., in contrast to lower energy results[8] and calculated spectrscopic factors[9] which suggest the strengths should be nearly equal.

Also, as is shown in Fig. B32, the overall strength of the DWBA cross section to the ground state becomes much larger than experiment as the mass of the target increases. For ^{40}Ca(p,d) $\sigma_{DWBA}/\sigma_{expt.} \sim 30$ for the $3/2^+$ ground state. It should be noted

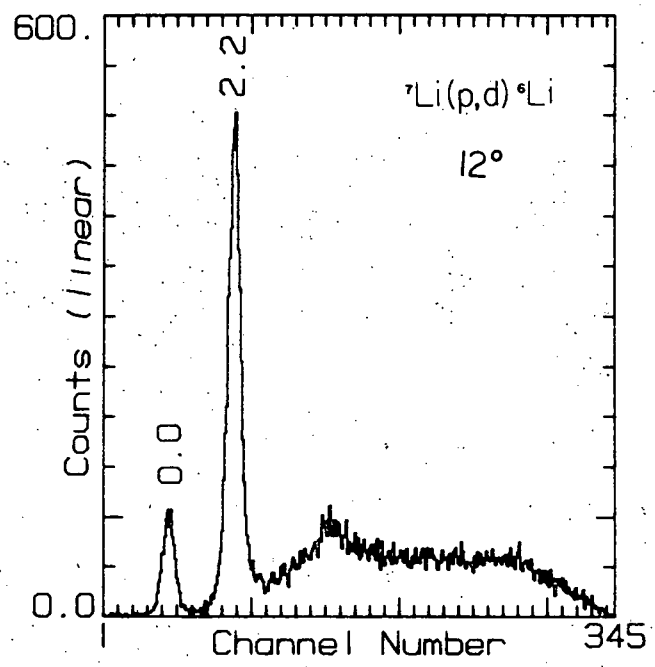

Fig. B24. Deuteron spectrum from the ^{7}Li(p,d)^{6}Li reaction.

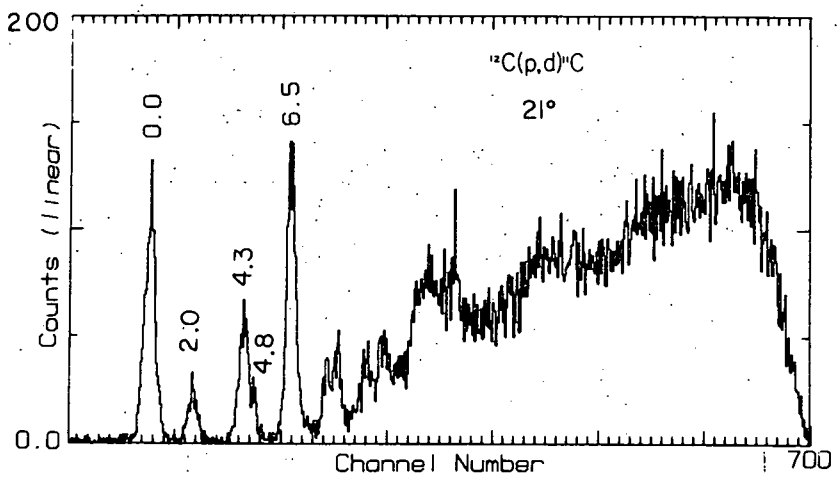

Fig. B25. Deuteron spectrum from the ^{12}C(p,d)^{6}Li reaction.

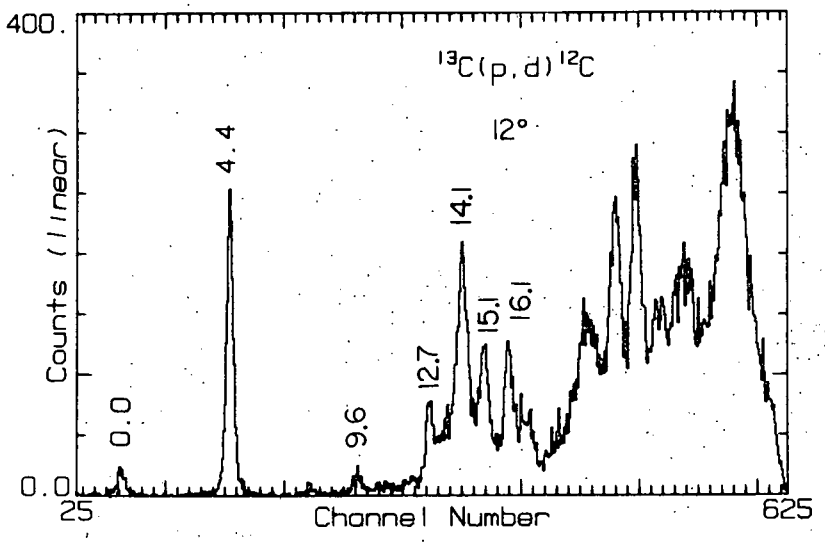

Fig. B26. Deuteron spectrum from the $^{13}C(p,d)^{12}C$ reaction.

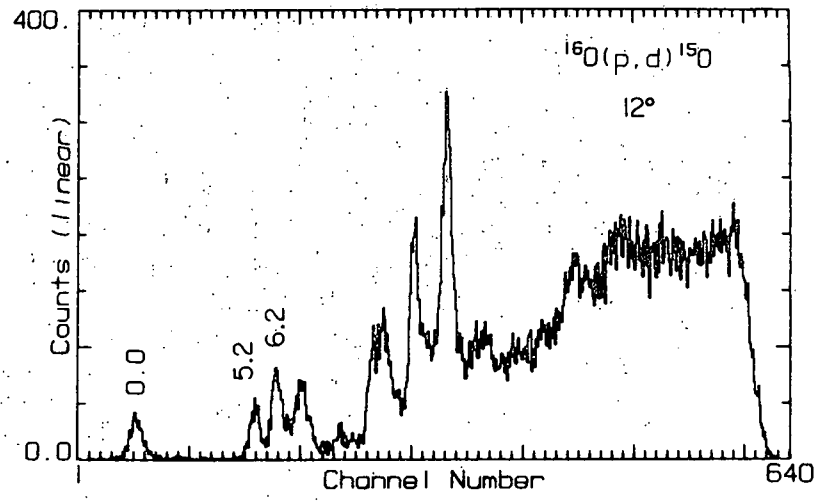

Fig. B27. Deuteron spectrum from the $^{16}O(p,d)^{15}O$ reaction.

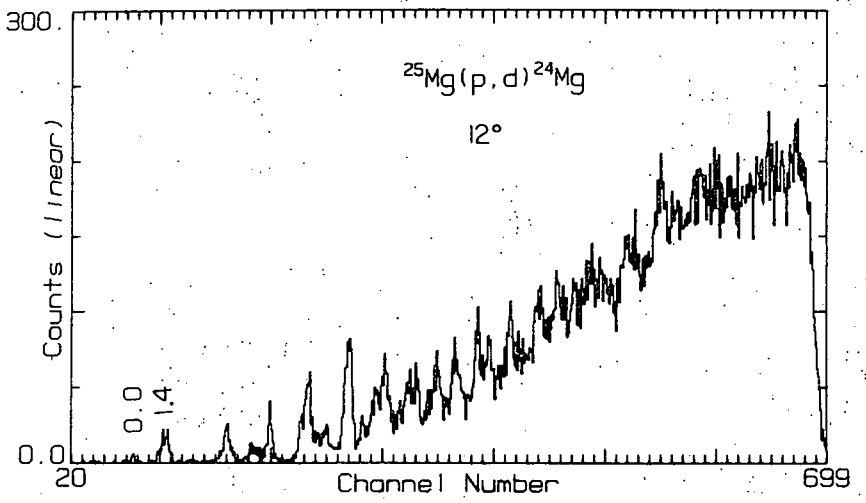

Fig. B28. Deuteron spectrum from the $^{25}Mg(p,d)^{24}Mg$ reaction.

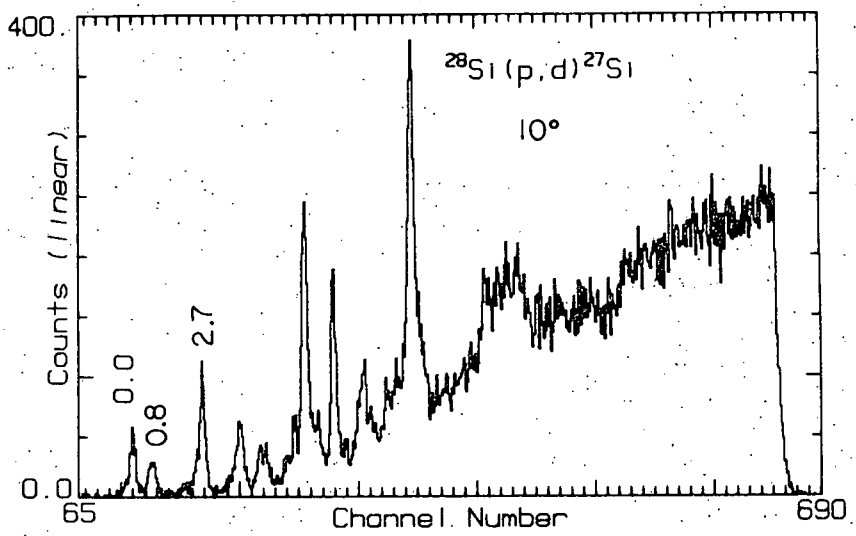

Fig. B29. Deuteron spectrum from the ^{28}Si(p,d)^{27}Si reaction.

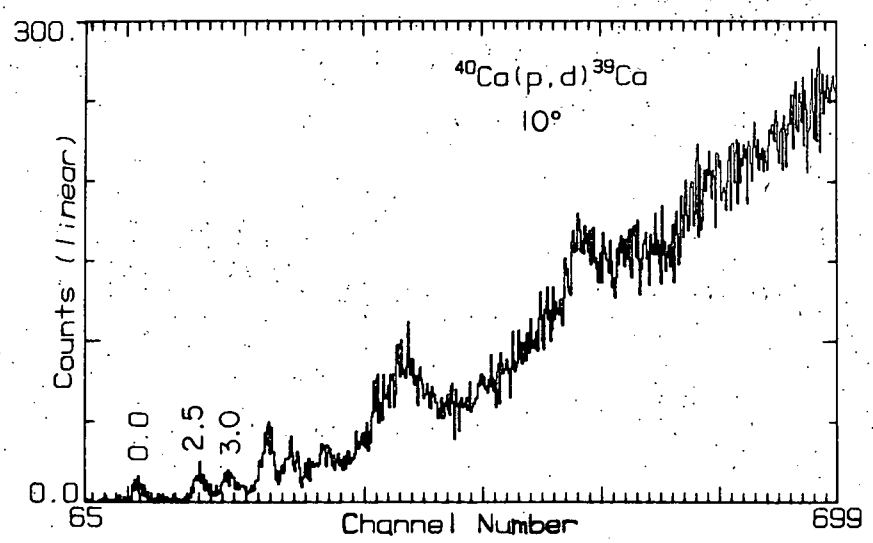

Fig. B30. Deuteron spectrum from the ^{40}Ca(p,d)^{39}Ca reaction.

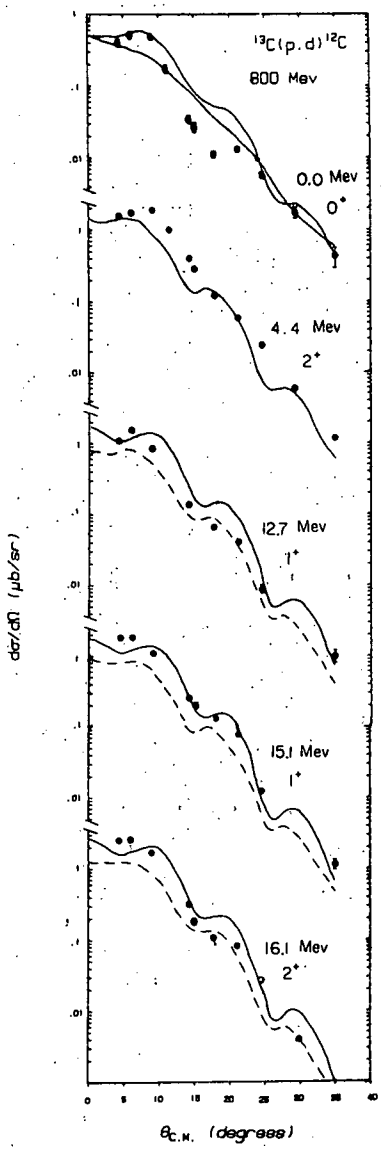

Fig. B31. DWBA calculations are compared with measured angular distributions for the $^{13}C(p,d)^{12}C$ reaction. Calculations are discussed in the text.

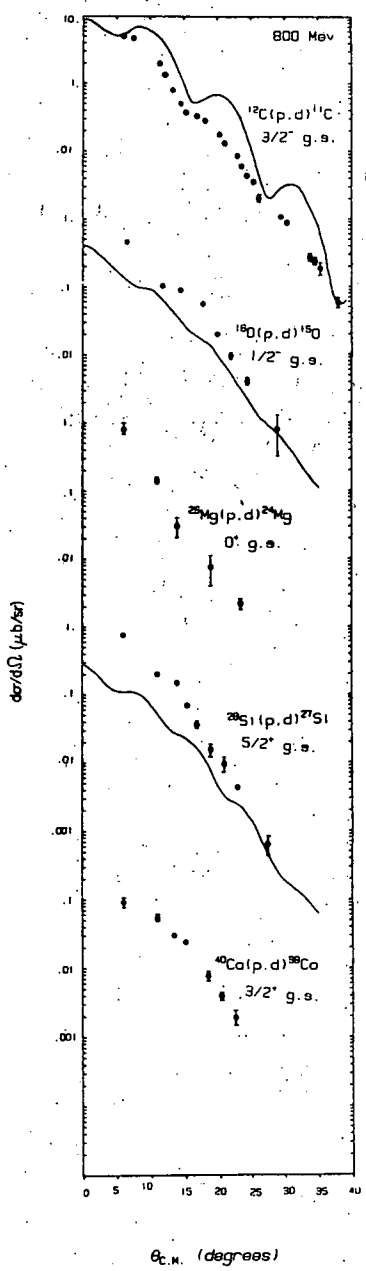

Fig. B32. Ground state angular distributions are shown. The solid lines are DWBA calculations; the ^{16}O and ^{28}Si calculations have been arbitrarily renormalized by factors of 1/20 and 1/35, respectively.

Table BVI

DWBA input parameters. Potentials are in MeV, and lengths are in fermis.

	V	r	a	W	r'	a'	V_{so}	W_{so}	r_{so}	a_{so}	r_c
Proton [a] Potential	+13.72	0.872	0.304	-68.93	0.948	0.472	+1.09	-0.48	1.041	0.745	1.25
Deuteron [b] Potential	-8.0	0.96	0.41	-72.0	0.96	0.41	--	--	--	--	1.30
Carbon S & K	--[e]	1.44	0.38				f)				
Bound State E & S	--[e]	1.36	0.55				f)				
Oxygen Bound State	--[e]	1.30	0.50				f)				
Silicon Bound State	--[e]	1.27	0.60				f)				
Calcium Bound State	--[e]	1.27	0.60				f)				

Assumed ground state spectroscopic factors

Target	C^2S
^{12}C	3.0
^{13}C	0.67
^{16}O	2.0
^{25}Mg	0.33
^{28}Si	3.5
^{40}Ca	3.0

a) From best fit to E_p=800 MeV ^{12}C elastic scattering of Ref. 10.
b) Ref. 11.
c) Ref. 6
d) Ref. 7
e) Central depth adjusted to give correct neutron separation energy.
f) Spin orbit strength proportional to central depth; λ=25.

that all calculations presented here used optical model potentials appropriate to ^{12}C (but with radii scaled by $A^{1/3}$) and that better optical model potentials may give significantly different results. This problem is currently under investigation.

---

[1] D. A. Miller, Indiana Univ., private communication.
[2] J. Källne, Univ. of Virginia, private communication.
[3] L. J. Parrish et al., Phys. Rev. C 9 (1974) 876.
[4] For description of the calculations, see E. Rost, J. R. Shepard, and D. A. Sparrow, Phys. Rev. C 17 (1978) 1513; note that both S and D state deuteron contributions are included in the present results.
[5] J. L. Norton and P. Goldhammer, Nucl. Phys. A165 (1971) 33 and
[6] J. L. Norton, Ph.D. Thesis, Univ. of Kansas, unpublished.
[7] J. R. Shepard and P. Kaczkowski, Bull. Am. Phys. Soc. 22 (1977) 529.
[8] L. R. B. Elton and A. Swift, Nucl. Phys. A94 (1967) 52.
[9] e.g., D. W. Devins et al., Nucl. Phys. A126 (1969) 261 or J. Källne et al., Phys. Lett. 52B (1974) 313.
[10] Using the wave functions of Ref. 5.
[11] G. S. Blanpied et al., Phys. Rev. Lett. 39 (1977) 1447.
S. D. Baker et al., Phys. Lett. 52B (1974) 57.

C. Apparatus and Facility Development

1. New In-House Computing Facilities - Dale E. Prull

The computing facilities at the University of Colorado Nuclear Physics Laboratory were greatly expanded last year with the purchase of a Digital Equipment Corporation PDP-11/34 computer. Delivery and installation were completed in December, and system generation for RSX-11M v3.0 was completed in early January.

The initial purchase consisted of a PDP-11/34 processor, 128K bytes MOS memory, floating point processor, a system console, two RK05 disk drives, a 9 track magnetic tape transport, a character printer, and a Tektronix 4010 alphanumeric-graphics display terminal. We have since added two RK05 disk drives, a card reader, a second Tektronix 4010 display terminal, a Tektronix 4662 interactive digital plotter, and two general device interface cards.

A primary goal is to utilize the PDP-11 for on-line data acquisition and experimental control. We have purchased a CAMAC crate, a dedicated crate controller, and a modest collection of CAMAC modules. We are building an interface and controller for three Northern Scientific NS-623 analog-to-digital converters and plan to interface our Nuclear Data ND-50/50 pulse-height analyzer system. This provides the basis for modernizing our experimental procedures.

A secondary goal in this purchase was to expand our data-reduction capabilities. The multi-user capability of RSX-11M permits analysis and program development to proceed in parallel with real-time data acquisition. Several analysis programs have already been written and are in general use while the data acquisition software is being developed.

This purchase represents a significant expansion of our computing facilities and will be the basis for continuing development. It provides the sophistication and flexibility required in modern nuclear physics experiments.

2. Computer Program Development - Dale E. Prull

PICSY

A program input and control system has been developed for the PDP-11 computer which provides user-oriented, interactive features for any program into which it is incorporated. Use of the system by a program requires that an outline of control words be supplied and that all input be performed via subroutine calls. The system, which consists of a package of subroutines, scans each line of free format input and checks to see if the fields conform to the prescribed outline. If errors are detected, diagnostic messages are returned to the user, and he is given the opportunity to make corrections before proceeding.

Plotting

A package of subroutines has been developed for the PDP-11 computer to provide Fortran callable plotting capability on the Tektronix 4010 display terminals and the Tektronix 4662 digital plotter. The functions available vary from simple plotting to lettering with sub- and super-scripting, italics, the Greek alphabet, and lower as well as upper-case characters. There are subroutines for axis plotting, array plotting, and patterned lines. The cursors on the Tektronix 4010 can be displayed and their coordinates returned for interactive capability.

SPECTR

Program SPECTR provides all of the operations required for handling large numbers of multichannel pulse-height spectra and for accomplishing basic data reduction of the spectra. The concepts, logic, and capabilities of the original SPECTR, which has been in use for several years on the PDP-9 computer, were used as the basis of a new SPECTR written for the PDP-11 computer. Approximately half of the original code was kept intact except for changes in common blocks and system library calls.

All program operations are controlled either from a terminal or from the card reader using free format user-oriented control sequences via the PICSY system. The commands are organized in such a way that after a short break-in period most users can recall the control sequences from memory and request program operations as desired. The basic philsophy is that if any command makes sense within the context of its use, then it should function accordingly.

For speed of development and ease of maintenance, Fortran was selected as the primary source language. Extremely limited use has been made of assembly language. Standard overlay techniques are employed with segments loaded via subroutine calls from the resident code. A linkage table is used so that any segment can, in effect, call or be called by any other segment. SPECTR presently includes twenty overlay segments.

A single multichannel pulse-height spectrum is considered to be the basic unit of data. All spectra are stored on a disk pack, which serves as a working file, where they are available for various types of reduction and manipulation. These operations usually result in the association of additional information such as peak locations and areas with each spectrum, but information already present may also be edited or deleted. Magnetic tape "master files" are used for permanent storage of the spectra and associated information.

SPECTR operations include a wide variety of listing and plotting options, editing functions, calibration, and data archiving. Extraction of peaks and peak areas is available using interactive display routines and least-squares Gaussian fitting or centroid calculations. Spectra may be added or subtracted from one another incorporating

zero shifts and changes in gain.

The current version of SPECTR has been in general use for the past several months. Several additions are expected in conjunction with the development of data acquisition hardware and software.

LSQ11

This program searches for least squares fits between data sets and arbitrary functions. LSQ11, written for the PDP-11 computer, was adapted from a similar program, LSQ9, written earlier for the PDP-9 computer. A skeleton subroutine forms the basis for the user to generate his own particular function. Functions of up to twenty independent variables can be fitted to data sets of up to 250 data points. Searches are based on the non-linear least squares regression technique.

FITIT

FITIT is a program to fit multichannel pulse-height spectra and extract peaks and peak areas using an arbitrary peak shape. The peak shape is defined from a user supplied table of counts versus channel number. A search is made on peak normalizations (or scale factors) and positions to find a least squares fit to data in the region. In the current version, a region may contain up to 250 channels and up to 9 peaks. A fixed or variable linear background is used. Searches are based on the non-linear least squares regression technique taken from LSQ11.

ACQTOF

Program ACQTOF is a two-parameter data acquisition package developed for the PDP-9 computer-ND 50/50 pulse-height analyzer system. Pairs of ADC conversions are used to generate spectra which are stored in the memory of the ND 50/50. Each spectrum is formed from a combination of the two conversions, such as $[(x+y) + A*(y-x)]/2$, gated by a second combination. Up to eight different spectra may be accumulated at once. A typical application of this program is the collection of neutron time-of-flight data using large volume scintillation detectors.

3. In-Beam Gamma-ray Spectroscopy Facility - M. E. Burroughs, R. A. Emigh, C. A. Fields, J. J. Kraushaar, D. L. Lingle, R. A. Ristinen and L. E. Samuelson

The laboratory facilities for in-beam gamma-ray spectroscopy are currently being upgraded. Target chambers designed especially for gamma-ray angular distribution and gamma-gamma coincidence measurements have been constructed and are now in use. The new angular distribution chamber allows measurements to be made between 15° and 90° relative to the incident beam direction. Angles less than 35° were not possible with earlier equipment. The γ-ray

coincidence chamber is designed for maximum coincidence count rate with detectors located at 45° and 135° relative to the incident beam direction. This geometry allows shielding between detectors to minimize coincidences due to Compton scattering between detectors.

A target chamber is presently being tested which will house a mini-orange electron spectrometer, discussed elsewhere in this report. This chamber will allow coincidence measurements between conversion electrons and γ-ray cascades, as well as measurements of conversion coefficients. A fourth chamber is presently being designed for angular distribution measurements with low-energy proton beams. The beam will be stopped either in the target or in a thin gold or lead foil placed behind the target. This set-up will allow measurements through 0° relative to the incident beam direction.

All chambers are interchangeable, using the same target ladder and vacuum system. About 30 minutes is required to change chambers. The angular distribution and electron spectrometer chambers have identical parts to accept a charged particle monitor for normalization purposes.

Improvements to the currently available apparatus for the measurement of magnetic moments of isomeric states by the perturbed angular distribution technique are currently in the design stages.

4. Cyclotron Orbit Calculations - D. H. Haynes and P. A. Smith

During the last year substantial effort has been put into preparing a proposal for a new light ion accelerator laboratory at the University of Colorado. This proposal is centered about a separated-sector cyclotron, which is to be injected by a smaller accelerator. It is our intent to modify the existing cyclotron to serve as the injector. For this reason certain aspects of cyclotron particle dynamics are under intensive study. A number of computer programs, under development, are being used to analyze the particle motion.

The existing cyclotron is a 52" fixed frequency alternating gradient machine with four spiral shims. The ion source is of the hooded arc variety and the ions are accelerated with a single 180° dee. Some of the modifications to this system which are being considered are:

1) Axial injection of the ions.
2) Use of three-sector geometry with radial shims.
3) Use of a single 60° dee to accelerate the ions.

With the above modifications, the only results ready for discussion at this time are the median-plane orbit calculations. Both equilibrium and accelerated orbits have been determined.

The shape of the magnetic field used for these test calculations is described by a finite Fourier series, determined analytically by applying the hard-edge approximation to the three-sector field. Consequently, the field near the center of the cyclotron is not adequately represented. An isochronous field is established by applying an iterative technique to the equilibrium orbit calculations.

For accelerated orbits the energy gains at the dee gaps are assumed to be discontinuous. That is, whenver an ion arrives at a dee gap, its energy is instantaneously incremented by an amount determined by its phase with respect to the radio-frequency. This delta-function representation of the electric field is a poor approximation near the center of the cyclotron. As a result of this, and the previously mentioned limitation of the magnetic field, orbit calculations have not yet been performed in the central region of the cyclotron.

The orbit plots summarize the results obtained to date. In all cases the average magnetic field was approximately 6500 gauss and the ratio of the field in the hills to the field in the valleys was approximately two.

In Fig. C1 an equilibrium orbit of a 1 MeV proton is shown. The dominant third-harmonic oscillation is clearly evident. For the

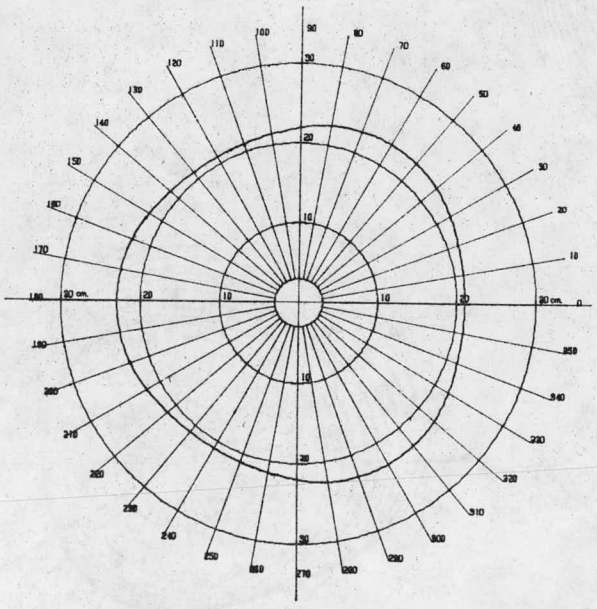

Fig. C1. An equilibrium orbit of a 1 MeV proton in a three-sector cyclotron with radial shims.

accelerated orbits shown in the remaining figures the proton was started with an energy of 1 MeV at 0° on the equilibrium orbit shown in Fig. C1. Using a 180° dee and a maximum energy-gain per turn of 0.150 MeV, a proton was accelerated to a final energy of 2.75 MeV. This orbit, shown in Fig. C2, has the desired characteristics of symmetry and centering. The maximum phase difference with respect to the electric field was only 6°. With a 60° dee and an energy gain per turn of 0.100 MeV the proton was accelerated to a final energy of 1.9 MeV. The resulting orbit shown in Fig. C3 is highly asymmetric and uncentered. The calculations for the 60° dee were then repeated with a first harmonic in the magnetic field oriented to correct the asymmetry. At a first harmonic field amplitude of 1½% of the main field the symmetry seen in Fig. C2 is regained.

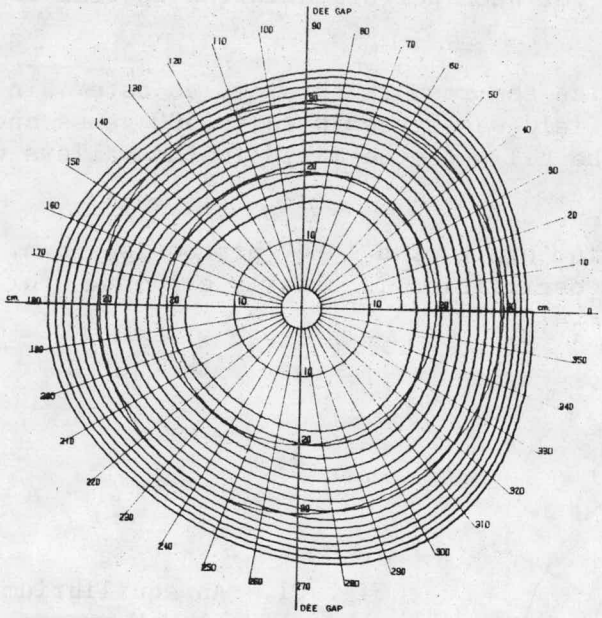

Fig. C2. The orbit of a proton accelerated with a single 180° dee.

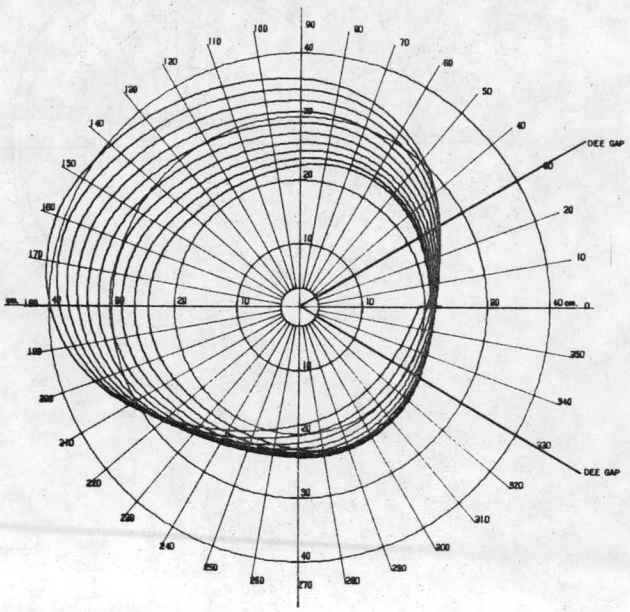

Fig. C3. The orbit of a proton accelerated with a single 60° dee.

5. Electronics Maintenance and Development - Lee A. Erb

a) Cyclotron

i. Magnet System

Cyclotron magnets and their power supplies have given little trouble this year. Only minor problems were encountered with the SCR regulated main magnet power supply. An adjustment trim pot for an SCR phase timing circuit became intermittent, causing a shift in SCR gate pulses to one pair of SCRs, resulting in unbalanced power line currents. When the supply was run at high magnet currents, the current in one power line phase would exceed the circuit breaker threshold resulting in a trip-off. Sufficient current handling capacity was available in the supply to avoid damage, and the current regulation of the supply was not sufficiently degraded to disrupt normal cyclotron operations below the circuit breaker trip-off threshold.

A beam extraction magnet known as the 5-degree magnet has again suffered a winding-to-ground short circuit. This problem has previously been experienced requiring the rewinding of the magnet coils. The magnet power supply normally floats with respect to ground which allows for a single magnet-to-ground short circuit before ground currents disrupt the regulation and magnetic fields. The problem was discovered when a second magnet on the same power supply system also shorted thus disrupting operation. The second magnet has been repaired and materials are being acquired to repair the 5-degree magnet at a convenient time. In the interim, normal operation can be continued in spite of the 5-degree magnet short circuit.

No trouble with the other cyclotron magnet systems has occurred this year.

ii. RF System

The RF system final amplifier power supply was rebuilt this past year because of the failure of a number of high voltage filter capacitors utilized in a series-parallel configuration in its ripple filter. Higher voltage capacitors, which replace the series-parallel stacks of lower voltage units, were installed and additional crowbar circuitry was added to reduce the discharge surge currents. Solid state rectifier assemblies, with adequate safety margins, replaced earlier units to improve reliability. These modifications have substantially reduced the trip-offs previously experienced with the system.

b) Safety Interlocks

A new personnel safety interlock system was completed and put into operation this year. Modifications of beam line and experimental hardware throughout the years had caused the original system to become out of date.

The new personnel interlock system was designed to be adaptable to the beamline conditions and only insist upon control over areas that require it at any given time. Operator convenience was also a concern, prompting a display of both interlocks required and their status.

c) Beam Transport System

i. 45^{o} Magnet Supply

The chopper stabilized regulator error amplifier failed in the 45^{o} magnet power supply. The high speed overcurrent detection circuitry previously installed protected the supply from damage due to unregulated overcurrent conditions. A more modern, higher performance operational amplifier is being used for replacements with no modifications required to the existing circuitry or mounting sockets.

ii. General 300 Amp and 600 Amp Supplies

The laboratory's standard 300 amp and 600 amp power supplies have demonstrated a high degree of reliability this last year. Other than the normal preventive maintenance, the only unusual repairs performed on the supplies have consisted of filter capacitor replacements which have been done during the annual preventive maintenance periods.

iii. Cooling Interlocks

Additional beamline devices have been added to the beamline cooling interlock system. The flexibility of the system allows for easy expansion.

iv. RF Beam Deflector

The high voltage RF beam deflector has been used on a number of experiments this past year with reasonable results. It was found that the voltage swing initially calculated to deflect the beam was somewhat conservative. This allows the hardware to run at reduced power levels thus reducing the stress on dielectrics and components. Some modifications are in order to make interlock trouble shooting easier and general operation more reliable.

v. Beam Swinger

The drive motor on the beam swinger target chamber sliding vacuum seal lost a field winding due to the failure of a limit switch. The motor control is a current limiting thyristor-type controller for the armature circuit but the field excitation is at a fixed voltage. The motor had driven into a mechanical stop and had stalled under armature circuit current limiting. Insufficient flow of cooling air resulted in the field winding failure. A motor mount problem was also repaired during the brief interval that was required to replace the windings and switch.

d) Data Processing

i) PDP-9 Computer

The Digital Equipment Corporation Model PDP-9 computer continued to perform well this year with only a moderate amount of trouble. A number of intermittent logic cards were tracked down earlier in the year when temperature-related failures were experienced. The high maintenance items are still the line printer and card reader. Data are still being acquired on-line with this computer in conjunction with the Nuclear Data ND 50/50 multi-channel pulse-height-analyzer.

ii) ND 50/50 PHA

Again this year only minor component failures were encountered with the Nuclear Data ND 50/50 pulse-height-analyzer system. It has seen much use as both a stand alone pulse-height-analyzer and as a front end ADC system for on-line computer controlled data acquisition.

iii. PDP-8E Computer

The Digital Equipment Corporation PDP-8E computer utilized with the x-ray fluorescence spectrometer has performed flawlessly this past year. The computer typically runs about 10 hours a day.

iv. PDP-11/34 Computer

This is the first year for operation of the new Digital Equipment Corporation PDP-11/34 computer. The performance of the standard hardware and software is superb. The flexibility of the system allows for multiple complex tasks to share simultaneously the machine's facilities. Data acquisition software and hardware are being readied for on-line use this coming year.

v. PDP-11/34 Interfacing

A multiple analog-to-digital converter control unit and interface to the PDP-11/34 has been built and software drivers are being readied. The ADC control allows for independent or coincident operation of any combination of the three ADC's and an eight bit routing register. CAMAC was not used as a computer entry port for the ADC control because the addition of a more efficient direct memory access port to the computer memory for the ADC data is planned as a modification next year. The DMA feature operating with the RSX-11M software system greatly reduces dead time effects of the resource sharing executive.

e) Experimental Support

i. Energy-Loss Spectrometer

The zoom lens quadrupole magnets at the entrance of the energy

loss spectrometer developed restrictions in some of the cooling water passages. A buildup of corrosion occurred at brazed joints near the end of two windings which in each case caused the restriction of cooling water flow in the winding. The water line to each magnet is protected by a flow switch and the individual windings in parallel water circuits within each magnet have their own temperature sensing switches. A restriction in a single water circuit may not result in a flow switch drop-out but the winding temperature rise will actuate the thermal switch. The restricted areas were drilled out and flows were measured. Additional checks were made on the temperature rise of individual magnet coils and the temperature sensing switches were tested for proper protection thresholds.

Position-sensitive proportional counter development has continued this past year. The detector signal and power cabling was expanded slightly to accommodate modified detector designs. Co-ax cable grounding was improved to reduce the coupling of noise into the detector housing. A high voltage interlock controlled by the chamber vacuum fault indicator was implemented so that damage to cables and circuitry would be avoided during poor vacuum conditions.

ii. X-ray Fluorescence Spectrometer

The x-ray fluorescence spectrometer has performed well this year with little down time due to corrective maintenance. The only failure of the x-ray source system was due to a Variac utilized in the x-ray tube anode voltage regulation circuit. A brush holder jammed which with the wear of its carbon element caused an intermittent contact to the transformer windings. Minor arcing was observed along with unstable operation of the anode supply. An immediate investigation discovered the problem before damage was caused to the Variac transformer. Repair was accomplished by replacing the brush assembly and cleaning the transformer windings.

iii. Ion Source Test Facility

An area is being set up in which will be housed the equipment necessary to test ion sources. The original cyclotron model magnet has been modified to a gap opening of six inches and is being outfitted with a vacuum chamber and pumping system. The magnet is powered by the old cyclotron main magnet power supply and regulator equipment. The facility will be used for maintenance on the present ion sources in use and will also serve as a development and evaluation facility for new ion source designs.

iv. NIM Module Service Program

A program of preventive maintenance has been initiated to decrease the down time of defective NIM modules in the laboratory. All modules will be checked for proper operation at least once a year. In addition, trouble reporting forms have been made available in an attempt to allow the experimenter the opportunity to communicate to the repair technician the troubles he is experiencing with the equipment.

v. General Purpose NIM Modules

A number of NIM modules were produced in-house to fulfill special experimental needs. When needed, we continue to develop and manufacture special purpose NIM modules which are not available on the commercial market.

6. Neutron Detector Development for TOF Studies - W. P. Alford, R. E. Anderson, A. Craig, P. Craig, R. A. Emigh, G. Feldkamp, D. A. Lind, A. Park, D. E. Prull, P. A. Smith and C. D. Zafiratos

In order to obtain better energy resolution in neutron time-of-flight data, an effort is currently under way to upgrade the 30-meter flight path facility. In the past an array of up to seven eight-inch diameter Colorado-style detectors has been used, but the problems associated with the low counting rate have made data acquisition difficult. This indicates a need for neutron detectors of larger volume. The large volume requirement is accompanied by two other requirements: 1) time resolution not worse than one nanosecond in order to achieve the overall goal of improved energy resolution, and 2) good n-γ discrimination. Two different detector types are under investigation to achieve these objectives.

One type of detector that has been assembled and tested is a long tube-style detector filled with NE-224 liquid scintillator, and viewed by a single two-inch RCA 8575 photomultiplier tube at one end. The length of the plexiglass tube used is 80 cm, with an inside diameter of 4.4 cm. The outer walls are wrapped with black construction paper to allow light collection by total internal reflection only, thus assuring good time characteristics. With this geometry, time compensation can be employed to correct for the range of positions in the detector at which the scintillation can occur; this time compensation is effected by merely tilting the axis of the detector with respect to the neutron flight path,[1,2] which forces neutrons that strike the scintillator nearest the photocathode to traverse a greater distance (see Fig. C4).

The detector was tested by using the reaction $^{9}Be(^{3}He,n)^{11}C$ at 25.4 MeV, at a laboratory scattering angle of 61° and with a mean flight path of 6.18 m. Resolution as a function of tilt angle was measured (see Fig. C5). At the observed optimum tilt angle, the time resolution obtained was 0.96 ns. In addition, the n-γ discrimination was nearly equal to that obtained from the 2-inch thick Colorado-style detectors.

In order to implement this design at the 30-meter stations and achieve the desired detector volume, it would be necessary to assemble an array of such tubes, with several light-piped onto a single 4-inch RCA4522 PMT (which might result in some degradation of the time resolution) or with a 2-inch phototube attached to each. Some modification of the earthen shielding at the 30-meter station would also be necessary to accommodate this geometry.

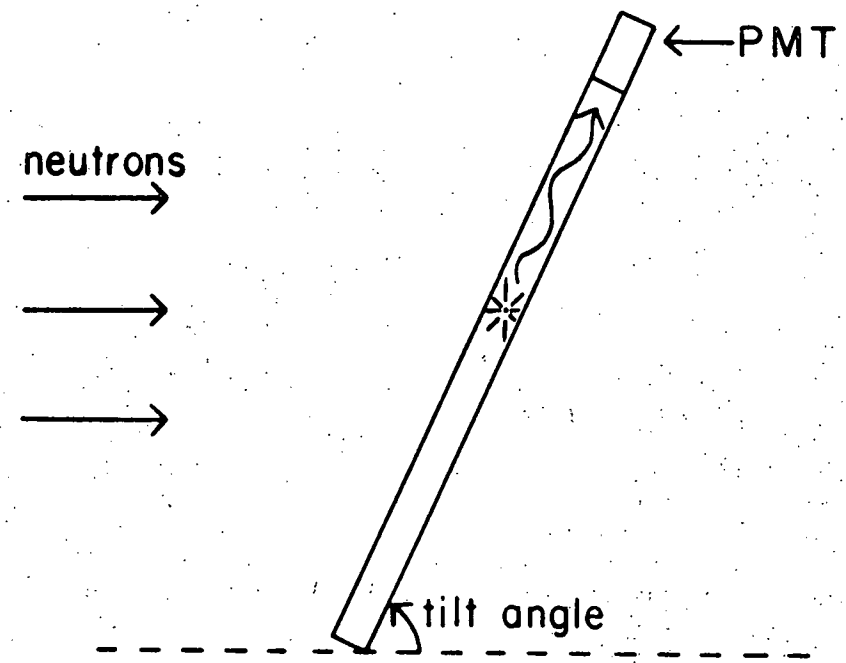

Fig. C4. Detector orientation for time compensation. Because of the tilted geometry neutrons strike the bottom end earlier, thus compensating for the increased delay time for scintillation light reaching the PMT.

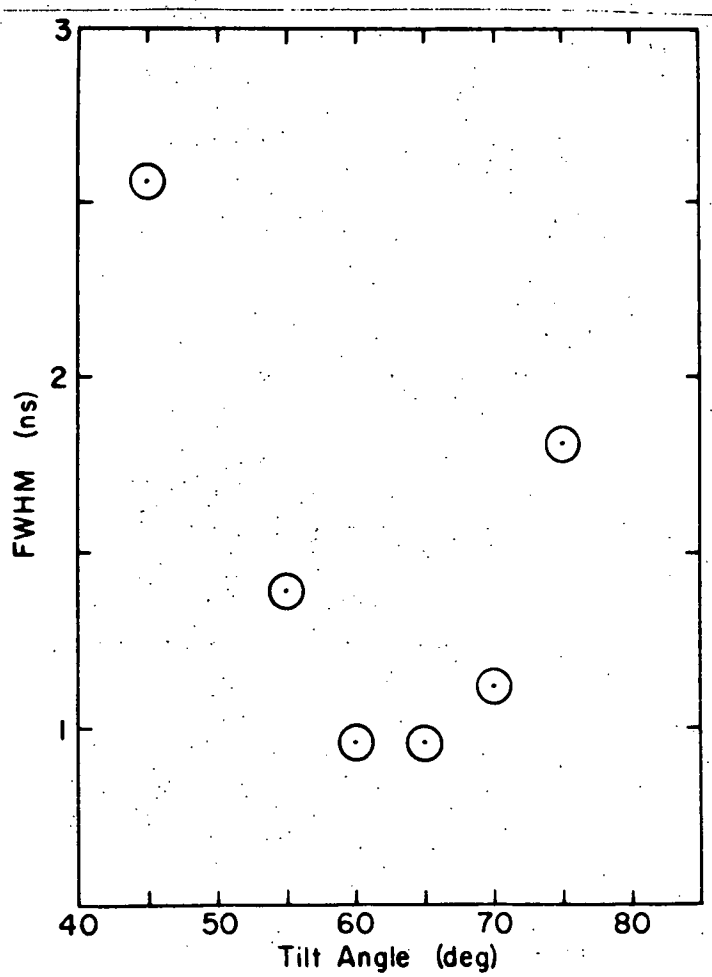

Fig. C5. Time resolution as a function of tilt angle for the time compensated long tube-style detector. Note that 68^{o} is the tilt angle for which light traveling parallel to the tube has a velocity component in the neutron's direction that is equal to the velocity of the neutrons.

A second type of neutron detector known as the very large detector has also been built and tested. Large volume detectors have an intrinsic uncertainty in the position of scintillation. For a detector with a single PMT located downstream from the scintillator and not time compensated, this position uncertainty gives a time uncertainty equal to the difference between neutron and scintillation light flight times through the detector. For 30 MeV neutrons in a 14" long detector this uncertainty is 3 ns. The very large detector (VLD) has two PMT's to eliminate this time uncertainty (see Fig. C6).[3]

Let t_1 be the timing signal taken from the upstream PMT and t_2 the timing signal taken from the downstream PMT; then timing spectra of the form $t_1-\alpha t_2$ are obtained, where α is chosen to give best time resolution. The constant α can be easily determined for axial rays. If x is the distance into the detector at which a scintillation occurs and v is the neutron velocity, then

$$t_o=t_0+\frac{x}{v}+\frac{xn}{c}$$

and $$t_2=t_0+\frac{x}{v}+\frac{(L-X)n}{c}$$

where L is the length of the detector and n is the index of refraction. If

$$\alpha=\frac{c-vn}{c+vn},$$

then $t_2-\alpha t_1$ will not depend upon x. The v dependence of α means that the faster neutrons require slightly smaller values of α than the slower neutrons.

Most of the scinillation rays are not axial. If the rays correspond to the maximum angle of total internal reflection, then

$$\alpha=\frac{c-vn^2}{c+vn^2}.$$

For 39.3 MeV neutrons the experimentally determined value of α was between .25 and .30. This is within the calculated bounds of α=.23 for rays at the maximum angle of total internal reflection and α=.41 for axial rays.

The first VLD was constructed from unannealed acrylic using a solvent cement and was filled with NE-224 liquid scintillator. A Dow Corning optical coupling compound was used to attach the RCA 4522 PMT's. The detector was surrounded with aluminum foil in order to improve the neutron-gamma ray discrimination. At a distance of 30 meters a time resolution of 2.4 ns FWHM was obtained.

A problem with crazing in the container caused by NE-224 attacking the acrylic material led to the construction of a new VLD using annealed acrylic and a cyanoacrylate cement. A new support structure that did not stress the container walls was also constructed.

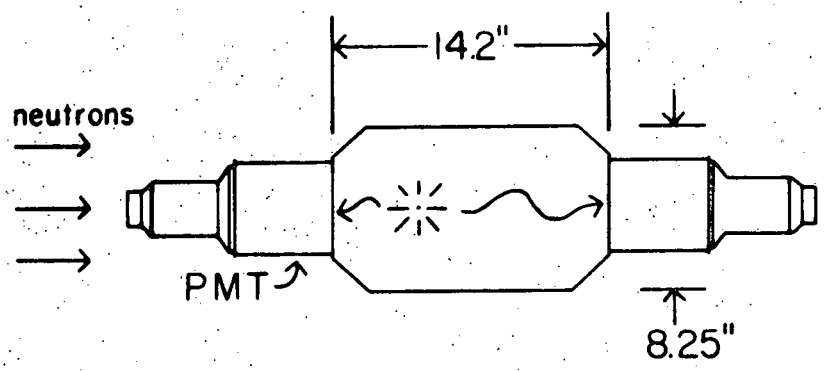

Fig. C6. Large volume detector orientation and dimensions. It has a volume of 11.3 liters.

Relative efficiencies of the VLD as compared to the Colorado-style 2" detector were measured as a function of neutron energy (see Fig. C7). The relative efficiencies do not account for the slight difference of areas presented to the neutron beam by the two detectors.

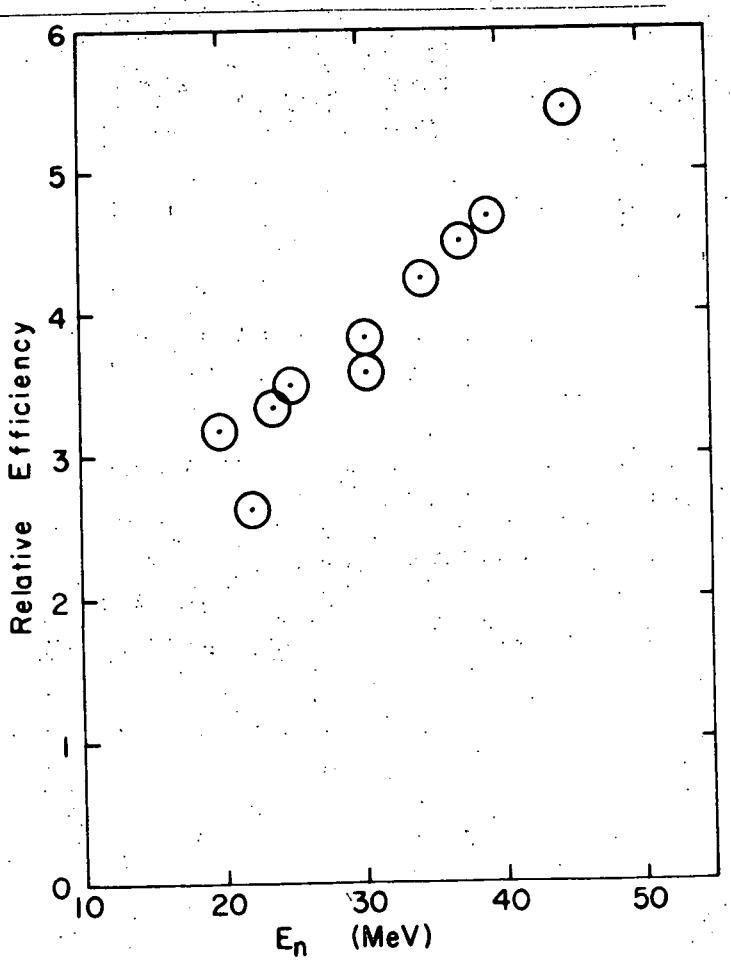

Fig. C7. The relative efficiency of the VLD to the Colorado-style 2" detector is shown as a function of neutron energy.

A comparison of the time spectra may be seen in Figs. C8, C9 and C10 using the reaction $^{9}Be(^{3}He,n)^{11}C$ at 6^{o} with $E(^{3}He) = 33$ MeV. The VLD at 25 m gave 1.7 ns FWHM for the ground state neutron peak. However, the beam burst length was excessive during this measurement as indicated by the 1.4 ns width of the ground state peak in the 2" detector spectrum.

A glass VLD has been assembled, filled with NE-213, and attached to the PMT's with acrylic light pipes and a transparent Dow Corning dielectric gel. It will be tested shortly.

[1] C. D. Goodman, J. Rapaport, D. E. Bainum and E. Bryant, Nucl. Inst. and Meth. 151 (1978) 125.

[2] C. D. Goodman, J. Rapaport, D. E. Bainum, M. B. Greenfield and C. A. Goulding, IEEE Trans. in Nucl. Sci. NS-25 (1978) 577.

[3] J. D. Carlson, R. W. Finlay and D. E. Bainum, Nucl. Inst. and Meth. 147 (1977) 353-360.

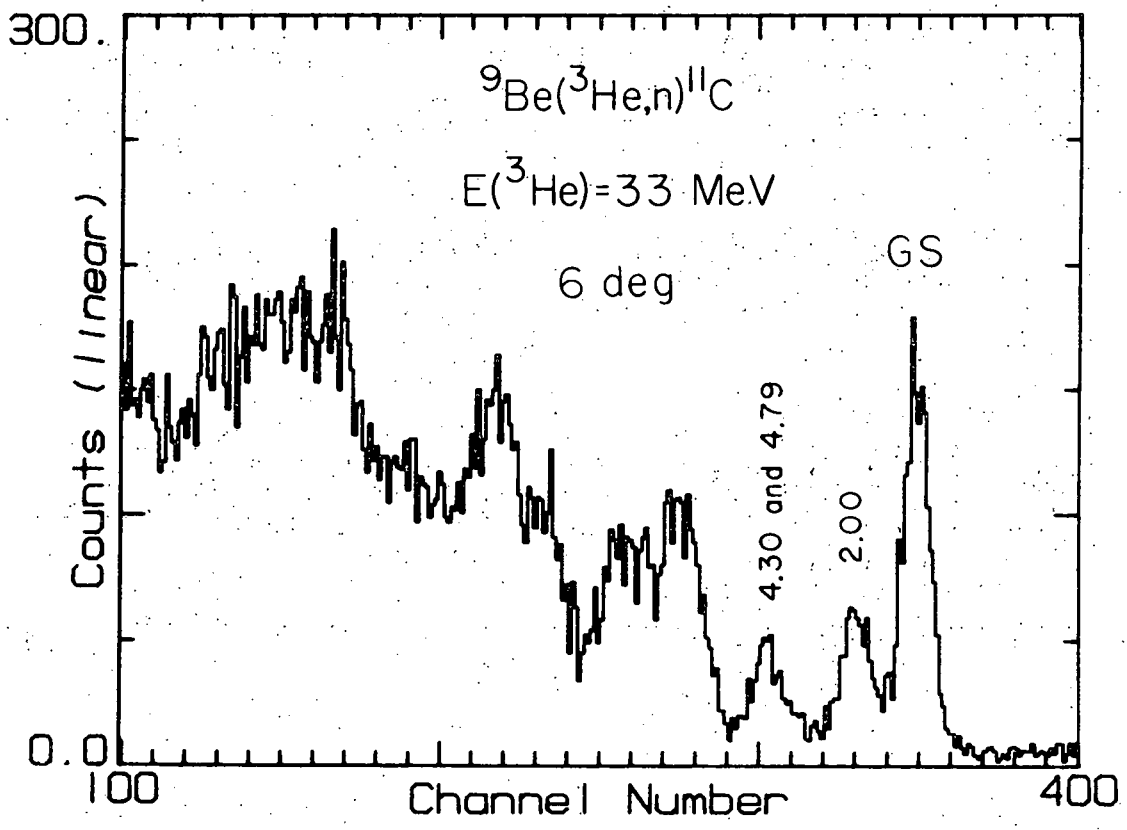

Fig. C8. Spectrum for a 2" detector at 9 m. The time per channel is 0.148 ns.

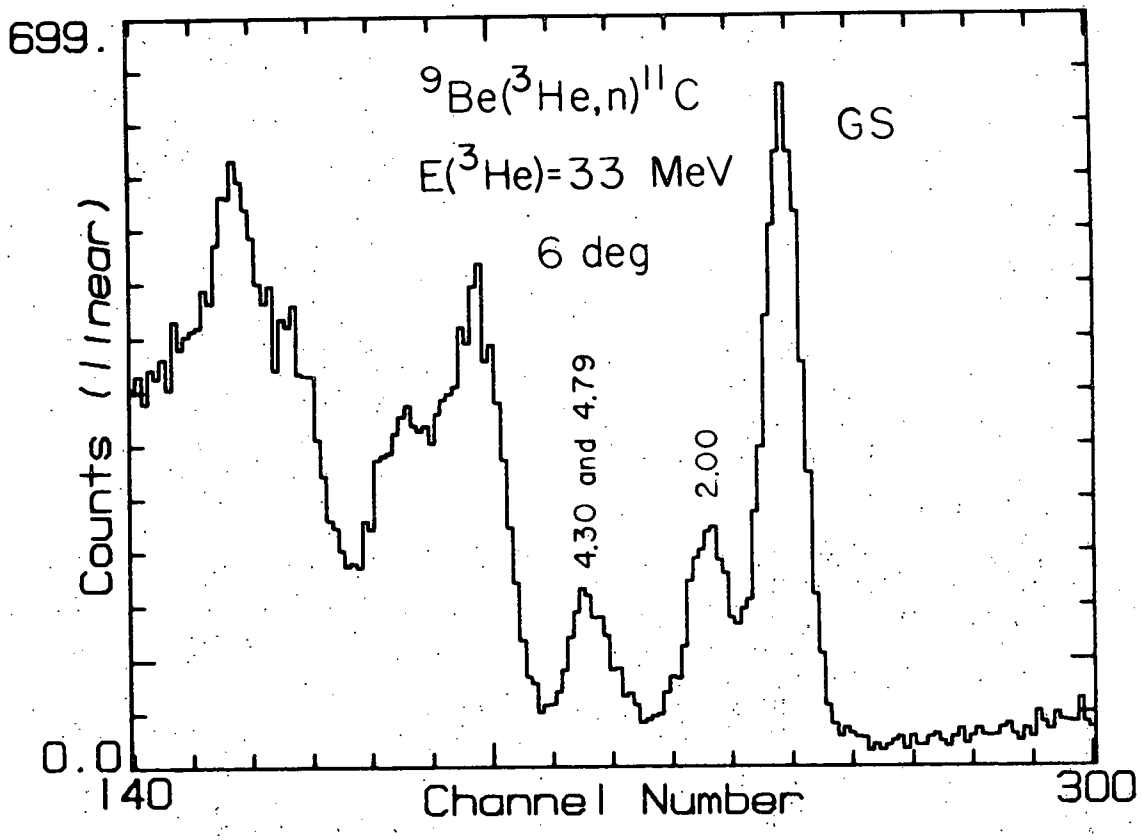

Fig. C9. Spectrum for the VLD at 9 m.

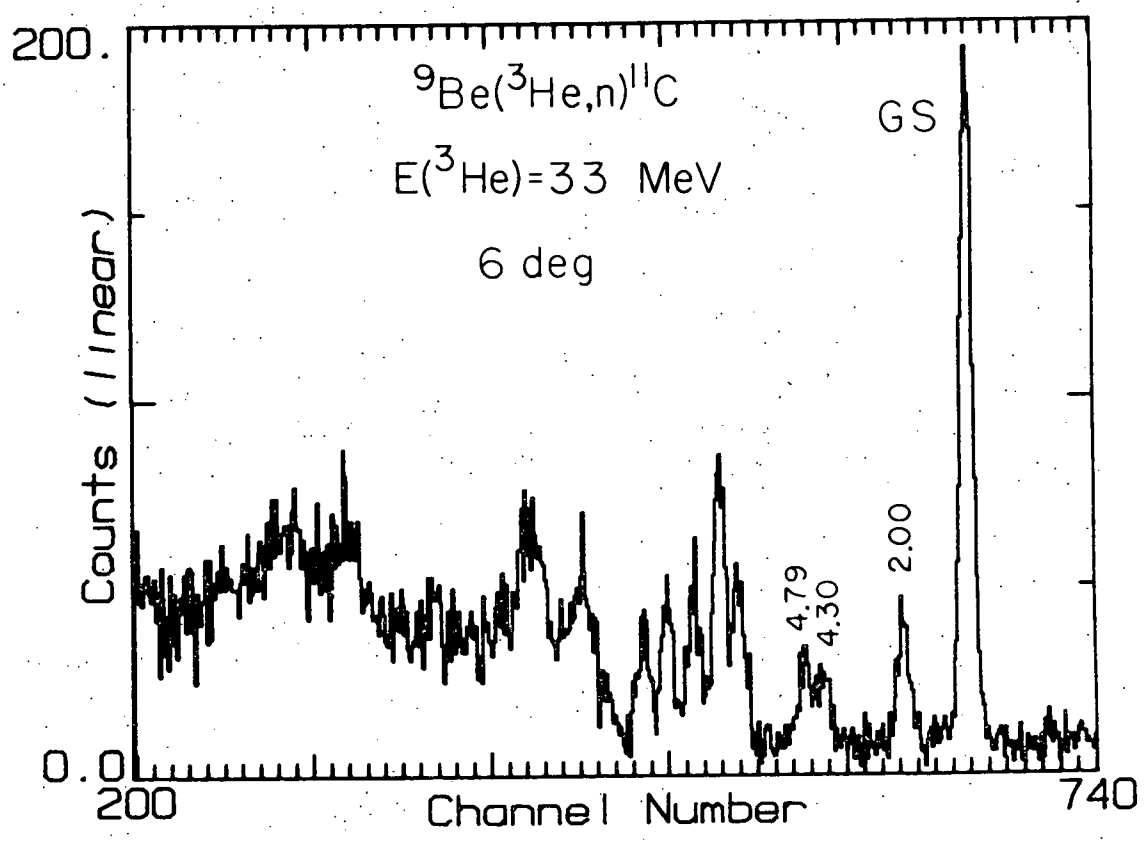

Fig. C10. Spectrum for the VLD at 25 m.

7. Construction of an Ion Source Test Facility - B. Smith, L. Erb, J. R. Homan, P. Kaczkowski, P. Smith and C. Zafiratos

Recently there has been considerable interest in the development of new ion sources at the University of Colorado. The ion sources under study now include: a) a large P.I.G. source for the newly proposed Colorado Light Ion Accelerator Facility, b) a smaller version of this source for the acceleration of lithium ions in the existing C.U. cyclotron, and c) an ion source optimized for pulsed-beam time-of-flight studies. In order to facilitate development of these sources without interfering with the operation of the cyclotron an ion source test facility is under construction.

The magnet for the facility is the original model magnet for the C.U. cyclotron. It had also served for some years as a beam analyzing magnet but has not been in use in recent years. This magnet has 15-inch diameter pole tips and has been modified to have a 6-inch gap suitable for testing the large ion source for the injector cyclotron of the proposed Colorado Light Ion Accelerator Facility. A 750-ampere power supply was needed for this magnet and fortunately the motor-generator set which at one time had provided main magnet excitation for the cyclotron was standing idle since being replaced by a solid-state supply several years ago.

Cables have been pulled from the motor-generator set to the test facility location. Control circuitry has been constructed and installed. Thermal sensing switches have been installed and made part of the interlock system. A complete 10-inch diffusion pumping system has been acquired to handle the large gas flow needed in an ion source test facility.

The vacuum chamber is in the initial phase of construction in our machine shop. One of its access ports will be an exact duplicate of the ion source port on the C.U. cyclotron so that present ion sources can be tested without interruption of normal cyclotron operation.

8. Shimming of the Central Region to Improve Cyclotron Performance - C. D. Zafiratos, P. A. Smith, A. B. Phillips and D. A. Lind

It had been known for some time that the beam in the C.U. cyclotron had a substantial vertical oscillation amplitude which caused loss of beam at about 7" radius where ν_z has a minimum.[1] Since this oscillation caused no serious difficulties it was ignored, as the most likely cause was thought to be a slight median plane field error in the central region which would require shimming. Since central region shimming would require removal of the RF liners and, hence, considerable down time, the problem was tolerated for several years.

The opportunity to correct the problem was created in part by the problem itself in October of 1977. The excursions of the beam from the median plane caused ion erosion of the leading edge of the dummy dee which finally reached a water line at that time as shown in Fig. C11. While the liners and dummy dee were out for repair a circular soft iron shim of 0.012" thickness and 3" diameter was attached to the bottom RF liner to raise the magnetic median plane slightly. Additionally, graphite protective blocks were placed over the dummy dee.

Fig. C11. Severe ion erosion of the dummy dee can be seen at the top of this photograph just left of center.

Several effects of the shimming operation have been noted since.

a) The puller slit and first-turn slit which previously glowed bright red on 35 MeV alpha tunes now run cool.
b) Ion erosion of the graphite blocks covering the dummy dee is minimal and is now symmetric between the top and bottom.
c) Beam on target increased only slightly for most tunes.

A differential probe trace is shown in Fig. C12 for the 15 MeV H_2^+ tune. The beam still strikes the top element of the

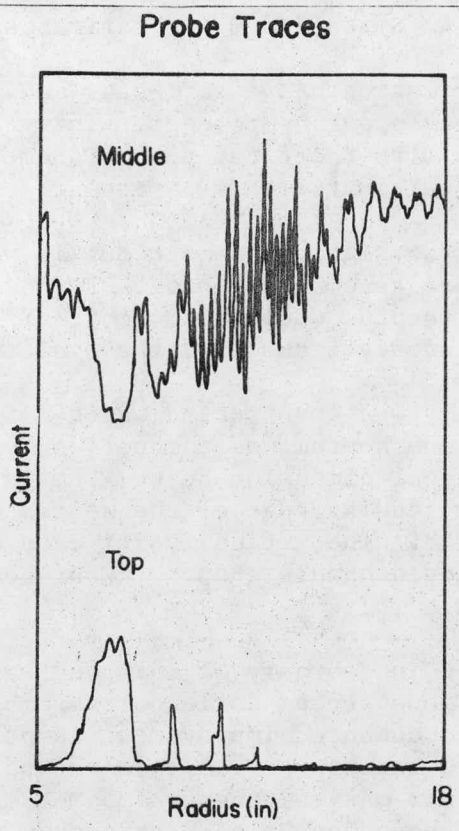

Fig. C12. A differential probe trace taken after shimming shows a tendency of the beam to strike the top element near 7" radius. However, this effect is greatly reduced when compared to the next figure which shows a similar trace before shimming.

differential probe near 7" radius but no longer does so in the central region. Fig. C13 is a similar trace obtained before the shimming and beam is seen to strike the top element at even the smallest radii. Further, the drop in the middle element intensity is more dramatic.

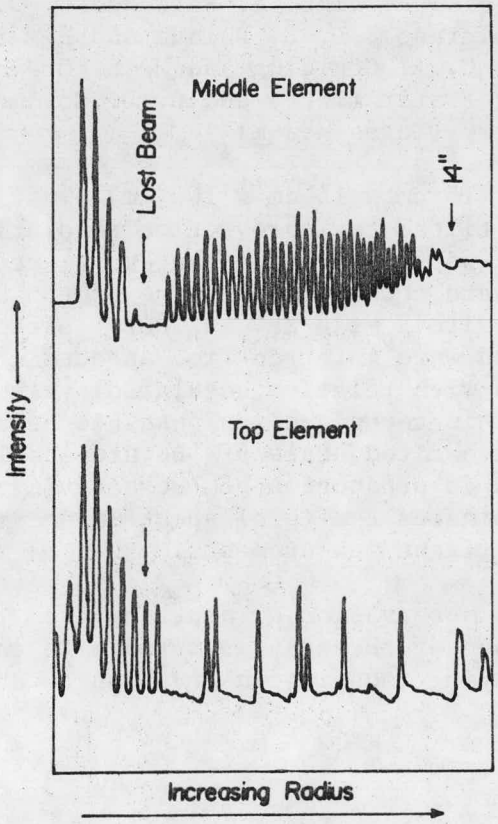

Fig. C13. The beam was seen to be high even at small radii in this differential probe trace taken before shimming. The turn pattern is more sharply defined at small radii than in the previous figure because a small first-turn defining slit was in place.

[1] D. A. Lind, Technical Progress Report (1967) 69; also P. A. Smith, C. D. Zafiratos and D. A. Lind, TPR (1977) 135.

9. Performance of the New Deflector-Septum Assembly - D. A. Lind, A. B. Phillips, P. A. Smith and C. D. Zafiratos

The University of Colorado cyclotron has a deflector and septum fabricated with water cooled copper components. This system has been extremely reliable with the first such system installed in 1963 serving continuously until this past year.

The original unit still shows no signs of damage but it was felt to be desirable to have a spare assembly on hand. Further, there was some hope that a thinner septum would allow more efficient extraction of the various maximum energy beams from the cyclotron.

A new deflector-septum assembly was constructed which differed from the original in three ways. The septum was thinner, only 3/4 mm thick. It was also larger in vertical dimension being 1 cm in height. Finally, the V-shaped notch on the leading edge of the septum was made with a sharp acute angle of 11^{o}. Theoretical worst case estimates indicated that this septum could handle about 2 kW of beam power and it was red-lined at 1 kW.

The new assembly was installed in February of 1978 and has operated reliably since. The previous septum-deflector assembly is now a spare. The most clearly documented improvement in performance which can be attributed to the new assembly is an approximate doubling of the intensity of the maximum energy (35 MeV) alpha beam. Up to 9 μA of 35 MeV alphas have been placed on target in the energy-loss spectrometer. Typical beam intensities now available for most experiments with the energy-loss spectrometer are 6 μA.

10. Efficiency Measurements of Large Neutron Detectors for Intermediate Energies - D. A. Lind, A. Park and C. D. Zafiratos (Univ. of Colorado); D. E. Bainum and J. Rapaport (Ohio Univ.); C. A. Goulding and M. B. Greenfield (Florida A & M); C. C. Foster (IUCF) and C. D. Goodman (ORNL); and S. D. Schery (Texas A & M)

The efficiency of a large (15 cm x 15 cm x 100 cm) plastic scintillator neutron detector, tilted to improve time resolution, was measured in three different ways. In one measurement, neutrons from the $^{7}Li(p,n)^{7}Be$ reaction were counted during the proton bombardment of a fresh ^{7}Li target with E_p=120 MeV at IUCF. Afterwards, the number of ^{7}Be nuclei created were inferred from an absolute count of ^{7}Be gamma rays coupled with relative angular distribution measurements of $^{7}Li(p,n)^{7}Be$. This technique was possible because only the ground state and first excited state of ^{7}Be are stable against particle decay and lead to production of ^{7}Be activity. The sum of these two states dominates the (p,n) spectrum and is easily measured in the time-of-flight measurements.

The second method involved observation of neutrons from $^{12}C(p,n)^{12}N$ (g.s.). A comparison of these data was made to the cross section predicted by applying isospin conservation to absolute

data for the $^{12}C(p,p')^{12}C$ (15.1 MeV) reaction. Both of these methods gave an effective solid angle of the tilted detector equivalent to 32% of its cross sectional face (15 x 15 cm).

A third measurement was made near E_n=45 MeV using neutrons from the $^{9}Be(^{3}He,n)^{11}C$ reaction and the 30-meter flight path facility at the University of Colorado. This region of neutron energies corresponded to those observed in previous (p,n) measurements at IUCF with E_p=60 MeV. In these measurements comparison was made to data simultaneously acquired with the Colorado-style 2" thick x 8" diameter neutron detectors. These detectors have measured efficiencies up to E_n=35 MeV and it was felt that extrapolation to 45 MeV guided by Monte Carlo efficiency calculations was reliable. However, when these results were compared with efficiencies inferred from a comparison of $^{12}C(p,n)^{12}N$ (g.s.) with $^{12}C(p,p')^{12}C'$ (15.1 MeV) at E_p=60 MeV a substantial discrepancy was observed, with the Colorado results indicating the larger efficiency. Whether this discrepancy indicates a breakdown of the assumed isospin symmetry in the (p,n) to (p,p') comparisons is unknown at present.

11. A Magnetic Filter for Conversion Electrons - D. L. Lingle and R. A. Emigh

A magnetic filter of the mini-orange design has been constructed for the in-beam study of conversion electrons. The design is essentially a copy of devices in use at Groningen[1] and at the University of Kentucky.[2] The filter transports electrons in a given momentum range from a target onto a Si(Li) detector for energy analysis. The magnetic filter is made up of 5 Recoma 20 magnets (each 30.5 mm x 15.0 mm x 2.0 mm) fixed into a radial geometry as shown in Fig. C14. We are now in the process of obtaining the curve of transmission efficiency versus electron momentum for the filter.

---

[1] J. Van Klinken et al., Nucl. Inst. and Meth. 130 (1975) 427.
[2] D. E. Miracle, University of Kentucky, 1977, to be published.

12. High-Purity Germanium Detectors for Charged-Particle Reaction Studies - R. A. Ristinen, J. L. Homan, R. E. Anderson, J. J. Kraushaar and J. R. Shepard

A detector telescope for charged-particle studies at intermediate energies was developed specifically for use in (p,t) investigations with E_p=175 MeV at the Indiana University Cyclotron Facility. The detectors were made at the University of Colorado with germanium obtained from General Electric Corporation. The two detectors, each 14 mm thick, have contacts of lithium and palladium. They are mounted back-to-back in a cryostat so that particles having ranges of up to 28 mm in germanium will be stopped in the detectors. Signals are taken separately off each detector.

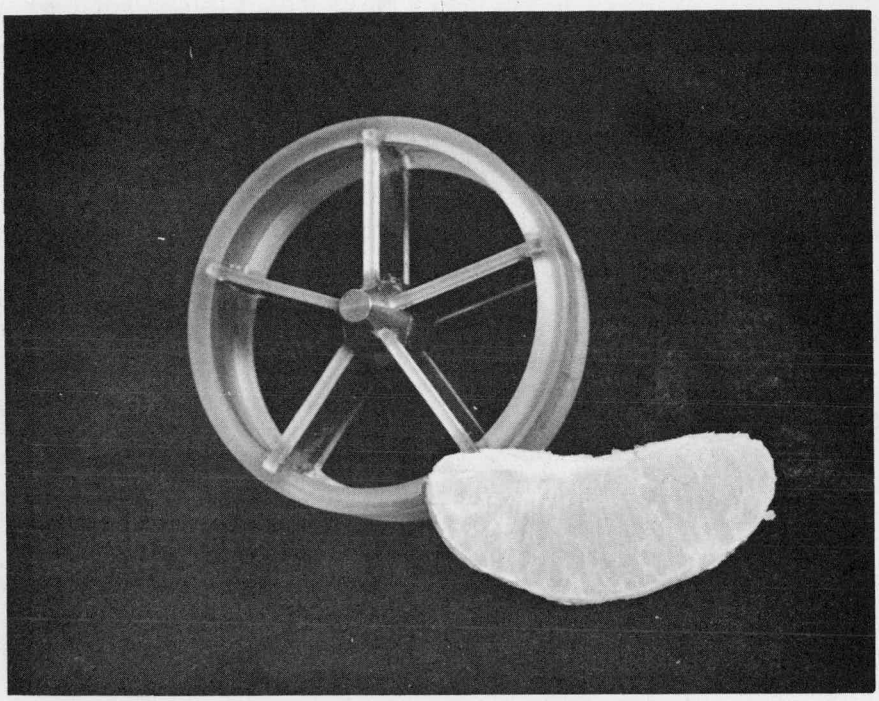

Fig. C14. The magnetic filter is made up of five magnets fixed into a radial geometry between a central lead plug and a lucite ring.

The cryostat shown in Fig. C15 was also designed and built at Colorado. The design was adapted from a device developed earlier at the University of California, Davis, by N. S. P. King and others. It is easily portable, and for the experiment it was mounted on one of the detector trays in the existing scattering chamber at Indiana with flexible LN_2 fill and vent lines connected through the scattering chamber wall. The vacuum jacket is sorption-pumped and sealed so as to be completely independent of the scattering chamber vacuum. The cryostat is super-insulated with several layers of silver-coated mylar and holds about 1 liter of LN_2 which lasts for a time in excess of 30 hours. The energetic charged particles incident on the detector pass through a thin window of aluminized mylar which separates the chamber vacuum from the cryostat vacuum. The cryostat has both entrance and exit windows for the charged particles so that a veto counter can be used to discriminate against long-range particles which pass through both detectors. As an entrance collimator, one may use either a conventional aperture or a "live" collimator made of scintillator material and used in the veto mode.

As an aid in monitoring the performance of the detectors a weak (<1 μCi) source of ^{207}Bi on a 0.0005 cm thick mylar film was mounted between the two detectors. The facing surfaces are the p-type palladium contacts toward which the detectors deplete as bias

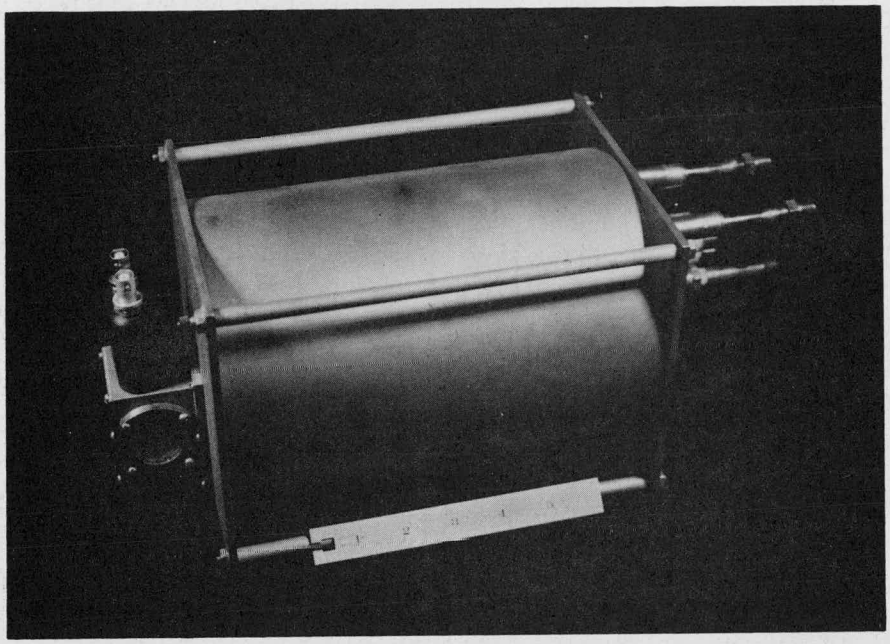

Fig. C15. The detector cryostat. The scale is in inches. The LN_2 fill and vent lines and the vacuum pumpout are to the right. The incident particles pass through the circular window on the rectangular box attached on the left. Signal connections are shown on the top of this box. The incident particle direction is perpendicular to the symmetry axis of the cylindrical LN_2 reservoir and vacuum jacket. This design allows particle detection at small scattering angles.

voltage is applied. Thus the presence in the spectrum of the conversion-electron lines from the ^{207}Bi source confirms that the detectors are fully depleted while providing a check on the energy calibration and resolution.

Preliminary data were taken at Indiana in April, 1978, for the (p,t) reaction on a number of targets. To our knowledge these data represent the first reaction (as opposed to scattering) data ever taken with multiple HPGe detectors mounted in a telescope configuration. Because of incompatibility of magnetic tape units at Indiana and Colorado we have not yet been able to analyze the data and have neither spectra nor angular distributions to present at this time. As an initial check of the detector system a spectrum was taken (using a different magnetic tape unit) of 88 MeV protons scattering from carbon. The spectrum shown in Fig. C16 was taken with no collimating aperture between target and detector. This spectrum was taken at a scattering angle of 45^{o} with the detector at a distance of 250 mm from the target.

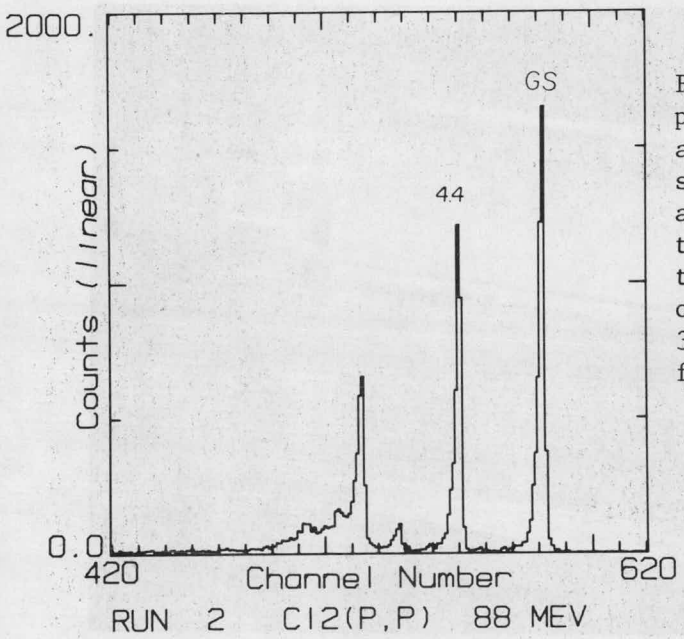

Fig. C16. A spectrum of 88 MeV protons scattered from carbon at an angle of 45°. The ground state and 4.4 MeV state of ^{12}C are labelled. For this spectrum there was no collimator between target and detector and the observed line width of about 350 keV is completely accounted for by reaction kinematics.

The detector entrance window is circular and 12 mm in diameter. The calculated value of $\frac{dE}{d\theta}$ =182 keV/degree results in a kinematics contribution of the order of 300 to 400 keV FWHM. The observed line width is about 350 keV FWHM. In order to evaluate the detector performance more completely, further measurements will need to be made with proper collimation and heavier targets.

13. A Scintillator Telescope for the Helical Cathode Proportional Chamber - R. C. Weiss

The particle identification capabilities of the charged-particle spectrograph have been enhanced by the addition of a scintillator telescope. In its initial use the system had a 1/16" thick scintillator backed by a 1/2" thick scintillator and was coupled to the back of an existing helical cathode proportional chamber. By taking energy-loss signals from both scintillators very good particle identification is achieved. A spectrum taken with this system for the $^{40}Ca(\alpha,p)^{43}Sc$ reaction is shown in Fig. C-17, where the protons have been clearly resolved from the other reaction products. Additional scintillators of 1/32", 1/8" and 1/4" thickness are being constructed so that a double scintillator system may be assembled for optimum particle identification in any particular reaction.

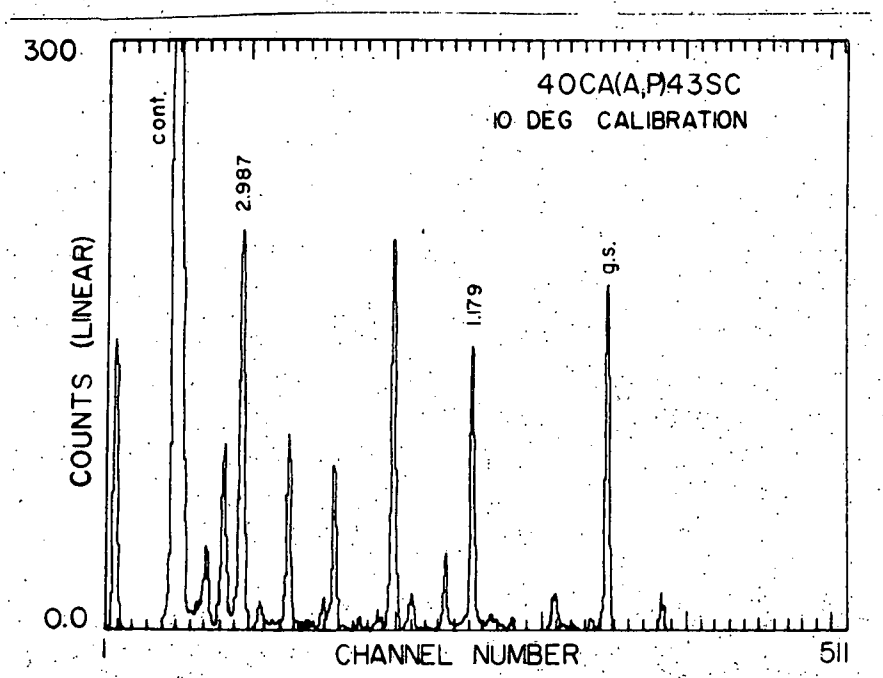

Fig. C17. A spectrum taken for the $^{40}Ca(\alpha,p)^{43}Sc$ reaction with the new double scintillator system. Excitation energies are given in MeV.

D. Cyclotron Operation - A. B. Phillips

Operation for the period 1 September 1977 to 31 August 1977 is covered below. Table D-I shows hours of cyclotron operation by purpose. Table D-II shows hours of operation by particle accelerated. An additional 211 hours were spent in tests of cyclotron components without beam.

Of the 8760 hours in the year, the cyclotron was ready for use 84% of the time, and was running 57% of the time. Actual beam-on-target time was 3657 hours, equal to 73% of cyclotron running time or 42% of the year.

The cyclotron was out of commission for 1366 hours or 16% of the year. 390 hours were spent on scheduled maintenance, 291 hours on scheduled repairs, and 685 hours on non-scheduled repairs. These figures include time lost to causes beyond our control, such as power outages and roof repairs, both of which are covered below.

Of the scheduled repair time, 97 hours were spent installing and testing results of adding an iron disc in the center of the cyclotron to remove a magnetic asymmetry in the median plane. 88 hours were spent installing a revised septum and deflector. Results achieved by both the disc and septum changes are covered elsewhere in this report. Another 88 hours were spent on changes and additions to the radiation safety interlock system, as required by the Health and Safety Division of DOE.

Of the non-scheduled repair time, 74 hours were spent on repairs to the rectifier bank of the 150 KVA power supply on the RF system. This included time spent replacing the mercury vapor rectifiers by solid state rectifiers. 23 hours were spent on overhauling the ion source gas system valves. 440 hours were spent on internal water leaks, and 59 hours on roof repairs, both covered below.

Power outages during storms occurred 10 times, varying from momentary to as long as 2½ hours. Even momentary outages cause the cyclotron to turn off and require time to get back to running status. In one case, several hours of data stored in an on-line computer were lost. In addition to power outages, scheduled running time was wiped out by a wind storm in December, which blew off about 5% of the roof in the experimental area. The same section was blown off two more times in December and January before final repairs could be completed.

In October, 1977, an internal water leak developed at one of the shim coil water connections. Inspection of the leak led to replacing 192 O-rings on these connections. 32 similar O-rings were left unchanged because of inaccessibility without further

extensive disassembly. At the same time, an incipient water leak was found on the lower dummy dee and repaired. The carbon shields on the dummy dees were also revised to eliminate the dummy dee water problem.

Also included in the cyclotron non-scheduled repair time, although not actually cyclotron repairs, were two cases of water leaks in experimental equipment. On two separate occasions, runs were interrupted for about 18 hours each time by water leaks which flooded the same scattering chamber. This situation has since been corrected by the addition of an interlock which removes responsibility from the experimenter.

Cyclotron runs in collaboration with outside users were as follows:

13 hours	Ball Brothers Research Corporation, Boulder, CO--calibrate detectors for use on Jupiter probe.
14 hours	National Center for Atmospheric Research, Boulder, CO--production of ^{209}Po for calibration source in alpha induced mutation studies.
165 hours	Comparison of neutron time-of-flight detectors from various laboratories.
9 hours	Colorado School of Mines, Golden, CO--low energy beam diagnostics for fusion program.

Table D-III is a list of scheduled visitors to the laboratory during the period.

Table D-I

Hours of Cyclotron Operation - Purpose

Month	Cyclotron Development & Test	Research Staff	Research Collaborate	Radionuclide Production Staff	Radionuclide Production Outside & Collaborate	Subtotal Hrs/mo.
Sept. 77	23T	293	--	--	--	293 + 23T
Oct. 77	7T	243	--	--	--	243 + 7T
Nov. 77	69T	16	--	--	--	16 + 69T
Dec. 77	77T	234	--	--	--	234 + 77T
Jan. 78	3T	567	--	--	--	567 + 3T
Feb. 78	--	382	13	14	--	409
Mar. 78	55 + 8T	396	--	--	--	451 + 8T
Apr. 78	--	242	165	--	--	407
May 78	--	556	--	--	--	556
June 78	24T	530	--	--	--	530 + 24T
July 78	--	550	9	--	--	559
Aug. 78	--	526	--	--	--	526
Totals	55 + 211T	4535	187	14	--	4791 + 211T

Table D-II

Hours of Cyclotron Operation - Particle and Energy Range Used This Year

Month	Protons 1-27 MeV	Deuterons 0.2-18 MeV	H_2^+ 14 MeV	^3He 24-44 MeV	^4He 3-36 MeV	Other	Sub-Total Hrs/mo.
Sept. 77	--	34	--	--	259	--	293
Oct. 77	--	75	--	--	168	--	243
Nov. 77	16	--	21	--	32	--	69
Dec. 77	191	--	--	43	--	--	234
Jan. 78	404	8	--	10	145	--	567
Feb. 78	13	14	--	75	307	--	409
Mar. 78	128	--	23	--	300	--	451
Apr. 78	--	--	--	197	210	--	407
May 78	38	--	--	344	174	--	556
June 78	208	--	--	121	201	--	530
July 78	74	9	--	190	286	--	559
Aug. 78	104	--	--	174	248	--	526
Totals	1176	140	44	1154	2330	--	4844

Table D-III

Scheduled Visitors - 9/1/77 to 8/31/78

Date	No.	From
9-22-77	7	C.U. EE class
9-22-77	16	C.U. Physics class
11-18-77	81	C.U. Physics 202 class
12-10-77	56	Junior Girl Scouts
12-10-77	51	C.U. Physics 213 class
1-12-78	8	South Dakota State School of Mines
2-24-78	25	C.U. Health Physics class
3-3-78	26	U.C.-Denver Physics classes
3-29-78	20	Colorado State Univ., Ft. Collins, CO, physics class
4-14-78	14	Community College of Denver Physics class
4-14-78	21	C.U. Physics 112 class
4-17-78	57	Greeley Central High School, Greeley, CO
4-17-78	30	Air Force Academy, Colorado Springs, CO
4-20-78	3	Lowry Air Force Base, Denver, CO
4-25-78	5	Coop. Inst. for Research in Environmental Sci. (CIRES)
4-28-78	18	C.U. Physics 104 class
5-6-78	18	U.C.-Denver Physics classes
6-6-78	8	Out-of-town student families
7-7-78	5	Prospective student and family
8-4-78	13	Colorado School of Mines, Golden, CO
8-21-78	20	C.U. High School Honors Institute in Engineering
8-22-78	32	C.U. High School Honors Institute in Engineering
TOTAL	534	

E. Outside Users of Cyclotron Facilities

The Nuclear Physics Laboratory encourages outside users of the cyclotron facility for both educational and research purposes. These uses include collaborative research in short visits, independent or collaborative research by long-term visitors, and brief service irradiations. This past year has included activity in all three of these areas.

A study at Colorado of the large-volume neutron detectors used for intermediate-energy studies at the Indiana University Cyclotron Facility involved several visitors: Dr. Charles Goodman (ORNL), Dr. Charles Foster (IUCF), Dr. Mark Greenfield and Dr. Charles Goulding (Florida State) and Dr. Jack Rapaport (Ohio University). These studies utilized 45 MeV neutrons produced by the $^{9}Be(^{3}He,n)^{11}C$ reaction.

In a short visit, Dr. C. Robert Emigh of Q-division, Los Alamos Scientific Laboratory, participated in a study of the nuclear structure of ^{106}Pd by the $^{103}Rh(\alpha,p)^{106}Pd$ reaction.

Dr. N. S. P. King of LASL visited to participate in a $^{11}B(^{3}He,d)^{12}C$ experiment investigating high-lying levels in the residual nucleus for purposes of comparison with recent $^{12}C(\pi,\pi')$ and $^{13}C(p,d)^{12}C$ experiments at LAMPF.

Professor W. Parker Alford, on sabbatical leave from the University of Western Ontario, is spending the current academic year at the laboratory and is participating primarily in $(^{3}He,n)$ reaction studies.

Professor F. W. N. deBoer of the Free University in Amsterdam has a visiting appointment in the laboratory for the 1978-79 year. Some details of his current research work are presented in sect. II-A-2-f of this report.

For the second year, Professor S. Shastry of SUNY at Plattsburgh, NY, spent the summer in Boulder. His work on the (p,t) reaction is described in sect. II-A-1-b-vii.

Professor W. Pratt of Pennsylvania State University participated in two experimental efforts while at the laboratory for the summer. These are reported in sects. II-A-2-a and II-A-2-c.

Professor Martha Iverson of the University of Northern Colorado has worked during the past year on measurements of nuclear reaction rates of astrophysical significance.

Professor Norbert Roughton, of Regis Collge, Denver, continued his research efforts in the laboratory throughout the year.

Radioactive sources of ^{209}Po were produced for Dr. E. Martell of the National Center for Atmospheric Research. These sources

are for use in his studies of the biological effects of alpha radiation.

A collaborative program with scientists from Colorado State University on the radiobiological effects of fast neutrons was completed during the past year and is described in sect. II-A-3-b.

Inquiries from potential outside users of our facility are welcome and should be directed to D. A. Lind, Chairman, Nuclear Physics Laboratory, University of Colorado, Boulder, CO 80309. A description of the facilities of the laboratory follows.

Accelerator: 132 cm AVF cyclotron. Maximum energies are: protons, 28 MeV; deuterons, 17.5 MeV; ^{3}He, 44 MeV; ^{4}He, 35 MeV. Energy is continuously variable with no strict lower energy limit. For example, copious beams of 0.25 MeV protons and 1 MeV alphas have been accelerated without difficulty.

Beam intensities for target box irradiations are in 10's of μamps; in external beam lines, several μamps. The temporal structure of the cyclotron beam consists of narrow bursts at the accelerating frequency. This frequency is of the order of 10 MHz in most cases, but facilities are available to reduce this frequency by factors up to 100. Beam burst widths are sub-nanosecond in most cases. The energy width of the extracted beam is typically about $\Delta E/E=2 \times 10^{-3}$.

An energy-loss spectrometer provides a final $\Delta E/E$ of 3×10^{-4} while accepting the full undispersed output of the cyclotron. The focal plane encompasses an energy range of about 20% of the central energy. A helical cathode proportional chamber and a resistive wire proportional chamber are available and both give spatial resolution sufficient to achieve the full resolution afforded by the spectrometer.

Neutron time-of-flight spectroscopy is carried out with both 9-meter and 30-meter flight paths. The overall time resolution is typically 1 ns. The angle of observation is varied by a beam swinger so that the well-shielded detector array is stationary.

Gamma-gamma coincidence studies can be made in-beam in a specially designed γ-ray line. The facility is also suitable for gamma-ray angular distribution measurements.

A conventional target chamber of 36" dia. is available. It has two separate arms for ΔE-E telescopes, and follows a dispersive system of magnets which reduce the energy spread of the beam.

A fast neutron irradiation facility provides fluxes of neutrons with a broad energy distribution centered at 10.8 MeV from the d+d reaction. The maximum fluxes available are 10^{11} neutrons/ μC·sr in the forward direction.

Data acquisition is presently carried out using a PDP-9 computer and ND-50/50 pulse height analyzer system. Analysis is performed on either the PDP-9 or PDP-11/34 computers. The interfaces permitting data acquisition through the PDP-11 via CAMAC are being installed at this time.

An x-ray fluorescence system for elemental analysis of small (300 μg) samples is in operation. The system consists of a 75 kV, 20 mA x-ray tube, an automatic target changer, and a PDP-8/E control and data handling computer. Elemental analyses for elements from potassium (Z=19) through uranium (Z=92) are performed.

III. THEORETICAL PROGRAM

A. The (t,d) and (^{3}He,d) Reaction Normalization - P. D. Kunz

The normalization for the zero range DWBA and the form factor for finite range DWBA calculations have never been satisfactorily calculated. We have attempted to construct a phenomenological wave function for the t and ^{3}He systems with adjustable parameters to fit the electron scattering data for these nuclei. The wave function is of the product form suggested by Pappademos[1] which has the correct asymptotic behavior for single nucleon separation. To keep the number of parameters reasonable, the wave functions are restricted to the fully symmetric S and mixed symmetry S' states. After adjustment of the parameters to fit electron scattering data some relevant physical quantities are shown in Table III-I for two choices of the hard core radius XC. The resulting (t,d) form factor in momentum space is shown in Fig. 1.

Table III-I

Coulomb energy and mixed symmetry state probability for two hard core radii.

XC	0.0	0.4	fm
Coulomb energy	.649	.643	MeV
S' state	1.3	1.4	%

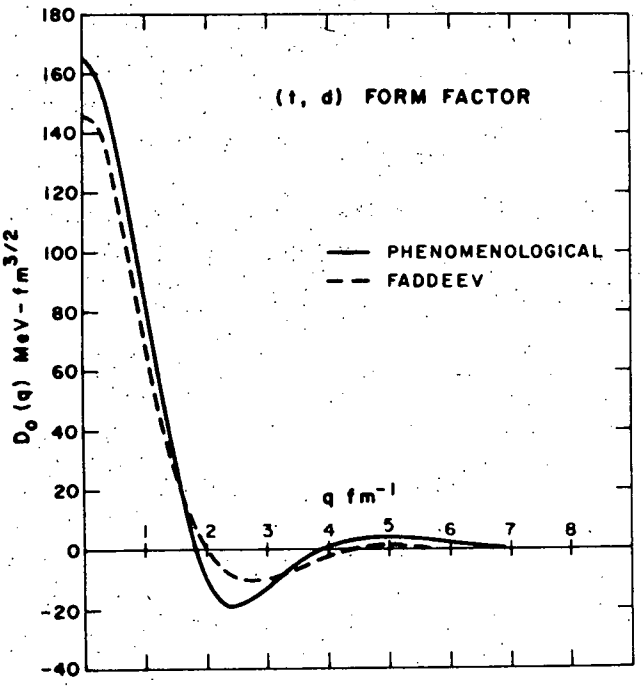

Fig. 1. The Fourier transform of the deuteron-triton overlap for the phenomenological triton wave function. Also shown is the same overlap for a Faddeev solution for the triton using the Reid soft core potential.

The value of the normalization constant $N=\frac{3}{2} D_o^2(0)$ is 4.07 MeV^2-fm^3 for the (t,d) and 3.56 MeV^2-fm^3 for the (^{3}He,d) reaction. These values are to be used when finite range effects or corrections are included in the DWBA calculation. The zero range normalization numbers can be obtained by comparing full finite range DWBA cases with zero range DWBA cases. This normalization number varies by ±10% depending upon the energy of the reactions, orbital of the transferred particle, or optical potential family used. The resulting normalization numbers are N=4.89 for the (t,d) and N=4.34 for the (^{3}He,d) reactions. A further comparison of zero range DWBA calculations with a Hulthén shape (R=0.83 fm) for the finite range correction factor gives N=3.71 for (t,d) and N=3.08 for (^{3}He,d) reactions.

---

[1] J. H. Pappademos, Nucl. Phys. 42 (1963) 122.

B. Four Particle Pickup Reactions on Te and Sn - P. D. Kunz with R. A. Broglia, H. Sofia and A. Vitturi (Niels Bohr Institute, Copenhagen, Denmark)

Recent data[1] for the (d,^{6}Li) reaction on the Te and Sn isotopes have been analyzed in terms of the transfer of an alpha particle cluster. The form factor has been calculated by assuming the transfer from the nucleus of a neutron and of a proton pairing mode. The wave functions are then averaged over the internal motion of the alpha particle. The neutrons in the Sn region partly fill a shell and there is considerable variation of strength of the transfer as a function of neutron number. This result can again be explained in a "back of an envelope" calculation utilizing what is known about two-nucleon transfer reaction.

In the Sn case the protons play a mainly passive role, while the neutron Fermi surface λ moves from being very closed to the $1d_{3/2}$ and $2s_{1/2}$ orbitals, which are almost degenerate, to being rather close to the $h_{11/2}$ orbital which is about 1 MeV higher in energy. This change in λ gives rise to an important change in the associated two-nucleon spectroscopic amplitudes $B(j^2(0)) \equiv \langle BCS(A+2) | [a_j^+ a_j^+]_0 | BCS(A) \rangle = \sqrt{j+\frac{1}{2}}\, U_j(A) V_j(A+2)$. (See Table III-II.) Here U_j and V_j are the BCS occupation parameters associated with the corresponding BCS wave functions used to describe initial and final states. As the Fermi surface moves away from the "hot" $s_{1/2}$ and $d_{3/2}$ orbitals towards the "cold" $h_{11/2}$ orbital, the cross section $\sigma_\nu = [\Sigma_{j\nu} B(j^2(0)) \sqrt{\sigma(j^2(0))}]^2$ for the transfer of a dineutron changes by a factor of two, and thus the alpha-transfer cross section is also expected to do so.

---

[1] F. Becchetti, private communication.

A microscopic calculation of the different four-particle transfer cross sections gave a nice overall account of the experimental data (see Fig.2a), provided that the parameters describing the relative motion of the dineutron (n^2) and the diproton (p^2) and the center of mass of n^2 with respect to p^2 are chosen in such a way that $\sigma_\alpha(j_\pi^2(0), j_\nu^2(0)) \approx C_\sigma(j_\pi^2(0))\sigma(j_\pi^2(0))$. Here C_σ is a constant with dimensions fm^{-2}. $\sigma_\alpha(j_\pi^2(0)), j_\nu^2(0)$ is the four-particle transfer cross section associated with the pure configuration $j_\pi^2(0)\ j_\nu^2(0)$, while $\sigma(j^2(0))$ is a two-paritcle transfer cross section associated with the pure configuration $j^2(0)$.

For the Te case the protons are not passive and an extra modulation of the cross sections is due to the changing order of the single particle levels. The proton $d_{5/2}$ level is the lowest level for the small neutron numbers while the $g_{7/2}$ level is the lowest for the larger neutron numbers. Since the $d_{5/2}$ level has a larger intrinsic strength than the $g_{7/2}$ level, the diproton transfer will be larger at mass 122 than at mass 130. This is seen in (^{3}He,n) reactions on the Sn isotopes. In Fig. 2b the crosses denote the relative strength of the Te(d,^{6}Li) reaction with the proton strength held constant. Thus better agreement with the data is obtained when the proton strength is changed.

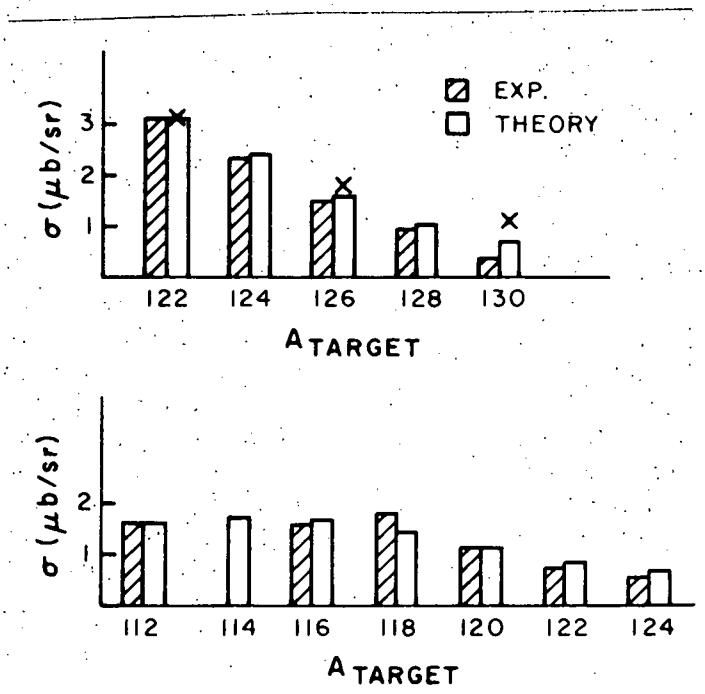

Fig. 2a and 2b. The theoretical cross section for the (d,^{6}Li) reactions on the Sn and Te isotopes shown with the experimental data at 15°. The calculated cross sections are relatively normalized to the ^{112}Sn and ^{122}Te isotopes for the two cases.

Table III-II

Relative cross sections for orbitals

			$B(j^2(0),A)$	
(ℓj)	$\sigma(j^2(0))$	116	118	120
$s_{1/2}$	1.3	0.5	0.4	0.3
$d_{3/2}$	0.5	0.8	0.7	0.6
$h_{11/2}$	0.1	0.9	1.1	1.3
$^{A+4}Sn(d,^6Li)^ACd$	Theory	1.0	0.7	0.5
	Exp.	1.0	0.6	0.4

In conclusion the $(d,^6Li)$ reaction to the ground states of spherical nuclei shows a strong correlation with a simple picture of the reaction strength as a product of the diproton and dineutron strengths.

C. Low Energy Pion Elastic and Inelastic Scattering--E. Rost and A. S. Rosenthal

A low energy pion-nucleus optical potential[1] has been applied to the elastic and inelastic scattering of $\pi^{\pm}$ by ^{12}C, ^{16}O, ^{28}Si, ^{56}Fe and ^{208}Pb. The potential is described in detail in refs. 1 and 2.

For nuclei lighter than ^{56}Fe our model underpredicts the back angle scattering somewhat. The underprediction worsens with decreasing mass number. For ^{56}Fe the agreement with data is excellent while for nuclei heavier than ^{56}Fe the potential overpredicts the data somewhat. The important forward angle region where structure is due to Coulomb-nuclear interference is adequately described for all nuclei except ^{12}C. Given the global character of the model we consider these cross sections to be in acceptable agreement with the data.

Inelastic cross sections to low lying collective states have been obtained by deforming the density $\rho(r)$ which appears in the optical potential. Angular distributions are generally well described by this procedure. However, at 50 MeV incident pion kinetic energy we underpredict the inelastic cross section magnitudes when standard deformation parameters are used. We believe that the poor agreement between our extracted deformation parameters and those obtained with strongly absorbed probes is related to the relative transparency of nuclei to low energy pions. At 116 MeV, where the scattering is largely diffractive, our extracted β_3 for ^{208}Pb is in

good agreement with other experiments. Work is continuing with other models for the transition densities.

---

[1] N. J. DiGiacomo et al., Phys. Lett 68B (1977) 40;
[2] A. S. Rosenthal, Ph.D. thesis, University of Colorado, 1978, unpublished.

D. Pi Meson Induced Excitation of Nuclear Giant Resonances - A. S. Rosenthal

In an attempt to explore further the consequences of the pion-nucleus optical potential discussed in the previous section, a series of calculations was performed for the pion-induced excitation of the nuclear giant dipole, isoscalar quadrupole and giant monopole resonances. The $|\Delta T|=1$ dipole resonance was treated with both a surface peaked (Goldhaber-Teller) and volume peaked (hydrodynamic) transition density. The giant quadrupole resonance was modelled with a derivative Woods-Saxon transition density and the monopole form factor was taken to be

$$\rho_{tr}(r) \propto \frac{1}{r^2} \frac{d}{dr} (r^3 \rho_o(r))$$

as in ref. 1. We have assumed that the breathing mode exists and exhausts 100% of the monopole energy weighted sum rule strength. The results of these calculations are summarized in Table III-III.

Low energy pions have a strong isovector interaction with nucleons which our calculations predict will be reflected in a strong excitation of the $|\Delta T|=1$ dipole resonance by 50 MeV pions. At higher energies the $|\Delta T|=0$ resonances appear to be more strongly excited. In particular the monopole breathing mode appears to be observable at all energies if the physical state has the assumed strength.

We conclude that pi mesons should be as useful for giant resonance spectroscopy as other hadronic probes and perhaps more useful at low energies for $|\Delta T|=1$ modes. Sufficient differences between π^+ and π^- excitations exist to suggest that comparison of experimental results obtained from both probes can be useful in studying giant resonances.

---

[1] G. R. Satchler, Particles and Nuclei, vol. 5 (1973) 105.

E. Effects of Pion-Nucleon Finite Range on Pion-Nucleus Elastic Scattering - A. S. Rosenthal and E. Rost

Simple configuration space, pion-nucleus optical potentials are based on the assumption that the elementary meson-nucleon interaction has zero range. More realistic models should include effects due to the finite range of the interaction. Fig. 3 compares the Kisslinger and cut-off Kisslinger off-shell scattering amplitudes

Table III-III

Calculated angle-integrated cross sections for the pion-induced excitation of giant resonances in units of mb.

Resonance	Pion Energy (MeV)	^{40}Ca		^{120}Sn		^{208}Pb	
		π^+	π^-	π^+	π^-	π^+	π^-
GDR	50	6.47	4.83	6.28	2.27	4.67	1.191
GT Form Factor	115	.355	.370	.247	.206	.178	.146
	180	.621	.679	.494	.462	.346	.325
GDR	50	23.85	19.57	20.85	5.48	12.42	5.32
Hydrodynamic	115	.934	.949	.481	.365	.219	.150
Form Factor	180	1.42	1.50	.886	.744	.412	.334
	50	.859	1.07	1.46	3.43	1.21	3.53
GQR	115	.774	.903	1.80	2.28	1.73	2.36
	180	1.15	1.27	2.80	3.48	2.84	3.78
	50	.597	2.70	.312	1.31	.249	1.76
GMR	115	.658	.810	.689	1.03	.765	1.25
	180	.918	1.06	1.00	1.39	1.16	1.74

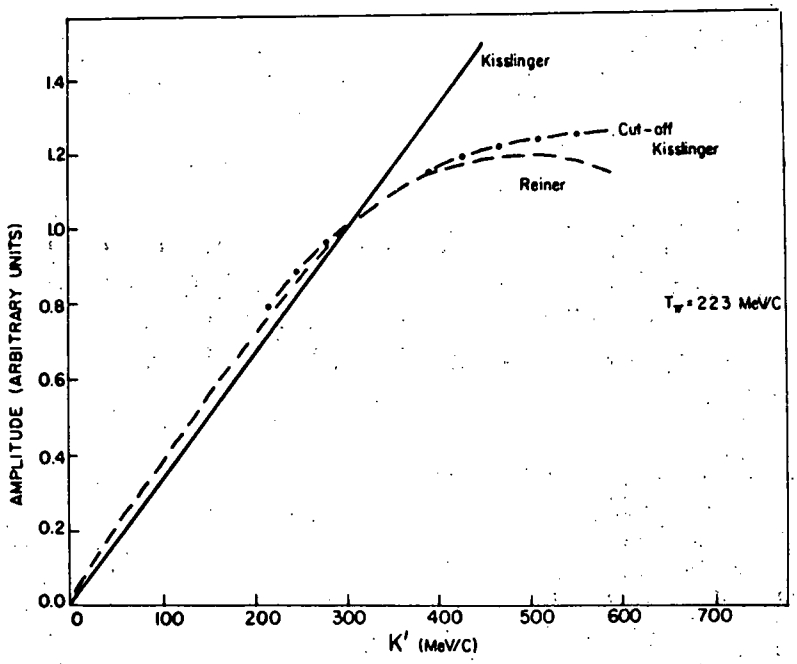

Fig. 3. Three models of the pion-nucleon half-off-shell T-matrix as a function of the off-shell momentum.

with the result of a dispersion-theoretic calculation due to Reiner.[1] The cut-off Kisslinger model is a good approximation to Reiner's results below about 600 MeV/c.

The meson-nucleon finite range gives rise to a non-local optical potential leading to an integro-differential wave equation. The effects of the non-locality have been approximated by treating the non-local potential in the distorted wave Born approximation, which yields useful results with tractable numerical computations. The finite range effects appear to be significant, especially for low energies and light nuclei. For energies above 100 MeV, the finite range calculations slightly improve the agreement with experiment at back angles. However, the finite-range predictions alter the structure of the Coulomb-nuclear and scalar-vector interference regions in ways which are not seen in the experimental cross sections. Although our non-locality corrections do not generally improve the agreement with data, we conclude that the meson-nucleon finite range is less than 1/3 fm.

---

[1] M. J. Reiner, Phys. Rev. Lett. 38 (1977) 1467.

F. A Technique for Determining Neutron Densities Using Low Energy π^- Nucleus Scattering - E. Rost with R. R. Johnson, T. Marks and B. Gyles (University of British Columbia)

A longstanding question of nuclear structure concerns the neutron density distribution which is not nearly as well known as the proton

distribution. Various methods have been applied but there are still sizable discrepancies between the results obtained by different techniques.[1] Several attempts have been made to exploit the properties of the pion in its different interactions with neutrons and protons. Initially ratios of π^+ and π^- total cross sections were measured[2,3] at energies near 1 GeV to exploit the asymmetric interaction of the pions with the nucleons. Although the π^--p (or π^+-n) interaction is about 3 times stronger than the π^--n (or π^+-p) interaction at these energies, the effect on the total cross section ratios σ^-/σ^+ of reasonable neutron density variations was only a few percent which is at the level of the model ambiguities in the analysis.

An alternate method often used in electron scattering measures differences in density distributions for neighboring nuclides, often isotopic pairs. These differences cancel many experimental and theoretical uncertainties and yet preserve sensitivity to the nuclear densities. Cooper[4] applied this type of analysis to pion total cross sections in the 100-200 MeV energy region and extracted rms neutron radii for ^{18}O and ^{48}Ca exploiting difference measurements with ^{16}O and ^{40}Ca targets, respectively. His analysis was based on the strong π^--n resonant interaction which occurs in any reasonable pion-nucleus optical model thereby making his results insensitive to the nuclear model used.

We have developed another method using angular distributions of low-energy π^- scattering from neighboring nuclei. A useful quantity to measure is the ratio of differential cross sections from the pair since normalization uncertainties in the data and theory cancel out approximately. This method depends on the large S-wave isovector part of the π-N interaction at low energies (the S-wave isoscalar term is small due to cancellations). This feature occurs in any reasonable low-energy, pion-nucleus optical model[5] and thus makes the results insensitive to the precise form of the model employed.

The basic optical model used is taken from pi-mesic atom theory[5] extended[6] to positive energies. The potential for the case of π^- scattering is

$$U(r) = U_o + U_p + U_{SA} + V_{COUL} \tag{1}$$

where

$$\begin{aligned} U_o = & -(1+\varepsilon)k^2\,[b_o(\rho_n+\rho_p) + 1/2\; c_o(\rho_n-\rho_p)] \\ & + (1+\varepsilon)^{-1}\vec{\nabla}\cdot[b_1(\rho_n+\rho_p) + 1/2\; c_1(\rho_n-\rho_p)]\,\vec{\nabla} \\ & -1/2(1+\varepsilon)^{-1}\nabla^2[b_1(\rho_n+\rho_p) + 1/2\; c_1(\rho_n-\rho_p)] \end{aligned} \tag{2}$$

$$U_p = 4\pi(b_o^2 + 1/2c_o^2)\left\langle\frac{1}{r}\right\rangle(\rho_n+\rho_p)$$

$$U_{SA} = -4\pi B_o(\rho_n+\rho_p)^2$$

representing a zero-range impulse approximation term, a Pauli blocking correction, an S-wave annihilation term and the usual Coulomb potential.

The impulse approximation term involves an angle transformation of the π-nucleon scattering amplitude into the π-nucleus center-of-momentum frame ($\varepsilon=\omega_\pi/\mu_p$). The off-shell form of this angle transformation has been chosen to preserve unitarity. In eq. (2), the isoscalar (b_o and b_1) and isovector (c_o and c_1) collision amplitudes are taken from the parametrized fit to pion-nucleon scattering of ref. 7. A Pauli correlation length $\langle\frac{1}{r}\rangle$ is obtained by a procedure due to Thies[6]; its value at 29 MeV is $0.32 + i0.29$ fm^{-1}. The S-wave annihilation strength $B_o=0.168$ $(-2+i)$ fm^4 has been extracted phenomenologically by Rosenthal[8] in his analysis of 50 MeV π^+ scattering from many target nuclei.

Eq. (2) is written in terms of separate neutron and proton densities, ρ_n and ρ_p, normalized to N and Z. For p-shell targets a harmonic oscillator form is usually used

$$\rho(r) = \rho_o\,[1+\alpha(r/a)^2][\exp -(r/a)^2] \qquad (3)$$

where α is either a free parameter or set to the shell model value $(Z-2)/3$ for proton density distributions. The root mean square (rms) radius is given by

$$\langle r^2\rangle^{\frac{1}{2}} = \left[1.5\left(\frac{1+2.5\alpha}{1+1.5\alpha}\right)\right]^{\frac{1}{2}} a. \qquad (4)$$

Charge density distributions have been measured in electron scattering experiments and the tabulated values[9] of a and α are listed in Table III-IV for the ^{12}C, ^{13}C and ^{16}O, ^{18}O pairs. We have used these

Table III-IV

Density parameters. A modified harmonic oscillator form was used: $\rho(r) = \rho_o(1+\alpha(r/a)^2)\exp(-(r/a)^2)$

Target	Type	a	α	$(r^2)^{\frac{1}{2}}$	Method
^{12}C	proton	1.564	1.247	2.294	ref. 11[a]
	neutron	1.564	1.247	2.294	
^{13}C	proton	1.550	1.403	2.287	ref. 12[a]
	neutron	1.592	1.333	2.343	this work
		1.565	1.667	2.328	
^{16}O	proton	1.756	1.544	2.604	ref. 13[a]
	neutron	1.706	1.544	2.604	
^{18}O	proton	1.808	1.544	2.681	ref. 13[a]
	neutron	1.931	1.544	2.863	this work
		1.908	2.000	2.862	

a) The proton form factor was subtracted out by the prescription $\langle r^2\rangle = \langle r^2\rangle_{e\ell} - \langle r_p^2\rangle$ where $r_p=0.78$ fm and $\langle r^2\rangle_{e\ell}^{\frac{1}{2}}$ is the rms radius measured in electron scattering.

densities after subtracting out the proton form factor as indicated. For the N=Z nuclei ^{12}C and ^{16}O we assume equal neutron and proton density distributions as is reasonable from their closed shell character, from Hartree-Fock calculations,[10] and from high energy pion scattering.[3] The calculation now consists of varying the neutron density ρ_n of ^{13}C or ^{18}O and comparing the resultant cross section ratios with the data. The experimental data were measured by a group at TRIUMF.

Figs. 4 and 5 show the results comparing a best-fit neutron rms radius with those differing by ±0.1 fm. Considerable sensitivity is found as is also indicated by the χ^2/N curves. This sensitivity may be understood in terms of the large S-wave isovector amplitude c_o tabulated in Table III-V. This is multiplied by a coefficient of order 1/26 for ^{13}C(2/36 for ^{18}O) relative to the isoscalar term and adds an appreciable amount to the total S-wave scattering. This S-wave amplitude interferes with the larger P-wave amplitude. In the π-nucleus system one has essentially only ℓ=0 and ℓ=1 partial waves which also interfere destructively, especially at backward angles. An increase in the neutron rms radius, say, will thus decrease the ℓ=1 contribution because of additional interference at larger radii thereby decreasing the cross section and ratio. This qualitative effect was always present in all the models we tested.

Table III-V

Optical parameters for pion scattering at 29 MeV. The units are fm^3.

	Isoscalar	Isovector
S-wave	$b_0 = -1.64 + 0.20\ i$	$c_0 = -14.58 - 0.55\ i$
P-wave	$b_1 = 6.43 + 0.31\ i$	$c_1 = 8.06 + 0.30\ i$

The extracted neutron rms radii are given in Table III-IV. Two values of α were tried which gives some indication of the model sensitivity (the plots in figs. 4 and 5 would be indistinguishable for the two α cases). Thus it is seen that our method basically measures only a neutron rms radius as is reasonable for a low momentum transfer experiment. Indeed, only a difference in rms values between neutron and protons densities is extracted. We have performed calculations with the unsubtracted proton rms radii, with other variants of optical potentials, and with Fermi density distributions. In all cases the results were within the limits:

$$r_n - r_p = 0.06 \pm 0.02 \text{ fm for } ^{13}C$$
$$r_n - r_p = 0.18 \pm 0.02 \text{ fm for } ^{18}O \qquad (5)$$

The later result agrees well with that of Cooper[4] who measured $r_n - r_p = 0.19 \pm 0.02$ fm for ^{18}O.

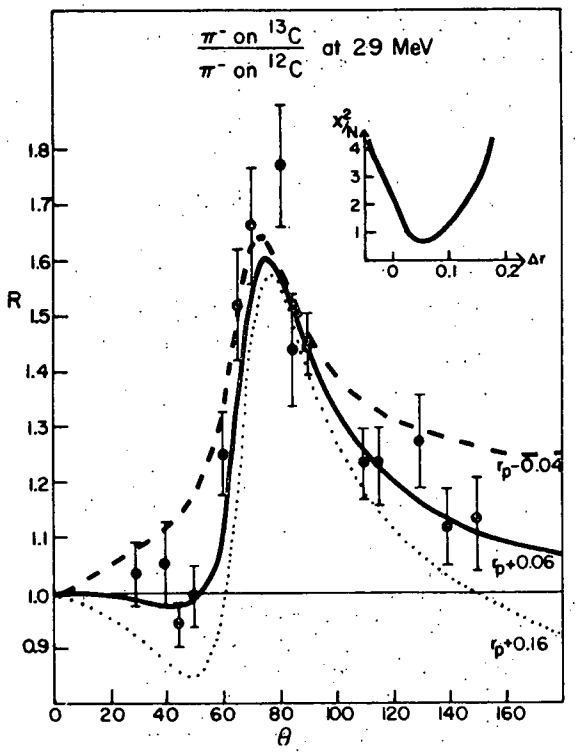

Fig. 4. Ratios of differential cross sections of 29 MeV π^- on ^{13}C relative to ^{12}C. The curves show variations of the neutron rms radius. In the inset, a plot of χ^2 per degree of freedom is given as a function of the difference between neutron and proton rms radii.

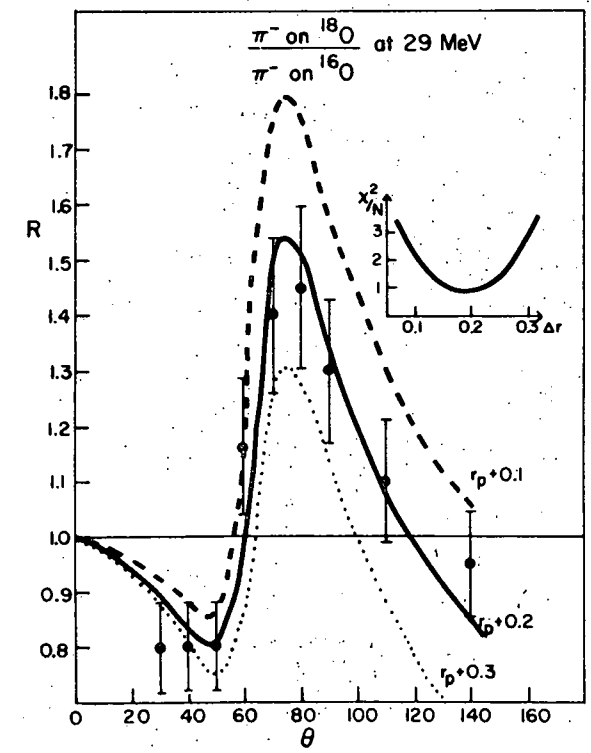

Fig. 5. Ratios of differential cross sections of 29 MeV π^- on ^{18}O relative to ^{16}O. The curves show variations of the neutron rms radius. In the inset, a plot of χ^2 per degree of freedom is given as a function of the difference between neutron and proton rms radii.

1 R. C. Barrett and D. F. Jackson, Nuclear Sizes and Structure, Clarendon Press, Oxford, 1977.
2 A. Abashian, R. Cool and J. W. Cronin, Phys. Rev. 104 (1956) 855.
3 B. W. Allardyce et al., Nucl. Phys. A209 (1973) 1.
4 M. D. Cooper, AIP Conf. Proc. 33 (1976) 237.
5 M. Ericson and T. E. O. Ericson, Ann. Phys. (N.Y.) 36 (1966) 323.
6 M. Thies, Phys. Lett. 63B (1976) 43.
7 M. Salomon, TRIUMF Report TR1-74-2.
8 A. S. Rosenthal, Ph.D. dissertation, University of Colorado, 1978 (unpublished).
9 C. W. DeJager et al., Atomic Data and Nuclear Data Tables 14 (1974) 479.
10 J. W. Negele, Phys. Rev. C 1 (1970) 1260.
11 I. Sick and J. S. McCarthy, Nucl. Phys. A150 (1970) 631.
12 J. Heisenberg, J. S. McCarthy and I. Sick, Nucl. Phys. A157 (1970) 435.
13 W. Schütz, Ph.D. thesis, T. H. Darmstadt, 1973 (unpublished) cited in ref. 9.

G. The ^{4}He(p,d)^{3}He Reaction at 770 MeV - W. S. Pong

In previous progress reports,[1] it was found that angular distributions from DWBA calculations do not agree with experiment. It was suggested that a pion emission and reabsorption process as proposed by Craigie and Wilkin[2] for back angle p+d elastic scattering might be important. We have included the contribution from this mechanism by calculating the Feynmann diagram in Fig. 6.

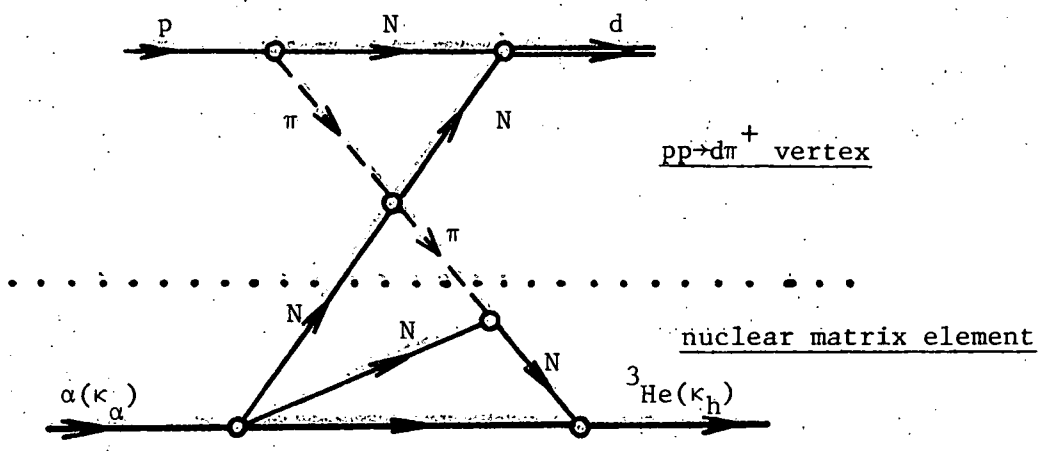

Fig. 6. Pion emission and reabsorption process in ^{4}He(p,d)^{3}He.

As sketched in Fig. 6, we consider the $pp \to d\pi^+ (pn \to d\pi^o)$ vertex and the nuclear matrix element separately. The $pp \to d\pi^+$ vertex is calculated with one of the protons and the pion off the mass shell, and we are checking this calculation with the experimental cross section of π^+ absorption on the deuteron. The nuclear matrix element displays the feature that the momentum transfer in the reaction, $\frac{3}{4}\vec{k}_\alpha - \vec{k}_h$, (where $\vec{k}_\alpha$ and $\vec{k}_h$ are the momenta of the incoming α particle and outgoing ^{3}He), is shared by two nucleons in the α-particle, rather than taken almost entirely by one nucleon as in previous DWBA calculations. Consequently, large momentum transfers are possible with this mechanism.

We are now folding the $pp \to d\pi^+$ vertex over the nuclear matrix element to obtain the plane wave scattering amplitude and differential cross sections.

---

[1] Univ. of Colorado Nuclear Physics Laboratory Technical Progress Reports, COO-535-763 (1976) 136, COO-535-764 (1977) 155.
[2] N. S. Craigie and C. Wilkin, Nucl. Phys. B14 (1969) 477.

H. The $\pi^+ + d \to p + p$ Reaction - W. S. Pong

The absorption of pions on deuterons between 100 to 250 MeV incident pion energy is dominated by pion rescattering via the (3,3) resonance,[1] as is illustrated by the Feynmann graphs in Fig. 7. We are interested in this reaction for two reasons. First, the amplitude of $\pi^+ d \to pp$, when continued off the mass shell for the pion and one of the protons, is required in the calculation of the high energy ^{4}He(p,d)^{3}He reaction, so that the experimental cross sections of $\pi^+ d \to pp$ provide a "physical" check for the (p,d) calculation. Secondly, we hope to examine this absorption mechanism in heavier nuclei.

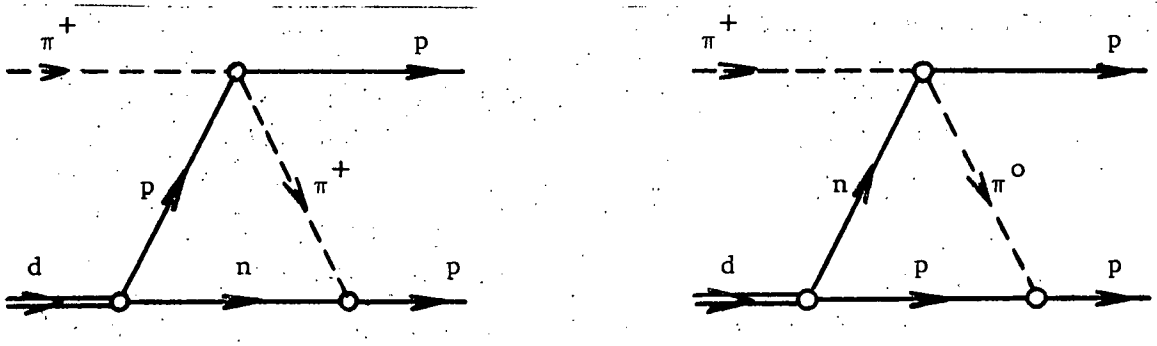

Fig. 7. Rescattering processes in π^+ absorption on deuteron.

---

[1] J. Hüfner, Phys. Reports 21C (1975) 1.

The Feynmann graphs are calculated with the following prescriptions. The total amplitude is assumed to be the sum of amplitudes, each calculated by putting one of the internal momenta (see Fig. 7) on the mass shell in turn. The deuteron vertex is obtained by analytic continuation of the deuteron wave function, following the method of Gourdin et al.)[2], and McGee's parametrization of the wave-function is used.[3] The π-N scattering is assumed to be dominated by the (3,3) resonance which is assumed to have a Breit-Wigner form as given by Deans and Holliday.[4] Also, the angle transformation is taken into account. The Ferrari-Selleri form factor[5] is included in the π-production vertex, corresponding roughly to a high momentum cutoff of 1.1 GeV/c.

The experimental[6] and the plane wave cross sections for the reaction are shown in Fig. 8. The plane wave cross section (dotted line)

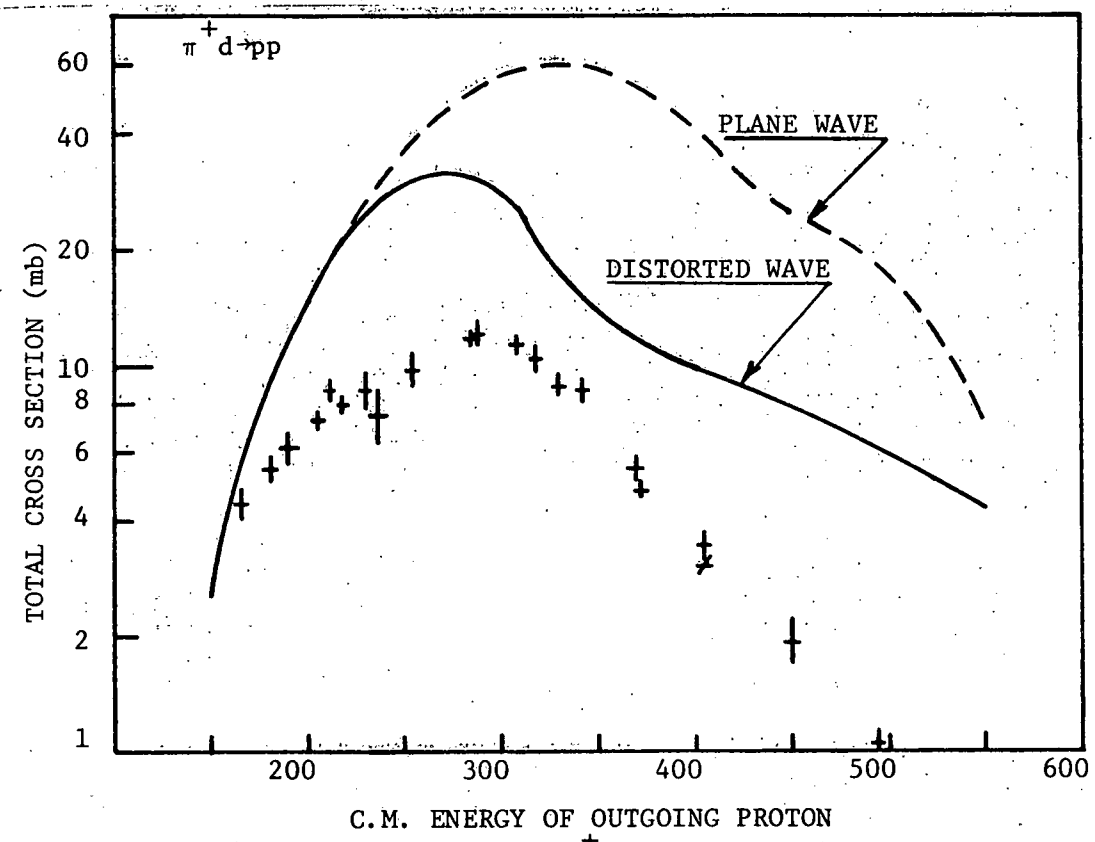

Fig. 8. Total cross section of π^+ absorption on deuteron.

is a factor of 2 to 10 larger than the experimental cross section, and the factor increases with energy. This is to be expected since the $\pi^+ d$ reaction is dominated by quasi-free scattering (about 70% of the total cross section) and because the proton-proton scattering becomes more inelastic. We estimated the effect of quasi-free scattering by including the graph in Fig. 9 approximately, where the internal lines with crosses are on the mass shell. The total cross section (full line in Fig. 8) is considerably reduced, especially at high energies; however, it is still about a factor of 3 larger than

experiment. It has been shown by Goplen et al.[7] that with a smaller momentum cutoff (∿300 MeV/c), the total cross section can be fitted, although the angular distributions do not agree with experiment.[8]

We are currently recalculating this reaction to include distortion in the entrance and the exit channels more carefully.

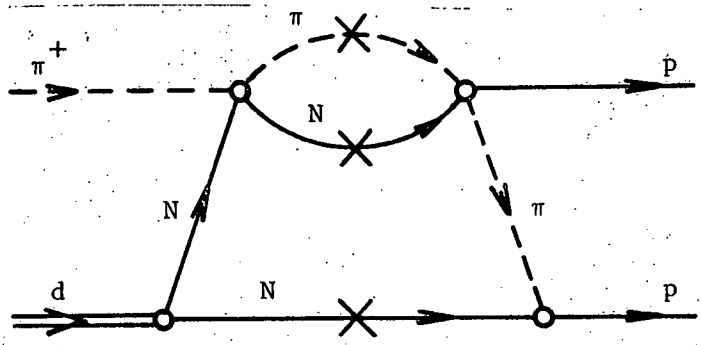

Fig. 9. Distortion of incident pion by quasi-free scattering.

2 M. Gourdin et al. Nuovo Cimento 37 (1965) 524.
3 I. McGee, Phys. Rev. 151 (1966) 772.
4 S. R. Deans and G. Holliday, Proc. Williamsburg Conf. on Intermediate Energy Phys. Vol. II, p. 551 (pub. College of William and Mary, Williamsburg, 1966).
5 E. Ferrari-Selleri, Nuovo Cimento Suppl. 24 (1963) 453.
6 C. Richard-Serre et al., Nucl. Phys. B20 (1970) 413.
7 B. Goplen et al., Phys. Rev. Lett. 32 (1974) 1012.
8 D. Aebischer et al., Nucl. Phys. B106 (1976) 214.

I. Pickup to Unbound Projectile States - P. D. Kunz, with A. Saha, (KVI, Groningen) and H. T. Fortune (Univ. of Pennsylvania)

The problem of calculating the DWBA matrix elements for a stripping reaction to an unbound target state requires integrations to very large radii in order to obtain the necessary convergence to these integrals. This is because the usual post interaction form uses the projectile interaction for stripping reactions and hence contains no convergence-producing factors in the radial matrix elements beyond the 1/r factor from the target bound state. Vincent and Fortune[1] proposed a scheme in which the radial integration progresses along the real r axis to a radius outside the nuclear surface after which it proceeds perpendicular to the real r axis into the complex plane. The oscillating functions then become decaying exponential forms and the integrals converge much more rapidly.

For pickup reactions to unbound projectile states the use of the prior interaction inserts the projectile interaction potential into the matrix elements and the DWBA integrals can be performed as usual with the convergence coming from the rapid falloff in the integrand from the potentials. We report a finite range DWBA

analysis of the proton pickup reaction $^{12}C(\alpha, ^{5}Li)^{11}B$ at 65 MeV in which the final ^{5}Li is unbound and in a p state. The projectile wave function is in the $p_{3/2}$ state where the width of the state is large ($\approx$2 MeV) with a resonance energy of $\sim$2.5 MeV. The $p_{3/2}$ phase shifts were fit with a Woods-Saxon potential model of radius $R=1.25(5^{1/3})$ fm, diffusivity a=0.65 fm and spin-orbit parameter λ=38. The fit to the phase shifts is shown in Fig. 10. For each

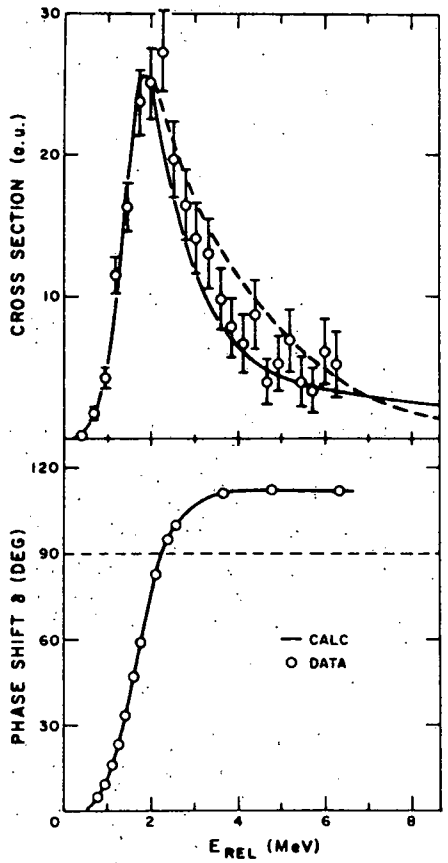

Fig. 10. The fit to the data. In the upper curve the solid line is the calculation. The dashed line is a $\alpha(p,d)\ ^{5}Li$ shape fit.

energy the wave function was then used to compute the differential cross sections. The result is an energy dependent cross section shown in Fig. 10 with the data. The $s_{1/2}$ and $p_{1/2}$ contributions to this cross section have been shown to be negligible (<10%) for relative energies less than 5 MeV in the p-α system. Thus the DWBA method is feasible for calculating reactions for unbound projectile or target states.

---

[1] C. M. Vincent and H. T. Fortune, Phys. Rev. C 2 (1970) 782.

IV. PUBLICATIONS AND REPORTS

A. Published Articles

A Study of the (^{3}He,n) Reaction on Isotopes of Tin. H. W. Fielding, R. E. Anderson, P. D. Kunz, D. A. Lind, C. D. Zafiratos and W. P. Alford, Nucl. Phys. A304 (1978) 520-532.

The Contribution of Second-Order Processes to (^{3}He,n) Calculations. I. Brissaud, J. Phys. G: Nucl. Phys. 4 (1978) L87.

Observation of the Proton Pairing Vibration in ^{206}Pb. R. E. Anderson, P. A. Batay-Csorba, R. A. Emigh, E. R. Flynn, D. A. Lind, P. A. Smith, C. D. Zafiratos and R. M. DeVries, Phys. Rev. Lett. 39 (1977) 987.

Level Structure of ^{99}Tc by Inelastic Scattering and Proton Stripping. R. J. Peterson, R. A. Emigh and R. E. Anderson, Nucl. Phys. A290 (1977) 155.

A Study of the ^{99}Tc(p,d)^{98}Tc Reaction. R. A. Emigh and R. E. Anderson, Nucl. Phys. A293 (1977) 379.

The ^{85}Rb(p,d)^{84}Rb Reaction. S. Shastry, R. A. Emigh, R. J. Peterson and R. E. Anderson, Nucl. Phys. A304 (1978) 40.

Uremic Hyperstannum: Elevated Tissue Tin Levels Associated with Uremia. L. L. Nunnelley, W. R. Smythe, A. C. Alfrey and L. S. Ibels, Jour. of Lab. and Clin. Medicine, 91 (1978) 72.

Energy Dispersive X-ray Fluorescence Spectrometric Determination of Trace Elements in Oil Samples. H. Kubo, R. Bernthal, T. Wildman, Analyt. Chem. 50 (1978) 899.

Two-Step Processes and Finite-Range Effects in the ^{60,62}Ni(p,t) Reaction. J. D. Burch, M. J. Schneider and J. J. Kraushaar, Nucl. Phys. A299 (1978) 117.

The ^{56}Fe(^{3}He,t)^{56}Co Reaction. W. R. Zimmerman, J. J. Kraushaar, M. J. Schneider and H. Rudolph, Phys. Rev. C 16 (1977) 2432.

A Study of the (^{3}He,t) Reaction on ^{60}Ni. W. R. Zimmerman, J. J. Kraushaar, M. J. Schneider and H. Rudolph, Nucl. Phys. A297 (1978) 263.

The Level Structure of ^{111}Ag via the ^{110}Pd(^{3}He,d)^{111}Ag Reaction. R. E. Anderson, J. J. Kraushaar, R. A. Emigh, P. A. Batay-Csorba and H. P. Blok, Nucl. Phys. A287 (1977) 265.

Energy Dependence of π^{+} Induced Two and Four-Nucleon Removal. G. R. Smith, R. L. Boudrie, J. J. Kraushaar, R. J. Peterson, R. A. Ristinen, C. L. Morris, J. E. Bolger, W. J. Braithwaite, C. F. Moore and L. E. Smith, Phys. Letts. 72B (1977) 176.

Pion Induced Single Nucleon Removal to Discrete Final States. C. L. Morris, R. L. Boudrie, J. J. Kraushaar, R. J. Peterson, R. A. Ristinen, G. R. Smith, J. E. Bolger, W. J. Braithwaite, C. F. Moore and L. E. Smith, Phys. Rev. C 17 (1978) 227.

High Spin States in ^{88,87,86}Zr. J. E. Kitching, P. A. Batay-Csorba, C. A. Fields, R. A. Ristinen and B. L. Smith, Nucl. Phys. A302 (1978) 159.

A Least-Squares Technique for Extracting Neutron Spectra from Bonner Sphere Data. C. S. Zaidins, J. B. Martin and F. M. Edwards, Med. Phys. 5 (1978) 42.

Neutron Pickup from ^{194,196,198}Pt. G. R. Smith, N. J. DiGiacomo, M. L. Munger and R. J. Peterson, Nucl. Phys. A290 (1977) 72.

Level Structure of ^{99}Tc by Inelastic Scattering and Proton Stripping. R. J. Peterson, R .A. Emigh and R. E. Anderson, Nucl. Phys. A290 (1977) 155.

Reappraisal of the ^{24}Mg(^{3}He,t)^{24}Al Reaction to Low-Lying 1^+ States. R. J. Peterson, Phys. Rev. C 16 (1977) 2424.

Definitive Test of Outgoing Nucleon Charge Exchange Using the Reaction ^{13}C($\pi^{\pm}$,πN) ^{12}C (4.44 and 15.11 MeV). C. L. Morris, H. A. Thiessen, W. J. Braithwaite, C. F. Moore, J. E. Bolger, L. E. Smith, R. J. Peterson, R. L. Boudrie, J. J. Kraushaar, R. A. Ristinen and G. R. Smith, Phys. Rev. Lett. 39 (1977) 1455.

Isoscalar Excitations of ^{24}Mg by Inelastic ^{3}He Scattering. R. J. Peterson and F. E. Cecil, Nucl. Phys. A297 (1978) 10.

^{14}C(t,p)^{16}C Reaction at 23 MeV. R. R. Sercely, R. J. Peterson and E. R. Flynn, Phys. Rev. C 17 (1978) 1919.

Elastic Scattering of 162 MeV Pions by Nuclei. B. Zeidman, C. Olmer, D. F. Geesaman, R. L. Boudrie, R. H. Siemssen, J. F. Amann, C. L. Morris, H. A. Thiessen, G. R. Burleson, M. J. Devereaux, R. E. Segel and L. W. Swenson, Phys. Rev. Lett. 40 (1978) 1316.

Structure of ^{88}Sr from the ^{86}Kr(^{3}He,n)^{88}Sr Reaction. W. P. Alford, R. E. Anderson, P. A. Batay-Csorba, D. A. Lind, H. H. Wieman and C. D. Zafiratos, Nucl. Phys. A293 (1977) 83.

Neutron Deformation Parameter from Comparative Study of π^+ and π^- Inelastic Scattering. S. Iversen, A. Obst, K. K. Seth, H. A. Thiessen, C. L. Morris, N. Tanaka, E. Smith, J. F. Amann, R. L. Boudrie, G. Burleson, M. Devereux, L. W. Swenson, P. Varghese, K. Boyer, W. J. Braithwaite, W. Cottingame and C. Fred Moore, Phys. Rev. Lett. 40 (1978) 17.

Is (^{3}He,t) Primarily A (^{3}He,α)(α,t) Reaction? L. A. Charlton and P. D. Kunz, Phys. Lett. 72B (1977) 7.

Observation of the Neutron Pairing Vibration in ^{206}Hg. E. R. Flynn, D. L. Hanson, R. V. Poore and S. D. Orbson, D. A. Lind, Phys. Lett. 76B (1978) 197.

Proton Stripping Reactions on ^{194}Pt, ^{196}Pt and ^{198}Pt. M. L. Munger and R. J. Peterson, Nucl. Phys. A303 (1978) 199.

DWBA Description of ^{4}He(p,d)^{3}He Reaction at E_p=770 MeV. E. Rost, J. R. Shepard and D. A. Sparrow, Phys. Rev. C 17 (1978) 1513.

Second Order Density Effects in Low Energy Pion Scattering. A. S. Rosenthal, E. Rost, D. A. Sparrow and N. J. DiGiacomo, Phys. Lett. 71B (1977) 237.

A Study of the ^{76}Se(^{3}He,d)^{77}Br and ^{78}Se(^{3}He,d)^{79}Br Reactions. B. M. Kluger, R. E. Anderson, R. J. Peterson and R. A. Ristinen, J. Phys. G: Nucl. Phys. 4 (1978) 1489.

B. Articles Accepted or Submitted for Publication

The (^{3}He,n) Reaction on N=82 Targets and Even Isotopes of Neodymium. W. P. Alford, R. E. Anderson, P. A. Batay-Csorba, R. A. Emigh, D. A. Lind, P. A Smith and C. D. Zafiratos, submitted to Nucl. Phys. A.

The ^{208}Pb(p,α)^{205}Tl Reaction. P. A. Smith, G. M. Crawley, R. G. Markham and D. Weber. Accepted for publication in Phys. Rev. C.

The Population of Intrinsic High Spin States with the ^{116}Sn(α,p)^{119}Sb Reaction. P. A. Smith, R. A. Emigh, N. J. DiGiacomo, G. R. Smith and R. J. Peterson, submitted to Phys. Rev. C.

The Proton Closure at ^{14}C. R. R. Sercely, R. J. Peterson, P. A. Smith and E. R. Flynn, submitted to Nucl. Phys.

The (^{3}He,n) Reaction Near and Above Z=82. R. E. Anderson, P. A. Batay-Csorba, R. A. Emigh, E. R. Flynn, D. A. Lind, P. A. Smith, C. D. Zafiratos, R. M. DeVries, submitted to Phys. Rev. C.

Pion Induced Double Charge Exchange Reaction. D. A. Sparrow and A. S. Rosenthal, accepted by Phys. Lett.

Elastic and Inelastic Scattering of $\pi^{\pm}$ by ^{208}Pb. J. Arvieux, J. P. Albanese, J. Bolger, E. Boschitz, C. H. Q. Ingram, L. Pflug, J. Jansen, J. Zichy, E. Rost and A. S. Rosenthal, accepted by Nucl. Phys.

Electrostatic Deflector for the University of Colorado Energy-Loss Spectrometer. R. A. Emigh. Accepted for publication in Nucl. Inst. and Meth.

Fast Neutron Irradiation of Microvasculature. J. R. Fike, E. L. Gillette, F. M. Edwards, J. J. Kraushaar, D. E. Prull, submitted to Radiology.

Two-Step Processes in the ^{54}Fe(^{3}He,t) Reaction. W. R. Zimmerman, J. J. Kraushaar and F. E. Cecil, accepted by Nucl. Phys.

Elastic and Inelastic Diffraction Scattering of 0.8 GeV Protons by ^{89}Y and ^{90}Zr. N. J. DiGiacomo, R. L. Boudrie, I. Brissaud, J. J. Kraushaar, R. J. Peterson, R. A. Ristinen, E. S. Rost and G. R. Smith, submitted to Phys. Rev. Lett.

A Study of the ^{58}Ni, ^{90}Zr and ^{208}Pb(p,d) Reactions at 121 MeV. R. E. Anderson, J. J. Kraushaar, J. R. Shepard and J. R. Comfort, accepted by Nucl. Phys.

Proton Spectroscopy of ^{96}Tc from the (^{3}He,d) Reaction. R. A. Emigh, J. J. Kraushaar and S. Shastry, submitted to Nucl. Phys.

Observation of Enhanced Excitation of ^{12}C by Inelastic Pion Scattering on the 3-3 Resonance. C. Fred Moore, W. Cottingame, K. G. Boyer, L. E. Smith, C. Harvey, W. J. Braithwaite, C. L. Morris, H. A. Thiessen, J. F. Amann, M. Devereux, G. Blanpied, G. Burleson, A. W. Obst, S. Iversen, K. K. Seth, R. L. Boudrie and R. J. Peterson, submitted to Phys. Lett.

The ^{85}Rb(p,d)^{87}Rb Reaction. S. Shastry, R. J. Peterson, R. A. Emigh and R. E. Anderson, accepted by Nucl. Phys.

The Level Structure of ^{78}Br. B. M. Kluger-Bell, R. E. Anderson, R. J. Peterson, D. E. Prull, R. A. Ristinen and B. L. Smith, submitted to Jour. Phys. G.

A Study of ^{80}Br by the ^{81}Br(p,d) Reaction. B. M. Kluger, R. E. Anderson, R. J. Peterson and R. A. Ristinen, accepted by J. of Phys. G.

Elastic Pion Scattering from ^{6,7}Li and ^{12,13}C. S. A. Dytman, J. F. Amann, P. D. Barnes, J. N. Craig, K. G. R. Doss, R. A. Eisenstein, J. D. Sherman and W. R. Wharton, G. R. Burleson, S. L. Verbeck, R. J. Peterson and H. A. Thiessen, submitted to Phys. Rev. C.

Low Energy π^{+} Scattering from Light Nuclei. A. Dytman, J. F. Amann, P. D. Barnes, J. N. Craig, K. G. R. Doss, R. A. Eisenstein, J. D. Sherman, W. R. Wharton, G. R. Burleson, S. L. Verbeck, R. J. Peterson and H. A. Thiessen, submitted to Phys. Rev. C.

A Study of the $^{80}Se(p,d)^{79}Se$ Reaction. B. M. Kluger, R. E. Anderson, R. J. Peterson and R. A. Ristinen, accepted by J. of Phys. G.

The Effect of Energy Straggling on the Relationship Between Cross Sections and Thick Target Yields. C. S. Zaidins, accepted by Nucl. Inst. and Meth.

Thick Target Measurements and Astrophysical Thermonuclear Reaction Rates: Proton Induced Reactions. N. A. Roughton, M. J. Fritts, R. J. Peterson and C. S. Zaidins, accepted by Atomic Data and Nuclear Data Tables.

C. Published Abstracts, Conference Presentations and Reports

Neutron Spectra from $^{9}Be(p,n)^{9}B$. C. D. Zafiratos, D. E. Bainum, J. Rapaport, C. A. Goulding, M. B. Greenfield, C. C. Foster and S. D. Schery, Bull. Am. Phys. Soc. 23 (1978) 526.

Efficiency Measurements of a Large Neutron Detector. C. A. Goulding, M. B. Greenfield, D. E. Bainum, J. Rapaport, C. C. Foster, T. E. Ward, C. D. Zafiratos, S. D. Schery and C. D. Goodman, Bull. Am. Phys. Soc. 23 (1978) 558.

The Neutron Pairing Vibration in ^{206}Hg Excited by the $^{204}Hg(t,p)^{206}$ Reaction. E. R. Flynn, D. L. Hanson, R. V. Poore, and S. D. Orbesen, and D. A. Lind, Bull. Am. Phys. Soc. 23 (1978) 613.

Invited Paper: The (p,d) Reaction Revisited at Medium Energies. J. R. Shepard, Bull. Am. Phys. Soc. 23 (1978) 11.

Pion Scattering on ^{12}C at 162 MeV. H. A. Thiessen, J. F. Amann, C. L. Morris, N. Tanaka, L. W. Swenson, P. Varghese, G. Burleson, M. Devereux, R. Boudrie, S. Iversen, A. W. Obst, K. K. Seth, K. Boyer, W. J. Braithwaite, W. B. Cottingame, C. Fred Moore, Bull. Am. Phys. Soc. 23 (1978) 592.

Elastic Scattering of 162 MeV Pions by Nuclei. C. Olmer, B. Zeidman, D. F. Geesaman, R. L. Boudrie, R. A. Siemssen, C. L. Morris, J. Amann, H. A. Thiessen, M. Devereaux, G. L. Burleson, R. E. Segel, L. W. Swenson, Bull. Am. Phys. Soc. 23 (1978) 592.

Differential Study of π^{+} and π^{-} Inelastic Scattering from ^{18}O. S. Iversen, A. Obst, K. K. Seth, H. A. Thiessen, C. L. Morris, N. Tanaka, J. Amann, R. Boudrie, G. Burleson, M. Devereux, W. Swenson, P. Varghese, K. Boyer, W. J. Braithwaite, W. Cottingame and C. Fred Moore, Bull. Am. Phys. Soc. 23 (1978) 592.

Pion Inelastic Scattering at 162 MeV. D. G. Geesaman, C. Olmer, B. Zeidman, R. L. Boudrie, R. H. Siemssen, C. L. Morris, J. Amann, A. H. Thiessen, M. Devereaux, G. L. Burleson, R. E. Segel and L. W. Swenson, Bull. Am. Phys. Soc. 23 (1978) 593.

Pion Scattering from ^{208}Pb. A. S. Rosenthal and E. Rost, Bull. Am. Phys. Soc. 23 (1978) 593.

Elastic and Inelastic Scattering of 800 MeV Protons from ^{89}Y and ^{90}Zr. N. J. DiGiacomo, R. L. Boudrie, I. Brissaud, J. J. Kraushaar, R. J. Peterson, R. A. Ristinen, E. Rost and G. R. Smith, Bull. Am. Phys. Soc. 23 (1978) 625.

The (p,d) Reaction on ^{7}Li at 800 MeV. J. R. Shepard, R. E. Anderson, R. L. Boudrie, J. J. Kraushaar, R. J. Peterson and G. R. Smith, Bull. Am. Phys. Soc. 23 (1978) 626.

The (p,d) Reaction on ^{13}C at 800 MeV. T. S. Bauer, G. Adams, G. Igo, G. Pauletta, C. Whitten, A. Wreikat, R. E. Anderson, R. L. Boudrie, J. J. Kraushaar, R. J. Peterson, J. R. Shepard and G. R. Smith, Bull. Am. Phys. Soc. 23 (1978) 626.

Energy Dependence of π^+ Induced Two-Nucleon Removal from ^{12}C. R. J. Peterson, J. E. Bolger, R. L. Boudrie, W. J. Braithwaite, J. J. Kraushaar, C. Fred Moore, C. L. Morris, R. A. Ristinen, G. R. Smith and L. E. Smith, Bull. Am. Phys. Soc. 23 (1978) 48.

Energy Dependence of π^+ Induced Four-Nucleon Removal from ^{16}O. W. J. Braithwaite, J. E. Bolger, R. L. Boudrie, J. J. Kraushaar, C. Fred Moore, C. L. Morris, R. J. Peterson, R. A. Ristinen, G. R. Smith and L. E. Smith, Bull. Am. Phys. Soc. 23 (1978) 48.

A Survey of the Pick-Up Reaction at 0.65 and 0.8 GeV. G. J. Igo, T. Bauer, G. Pauletta, J. Soukup, C. A. Whitten, Jr., G. Blanpied, R. Liljestrand, G. W. Hoffmann, M. Oothoudt and R. L. Boudrie, Bull. Am. Phys. Soc. 23 (1978) 47.

Elastic and Inelastic Scattering of 800 MeV Protons from ^{89}Y and ^{90}Zr. N. J. DiGiacomo, R. L. Boudrie, I. Brissaud, J. J. Kraushaar, R. J. Peterson, R. A. Ristinen and G. R. Smith, Bull. Am. Phys. Soc. 23 (1978) 80.

The ^{208}Pb(p,α) and ^{206}Pb(p,α) Reactions at 35 MeV. D. Weber, G. M. Crawley, R. G. Markham and P. A. Smith, Bull. Am. Phys. Soc. 23 (1978) 613.

Trace Element Abnormalities in Chronic Uremia. P. Craswell, A. C. Alfrey, L. Ibels and W. R. Smythe, presentation at the Queensland State Branch Meeting of the Australasian Society of Medical Research, Brisbane, Australia, August 1978.

Microscopic Description of Alpha-Transfer Reactions. R. A. Broglia, L. Ferreira, P. D. Kunz, H. Sofia and A. Vitturi, Conference on Clustering Aspects of Nuclei, Winnipeg, Manitoba, Canada, 19-23 June 1978.

A Study of the $^{88}Sr(^{3}He,n)^{90}Zr$ Reaction. C. D. Zafiratos, R. E. Anderson, R. A. Emigh, E. R. Flynn, D. A. Lind, P. A. Smith and W. P. Alford, Bull. Am. Phys. Soc. 23 (1978) 14.

Coupling of Single Particle and Core Excitations in $^{207,211}Bi$. R. E. Anderson, R. A. Emigh, E. R. Flynn, R. J. Peterson and P. A. Smith, Bull. Am. Phys. Soc. 23 (1978) 92.

The $^{116,118}Sn(\alpha,p)^{119,121}Sb$ Reactions at E_α=35 MeV. P. A. Smith, N. J. DiGiacomo, R. A. Emigh, R. J. Peterson and G. R. Smith, Bull. Am. Phys. Soc. 23 (1978) 539.

Proton Spectroscopy of ^{96}Tc from the (^{3}He,d) Reaction. S. Shastry, R. A. Emigh and J. J. Kraushaar, Bull. Am. Phys. Soc. 23 (1978) 554.

The $^{205}Tl(p,d)^{204}Tl$ Reaction. R. A. Emigh, R. E. Anderson, P. A. Smith and R. J. Peterson, Bull. Am. Phys. Soc. 23 (1978) 527.

Comparisons of 50 MeV π^+ Scattering from $^{6,7}Li$ and $^{12,13}C$. R. A. Eisenstein, J. F. Amann, P. D. Barnes, J. N. Craig, K. G. R. Doss, S. A. Dytman, J. D. Sherman, W. R. Wharton, R. J. Peterson, G. R. Burleson, S. L. Verbeck and H. A. Thiessen, Bull. Am. Phys. Soc. 23 (1978) 80.

Thick Target Yields for Alpha-Induced Reactions on Ca, Ti, Fe, Ni, Cu, Ge and Mo. N. A. Roughton, R. J. Peterson, C. S. Zaidins, C. J. Hansen, P. Batay-Csorba and M. S. Iverson, Bull. Am. Phys. Soc. 23 (1978) 67.

A Facility for Studying Neutron Energy Spectra at Intermediate Energies. C. D. Goodman, C. C. Foster, M. B. Greenfield, C. A. Goulding, D. A. Lind and J. Rapaport, 1978 International Cyclotron Conference at Indiana, to be published in IEEE Trans. Nuc. Sci. NS 26, April (1979).

Low Lying Isoscalar E3 Excitations in 0.8 GeV Inelastic Proton Scattering by ^{89}Y and ^{90}Zr. N. J. DiGiacomo, R. L. Boudrie, I. Brissaud, J. J. Kraushaar, R. J. Peterson, R. A. Ristinen, E. Rost and G. R. Smith, Bull. Am. Phys. Soc. 23 (1978) 927.

Normalization of the (t,d) Reaction with Realistic 3-Body Wave Functions. P. D. Kunz and A. E. L. Dieperink, Bull. Am. Phys. Soc. 23 (1978) 931.

Analysis of Energetic Proton Spectra by Thick Target Activation Method. T. Intrator, R. J. Peterson, C. S. Zaidins and N. A. Roughton, Bull. Am. Phys. Soc. 23 (1978) 926.

Measurements of the ^{138}Ba, ^{139}La and ^{144}Sm (^{3}He,n) Reactions at 25.4 MeV. W. P. Alford, R. E. Anderson, R. A. Emigh, D. A. Lind, P. A. Smith and C. D. Zafiratos, Bull. Am. Phys. Soc. 23 (1978) 962.

Level Structure of ^{112}In. L. E. Samuelson, R. A. Emigh and R. E. Anderson, Bull. Am. Phys. Soc. 23 (1978) 962.

Neutron Spectroscopy of ^{114}In from the (p,d) Reaction. R. A. Emigh, R. E. Anderson, L. E. Samuelson, Bull. Am. Phys. Soc. 23 (1978) 962.

A Study of the ^{90}Zr(α,d)^{92}Nb Reaction. R. A. Emigh, R. E. Anderson, L. E. Samuelson and P. A. Smith, Bull. Am. Phys. Soc. 23 (1978) 930.

Population of Spin-Flip States in ^{12}C. R. L. Boudrie, G. W. Hoffmann, H. A. Thiessen, N. Hintz, C. Glashausser and M. Barlett, Bull. Am. Phys. Soc. 23 (1978) 952.

Neutron Radius of ^{18}O by Elastic Scattering of π^+ and π^-. S. Iversen, A. Obst, H. Nann, K. K. Seth, C. L. Morris, N. Tanaka, H. A. Thiessen, K. Boyer, W. Cottingame, C. Fred Moore, R. L. Boudrie and D. Dehnhard, Bull. Am. Phys. Soc. 23 (1978) 935.

Survey of the (p,d) Reaction at 800 MeV. C. A. Whitten, Jr., G. Adams, T. S. Bauer, G. Igo, G. Pauletta, A. Wriekat, R. L. Boudrie, J. R. Shepard, G. R. Smith, G. W. Hoffmann and B. Hoistad, Bull. Am. Phys. Soc. 23 (1978) 934.

A Technique for Determining Neutron Densities Using Low Energy π^- Nucleus Scattering. E. Rost, Bull. Am. Phys. Soc. 23 (1978) 964.

Multistep Phenomena in the ^{20}Ne(d,^{6}Li) Reaction. J. R. Shepard and N. S. P. King, Bull. Am. Phys. Soc. 23 (1978) 953.

Measurement of the (t,p) Reaction on ^{58,60,64}Ni. W. P. Alford, R. N. Boyd, E. Sugarbaker, E. R. Flynn and D. Hansen, Bull. Amer. Phys. Soc. 23 (1978) 962.

Neutron Pickup from ^{7}Li and ^{13}C at Large Momentum Transfer. G. R. Smith, J. R. Shepard, R. J. Peterson and N. J. DiGiacomo, Bull. Am. Phys. Soc. 23 (1978) 951.

Weak Coupling Structure in ^{203}Tl from the ^{205}Tl(p,t)^{203}Tl Reaction. R. E. Anderson, J. J. Kraushaar, R. A. Ristinen, S. Shastry and R. C. Weiss, Bull. Am. Phys. Soc. 23 (1978) 945.

Elastic and Inelastic Proton Scattering from ^{16}O at 800 MeV. G. S. Adams, T. S. Bauer, G. Igo, G. Pauletta, C. Whitten, A. Wriekat, G. W. Hoffmann, G. R. Smith, M. Gazzaly and L. Ray, Bull. Am. Phys. Soc. 23 (1978) 934.

D. Theses

The Level Structure of ^{78}Br. B. M. Kluger, Ph.D., 1978.

A Configuration Space Study of Low Energy Pion-Nucleus Scattering. A. S. Rosenthal, Ph.D., 1978.

V. PERSONNEL

A. Academic and Scientific

W. P. Alford[1]	Visiting Professor
R. E. Anderson[2]	Assistant Professor
R. R. Borchers	Professor, Vice-Chancellor of University
R. L. Boudrie[3]	Research Associate
F. W. N. deBoer[4]	Visiting Associate Professor
R. A. Emigh	Research Associate
M. L. Gartner[5]	Research Associate
J. J. Kraushaar[6]	Professor, Chairman of Laboratory until August 1, 1978
H. Kubo[7]	Research Associate
P. D. Kunz[8]	Professor
D. A. Lind	Professor, Chairman of Laboratory beginning August 1, 1978; Chairman of Department until July, 1978
R. J. Peterson[9]	Professor
B. W. Ridley	Professor, on leave
R. A. Ristinen	Professor
E. S. Rost	Professor
W. S. Pong	Research Associate
J. R. Shepard	Assistant Professor
W. R. Smythe	Professor
L. E. Samuelson	Research Associate
P. A. Smith	Research Associate
C. D. Zafiratos	Professor, Chairman of Department beginning July, 1978
C. S. Zaidins	Professor

B. Technical and Support Staff

R. C. Armstrong	Research Aide
C. A. Crouch[10]	Laboratory Technician
E. C. DeGabain	Equipment Fabricator
L. A. Erb	Electrical Engineer
J. L. Homan	Research Aide
A. B. Phillips	Cyclotron Engineer
D. E. Prull	Scientific Programmer
J. N. Sonnenberg	Staff Assistant
J. W. V. Trish[11]	Computer Programmer
A. K. Wiles	Equipment Fabricator

C. Research Assistants

A. D. Craig[12]	T. P. Intrator[13]	R. R. Sercely[13]
P. N. Craig[12]	B. M. Kluger[14]	B. L. Smith
N. J. DiGiacomo	J. A. Mulvaney[10]	G. R. Smith
G. E. Feldkamp[13]	D. L. Lingle[12]	A. D. Streater[13]
C. A. Fields	A. E. Park	R. C. Weiss
D. H. Haynes[12]	A. S. Rosenthal[14]	
J. P. Huennekens[13]	M. D. Rayman[12]	

D. Other Students (part-time)

J. Anderson
J. Alvistur
D. Bass
C. Bowker[13]
M. Burroughs[13]
B. Campbell[15]
K. Casey
R. Chinnock
D. Cooke[13]
S. Dowis[13]
L. Drury[13]
P. Eggers[13]
J. Flora[13]
P. Kaczkowski[13]
L. Kermish[13]
M. Kirshner[13]
P. Orum
P. Pfister
M. Sares
G. Snyder
C. Spahr
J. Suekama[13]
T. Talbot[13]

E. Summer Visitors (Supported in part by contract funds; see section II-E for a complete list of Visiting Scientists)

W. Pratt (Pennsylvania State University, University Park, PA)
N. Roughton (Regis College, Denver)
S. Shastry (SUNY, Plattsburgh, NY)

---

[1] On leave from Univ. of Western Ontario, London, Ontario.
[2] Appointment ended September, 1978; now at LASL.
[3] Working at Los Alamos Scientific Laboratory.
[4] On leave from Vrije Universiteit, Amsterdam, The Netherlands.
[5] Appointment began August, 1978.
[6] On leave at Univ. of British Columbia, starting Sept., 1978.
[7] Appointment ended August, 1978; supported by NIH.
[8] Returned from leave at Niels Bohr Inst., Copenhagen, June, 1978.
[9] On leave at NSF, Washington, D. C., starting Sept., 1978.
[10] Supported by NIH.
[11] Supported in part by NIH; appointment ended May, 1978.
[12] Appointment began summer, 1978.
[13] Appointment ended, 1978.
[14] Received Ph.D., 1978.
[15] Summer visitor from Liverpool, England.